UNIVERSIDADE FEDERAL DE SANTA CATARINA
CENTRO TECNOLÓGICO
PROGRAMA DE PÓS-GRADUAÇÃO EM ENGENHARIA AMBIENTAL

Carlos Eduardo Lach

Avaliação do processo de tratamento integrado utilizando célula a combustível microbiana (CCM) e eletro-Fenton (EF) na degradação de azo-corante têxtil

Florianópolis
2023

Carlos Eduardo Lach

Avaliação do processo de tratamento integrado utilizando célula a combustível microbiana (CCM) e eletro-Fenton (EF) na degradação de azo-corante têxtil

Dissertação submetida ao Programa de Pós-Graduação em Engenharia Ambiental da Universidade Federal de Santa Catarina como requisito para a obtenção do título de mestre em Engenharia Ambiental.

Orientadora: Profª. Maria Ángeles Lobo Recio, Drª.
Coorientador: Prof. Flávio Rubens Lapoli, Dr.

Florianópolis

2023

Lach, Carlos Eduardo
Avaliação do processo de tratamento integrado utilizando célula a combustível microbiana (CCM) e eletro-Fenton (EF) na degradação de azo-corante têxtil / Carlos Eduardo Lach ; orientadora, Maria Ángeles Lobo Recio, coorientador, Flávio Rubens Lapolli, 2023.
195 p.

Dissertação (mestrado) - Universidade Federal de Santa Catarina, Centro Tecnológico, Programa de Pós-Graduação em Engenharia Ambiental, Florianópolis, 2023.

Inclui referências.

1. Engenharia Ambiental. 2. Engenharia Ambiental. 3. Azo-corante têxtil. 4. Célula a combustível microbiana. 5. Processo híbrido de tratamento. I. Lobo Recio, Maria Ángeles . II. Lapolli, Flávio Rubens . III. Universidade Federal de Santa Catarina. Programa de Pós-Graduação em Engenharia Ambiental. IV. Título.

Carlos Eduardo Lach

Avaliação do processo de tratamento integrado utilizando célula a combustível microbiana (CCM) e eletro-Fenton (EF) na degradação de azo-corante têxtil

O presente trabalho em nível de mestrado foi avaliado e aprovado em 20 de dezembro de 2023, pela banca examinadora composta pelos seguintes membros:

Profª. Erica Janaina Rodrigues de Almeida, Drª.
Serviço Nacional de Aprendizagem Industrial - SENAI

Profª. Maria Eliza Nagel Hassemer, Drª.
Universidade Federal de Santa Catarina - UFSC

Certificamos que esta é a versão original e final do trabalho de conclusão que foi julgado adequado para obtenção do título de mestre em Engenharia Ambiental.

ICP-Edu
Documento assinado digitalmente
Alexandra Rodrigues Finotti
Data: 09/02/2024 07:42:34-0300
CPF: ***.114.321-**
Verifique as assinaturas em https://v.ufsc.br

Profª. Alexandra Rodrigues Finotti, Drª.
Coordenadora do Programa de Pós-Graduação em Engenharia Ambiental

ICP-Edu
Documento assinado digitalmente
Maria Angeles Lobo Recio
Data: 08/02/2024 15:22:55-0300
CPF: ***.111.569-**
Verifique as assinaturas em https://v.ufsc.br

Profª. Maria Ángeles Lobo Recio, Drª.
Orientadora

Florianópolis, 2023

Dedico este trabalho à minha família.

AGRADECIMENTOS

À Deus, por todas as bençãos e discernimento nesta caminhada.

Aos meus pais, pelos ensinamentos e por todo apoio e confiança nas minhas escolhas. À minha irmã e minha avó, que sempre estiveram ao meu lado.

À minha orientadora, a profª. Drª. María Ángeles Lobo Recio, pelo aceite de orientação e por acreditar em minha capacidade de executar a pesquisa, pelas valiosas orientações recebidas e experiências compartilhadas. Obrigado pelos ensinamentos, pela dedicação constante, pela compreensão e resiliência no desenvolvimento da dissertação.

Ao meu coorientador, o prof. Dr. Flávio Rubens Lapolli, pelo aceite na coorientação, pela confiança e oportunidade em mim depositadas.

Ao Programa de Pós-Graduação em Engenharia Ambiental (PPGEA), ao Departamento de Engenharia Sanitária e Ambiental e à Universidade Federal de Santa Catarina por toda estrutura física e intelectual disponibilizada.

Aos professores do PPGEA, por todos os ensinamentos, que certamente contribuíram para minha formação.

Ao Laboratório de Reúso de Águas (LaRA), coordenado pelo prof. Dr. Flávio R. Lapolli e toda equipe de alunos-pesquisadores por todo suporte e parceria no desenvolvimento da pesquisa. Ao Laboratório Integrado de Meio Ambiente (LIMA), coordenado pelo prof. Dr. Rodrigo A. Mohedano, por toda ajuda e suporte durante esses dois anos de pesquisa.

Aos técnicos do LIMA, a Drª. Aline A. Freitas e ao Jorge C. da Silva Júnior, por toda ajuda prestada nas análises laboratoriais e por todas as dúvidas sanadas.

Ao Sr. Dagoberto pela construção, ajustes e manutenção do reator bioeletroquímico utilizado nesta pesquisa. Obrigado por aceitar a missão com dedicação e paciência.

À empresa Dystar® (filial Apiúna, SC) pelo fornecimento do azo-corante, em especial, ao Sr. Luiz B. Santana, pela atenção e cordialidade.

Aos professores e pesquisadores Dr. Dipak A. Jadhav, Dr. Luigi Rizzo e a Drª. Erica J. R. de Almeida, pelas conversas, pelas “trocas de e-mails”, pelo compartilhar de experiências e sugestões. Agradeço a disponibilidade e atenção que sempre tiveram comigo.

À Drª. Daniele D. Silveira pela sua disponibilidade e expertise no acompanhamento das análises da comunidade microbiana. Obrigado pela parceria e pelas valiosas contribuições no desenvolvimento desta pesquisa.

Aos membros da banca avaliadora, Drª. Erica J. R. de Almeida e a profª. Drª. Maria E. Nagel Hassemer, por aceitarem o convite e por contribuírem com suas experiências para a melhoria deste trabalho.

Às secretárias do PPGEA, Lays e Clara e a secretária de ensino, Miriane, por toda ajuda, pelas conversas e orientações. Obrigado pela atenção e dedicação.

Ao Conselho Nacional de Desenvolvimento Científico e Tecnológico (CNPq) e a Coordenação de Aperfeiçoamento de Pessoal de Nível Superior (CAPES), pela concessão da bolsa de estudo e de recursos necessários para o desenvolvimento desta pesquisa.

RESUMO

A integração da célula a combustível microbiana (CCM) com eletro-Fenton (EF), denominado sistema bio-eletro-Fenton (BEF), tem demonstrado resultados promissores na remoção de azo-corantes e geração simultânea de corrente elétrica. Neste estudo, foi investigada a aplicação do BEF ao tratamento de soluções do corante Violeta Brilhante de Remazol-5R (VBR-5R) em três diferentes fases, sendo: i) inoculação e aclimatação bacteriana; ii) remoção do azo-corante via BEF; e iii) tratamento via sistema híbrido em biofilme anódico de CCM e BEF catódico. Na primeira fase, foi investigado o processo de aclimatação das bactérias na CCM a partir de um lodo anaeróbio para a síntese de peróxido de hidrogênio (H_2O_2). Após 20 dias de aclimatação, a CCM alcançou uma densidade de potência máxima de 60,6 mW m^{-2}, com 15,17 ± 0,3 mg H_2O_2 L^{-1}. Houve uma notável mudança na estrutura da comunidade microbiana do biofilme, com incremento na abundância relativa de Proteobactérias (de 28,1% para 62%) e Firmicutes (de 7% para 19,6%). Alguns gêneros, como Kerstersia (42%) e Pandoraea (1%), apresentaram correlações positivas ($r > 0,850$) na conversão de substrato em corrente elétrica e subsequente síntese de H_2O_2. Na segunda fase, foram avaliadas as eficiências de remoção e degradação do VBR-5R utilizando diferentes concentrações de VBR-5R (5, 10 e 20 mg L^{-1}) e resistências externas (R_{ext}) (1000, 100 e 10 Ω). A estratégia mais eficaz foi aquela que usou 20 mg VBR-5R L^{-1} e 10 Ω R_{ext}. O sistema sintetizou 12,1 ± 0,2 mg H_2O_2 L^{-1} e alcançou uma densidade de potência máxima de 69,4 mW m^{-2}, com uma eficiência de Coulomb (EC) de 7,2 ± 0,4%. Nesse cenário, obtiveram-se eficiências notáveis, como 95,5 ± 0,3% na remoção de cor, 73,6 ± 0,4% na degradação de grupos aromáticos e 82,4 ± 0,3% na remoção de DQO. No entanto, a análise de fitotoxicidade revelou que, após 12 horas de detenção hidráulica (TDH), os índices de germinação (IG) das sementes de alface (*Lactuca sativa*) e rabanete (*Raphanus sativus*) permaneceram < 80%, indicando que o efluente tratado via BEF era tóxico. Na terceira fase, a aplicação de um TDH de 6 h no biofilme anódico da CCM e de 12 h no BEF catódico para 20 mg VBR-5R L^{-1} + 0,25 g acetato de sódio L^{-1}, se destacou. O sistema atingiu uma densidade de potência máxima de 70,3 mW m^{-2} e sintetizou 12,5 ± 0,3 mg H_2O_2 L^{-1}, com EC de 8,34 ± 0,23%. Além disso, foram obtidas boas eficiências na remoção de cor (99,8 ± 0,1%), DQO (79,6 ± 0,3%) e grupos aromáticos (78,7 ± 1,0%). A análise de fitotoxicidade revelou que o ajuste do pH de 3,0 para 7,0 resultou em menor toxicidade para as sementes de alface (IG = 30,1 ± 1,5%) e rabanete (IG = 43,8 ± 1,6%) em comparação com o efluente bruto (IG = 1,90 ± 0,2%; IG = 3,1 ± 0,4%). Na comunidade microbiana do biofilme anódico, os gêneros da família Rhizobiaceae ($r = 0,9475$), Soehngenia ($r = 0,9750$) e Pandoraea ($r = 0,8307$) apresentaram correlações positivas, desde a etapa de degradação do VBR-5R, até a conversão em corrente elétrica e síntese de H_2O_2. Portanto, de acordo com as três fases da pesquisa, o sistema de tratamento que apresentou os melhores resultados para degradação do VBR-5R foi o BEF (20 mg VBR-5R L^{-1}; e 10 Ω). A remoção de DQO foi superior no BEF em comparação com o sistema híbrido, apresentando eficiências de remoção de cor e degradação de grupos aromáticos muito próximas aos valores obtidos no sistema híbrido. Os elevados TDH's e a alta carga de DQO na entrada do sistema híbrido podem ter favorecido a formação de subprodutos tóxicos adicionais. Em síntese, as três fases da pesquisa demonstraram a viabilidade de abordagens bioeletroquímicas na síntese de H_2O_2 e na remoção eficiente do azo-corante têxtil, com contribuições significativas para aplicações futuras em tratamento de efluentes e questões ambientais.

Palavras-chave: célula a combustível microbiana; bio-eletro-Fenton; azo-corante; fitotoxicidade; sequenciamento 16S rRNA; comunidade microbiana eletroativa.

ABSTRACT

The integration of the microbial fuel cell (MFC) with electro-Fenton (EF), named bio-electro-Fenton (BEF) system, has demonstrated promising results in the azo dyes removal and simultaneous electric current generation. In this study, the BEF application to the Remazol Brilliant Violet-5R (RBV-5R) dye solutions treatment was investigated in three different phases, namely: i) inoculation and bacterial acclimation; ii) azo dye removal via BEF; and iii) treatment via hybrid treatment system MFC anodic biofilm and cathodic BEF. In the first phase, the acclimation process of bacteria in the MFC from anaerobic sludge for the hydrogen peroxide (H_2O_2) synthesis was investigated. After 20 days of acclimation, the MFC reached a maximum power density of 60.6 mW m^{-2}, with 15.17 ± 0.3 mg H_2O_2 L^{-1}. There was a notable change in the structure of the microbial community, with an increase in the relative abundance of Proteobacteria (from 28.1% to 62%) and Firmicutes (from 7% to 19.6%). Some genera, such as Kerstersia (42%) and Pandoraea (1%), showed positive correlations (r > 0.850) in the conversion of substrate into electrical current and subsequent H_2O_2 synthesis. In the second phase, the removal and degradation efficiencies of VBR-5R were evaluated using different concentrations of VBR-5R (5, 10, and 20 mg L^{-1}) and external resistances (R_{ext}) (1000, 100, and 10 Ω). The most effective strategy was the one using 20 mg RBV-5R L^{-1} and 10 Ω R_{ext}. The system synthesized 12.1 ± 0.2 mg H_2O_2 L^{-1} and achieved a maximum power density of 69.4 mW m^{-2}, with a Coulomb efficiency (CE) of 7.2 ± 0.4%. In this scenario, notable efficiencies were obtained, including 95.5 ± 0.3% in color removal, 73.6 ± 0.4% in aromatic group removal, and 82.4 ± 0.3% in COD removal. However, a phytotoxicity analysis revealed that, after 12h of hydraulic retention time (HRT), the germination indexes (GI) of lettuce (*Lactuca sativa*) and radish (*Raphanus sativus*) seeds were < 80%, which provided the effluent treated via BEF was toxic. In the third phase, HRT 6 h on the MFC anodic biofilm and 12 h on the cathodic BEF for 20 mg RBV-5R L^{-1} + 0.25 g sodium acetate L^{-1} stands out. The system achieved a maximum power density of 70.3 mW m^{-2} and synthesized 12.5 ± 0.3 mg H_2O_2 L^{-1}, with a CE of 8.34 ± 0.23%. Furthermore, good efficiencies were obtained in removing color (99.8 ± 0.1%), COD (79.6 ± 0.3%), and aromatic groups (78.7 ± 1.0%). A phytotoxicity analysis revealed that adjusting the pH from 3.0 to 7.0 was proven to have lower toxicity for lettuce (GI = 30.1 ± 1.5%) and radish (GI = 43.8 ± 1.6%) seeds, compared to raw effluent (GI = 1.90 ± 0.2%; GI = 3.1 ± 0.4%). In the microbial community of the anode biofilm, the genera of the family Rhizobiaceae (r = 0.9475), Soehngenia (r = 0.9750), and Pandoraea (r = 0.8307) showed positive correlations since the RBV-5R degradation, until conversion into electrical current and H_2O_2 synthesis. Therefore, according to the three phases of the research, the treatment system that presented the best results for handling RBV-5R was BEF (20 mg RBV-5R L^{-1}; and 10 Ω). The COD removal was increased in BEF compared to the hybrid system, presenting color removal and aromatic group handling efficiencies very close to the values obtained in the hybrid system. The high HRTs and the high COD load at the hybrid system inlet may have favored the formation of additional toxic byproducts. In summary, the three phases of research provide options for bioelectrochemical approaches in the H_2O_2 synthesis and the efficient textile azo dye removal, with significant contributions to future applications in wastewater treatment and environmental issues.

Keywords: microbial fuel cell; bio-electro-Fenton; azo dye; phytotoxicity; 16S rRNA sequencing; electroactive microbial community.

LISTA DE FIGURAS

Figura 1 - Representação esquemática de uma CCM 10
Figura 2 - Mecanismo de degradação de azo-corante via azorredutase 17
Figura 3 - Representação esquemática do sistema BEF 23
Figure 4 - Schematic MFC reactor setup 47
Figure 5 - Development of MFC acclimation: (A) relation of the increase in electric current density (mA m^{-2}) with H_2O_2 (mg L^{-1}) for R_{ext}=1000 Ω; (B) polarization curve 52
Figure 6 - PCoA ordination using the genera abundance data to represent the differences between the investigated microbial communities 58
Figure 7 - (A) Taxonomy of the most prevalent genera in the Inoculum and MFC samples; and (B) The 20 top phyla's relative abundance in percentage according to inoculum and MFC-acclimated biofilm 60
Figure 8 - CCA diagram showing relationships of 20 dominant genera associated with the variables highlighted in red color (pH, substrate, and temperature) 63
Figure 9 - Pearson's correlation analysis (r) between the 20 dominant microbial genera in the MFC and the efficiencies of substrate conversion into electric current and H_2O_2 65
Figure 10 - The BEF reactor configuration with the data acquisition system 72
Figure 11 - UV-vis spectra evolution as a function of reaction time for (A) S1, (B) S2, (C) S3 strategies, and (D) RBV-5R removal rate 77
Figure 12 - Relationship between the electric current generation and H_2O_2 synthesis in the BEF system applying different R_{ext}: (A) S1, 1000 Ω; (B) S2, 100 Ω; and (C) S3, 10 Ω 81
Figure 13 - Proton exchange membrane (PEM) with fouling characteristics 83
Figure 14 - (A) Increased CE and FE values in the BEF system fed 1 g L^{-1} sodium acetate with an HRT = 12 h; (B) polarization curve for each operational strategy 84
Figure 15 - COD removal according to operational strategies compared to RBV-5R and aromatic group removal efficiencies after HRT = 12 h 86
Figure 16 - GI of *L. sativa* and *R. sativus* seeds for raw azo dye wastewater (A and C, t = 0 h) and the treated effluent (B and D, t = 12 h) for the different operational strategies 89
Figure 17 - Schematic representation of the MFC+BEF reactor with the data acquisition system 98

Figure 18 - UV–visible spectra evolution for (A) S1, (B) S2, and (C) S3 in primary treatment via MFC anodic biofilm and (D) S1, (E) S2, and (F) S3 in oxidative posttreatment via cathodic BEF for the different operational strategies 105
Figure 19 - COD removal as a function of HRT (1) according to the operational strategy for the study and (2) an extended 12-h HRT for BEF. The results in graph (A) correspond to MFC decolorization, (B) BEF oxidative treatment, and (C) represent the overall removal efficiency with joint MFC+BEF..109
Figure 20 - An increase in Coulomb and Faraday efficiency values for an MFC+BEF system fed with azo dye and sodium acetate for different HRTs.............................111
Figure 21 - Relationship between electric current generation and H_2O_2 synthesis in the MFC+BEF hybrid system to (A) S1, (B) S2 and (C) S3 applying 10 Ω R_{ext} 114
Figure 22 - Polarization curve performed after the operating HRT: (S1) 2 h; (S2) 4 h; and (S3) 6 h 116
Figure 23 - Germination index (GI) of (A) *L. sativa* and (B) *R. sativus* seeds for azo dye solution in the different operational strategies 119
Figure 24 - PCoA ordering using overall abundance data to represent differences between the investigated microbial communities..122
Figure 25 - CCA diagram showing the relationships of 20 dominant genera associated with the variables highlighted in red (temperature and RBV-5R azo dye) 123
Figure 26 - The 20 top genera's relative abundance in percentage according to MFC-acetate and MFC-RBV-5R+acetate 124
Figure 27 - Pearson's correlation analysis (r) between the 20 dominant microbial genera in the MFC and the efficiencies of RBV-5R+acetate conversion into electric current and H_2O_2..126

LISTA DE TABELAS

Tabela 1 - Reações na CCM usando acetato como substrato com sua tensão potencial 10
Tabela 2 - Aplicação da CCM na degradação de corantes têxteis com diferentes inóculos 13
Tabela 3 - Vantagens e limitações direcionadas ao processo Fenton e seu efeito sinérgico com a CCM relatadas para tratamento de águas residuais de corante 20
Tabela 4 - Aplicação do processo BEF na remoção de corantes têxteis 25
Table 5 - COD removal and electrochemical parameters in MFC-1000 Ω R_{ext} during the acclimation 54
Table 6 - Numbers of rRNA sequences analyzed and alpha diversity indices for the microbial communities in the inoculum and MFC biofilm after 20 days of acclimation 57
Table 7 - Chemical structure of the reactive azo dye 71
Table 8 - Operational strategies applied in the BEF for HRT = 12 h 73
Table 9 - Maximum decolorization efficiency applying the BEF system for different azo dyes 79
Table 10 - Effects of phytotoxicity on the average root length (cm) of *L. sativa* and *R. sativus* for the different operational strategies according to the raw sample (t=0 h) and after oxidative treatment (t=12 h) 88
Tabela 11 - Chemical structure of the reactive azo dye 97
Table 12 - Operational strategies applied in the MFC+BEF hybrid treatment system 99
Table 13 - Color and aromatic groups removal efficiency for each stage of the hybrid treatment system 106
Table 14 - Phytotoxicity effects on the mean root length (cm) of *L. sativa* and *R. sativus* 118
Table 15 - The number of rRNA sequences analyzed and alpha diversity indices for the microbial communities in the inoculum and MFC-acclimated 121

LISTA DE ABREVIATURAS E SIGLAS

A	Ampère
AM	Azul de metileno
AOP	Advanced oxidative process
BEF	Bio-eletro-Fenton
BES	Bioelectrochemical system
$C_2H_3NaO_2$	Sodium acetate
CCA	Canonical coordinate analysis
CCM	Célula a combustível microbiana
CCM+EF	Célula a combustível microbiana+eletro-Fenton
CE	Coulomb efficiency
CO_2	Dióxido de carbono
COD	Chemical oxygen demand
DIET	Direct interspecies electron transfer
DNA	Ácido desoxirribonucleico
DP	Densidade de potência
DPV	Densidade de potência volumétrica
DQO	Demanda química de oxigênio
EC	Eficiência de Coulomb
EF	Electro-Fenton
FAD^+	Dinucleótido de flavina e adenina
FC	Feltro de carbono
FE	Faraday efficiency
$Fe(CN)_6$	Ferrocianeto
Fe^{2+}	Iron II
Fe_2O_3	Óxido férrico
FeOOH	Oxihidróxido de ferro
$FeSO_4.7H_2O$	Sulfato de ferro (II) heptahidratado
$g\ L^{-1}$	Grama por litro
GI	Germination index
H^+	Hydrogen ion
H^+	Íon hidrogênio
H_2O	Monóxido de di-hidrogênio
H_2O_2	Peróxido de hidrogênio
H_2SO_4	Ácido sulfúrico
HRT	Hydraulic retention time
I_3^-	Iodine
Kg	Quilograma
$KHC_8H_4O_4$	Biftalato de potássio
KI	Iodeto de potássio
$KWh\ m^{-3}$	Quilo Watts-hora por metro cúbico
LA7	Laranja ácido 7
LM	Laranja de metila
$mA\ m^{-2}$	Mili Ampère por metro quadrado
MFC	Microbial fuel cell
$mg\ L^{-1}$	Miligramas por litro
$mL\ min^{-1}$	Mililitro por minuto
mm	Milimetro

$mM\ L^{-1}$	Milimol por litro
MnO_4	Peróxido de manganês
MTP	Membrana de troca de prótons
$mW\ m^{-2}$	Mili Watts por metro quadrado
$mW\ m^{-3}$	Mili Watts por metro cúbico
Na_2SO_4	Sulfato de sódio
NAD^+	Dinucleótido de nicotinamida e adenina
$NADP^+$	Fosfato de dinucleótido de nicotinamida e adenina
NaOH	Hidróxido de sódio
$(NH_4)_2MoO_4$	Ortomolibdato de amônio
nm	Nanometer
•OH	Radical hidroxila
OMC	Outer membrane cytochromes
OTU	Operational taxonomic unit
PBS	Phosphate buffer solution
PCoA	Principal coordinate analysis
PD	Power density
PEM	Proton exchange membrane
pH	Potencial hidrogeniônico
POA's	Processos oxidativos avançados
ppm	Partes por milhão
RBV-5R	Remazol brilliant violet – 5r
R_{ext}	External resistance
R_{int}	Internal resistance
RNA	Ácido ribonucleico
SPE's	Substâncias poliméricas extracelulares
$t_{1/2}$	Reaction half-life
TDH	Tempo de detenção hidráulica
TEE	Transferência extracelular de elétrons
V	Voltagem
VBR-5R	Violeta brilhante de remazol – 5r
$ZnSO_4$	Zinc sulfate
Ω	Ohm
2e-ORR	Two-electron oxygen reduction reaction
4e-ORR	Four-electron oxygen reduction reaction

SUMÁRIO

APRESENTAÇÃO **1**

1 CAPÍTULO 1 - CONTEXTUALIZAÇÃO E OBJETIVOS **2**

1.1 INTRODUÇÃO 2

1.2 HIPÓTESES 4

1.3 OBJETIVOS 5

1.3.1 Objetivo geral **5**

1.3.2 Objetivos específicos **5**

2 CAPÍTULO 2 - REFERENCIAL TEÓRICO E ESTRUTURAÇÃO METODOLÓGICA **5**

2.1 MEIO AMBIENTE, ENERGIA E EFLUENTES TÊXTEIS 5

2.2 CORANTES SINTÉTICOS 8

2.3 CÉLULA A COMBUSTÍVEL MICROBIANA (CCM) 9

2.3.1 Remoção de corantes têxteis **16**

2.4 SISTEMA HÍBRIDO DE TRATAMENTO 19

2.5 BIO-ELETRO-FENTON (BEF) 21

2.5.1 Tipo de inóculo **28**

2.5.2 Substrato **30**

2.5.3 Síntese de H_2O_2 ..... **34**

2.5.4 Tempo de detenção hidráulica (TDH) **38**

2.6 METODOLOGIA DA PESQUISA 41

3 CAPÍTULO 3 - EXPLORING MICROBIAL COMMUNITY DYNAMICS IN MICROBIAL FUEL CELL (MFC) ACCLIMATION FOR HYDROGEN PEROXIDE (H_2O_2) SYNTHESIS **43**

3.1 INTRODUCTION 44

3.2 MATERIAL AND METHODS 47

3.2.1 MFC setup **47**

3.2.2 Inoculum and acclimation **47**

3.2.3 Analysis and calculation **48**

3.2.4 Microbial community analysis **50**

3.2.5 Data analysis **51**

3.3 RESULTS AND DISCUSSION 51

3.3.1 Current density output and H_2O_2 synthesis **51**

3.3.2 Coulomb and Faraday efficiency ... 54
3.3.3 Microbial community analysis ... 56
3.4 CONCLUSION ... 66
4 CAPÍTULO 4 - EVALUATING THE BIO-ELECTRO-FENTON (BEF) PROCESS FOR REMOVAL OF THE REMAZOL BRILLIANT VIOLET-5R (RBV-5R) AZO DYE ... 67
4.1 INTRODUCTION ... 68
4.2 MATERIALS AND METHODS ... 71
4.2.1 Azo dye ... 71
4.2.2 BEF setup ... 72
4.2.3 Operational strategies ... 72
4.2.4 Analytical procedures ... 73
4.2.5 Calculation ... 74
4.2.6 Phytotoxicity assessment ... 75
4.2.7 Data analysis ... 76
4.3 RESULTS AND DISCUSSION ... 76
4.3.1 RBV-5R removal ... 76
4.3.2 H_2O_2 synthesis ... 80
4.3.3 Coulomb and Faraday efficiency ... 83
4.3.4 COD removal ... 86
4.3.5 Phytotoxicity assessment ... 88
4.4 CONCLUSION ... 91
5 CAPÍTULO 5 - HYBRID BIOELECTROCHEMICAL PROCESS MFC ANODIC BIOFILM AND CATHODIC BEF (MFC+BEF) FOR RBV-5R DYE REMOVAL WITH SIMULTANEOUS ELECTRIC CURRENT GENERATION AND H_2O_2 SYNTHESIS ... 92
5.1 INTRODUCTION ... 93
5.2 MATERIALS AND METHODS ... 96
5.2.1 Azo dye ... 96
5.2.2 Hybrid system setup ... 97
5.2.3 Operational strategies ... 98
5.2.4 Analytical methods ... 99
5.2.5 Calculations and measurements ... 100
5.2.6 Bioassay assessment ... 101

5.2.7	**Microbial community analysis**	**102**
5.2.8	**Data analysis**	**103**
5.3	RESULTS AND DISCUSSION	103
5.3.1	**MFC anodic biofilm: color and aromatic group removals**	**103**
5.3.2	**Cathodic BEF: color and aromatic group removals**	**107**
5.3.3	**COD removal**	**108**
5.3.4	**Coulomb and Faraday efficiency**	**111**
5.3.5	**H_2O_2 synthesis**	**113**
5.3.6	**Output power density**	**115**
5.3.7	**Phytotoxicity assessment**	**117**
5.3.8	**Microbial community analysis**	**120**
5.4	CONCLUSION	127
6	**CAPÍTULO 6 – CONCLUSÕES GERAIS E RECOMENDAÇÕES**	**128**
6.1	CONCLUSÃO	128
6.2	RECOMENDAÇÕES	130
	REFERÊNCIAS	**131**

APRESENTAÇÃO

A dissertação está estruturada em 6 capítulos:

- O capítulo 1 inclui a introdução geral, hipóteses e objetivos.
- O capítulo 2 apresenta a revisão bibliográfica, que compreende aspectos relevantes em relação à problemática ambiental da disposição de azo-corantes, célula combustível microbiana (CCM), sistemas híbridos de tratamento e condições operacionais do processo bio-eletro-Fenton (BEF).
- O capítulo 3 apresenta a investigação sobre o processo de aclimatação da CCM para otimização da eletrossíntese de H_2O_2. Este capítulo está apresentado na forma de artigo, intitulado "*Exploring microbial community dynamics in microbial fuel cell (MFC) acclimation for hydrogen peroxide (H_2O_2) synthesis*".
- O capítulo 4 abrange a aplicação do BEF na remoção do azo-corante têxtil Violeta Brilhante de Remazol-5R (VBR-5R) através de soluções de diferentes concentrações e diferentes resistências externas na CCM, avaliando a remoção de cor e DQO, degradação de grupos aromáticos e avaliação fitotoxicológica do efluente tratado. Este capítulo está apresentado na forma de artigo, intitulado *"Evaluating the bio-electro-Fenton (BEF) process for removal of the Remazol Brilliant Violet-5R (RBV-5R) azo dye"*.
- O capítulo 5 aborda a eficiência operacional e a investigação da comunidade microbiana com aplicação do processo híbrido de tratamento via biofilme anódico da CCM e BEF catódico na remoção de azo-corante. Este capítulo está estruturado na forma de artigo, intitulado *"Hybrid bioelectrochemical process MFC anodic biofilm and cathodic BEF for RBV-5R dye removal with simultaneous electric current generation and H_2O_2 synthesis"*.
- O capítulo 6 apresenta as conclusões gerais e contribuições científicas da pesquisa, bem como as recomendações para estudos posteriores.

1 CAPÍTULO 1 - CONTEXTUALIZAÇÃO E OBJETIVOS

1.1 INTRODUÇÃO

A indústria têxtil é um dos setores mais importantes para o desenvolvimento da economia global, principalmente em países como China, Índia, Paquistão e Brasil (SOUZA et al., 2023). Entretanto, é considerada um dos principais setores que contribuem para a poluição ambiental devido à geração de grande volume de efluentes carregados de corantes (OLIVEIRA et al., 2018). Dentre os corantes têxteis, os azo-corantes correspondem a um importante grupo, sendo caracterizados quimicamente pela presença de uma ou mais ligações azo (N=N). Devido sua estrutura química complexa, quando descartados de maneira incorreta no meio ambiente, os subprodutos desses corantes podem se transformar em substâncias tóxicas e recalcitrantes de caráter cancerígeno (CHAUHAN; GAUTAM; KANWAR, 2022; MAJUMDAR et al., 2022).

Os processos oxidativos avançados (POA's) são tecnologias eficazes para a remoção de uma grande variedade de poluentes orgânicos recalcitrantes (OLVERA-VARGAS et al., 2017; RAMOS et al., 2021). Os POA's, como a eletro-oxidação, foto-Fenton e Fenton convencional, são os mais eficazes na redução da cor (> 90%) e da matéria orgânica (>78%) de efluentes contendo corantes têxteis (ZHANG et al., 2021). Isso se deve à geração de espécies fortemente oxidativas como, por exemplo, os radicais hidroxila (•OH) gerados a partir da reação entre Fe^{2+} e H_2O_2. No entanto, o fornecimento sustentável de H_2O_2 é considerado o principal desafio associado à aplicação bem-sucedida de POA's no tratamento de água contendo poluentes tóxicos, como por exemplo, azo-corante têxtil. Uma tendência recente na produção de H_2O_2 concentra-se na reação de redução do oxigênio pela via de 2 elétrons (2e-RRO), o que representa um método viável para geração *in situ* de H_2O_2 (LI et al., 2023; ZHANG et al., 2020; ZHOU et al., 2019). Por isso, a possibilidade de integração de técnicas de tratamento, como processos biológicos e POA's, pode fornecer uma maneira econômica de síntese de H_2O_2, favorecendo a descoloração e degradação de corantes tóxicos (CHUNG et al., 2020; SABA; KJELLERUP; CHRISTY, 2021; SURESH et al., 2022).

Recentemente, a combinação da célula a combustível microbiana (CCM) com eletro-Fenton (EF), denominado sistema bio-eletro-Fenton (BEF), tem demonstrado resultados promissores na remoção de azo-corantes (YANG et al., 2021). A popularidade do BEF decorre do fato de que os íons de hidrogênio (H^+) e os elétrons necessários no cátodo para a formação de H_2O_2 são gerados no ânodo pela oxidação de substratos orgânicos por bactérias eletrogênicas, liberando assim H^+, elétrons e CO_2 (OLVERA-VARGAS et al., 2017; SATHE et al., 2022a). A geração e transferência de H^+ e elétrons através da solução em massa e de um circuito elétrico externo, respectivamente, é um processo espontâneo que ocorre sem qualquer entrada de energia externa (ZHAO; ZHANG, 2021). Por isso, o processo BEF pode ser empregado no tratamento de diferentes tipos de contaminantes, tais como: cloreto de trifenil-estanho (YONG et al., 2017); anti-inflamatórios (NADAIS et al., 2018); surfactantes (SATHE et al., 2022b); polietilenos sulfonados (GHATGE et al., 2022); ervas medicinais (BIRJANDI et al., 2020); paracetamol (ZHANG; YIN; LI, 2015); metropolol (YANG et al., 2021); arsênio (WANG et al., 2014); mesotriona (ZHAO; ZHANG, 2021); lixiviado de aterro sanitário (HASSAN et al., 2017; LINH; HO, 2020; YANG et al., 2022); antibióticos (LI et al., 2022); remoção biológica de nitrogênio (NGUYEN; BABEL, 2022); efluente do cultivo hidropônico (BRYSZEWSKI; RODZIEWICZ; JANCZUKOWICZ, 2022); sulfatos (DAI et al., 2022); efluentes de indústrias de bebidas (AFOLABI; ADEKALU; OKUNADE, 2022); p-nitrofenol (WANG et al., 2022c), e inclusive na remoção e degradação de azo-corantes têxteis (FENG et al., 2010b; LIU et al., 2012; WANG et al., 2022b; XU et al., 2020b; YUAN et al., 2017; ZHANG; WANG; ANGELIDAKI, 2015a).

Aplicando o BEF, Wang et al. (2022b) alcançaram 93,5% na degradação do azul de metileno com sintetização de 20,18 mg L^{-1} de H_2O_2 e densidade de potência 1,99 W m^{-3}. Ling et al. (2016) obtiveram 86,7% de remoção para 5 mg L^{-1} de laranja de metila (LM) com apenas 88,63 mmol L^{-1} de H_2O_2. No estudo de Dios et al. (2022), as eficiências de remoção de verde lisamina B (10 mg L^{-1}), índigo de carmim (20 mg L^{-1}), violeta cristal (5 mg L^{-1}) e preto reativo 5 (50 mg L^{-1}) foram de 98,2%, 97,2%, 96,2% e 88,2%, respectivamente, em apenas 15 minutos. Yang et al. (2016) obtiveram 94,90 ± 0,01% de eficiência de descoloração do LM, correspondentemente, com taxa de reação constante (k) de 0,503 ± 0,001 h^{-1}. Embora os estudos tenham avaliado o BEF para remoção de corantes, o foco permanece mais na geração de energia elétrica e descoloração do que na degradação e na minimização da toxicidade de águas com azo-corantes têxteis (FATIMA et al., 2017; ILAMATHI; JAYAPRIYA, 2018; SABA et al., 2018; SINGH; DAHIYA; MISHRA, 2021; SOLANKI; SUBRAMANIAN; BASU, 2013).

Em consideração aos avanços no campo da pesquisa, neste estudo foi avaliada a capacidade de descoloração e degradação do azo-corante têxtil Violeta Brilhante de Remazol-5R (BVR-5R) com produção simultânea de corrente elétrica e síntese de H_2O_2 via processo BEF. Foram também conduzidas estratégias de remoção de azo-corante no compartimento anódico da CCM, com pós-tratamento BEF no compartimento catódico. Para comparação, diferentes concentrações do azo-corante, resistências externas (R_{ext}) e tempos de detenção hidráulica (TDH's) foram investigados na eficiência global do processo. Além disso, foi realizada análise de fitotoxicidade de amostras brutas e tratadas com sementes de alface e rabanete. Potenciais correlações entre o biofilme bacteriano anódico e as métricas operacionais foram evidenciadas através da análise da comunidade microbiana dos biofilmes anódicos, desenvolvidos durante o processo de aclimatação e a partir da alimentação com azo-corante.

Este estudo se enquadra na linha de pesquisa de tratamento de águas e efluentes domésticos, industriais e agropecuários do Programa de Pós-Graduação em Engenharia Ambiental (PPGEA) da Universidade Federal de Santa Catarina (UFSC). O Laboratório de Reuso de Águas (LaRA) já tem iniciado pesquisas com CCM para o tratamento de efluente doméstico (SORGATO, 2022). A aplicação do processo Fenton para tratamento de efluente têxtil também foi investigada em estudos anteriores (DALARI, 2018; JUSTINO, 2016). No entanto, esta foi a primeira pesquisa desenvolvida no LaRA abordando a integração da CCM e eletro-Fenton, com objetivo de degradar azo-corante têxtil com geração simultânea de corrente elétrica e sintetização *in situ* de H_2O_2.

1.2 HIPÓTESES

I - O desenvolvimento de bactérias eletrogênicas durante o processo de aclimatação favorece e incrementa a síntese de H_2O_2. A correlação positiva entre a comunidade microbiana e as métricas operacionais é indicativa de uma relação simbiótica entre os microrganismos e o desempenho do sistema.

II – A eficácia do BEF na remoção de azo-corante é aprimorada pela aplicação de menor resistência externa (R_{ext}) no sistema bioeletroquímico proposto. Isso porque o fluxo de elétrons é favorecido em menores R_{ext}, por consequência espera-se maior taxa de síntese de H_2O_2.

III - A combinação do processo de tratamento biológico com o oxidativo (biofilme anódico de CCM e BEF catódico) resulta em uma melhor degradação de azo-corante em comparação com o BEF. Enquanto ocorre a clivagem da ligação N=N em ambiente anaeróbio, a degradação oxidativa dos grupos aromáticos pela reação de Fenton é condicionada no processo híbrido.

1.3 OBJETIVOS

1.3.1 Objetivo geral

Avaliar a eficiência de remoção e degradação do azo-corante têxtil Violeta Brilhante de Remazol-5R (VBR-5R) aplicando o processo de tratamento integrado CCM+BEF em escala de bancada.

1.3.2 Objetivos específicos

a) Investigar o processo de aclimatação da CCM sob condições controladas de operação com exploração da estrutura e dinâmica da comunidade microbiana desenvolvida no biofilme anódico;
b) Analisar como diferentes concentrações de azo-corante, variações do tempo de detenção hidráulica (TDH) e aplicações de diferentes resistências externas (R_{ext}) afetam a eficiência do processo BEF, abrangendo a geração de corrente elétrica, síntese de H_2O_2 e toxicidade do efluente tratado;
c) Avaliar a eficiência operacional e estrutura e dinâmica da comunidade microbiana do sistema híbrido de tratamento (biofilme anódico de CCM e BEF catódico – CCM+BEF) quanto a remoção de azo-corante na câmara anódica da CCM, com pós-tratamento oxidativo via BEF na câmara catódica.

2 CAPÍTULO 2 - REFERENCIAL TEÓRICO E ESTRUTURAÇÃO METODOLÓGICA

2.1 MEIO AMBIENTE, ENERGIA E EFLUENTES TÊXTEIS

O vestuário, uma das necessidades básicas da sociedade, demanda o crescimento da indústria têxtil em todo o mundo (JAHAN et al., 2022). Considerado um dos maiores segmentos da indústria do mundo, contribui significativamente para a economia de um país (SHOAIB et al., 2022). Entretanto, a indústria têxtil é uma das maiores consumidoras de água potável e, consequentemente, produz uma grande quantidade de efluentes (KHANDAKER et al., 2022; YASEEN; SCHOLZ, 2019). Em média, são necessários aproximadamente 40 litros de água limpa para colorir apenas 1 kg de tecido, podendo aumentar de acordo com o material têxtil e o processo de tingimento (BEHERA et al., 2021). Ademais, cerca de 93% da água utilizada durante a produção de tecidos coloridos na indústria têxtil é descartada como efluente de tingimento (HORCIU et al., 2020). Desse modo, ao longo das várias operações da indústria têxtil, os corantes não se fixam completamente nos tecidos e cerca de 10 a 15% dos corantes utilizados não são fixados nas fibras têxteis (BHAGAT et al., 2022; PRATAP et al., 2022).

Existem há mais de 20 anos processos de tingimento têxtil sem água, conhecidos como tingimento assistido por air-dye e dióxido de carbono supercrítico (MAHMUD; KAISER, 2020). Essas tecnologias de tingimento sem água ainda não foram totalmente aceitas pela indústria têxtil. As principais razões para isso podem ser o fato de que as indústrias são passivas e sem pretensão ou motivação fiscal para implantação do tingimento sem água. Além disso, o custo elevado de instalação das máquinas e equipamentos desmotiva a restruturação e aplicação no processo produtivo já consolidado.

Em todo o mundo, aproximadamente 7×10^7 toneladas de diferentes corantes são produzidos anualmente, e mais de 280.000 toneladas de diferentes corantes sintéticos são descarregados no meio ambiente (KISHOR et al., 2021; KUMAR, 2022). Desse montante, os azo-corantes são considerados a maior classe de corantes sintéticos utilizados nas indústrias têxteis e estão presentes em quantidades significativas em seus efluentes. São altamente estáveis devido à sua estrutura aromática complexa e ligações azoicas covalentes (FATIMA et al., 2017).

Normalmente, a razão DBO/DQO para águas residuais com azo-corante varia de 0,2 a 0,5, indicando que esses efluentes contêm uma grande proporção de matéria orgânica não biodegradável (SOLÍS et al., 2012).

O aumento das concentrações de corantes nos corpos d'água impede a capacidade da água de se reoxigenar e bloqueia a luz solar, o que perturba a atividade biológica nos ecossistemas aquáticos. O acúmulo de corante orgânico sintético nas fontes de água aumenta a DBO e DQO, afetando também o pH (ROY; SAHA, 2020). Em contraste com a descoloração rápida e fácil, é mais difícil degradar os azo-corantes por causa de sua estrutura complexa de alto peso molecular (YOGALAKSHMI et al., 2020). Sua descarga é indesejável, não apenas por causa de sua cor, mas também porque muitos azo-corantes e seus subprodutos de degradação são tóxicos e/ou mutagênicos (SOLANKI; SUBRAMANIAN; BASU, 2013; VENKATACHALAM et al., 2022; ZHANG; TAO, 2018). A presença do grupo azo na estrutura química torna os azo-corantes altamente tóxicos, e após a decomposição podem gerar subprodutos tóxicos como, por exemplo: 1,4-fenilenodiamina e o-toluidina (HASHEMI; KAYKHAII, 2022). Além disso, mesmo em pequenas concentrações, os azo-corantes podem entrar na cadeia alimentar favorecendo a recalcitrância e bioacumulação. Por consequência, podem promover toxicidade, mutagenicidade e carcinogenicidade, problemas imunológicos e neurológicos à biota aquática e aos seres humanos (AL-TOHAMY et al., 2022; LELLIS et al., 2019; PALANISAMY et al., 2019).

A União Europeia, de acordo com o regulamento da Agência Europeia para Segurança e Saúde no Trabalho n° 1272/2008 (2008), classifica como carcinogênicas cerca de 22 tipos de aminas aromáticas, proibindo os usos desses compostos químicos em corantes têxteis. No entanto, no Brasil não existe uma lei específica para o controle da comercialização e uso de corantes na indústria têxtil. Após forte pressão, a Associação Brasileira de Normas Técnicas (ABNT) criou a normativa NBR16787/2019 que trata sobre a segurança química em produtos têxteis (ABNT, 2019).

As estações de tratamento de efluentes demandam extensos processos energéticos para a remoção de corantes, o que pode prejudicar o seu desempenho econômico e ambiental (GANDIGLIO et al., 2017; MARAMI et al., 2022). O tratamento de efluentes é um processo de alto consumo de energia, e sua demanda energética está aumentando consideravelmente devido à introdução de padrões mais restritivos, que exigem tecnologias avançadas para remoção de poluentes (BAGHERZADEH et al., 2021; DI FRAIA; MASSAROTTI; VANOLI, 2018; MUNOZ-CUPA et al., 2021; SEAN et al., 2020; YANG; CHEN, 2021). Panepinto et al. (2016) afirmam que em uma estação convencional de tratamento de efluentes, cerca de 25 a 40% dos custos operacionais são devidos ao consumo de eletricidade. Este valor varia na faixa de aproximadamente 0,3 - 2,1 kWh m^{-3} de efluente tratado. O Relatório Especial do Panorama Energético Mundial da *International Energy Agency* (IEA, 2017) descreve que, nos próximos 25 anos, a quantidade de energia usada no setor de água mais que dobrará, em parte devido à crescente demanda por tratamento em níveis mais restritivos de lançamento. Entretanto, as fontes de energia não renováveis estão se esgotando e as fontes de energia renováveis não são utilizadas adequadamente. Por isso, há uma necessidade imediata na busca de rotas alternativas para geração de energia (CHATURVEDI; VERMA, 2016).

Ao mesmo tempo, a recuperação de energia do tratamento e seus subprodutos está sendo implementada a fim de reduzir os custos econômicos e o impacto ambiental dos processos (ANDREIDES; DOLEJŠ; BARTÁČEK, 2022; BEHERA et al., 2020; DI FRAIA; MASSAROTTI; VANOLI, 2018). Algumas tecnologias modernas têm sido aplicadas para a degradação de azo-corantes, como: métodos eletroquímicos, oxidação por ozônio, foto-Fenton, precipitação química, separação por membranas, adsorção e foto-catálise (CHANKHANITTHA et al., 2020; LIU et al., 2022; PUNZI et al., 2015; SUBRAMANIAM; PONNUSAMY, 2015). Esses métodos apresentam vários inconvenientes como: alto consumo energético; economicamente inviáveis; mineralização incompleta dos corantes e seus metabólitos; e aumento da geração de lodo, causando poluição secundária (MOHANTY; KUMAR, 2021; SARKAR et al., 2017; VIKRANT et al., 2018). Além disso, nem sempre são completamente eficazes, devido a fatores como pH, temperatura e concentração do contaminante serem parâmetros que afetam diretamente a eficiência do processo de tratamento (SELVARAJ et al., 2021). Consequentemente, a indústria têxtil necessita de uma tecnologia de tratamento que evite o lodo tóxico, exija menos energia e permaneça segura para o meio ambiente (RAMOS et al., 2021; SURESH et al., 2022; YADAV et al., 2022). Por este motivo, as estações de tratamento de efluentes industriais podem obter maiores benefícios com a aplicação do BEF, porque os fluxos de resíduos são altamente concentrados em demanda química de oxigênio (DQO), o que pode aumentar seu potencial de recuperação de energia (TABASSUM; ISLAM; AHMED, 2021).

2.2 CORANTES SINTÉTICOS

Os corantes são compostos orgânicos coloridos que se ligam quimicamente ao substrato aplicado. São classificados de acordo com sua aplicação e estrutura química, pois, possuem diferentes estruturas e pesos moleculares (KADHOM et al., 2020; POPLI; PATEL, 2015). A estrutura básica de um corante consiste em dois componentes-chave, sendo um cromóforo que absorve a luz na região do visível e é responsável pela cor específica do corante; e o segundo é um auxocromo, que aprofunda a cor exibida pelo cromóforo e ajuda na fixação do corante (SINGH; DAHIYA; MISHRA, 2021).

A estrutura básica dos corantes e compostos químicos relacionados compreende um grupo cromóforo representado pelo grupo azo (–N=N–), grupo etileno (>C=C<), grupo metinila (–CH=), grupo carbonila (>C=O), grupos imina (>C=NH; –CH=N–), grupos carbono-enxofre (>C=S; ≡C–S–S–C≡), nitro (–NO_2; –NO–OH), nitroso (–N=O; =N–OH) ou grupos quinoides. Os grupos auxocromos são grupos ionizáveis que conferem aos corantes a capacidade de ligação ao tecido ou qualquer material. Os grupos auxocromos usuais são: –NH_2 (amino), –COOH (carboxila), –SO_3H (sulfonato) e, –OH (hidroxila). Em geral, as principais classes de corantes incluem grupos azo ou antraquinona.

Os azo-corantes são um grupo de corantes bem conhecidos por sua variedade e seu uso extensivo na indústria têxtil (SELVARAJ et al., 2021). São considerados os mais importantes e a maior classe de corantes comerciais, representando entre 65% a 75% de todos os produtos de corantes têxteis (CASTRO et al., 2021; HASHEMI; KAYKHAII, 2022; RAFAQAT et al., 2022). Apresentam resistência à degradação química e biológica, pois são caracterizados por anéis aromáticos unidos por uma ou mais ligações duplas N=N (CHAUHAN; GAUTAM; KANWAR, 2022; ESKANDARI; SHAHNAVAZ; MASHREGHI, 2019).

Os corantes reativos são os mais usados dentre todos os demais tipos, respondendo por 30% do total de corantes usados na indústria têxtil (UJIIE, 2015).

Esse grupo de corantes possuem um grupo eletrofílico (reativo) capaz de fazer ligações covalentes com a hidroxila da fibra celulósica (IMMICH; ULSON DE SOUZA; ULSON DE SOUZA, 2009). Devido a essas características químicas, a popularidade dos corantes reativos em escala comercial deve-se principalmente ao seu preço aceitável, brilho da tonalidade, ampla gama de cores, e propriedades de firmeza de cor razoavelmente boas (MAULIK et al., 2022). São usados principalmente para tingir fibras de celulose, como algodão e viscose, mas também estão ganhando cada vez mais importância para lã e poliamida (CHAVAN, 2011; SILVA et al., 2022). Cerca de 95% dos corantes reativos são azo-corantes, cobrindo uma ampla gama de cores (PAL, 2017).

2.3 CÉLULA A COMBUSTÍVEL MICROBIANA (CCM)

A célula a combustível microbiana (CCM), também conhecida como sistema bioeletroquímico, foi descrita pela primeira vez há mais de 110 anos. Desde que Potter (1911), inspirado nas descobertas de outros biólogos no final do século XIX e início do século XX concebeu a primeira CCM, esse dispositivo passou por pesquisas e desenvolvimentos substanciais (ARENDS et al., 2012). A tecnologia CCM é uma alternativa promissora capaz de degradar poluentes orgânicos e inorgânicos, permitindo o tratamento de efluentes sincronizado com a produção de bioeletricidade (KHAJEH et al., 2020; KITAFA; AL-SANED, 2021; KUMAR et al., 2019a; MOYO; MAKHANYA; ZWANE, 2022).

A CCM é um biorreator no qual a energia química das ligações químicas de compostos orgânicos é convertida em eletricidade em condições anaeróbias, através de reações catalíticas de bactérias eletrogênicas (AIYER; VIJAYAKUMAR, 2021; BORJA-MALDONADO; ZAVALA, 2022; CETINKAYA et al., 2017; KITAFA; AL-SANED, 2021). Conforme a Figura 1, uma CCM típica consiste em duas câmaras denominadas de compartimento anódico e catódico, que são separadas por uma membrana trocadora de prótons (MTP). Os eletrodos alojados nas respectivas câmaras são conectados por meio de um circuito externo, através do qual a eletricidade gerada pode ser coletada (GANTA; BASHIR; DAS, 2022). No compartimento anódico, a matéria orgânica (ex. acetato) que atua como doadora de elétrons é oxidada em CO_2 e H_2O (WANG; YANG; LIN, 2020). Essa oxidação gera elétrons (e^-) e prótons (H^+). Os elétrons fluem para o compartimento catódico através do circuito elétrico externo. Já os íons H^+ produzidos pela semirreação de oxidação transpassam através da membrana para o compartimento catódico, onde reduzem o oxigênio a água (BANERJEE; CALAY; MUSTAFA, 2022; YULIASNI et al., 2021). Como resultado dessas duas semirreações, uma diferença de potencial se desenvolve entre o ânodo e o cátodo e a corrente flui pelo circuito elétrico externo (NARAYANASAMY; JAYAPRAKASH, 2018; PUTHILIBAI; JEYASHRI; SANGAVI, 2020). As semirreações do compartimento anódico e catódico e a reação global que usa acetato como substrato são mostradas na Tabela 1.

Figura 1 - Representação esquemática de uma CCM

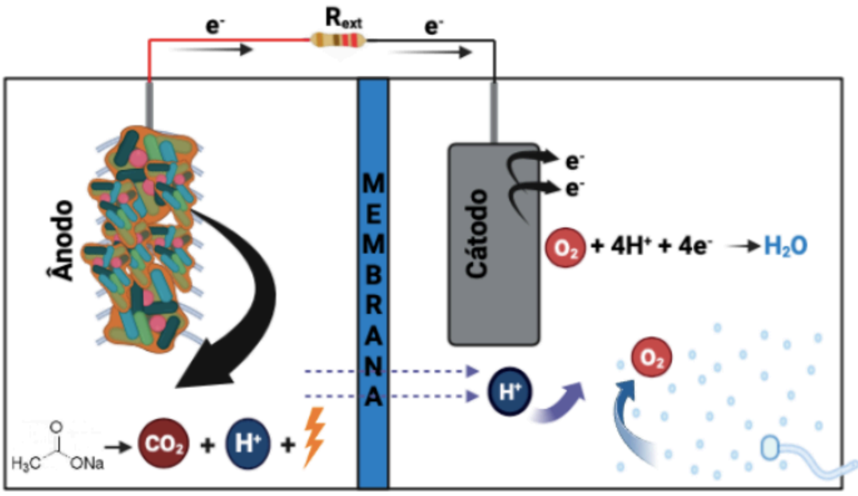

Fonte: Elaborado pelo autor (2023)

Tabela 1 - Reações na CCM usando acetato como substrato com sua tensão potencial

Reação	$E_{potencial}$ (V vs. NHE)
Ânodo: $CH_3COOH + 2H_2O \rightarrow 2CO_2 + 8H^+ + 8e^-$	- 0,300V
Cátodo: $4O_2 + 8H^+ + 8e^- \rightarrow 4H_2O$	+ 0,805 V

NHE: *Normal hydrogen electrode* (eletrodo de hidrogênio padrão)

Fonte: Obileke et al. (2021)

Neste sentido, o desempenho de uma CCM em termos de geração de energia e degradação da matéria orgânica, depende de uma comunidade versátil de bactérias eletroativas (LU et al., 2019; WANG et al., 2022a). O biofilme é uma massa agregada complexa de comunidades microbianas formadas por crescimento auto imobilizado em um substrato sólido pela excreção de adesivo e matriz protetora, também chamado de substâncias poliméricas extracelulares (SPE's). Por isso, as SPE's são importantes para o contato físico com a superfície do eletrodo e transferência de elétrons extracelulares (TEE) dentro do biofilme (GUO et al., 2021).

Em biofilmes, o contato célula a célula é possível se alta densidade celular puder ser criada, o que ajuda a estimular o mecanismo de transferência de elétrons (CHOUDHURY et al., 2017). A formação e a espessura do biofilme do ânodo são dois fatores importantes que contribuem para o maior desempenho bioelétrico. Biofilmes estáveis apresentam maior potencial de degradação dos corantes quando comparados aos consórcios bacterianos suspensos (SABA; KJELLERUP; CHRISTY, 2021). As bactérias eletrogênicas se adaptam à superfície do ânodo para criar um biofilme entre 30-50 μm de espessura (GAJDA; GREENMAN; IEROPOULOS, 2018). As bactérias eletrogênicas presentes no biofilme, em sua grande maioria, transferem elétrons diretamente por condutância através da membrana celular e atuam como aceptor final de elétrons no biofilme, o que ocorre devido ao envolvimento da cadeia respiratória dissimilatória dos microrganismos (AGRAWAL et al., 2019; NAWAZ et al., 2022). Os elétrons são produzidos no ânodo com um baixo potencial redox e a redução no aceptor de elétrons do cátodo cria um alto potencial redox. Essa diferença de potencial direciona os elétrons do ânodo para o cátodo para gerar eletricidade (DAS; MISHRA, 2019). Por isso, os biofilmes eletroativos são promissores na obtenção de tratamento eficiente de efluentes e conversão de energia em sistemas bioeletroquímicos (GUO et al., 2021).

Como a densidade de potência obtida na CCM é geralmente muito baixa, devido à perda de concentração, ativação, metabolismo bacteriano e altas perdas ôhmicas associadas à resistência ao fluxo de íons através da membrana de troca iônica, suas aplicações comerciais também têm sido limitadas (KHALID et al., 2018). Todavia, CCM's de câmara dupla com membrana provaram ser mais eficientes e com maior geração de energia. A membrana facilita a transição de H^+ do ânodo para o cátodo, bloqueando simultaneamente a difusão do oxigênio no ânodo (GURIKAR et al., 2021; QIU et al., 2022). Além disso, a CCM de câmara dupla é viável para a recuperação de nutrientes e/ou oxidação de compostos recalcitrantes em um sistema bioeletroquímico abrangente (YE et al., 2019). Por estes motivos, as CCM's podem apresentar potencial no tratamento de poluentes recalcitrantes, como corantes têxteis, além da geração simultânea de corrente elétrica (Tabela 2). A eletricidade é produzida durante a degradação de azo-corantes com outras fontes de carbono. As bactérias eletroquimicamente ativas na câmara anódica catalisam a oxidação de fontes de carbono em CO_2 através de várias reações metabólicas. Os elétrons das reações são conduzidos através de um circuito elétrico externo para o cátodo e reduzem O_2 a H_2O ou H_2O_2 ou podem ser usados para reduzir azo-corantes (CAO et al., 2010; LIU et al., 2009; SOLÍS et al., 2012).

Por outro lado, as diferentes condições operacionais levam ao estabelecimento de diferentes consórcios microbianos que podem influenciar na produção de energia e concomitantemente, na eficiência do tratamento via CCM. Apesar destas dificuldades, os indicadores mais comuns utilizados para avaliar a eficiência da CCM são, essencialmente: a taxa de remoção de DQO; densidade de potência (DP) ou densidade de potência volumétrica (DPV) para avaliar a produção de energia; e eficiência de Coulomb (EC). Esses indicadores fornecem informações gerais sobre a eficiência geral da CCM, tratamento de efluentes e geração de energia (BOAS et al., 2022; BORJA-MALDONADO; ZAVALA, 2022). A Tabela 2 apresenta uma análise resumida da aplicação da CCM na remoção de corantes têxteis em diferentes condições operacionais.

Tabela 2 - Aplicação da CCM na degradação de corantes têxteis com diferentes inóculos

Corante	Câmara CCM	Tipo de eletrodo		Inóculo	Densidade de potência ($mW\ m^{-2}$)	Remoção	Referência
		Ânodo	Cátodo				
Vermelho congo (300 ppm)	Única	Papel carbono	Papel carbono	Mistura de lodo aeróbio e anaeróbio	103,0	98% em 36h	Kumar et al. (2019b)
Vermelho congo (200 ppm)	Única	Escova de fibra de grafite	Fibra de grafite com platina	Lodo anaeróbio	23,5	≥ 88% em 24h	Dai et al. (2020a)
Diazo (100 $mg\ L^{-1}$)	Dupla	Feltro de grafite	Luva de grafite	Proteobacteria, Deltaproteobacteria e Desulfovibrio	258,0 ± 10	90% em 24h	Miran et al. (2018)
Vermelho congo	Dupla	Haste de grafite	Haste de grafite	Mistura de lodo anaeróbio	808,3	90% em 72h	Yuan et al. (2017)
Laranja ácido 7 (75 $mg\ L^{-1}$)	Única	Feltro de carbono	Feltro de carbono	Lodo de cultura mista anaeróbia	174,3 ± 5,8	90% em 2160h	Thung et al. (2015)
Efluente têxtil	Única	Fibra de carbono	Fibra de carbono	Algas	123,2 ± 27,5	42% em 720h	Logroño et al. (2017)
Laranja de metila (0,5 mM)	Dupla	Composto de grafite/poliéster	Composto de grafite/poliéster	*P. aeruginosa*	1575,0 ± 223,26	89,55% em 12h	Narayanasamy; Jayaprakash (2018)
Laranja reativo (10 $mg\ L^{-1}$)	Dupla	Luva de carbono	Luva de carbono	Cultura mista de lodo	84,0	98% em 24h	Shahi; Rai; Singh (2020)
Laranja de metila (0,92 mM)	Única	Grafite granulado	Grânulo de grafite	Lodo anaeróbio	-	91,74% em 0,48h	Li et al. (2016b)
Azul Victoria R (75-262 $mg\ L^{-1}$)	Dupla	Luva de carbono com platina	Luva de carbono com platina	*Shewanella putrefaciens* SW-5 e *Acinetobacter calcoaceticus* SW-12	> 194,8	98,7%	Wu et al. (2020a)
Vermelho Congo (190 ppm) com riboflavina (20 μM)	Dupla	Fibra de carbono	Fibra de carbono	*Shewanella oneidensis*-MR1	45,0	100% em 50h	Gomaa et al. (2017)
Vermelho scarlet e efluente têxtil (150 $mg\ L^{-1}$)	Única	Carbono-grafeno nano estruturado	Carbono-grafeno nano estruturado	Consórcio microbiano de efluente têxtil	76,9	89%	Deng; Zhao (2015)
Preto reativo 5 (200 $mg\ L^{-1}$)	Dupla	Placa de grafite	Feltro de grafite	Fluído ruminal	-	>90% em 225 min	Saba et al. (2018)
Azul reativo 4 (100 $mg\ L^{-1}$)	Dupla	Placa de grafite	Feltro de grafite	Fluído ruminal	-	90% em 300 min	Saba et al. (2018)

Vermelho brilhante X-3B (150 mg L^{-1})	Única	Carbono ativado granular (CAG)	Malha de aço inox dopado com CAG	Lodo anaeróbio	610,0	91,24%	Fang et al. (2013)
Laranja ácido 7 (100 mg L^{-1})	Dupla	Placa de grafite	Placa de grafite	Lodo ativado e anaeróbio	44,0	92,18% em 117h	Khajeh et al. (2020)
Laranja de metila (0,15 mM)	Dupla	Grafite granulado	Feltro de carbono	Lodo anaeróbio	-	94,9 %	Yang et al. (2016)

Fonte: Elaborado pelo autor (2023)

Recentemente, Reyes et al. (2021) empregaram um consórcio bacteriano para degradar quatro corantes de antraquinona, azul ácido 62, azul ácido 25, azul ácido 40 e azul reativo 19 a uma concentração inicial de corante de 50 mg L^{-1} usando uma CCM. O estudo mostrou que o consórcio foi capaz de degradar os corantes com eficiências de remoção de corantes de 48%, 17%, 9% e 5%, respectivamente. Os resultados mostraram uma diminuição na eficiência de remoção do corante à medida que a complexidade das estruturas do corante aumentava. O azul reativo 19 teve a menor eficiência de remoção de corante (5%) devido à presença do substituinte 2-[(3-aminofenil)sulfonil]etil sulfato de sódio, que criou uma transferência de elétrons mais eficiente em toda a estrutura química do corante, aumentando seu comprimento de conjugação e, consequentemente, sua estabilidade. Isso mostra que o azul reativo 19 foi o mais recalcitrante entre os corantes estudados e o consórcio bacteriano falhou em degradar efetivamente o corante. Da mesma forma, em outro estudo Saba et al. (2018) investigaram a descoloração de um azo-corante preto reativo 5 (PR5) e um corante antraquinona azul reativo 4 (AR4) em uma CCM de circuito aberto com um consórcio microbiano extraído do fluído ruminal bovino. Os resultados do estudo revelaram que o PR5 foi descolorido com eficiência superior a 90% em 120, 165 e 225 min nas concentrações de 50, 100 e 200 mg L^{-1}, respectivamente. O corante AR4 a 50 e 100 mg L^{-1} levou 225 e 300 min para descolorir, enquanto em 200 mg L^{-1} não foi descolorido. As diferenças na eficiência de descoloração dos corantes pelo consórcio bacteriano indicam que a degradação dos corantes foi mais rápida em PR5 do que em AR4. O AR4 contém o grupo diclorotriazina que, juntamente com o grupo cromóforo C=O, torna o corante mais estável, tornando-o difícil de degradar. No estudo de Oon et al. (2017) as taxas de descoloração dos monoazo-corantes foram aproximadamente 50% maiores do que os diazo-corantes. Os resultados revelaram que a estrutura do corante influenciou a descoloração e o desempenho de energia da CCM.

Apesar da excelente remoção de cor, a degradação incompleta e a baixa DP limitam a aplicação da CCM em escala real (SINGH; DAHIYA; MISHRA, 2021; SIVASANKAR et al., 2019). Além disso, a toxicidade de um corante pode fazer com que os microrganismos levem mais tempo para se adaptarem com a formação de biofilme nos eletrodos (SABA; KJELLERUP; CHRISTY, 2021; ZHONG et al., 2018).

Portanto, com base na discussão acima, uma única técnica de tratamento não é eficientemente capaz de remover azo-corantes.

2.3.1 Remoção de corantes têxteis

As técnicas de tratamento biológico receberam maior atenção em comparação com as tecnologias de tratamento físico-químico convencionais para efluentes têxteis, devido à diminuição da deposição de lodo, boa eficiência operacional e pela sua sustentabilidade (ROBLEDO-PADILLA et al., 2020; SHU et al., 2016). Os processos biológicos podem ser aplicados facilmente, pois, diferentes linhagens de microrganismos são capazes de absorver ou liberar enzimas que podem remover ou neutralizar poluentes nocivos de locais contaminados, transformando-os em composto menos tóxicos (AL-TOHAMY et al., 2022; SAHOO; DAHIYA; PATEL, 2022; VERMA et al., 2021a; VIKRANT et al., 2018).

Em uma CCM, a degradação de corante pode ser realizada tanto no ânodo quanto no cátodo. O passo inicial na degradação bacteriana de azo-corantes é a clivagem redutiva da ligação azoica (N=N) altamente eletrofílica sob condições estáticas, anóxicas ou anaeróbias, o que leva à formação de aminas aromáticas incolores (SINGH; SINGH; SINGH, 2017). A clivagem da N=N leva à quebra da estrutura do corante complexo ao aceitar elétrons liberados durante reações metabólicas intracelulares ou extracelulares por bactérias, por exemplo, *Bacteroides sp., Closteridium sp., Geobacter sp., Pseudomonoas sp.* (DEKA et al., 2022). Durante a redução intracelular, os azo-corantes são reduzidos dentro da célula bacteriana na presença da enzima azorredutase, enquanto, durante a redução extracelular que ocorre fora da célula bacteriana, os azo-corantes atuam como potenciais aceptores de elétrons (SINGH; DAHIYA; MISHRA, 2021). Após a biotransformação redutiva do azo-corante, as aminas aromáticas raramente são degradadas em compostos mais simples se o ambiente for mantido redutor. Portanto, as aminas aromáticas são consideradas compostos recalcitrantes em condições anaeróbias. Condições de baixa oxigenação fornecem condições ideais para a clivagem redutiva de azo-corantes, resultando em aminas aromáticas descoloridas (SELVARAJ et al., 2021; YADAV et al., 2022).

Acredita-se que a clivagem da ligação N=N possa ocorrer por mecanismos diretos, onde as enzimas azorredutase interagem fisicamente com as moléculas de corante têxtil transferindo os elétrons (IMRAN et al., 2015), ou por mecanismos indiretos, onde a cooperação de coenzimas é necessária, como dinucleótido de nicotinamida adenina (NAD^+), fosfato de dinucleótido de nicotinamida adenina ($NADP^+$) e dinucleótido de flavina e adenina (FAD) (SEN et al., 2016). As enzimas azorredutase transferem então os elétrons para estas coenzimas que por sua vez os transportam para as moléculas dos corantes têxteis promovendo a quebra das suas ligações azoicas. Portanto, as coenzimas não fazem parte da estrutura enzimática, mas são transportadores intermediários (VANMETER; HUBERT, 2021), ou mediadores redox (TELKE; KADAM; GOVINDWAR, 2015) que aceleram a taxa do processo de transferência de elétrons responsável pela clivagem redutiva (RATHER; AKHTER; HASSAN, 2018). Em suas formas oxidadas NAD^+, $NADP^+$ e FAD, as coenzimas recebem elétrons das enzimas azorredutase e são reduzidos a NADH, NADPH e FADH. Essas formas reduzidas são então oxidadas quando doam esses mesmos elétrons para as moléculas dos corantes e retornam às suas formas originais NAD^+, $NADP^+$ e FAD (Fig. 2).

Figura 2 - Mecanismo de degradação de azo-corante via azorredutase

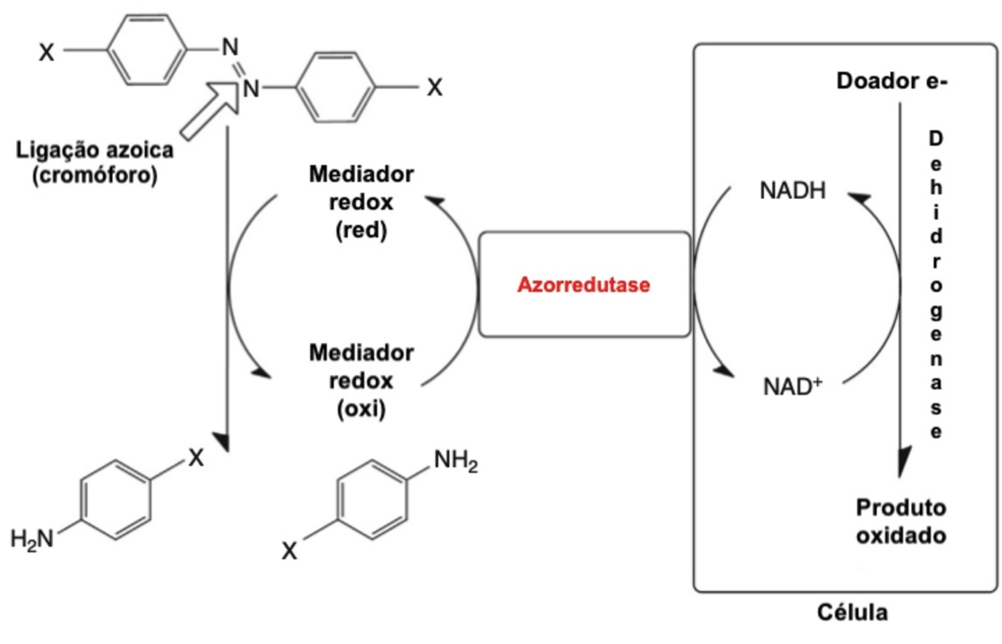

Fonte: Adaptado de Lellis et al. (2019); Khan et al. (2013)

A descoloração biológica anaeróbica de azo-corantes ocorre via enzimas redutoras extracelulares e é positivamente afetada por maior tempo de detenção hidráulica (TDH), maior concentração de biomassa e co-substrato primário simples (por exemplo, acetato e glicose); e negativamente afetado pela complexidade da estrutura do corante, presença de aceptor de elétrons alternativo e alta concentração inicial do corante (POPLI; PATEL, 2015). A persistência dos corantes têxteis depende principalmente do tipo de corante, pois a maioria dos corantes utilizados para coloração de tecidos diferem de acordo com sua estabilidade química e não pela sua biodegradabilidade (GADEKAR; AHAMMED, 2019).

Os consórcios aclimatados gradualmente maximizam o desempenho da descoloração e diminuem o efeito adverso da toxicidade para a população bacteriana (TACAS et al., 2021). Populações microbianas mistas/consórcio apresentam maior nível de biodegradação devido aos exercícios metabólicos sinérgicos do grupo microbiano e oferecem pontos de interesse significativos sobre a utilização de culturas puras na descoloração e degradação de azo-corantes (SINGH; SINGH; SINGH, 2017). A aclimatação e estabilização completa de uma CCM é muito importante para o melhor desempenho na descoloração de corantes. Assim, a CCM inoculada com lodo anaeróbio têxtil pode favorecer a redução intracelular e extracelular do corante no ânodo (ILAMATHI; JAYAPRIYA, 2018).

Na degradação de corantes no compartimento catódico, o pH elevado do católito afeta negativamente a concentração de prótons e inibe a reação de redução do azo-corante (LIU et al., 2009). Em alguns estudos, o $Fe(CN)_6$ (WANG et al., 2013b) e o MnO_4^- (LI et al., 2016b) são preferidos com base no alto potencial de redução para melhorar o desempenho da CCM. Azo-corante e oxigênio tem competição como aceptores de elétrons, o que reduz a EC para descoloração (LI et al., 2016b). Alguns azo-corantes são bons aceptores de elétrons e se forem adicionados para aceitar os elétrons, pode-se alcançar a biorremediação na reação eletroquímica do compartimento catódico (SABA; KJELLERUP; CHRISTY, 2021). Os azo-corantes foram testados como católitos em CCM com o duplo objetivo de fornecer um facilitador para o aceptor de elétrons e a possibilidade de descoloração. As reações de redução na câmara catódica são apresentadas por Goyal e Minocha (1985) e Menek e Karaman (2005), afirmando que a ligação –N=N– é reduzida a hidrazo (Eq. 1) ou amina (Eq. 2), consumindo dois ou quatro elétrons, respectivamente.

$$-N{=}N- + 2e^- + 2H^+ \rightarrow -NH{-}NH- \quad (1)$$

$$-N{=}N- + 4e^- + 4H^+ \rightarrow -NH_2 + H_2N- \quad (2)$$

A clivagem da ligação azoica causa a redução da estrutura complexa do corante de cadeia longa em compostos de menor peso molecular, como aminas aromáticas (SINGH; DAHIYA; MISHRA, 2021). Entretanto, a capacidade de descoloração de um azo-corante pode ser influenciada pelo número de ligações azoicas, grupo funcional e arranjo no composto (CHENGALROYEN; DABBS, 2013). Além disso, o peso molecular e a estrutura química do corante influenciam muito a taxa de descoloração (CHEN et al., 2010; REDDY; MOHAN, 2016). Por isso, monoazo-corantes podem ser mais favoráveis à descoloração do que os diazo-corantes, pois as moléculas de corante são mais prontamente reduzidas em ligações químicas menos complexas (OON et al., 2017).

Independentemente das vantagens fornecidas pelas CCM's, certas limitações como toxicidade para o biofilme, baixa potência, eficiência diminuída ao longo do tempo, instabilidade de eletrodos e degradação incompleta limitam o uso de CCM para degradação de corantes em aplicações em escala real. Para superar essas limitações, a integração das CCM's com outros sistemas de tratamento podem superar as limitações individuais com sinergismo (KABUTEY et al., 2019; ZHANG et al., 2019e).

2.4 SISTEMA HÍBRIDO DE TRATAMENTO

Nos últimos anos, o número de processos de tratamento de efluentes aumentou drasticamente com o desenvolvimento de tecnologias híbridas sinérgicas baseadas na combinação de vários POA's (DEWIL et al., 2017; WU et al., 2020b). A utilização da oxidação eletroquímica aliada ao tratamento biológico pode levar à remoção e degradação de azo-corantes, melhorando significativamente a eficiência do tratamento (ALMEIDA et al., 2019; SHOKRI; FARD, 2022; XU; XU; SHI, 2018). A reação de Fenton é um dos processos de oxidação mais eficazes e avançados, que tem sido amplamente utilizada no tratamento de vários contaminantes recalcitrantes (RAJARAMAN; GANDHI; PARIKH, 2021; SARAVANAN et al., 2022). No entanto, a principal desvantagem deste método é o custo relativamente alto devido ao consumo de energia e uma quantidade substancial de H_2O_2, quando é necessária uma degradação completa. Portanto, novos processos Fenton capazes de sintetizar H_2O_2 *in situ*, com baixo consumo de energia e de forma sustentável têm atraído muita atenção (MONTEIL et al., 2019; ZHAO; ZHANG, 2021).

As CCM's foram desenvolvidas com sucesso para o tratamento de águas residuais e podem recuperar energia diretamente das águas (ZHANG et al., 2019d). O desempenho de uma CCM integrada com POA pode ser muito superior ao de uma CCM autônoma em termos de tratamento e geração de energia (PATWARDHAN et al., 2021). Neste sentido, o sistema BEF difere favoravelmente de outros sistemas bioeletroquímicos pela sua alta taxa de remoção de vários poluentes com zero consumo de energia elétrica. Vários estudos comprovaram o conceito de que H_2O_2 catódico pode ser sintetizado nas superfícies de materiais de carbono e/ou grafite, através de elétrons biológicos gerados em sistema CCM sem a necessidade de alimentação externa (APOLLON et al., 2022; SOLTANI; NAVIDJOUY; RAHIMNEJAD, 2022). Sendo uma tecnologia inovadora, as vantagens duplas da geração de corrente elétrica e simultaneamente com a descoloração de corante também foram relatadas, conforme Tabela 3.

Tabela 3 - Vantagens e limitações direcionadas ao processo Fenton e seu efeito sinérgico com a CCM relatadas para tratamento de águas residuais de corante

Sistema	**Vantagens**	**Limitações**
Fenton	Formação de •OH, responsável por degradar poluentes recalcitrantes Geração de lodo	pH ácido Exigência externa de H_2O_2 Controle operacional exigente Alto custo dos eletrodos
CCM+EF/ BEF	Conversão do substrato orgânico em corrente elétrica Melhor custo-benefício Geração *in situ* de H_2O_2 Eficiência de tratamento aprimorada	Baixa corrente elétrica de saída Instabilidade a longo prazo dos eletrodos pH ácido

Fonte: Adaptado de Singh; Dahiya; Mishra (2021)

Ademais, estabelecer tecnologias econômicas é a necessidade do momento para a produção sustentável de eletricidade e, concomitantemente, do tratamento de efluentes. O desenvolvimento de novas tecnologias ou a integração de mais de uma tecnologia existente baseada em recuperação de subprodutos e resíduos como outras fontes de energia devem ser investigados. Com isso, pode-se minimizar a pegada de carbono que portanto, ajuda a reduzir a carga sobre o meio ambiente (PRIYANKA; SHEELA, 2021; SELVASEMBIAN et al., 2022). Como a energia renovável gerada a partir de uma única tecnologia é cara, combinar essas tecnologias comercialmente pode somar na produção total de energia renovável, tornando-a economicamente viável (NAWAZ et al., 2022). Contudo, em uma aplicação em larga escala, o conceito BEF é uma técnica promissora para o gerenciamento de diferentes fontes de matéria orgânica e pode ser usado simultaneamente para geração de eletricidade, a fim de minimizar a crise global de energia e reduzir a pressão sobre os recursos energéticos não renováveis (GURIKAR et al., 2021).

Com base no fato de que cada processo de remoção de corante tem suas próprias vantagens e desvantagens, a combinação de diferentes técnicas pode ser uma alternativa interessante para obter uma remoção de corante de maneira mais eficiente (BENKHAYA; RABET; EL HARFI, 2020; YASEEN; SCHOLZ, 2019). Assim, um processo combinado anaeróbio-oxidativo usando a CCM e POA pode ser uma opção viável para a degradação efetiva de substratos e corantes complexos, juntamente com a produção de bioeletricidade (KHAN et al., 2015; MURALI et al., 2013; ZHAO; ZHANG, 2021).

2.5 BIO-ELETRO-FENTON (BEF)

O processo eletro-Fenton (EF) é considerado como um dos POA’s que ocorrem a temperatura e pressão ambiente. A combinação de Fe^{2+} e H_2O_2 em condições ácidas resulta na formação de •OH (reação de Fenton) (MIKLOS et al., 2018). Os radicais •OH exibem elevada capacidade oxidativa (E = 2,8V), proporcionando uma eficaz remoção de poluentes orgânicos refratários presentes em águas coloridas (CASADO, 2019; SINGH; DAHIYA; MISHRA, 2021). Devido à alta atividade e não seletividade de •OH ($k = 109\ M^{-1}\ s^{-1}$), a reação Fenton ou reações do tipo Fenton podem oxidar numerosos contaminantes tóxicos e persistentes e, finalmente degradá-los em moléculas mais simples (CO_2 e H_2O) (SHAN et al., 2020; XU et al., 2020a).

No entanto, o processo tradicional de Fenton consome muita energia e requer reagentes instáveis adicionais (ZHANG; TAO, 2018). O bio-eletro-Fenton (BEF) é uma forma inovadora de tecnologia bioeletroquímica, que combina a biorremediação de resíduos e a remoção de poluentes simultaneamente nas câmaras anódica e catódica com a produção de bioeletricidade (HASSAN et al., 2019). No processo BEF, os métodos biológicos econômicos são acoplados ao processo EF (RAJARAMAN; GANDHI; PARIKH, 2021). Ou seja, o sistema resultante denominado como BEF, é capaz de degradar o contaminante na câmara catódica, enquanto coleta bioeletricidade e simultaneamente remove matéria orgânica oxidável do efluente na câmara anódica (SATHE et al., 2022a). Por isso, a energia elétrica necessária para o processo EF é fornecida pela oxidação da matéria orgânica no compartimento anódico, sem a entrada tradicional de eletricidade (ZOU et al., 2020). Portanto, a produção *in situ* de H_2O_2 é alcançada através de uma redução de dois elétrons do oxigênio no compartimento catódico (FERNANDO; KESHAVARZ; KYAZZE, 2012)

Um sistema BEF, representado na Figura 3, geralmente tem duas câmaras (anódica e catódica) separadas por uma membrana trocadora de prótons (MTP). Esse tipo de sistema híbrido combina reações de oxidação anódica e EF catódica em um único reator integrado. Os elétrons gerados pela oxidação da fonte de carbono na câmara do ânodo são doados ao ânodo e depois transportados para o cátodo através de um circuito elétrico externo. Os prótons migram da câmara do ânodo para a câmara do cátodo através da membrana. O H_2O_2 é produzido na superfície do cátodo através da redução de O_2 em uma via de dois elétrons. Os íons de Fe^{2+} adicionados na solução, reagem com H_2O_2 para gerar radicais •OH (ZHANG et al., 2019d).

Figura 3 - Representação esquemática do sistema BEF

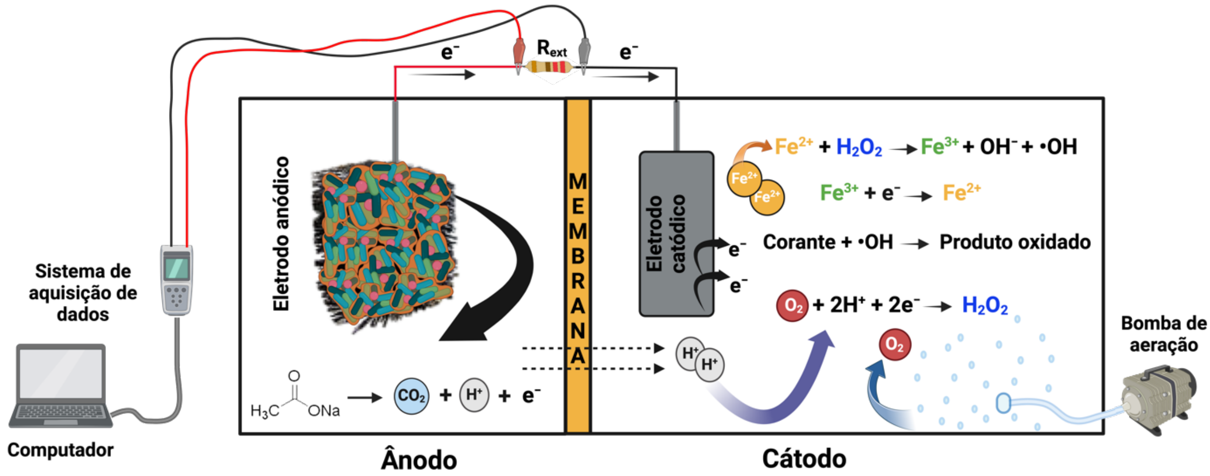

Fonte: Elaborado pelo autor (2023)

No ânodo do reator BEF (Figura 3), elétrons e prótons são produzidos primeiro devido à matéria orgânica (por exemplo, acetato) ser consumida pelas bactérias eletroativas (Eq. (3)) e, em seguida, são transferidos através do circuito externo e da MTP, respectivamente, para o cátodo. No cátodo do reator BEF, a geração *in situ* de H_2O_2 é alcançada seguindo a reação de redução de oxigênio de dois elétrons de acordo com a Eq. (4), que posteriormente reage com Fe^{2+} e gera •OH através das Eq. (5 - 7). Os radicais •OH atacam por via oxidativa as moléculas de corante, degradando-as em fragmentos menores (Eq. (8)) (HASSAN et al., 2019; ZOU et al., 2020).

Reações no ânodo:

$$CH_3COOH + H_2O \rightarrow 2CO_2 + 8H^+ + 8e^- \quad (3)$$

Reações no cátodo:

$$O_2 + 2H^+ + 2e^- \rightarrow H_2O_2 \quad (4)$$

$$Fe^{2+} + H_2O_2 \rightarrow Fe^{3+} + \bullet OH + OH^- \quad (5)$$

$$Fe^{3+} + H_2O_2 \rightarrow Fe^{2+} + HO_2\bullet + H^+ \quad (6)$$

$$Fe^{2+} + \bullet OH \rightarrow Fe^{3+} + OH^- \quad (7)$$

$$\text{Corante} + \bullet OH \rightarrow \text{Produto oxidado} \quad (8)$$

Por isso, a principal vantagem da configuração de câmara dupla da CCM em relação à câmara única é que o desempenho do cátodo pode ser controlado fornecendo oxigênio, adicionando mediadores na câmara catódica e oxigênio, melhorando assim o desempenho geral da reação do EF (FLIMBAN et al., 2018; NAWAZ et al., 2020). Ao utilizar os elétrons continuamente liberados das reações do ânodo, o H_2O_2 pode ser gerado continuamente na câmara do cátodo. Quando fornecidas fontes de ferro solúvel, são gerados radicais •OH, considerados como um poderoso oxidante para a degradação de poluentes orgânicos (XU et al., 2016). Os sistemas BEF's também podem liberar *in situ* íons ferrosos necessários na reação de Fenton que podem ser incluídos nos cátodos compostos (dopagem) (KAHOUSH et al., 2018; SINGH; DAHIYA; MISHRA, 2021).

Considerando o sucesso do processo baseado em Fenton no tratamento de corantes têxteis, o sistema acoplado BEF tem grande potencial de geração de energia durante a remoção corantes em efluentes têxteis com altos valores de DQO, DBO, sólidos em suspensão, cloretos, nitratos e metais (Fe, Cr, Pb, Cu, Mn, etc.) (WANG et al., 2023). Nos últimos anos, os pesquisadores se concentraram nos sistemas BEF para degradar poluentes coloridos e evitar seus efeitos negativos no meio ambiente. De acordo com a Tabela 4, a degradação de alguns corantes industriais, como Rodamina B, amaranto, laranja II, laranja de metila, laranja ácido etc. foram relatados aplicando o sistema BEF em diferentes condições operacionais.

Tabela 4 - Aplicação do processo BEF na remoção de corantes têxteis

Corante	Membrana	Tipo de eletrodo – Ânodo	Tipo de eletrodo – Cátodo	Condições operacionais	Potência	Remoção	Referência
Laranja ácido 7 (LA7)	MTP[(a)]	Papel carbono	Placa de ferro	1000 Ω; lodo anaeróbio; acetato de sódio; 200 mL os reatores; pH 7,0 PBS anódico; pH 3,0 catódico; anólito CCM: 0,1 a 2mM LA7, 0,16M NaCl; católito CCM: 0,16M NaCl	0,3 mW	85% em 30 min	Liu et al. (2012)
Vermelho Congo	MTP[(a)] (Nafion 117)	Haste com grânulos de grafite	Catalisador esférico à base de antraquinona e haste de grafite	1000 Ω; comunidade microbiana de CCM em operação; glicose; 100 mL cada reator; pH catódico 7,0, católito: (100μM corante e 0,1M PBS); fluxo de ar: 8,0 ±0,5 mg L^{-1}; 20˚C	808,3 mW m^{-3}	90% em 72 h	Yuan et al. (2017)
Azul de metileno	MTP[(a)] (Nafion 112)	Escova de fibra de carbono	Escova de fibra de carbono	1000 Ω; glicose; 550 e 360 mL ânodo e cátodo; pH catódico 3,0; católito: (30 mg L^{-1} AM; 0,1M Na_2SO_4; FC/Fe-Mn-Mg; 20 ˚C	1,99 W m^{-3}	93,5% em 5 h	Wang et al. (2022b)
Azo-corante (laranja II)	MTC[(b)]	PPy/AQDS feltro de carbono	PPy/AQDS feltro de carbono	1000 Ω; *Shewanella decolorationis* S12; lactato; 75 mL cada reator; pH catódico 7,0 católito: (0,2 mM laranja II, 0,1 M PBS e 1 g L^{-1} γ-FeOOH; fluxo ar: 100 mL min^{-1}; 30 ˚C	823 mW cm^{-2}	K=0,142-0,358 h^{-1} em 20 h	Feng et al. (2010a)
Rhodamina B	MTC[(b)]	Feltro de carbono ativado	$Fe@Fe_2O_3$/ feltro de carbono ativado	120 Ω; lodo anaeróbio; lactato; 200 mL cada reator; pH anódico 10 e catódico 3; anólito: efluente suíno; católito: (10 mg L^{-1} Rh B; 0,1M NaCl); fluxo de ar: 3 L min^{-1}; 25 ˚C	16,7 W m^{-3}	95,0 ±3,5 % em 24 h	Xu et al. (2020b)
Azul de metileno	Membrana bipolar	Escova fibra de carbono	Placa de grafite e papel carbono revestido com Pt	5 Ω; efluente doméstico; acetato; 250 mL cada reator; pH catódico 3,0; católito: (50 mg L^{-1} AM; 0,1 M Na_2SO_4 e 2 mM Fe; fluxo de ar: 10 mL min^{-1}; 25 ± 5˚C	50,1 mW m^{-2}	97% em 16 h	Zhang; Wang; Angelidaki (2015b)
Laranja de metila (LM)	MTC[(b)]	Escova fibra de grafite	Fe_2O_3/feltro de carbono ativado	100 Ω; lodo anaeróbio; 550 mL cada reator; pH catódico 3,0; católito: 5,0 mg L^{-1} LM e 0,05 M Na_2SO_4); fluxo de ar: 750 mL min^{-1}	268,1 mW m^{-3}	73,9-86,7% em 2 h	Ling et al. (2016)

Rhodamina B (Rh B)	GORE-TEX®	Feltro de carbono	$Fe@Fe_2O_3$/Feltro de carbono	1000 Ω; consórcio microbiano de CCM em operação; 75 mL cada reator; pH catódico 3,0 (HCl); católito: (efluente sintético têxtil com 15 mg L^{-1} Rh B); 30 ˚C	307 mW m^{-2}	95% em 12 h	Zhuang et al. (2010)
Laranja II	MTC[b]	Feltro de carbono	CNT/PTFE/ γ-FeOOH	1000 Ω; *Shewanella decolorationis* S12; lactate; 75,6 mL cada reator; pH catódico 7,0; católito: (0,1 mM laranja II, 100 mM PBS); fluxo ar: 100 mL min^{-1}; 30 ˚C	230 mW m^{-2}	100% em 14 h	Feng et al. (2010b)
Laranja ácido 7 (LA7)	MTP[a] (Nafion 212)	Luva de carbono	Feltro de carbono	1000 Ω; lodo anaeróbio; glicose; 100 mL cada reator; pH catódico 3,0; católito: (50 mg L^{-1} LA7; 20 g L^{-1} Na_2SO_4 e 1 g de $FeVO_4$)	15 mW m^{-3}	89% em 60 h	Luo et al. (2011)
Índigo carmim (IC)	Ponte salina	Folha de grafite	Folha de grafite	1000 Ω; lodo de esgoto; sedimento marinho com acetato; volume dos reatores: 150 mL; católito: (15 mg de corante, 0,01M Na_2SO_4 e 150 mg Fe L^{-1}); fluxo de ar: 1,0 L min^{-1}	1033-1046 mV	97,2%	Dios et al. (2014)

Obs: [a] MTP: membrana trocadora de prótons; [b] MTC: membrana trocadora de cátion   Fonte: Elaborado pelo autor (2023)

Nos primeiros estudos, Fu et al. (2010b) focaram na degradação do amaranto, que é um azo-corante estável e resistente à degradação por H_2O_2, no sistema BEF em pH 3,0. O BEF removeu 82,59% do amaranto em 1 h quando a concentração ótima de 1 mmol L^{-1} de ferro ferroso foi adicionada ao cátodo. Além disso, este corante foi degradado no sistema BEF com 0,5 mmol L^{-1} de íons férricos como catalisador de Fenton, com remoção de 76,4%. Além disso, a DP máxima foi de 28,3 W m^{-3}. A completa descoloração e mineralização do Orange II foi alcançada no estudo de Feng et al. (2010b) em pH 7,0 durante 14 e 43 h, respectivamente, via processo BEF, usando um eletrodo anódico de feltro de carbono (FC), um eletrodo catódico de γ-FeOOH e *Shewanella decolorationis* S12 como inóculo ativo no compartimento anódico. Quando a proporção de FC para γ-FeOOH foi de 1:1, o laranja II foi degradado rapidamente, e a maior quantidade de H_2O_2 foi produzida devido ao efeito da composição catódica do eletrodo no desempenho do sistema BEF. Além disso, a concentração de Fe^{2+} produzido *in situ* foi de 1,62 mg L^{-1} após 50 h de reação, a DP máxima de 230 mW m^{-2} também foi obtida simultaneamente. No estudo de Wang et al. (2022b), a bioeletricidade gerada a partir da degradação do lodo de esgoto foi utilizada pela CCM para gerar H_2O_2 *in situ* para estimular a degradação do azul de metileno (AM). Em pH 3,0 com 100 Ω R_{ext} e vazão de ar de 400 mL min^{-1}, EC, EF, produção de H_2O_2 e as taxas de remoção da DQO e AM foram 1,26 %, 74,25 %, 20,18 mg L^{-1}, 31,58% e 93,50%, respectivamente. A tensão de circuito aberto e a densidade de potência foram aprimoradas para 0,96 V e 1,99 W m^{-3}.

Li et al. (2010) afirmam que a ligação azoica foi clivada biologicamente na câmara anódica. Os intermediários tóxicos, aminas aromáticas, foram removidos por tratamento oxidativo. O sistema acoplado a CCM e reator sequencial ânodo-cátodo pode ser aplicado para obter a produção de eletricidade com degradação simultânea de azo-corante. Outro estudo semelhante relatou que o BEF é um sistema ecológico capaz de degradar azo-corantes de forma eficaz. Com base nesse ponto, Ling et al. (2016) conduziram uma pesquisa e chegaram à conclusão de que o LM foi efetivamente degradado durante oito operações em batelada no sistema BEF com haste de fibra de grafite e Fe_2O_3/FC como eletrodo anódico e catódico, respectivamente. A eficiência de degradação oxidativa do corante variou de 73,9% a 86,7% e a quantidade de geração de H_2O_2 atingiu 88,63 mmol L^{-1} nas condições ótimas de operação.

A degradação de poluentes orgânicos refratários nas câmaras anódica e catódica do BEF foi realizada simultaneamente com a produção de uma DPV máxima de 15,9 W m^{-3} em um estudo conduzido por Luo et al. (2011). A partir da reação de H_2O_2 e $FeVO_4$ obteve-se a remoção de 89% do laranja ácido 7 (LA7) e 81% de DQO na câmara catódica sob o pH 3,0 e 0,8 g de $FeVO_4$. Liu et al. (2012) desenvolveram um sistema inovador com o cátodo da CCM exposto ao ar-ambiente e geração *ex situ* de H_2O_2 para tratar poluentes orgânicos via Fenton. A taxa de degradação do LA7 em sistema integrado foi maior do que na reação de Fenton. Além disso, verificou-se que o aumento do oxigênio da solução catódica do sistema CCM, que levou a um aumento da densidade de potência, ocorreu junto com o aumento da taxa de degradação do LA7. Ou seja, cerca de 85% do LA7 foi degradado em pH 3,0 e com a adição de 2 mM H_2O_2 com uma potência de 0,3 mW.

Embora promissores, os sistemas BEF's ainda enfrentam vários desafios, como baixa DP, materiais catódicos caros, concentração de Fe^{2+} e pH (LI et al., 2020a). Para aplicação em larga escala, um grande obstáculo encontrado no BEF é sua menor taxa de sintetização de H_2O_2 do que a necessária (SINGH; DAHIYA; MISHRA, 2021). A seleção adequada de materiais anódicos e catódicos, pH, fonte de substrato, inóculo, fonte de catalisador de ferro, concentração de H_2O_2, modo de operação adequado interferem diretamente na eficiência operacional do processo (SOLTANI; NAVIDJOUY; RAHIMNEJAD, 2022). Nos tópicos a seguir, são apresentados alguns dos principais parâmetros operacionais que podem interferir na eficiência global do processo BEF, especificamente, quando se tem como objetivo a remoção e degradação de corantes têxteis.

2.5.1 Tipo de inóculo

A escolha do material de partida utilizado como inóculo para o processo BEF é importante, pois a comunidade microbiana presente no inóculo influencia o desempenho na degradação do corante (SABA et al., 2018). A maioria das bactérias tem capacidade de transferir elétrons liberados da oxidação da matéria orgânica para o eletrodo (AIYER; VIJAYAKUMAR, 2021; NGUYEN; BABEL, 2022). As bactérias que podem transferir elétrons extracelularmente de orgânicos para o eletrodo anódico são chamadas de bactérias exoletrogênicas (SUN et al., 2016). Entretanto, o mecanismo de descoloração e degradação do corante depende da capacidade das bactérias de produzir enzimas como as azorredutases que podem quebrar a ligação azoica (N=N) (KHAN; BHAWANA; FULEKAR, 2013; QI; SCHLÖMANN; TISCHLER, 2016; SARATALE et al., 2011). Além disso, a capacidade das bactérias de reduzir ou decompor aminas aromáticas, seja aeróbia ou anaerobiamente, permite que elas tenham mais versatilidade em comparação com outros organismos (MISHRA et al., 2020; NGO; TISCHLER, 2022).

Recentemente, CCM inoculada por comunidades microbianas mistas tem atraído muita atenção devido à sua estabilidade, robustez devido à adaptabilidade de nutrientes, resistência ao estresse e tendência geral de produzir densidades de corrente mais altas do que aquelas obtidas usando culturas puras (HALFELD et al., 2022; KHAN; PATEL; KHAN, 2020; LOGAN et al., 2006; MANCÍLIO et al., 2020). Além disso, culturas mistas não necessariamente requerem manutenção de condições estéreis e são mais adequadas para o uso de substratos complexos (PRATHIBA; KUMAR; VO, 2022; VERMA et al., 2021a). O uso de cepas específicas na descoloração não é prático para o tratamento de efluentes têxteis. Tem sido reportado que os sistemas de tratamento com populações microbianas mistas são mais efetivos na descoloração de diferentes tipos de corantes do que cepas específicas (CUI et al., 2016).

Tkach et al. (2017) alcançaram uma DP máxima de 465,3 ± 5,8 mW m^{-2} para a cultura mista a 10°C, enquanto apenas 68,7 ± 3,7 mW m^{-2} para cultura pura. Foi demonstrado que o biofilme anódico de cultura mista tinha um sobrepotencial e resistência menor do que o biofilme de cultura pura. Nos sistemas de cultivo misto proposto por Ren et al. (2021), o biofilme composto por *Saccharomyces cerevisiae* e *Bacillus subtilis* teve um aumento significativo na capacidade de geração de energia (554 mV) devido ao efeito de sinergia. O compartimento anódico inoculado pela co-cultura de *Klebsiella pneumonia* e *Lipomyces starkeyi* produziu uma DP de pico de 12,87 W m^{-3} (ISLAM et al., 2018). Jadhav & Ghangrekar (2020) inocularam CCM's com diferentes proporções de *Shewanella putrefaciens* e lodo anaeróbico misto. O desempenho de potência aumentou de 2,21 para 2,56 W m^{-3} com aumento da fração de *Shewanella* de 10 para 30% no inóculo e a DP aumentou ainda mais para 3,1 W m^{-3} quando inoculada com fração igual de *Shewanella* e lodo misto. Aiyer (2021) inoculou o BEF com uma co-cultura, que atingiu 190,44 mW m^{-2}, enquanto *E. coli* e *P.*

aeruginosa como culturas puras geraram apenas 139,24 e 158,76 mW m^{-2}, respectivamente. Para Albarracin-Arias et al. (2021), o inóculo enriquecido com uma comunidade mista de bactérias atingiu uma densidade de corrente de 247 mA m^{-2} e 2,36 W m^{-3}. Por outro lado, a inoculação com *Shewanella* sp. levou a um processo de diversificação, resultando em uma menor geração de corrente de 52 mA m^{-2}.

Consórcios de bactérias são comprovadamente mais eficientes na transferência de elétrons do que culturas puras, pois há uma maior diversidade de bactérias que podem gerar mediadores para uma transferência de elétrons mais bem-sucedida (FADZLI; BHAWANI; MOHAMMAD, 2021). Entretanto, uma das principais limitações associadas à cultura mista é o desenvolvimento de microrganismos não-eletrogênicos durante a aclimatação (PANDEY et al., 2016). Enquanto numerosas bactérias são conhecidas por serem eletroquimicamente ativas na natureza, certos biofilmes desenvolvem mecanismos distintos de transferência de elétrons para estabelecer comunicação elétrica com as superfícies dos eletrodos (CHEN et al., 2020; LUO et al., 2023). Essas bactérias são geralmente avaliadas com base em sua estrutura de superfície e propriedades bioquímicas, que podem ser confirmadas por um experimento de sequenciamento metagenômico 16S rRNA (IDRIS et al., 2022).

No BEF, análises de sequenciamento de genes 16S rRNA são geralmente empregadas para identificar microrganismos dominantes e fornecem uma visão geral da diversidade filogenética presente no biofilme anódico (CHIRANJEEVI; PATIL, 2020; SARATALE et al., 2017). Na aplicação da técnica de sequenciamento as moléculas de rRNA são funcionalmente conservadas com alto número de cópias e desempenham um papel crucial em toda a atividade funcional celular. A análise da sequência do gene 16S rRNA pode ser ainda implementada para a avaliação da riqueza da comunidade microbiana e da diversidade de espécies (WATANABE; KODAMA; HARAYAMA, 2001).

2.5.2 Substrato

A degradação do azo-corante pode ser melhorada pela adição de diferentes fontes de carbono, nitrogênio e mediadores redox (NGO; TISCHLER, 2022). O substrato afeta o desempenho de bactérias eletroativas na superfície de um ânodo (DWIVEDI et al., 2022). Em um processo de degradação microbiana de corantes, o substrato primário ajuda de duas maneiras: (1) como fonte de energia e carbono para o crescimento e sobrevivência de microrganismos; e (2) como doador de elétrons, por exemplo, para clivagem de ligações azoicas de corantes têxteis (POPLI; PATEL, 2015). Os elétrons obtidos na oxidação do substrato primário são transferidos para poluentes que aceitam elétrons, como azo-corantes, direta ou indiretamente por meio de mediadores redox, resultando em descoloração (PANDEY; SINGH; IYENGAR, 2007; SARATALE et al., 2011).

No compartimento anódico, o corante e os substratos de carbono são co-metabólitos. A alimentação apenas com corante não é capaz de fornecer energia suficiente para as bactérias do biofilme liberarem elétrons (SABA et al., 2018). As bactérias degradadoras de corantes extraem energia suplementar de fontes de carbono, como extrato de levedura, glicose, acetato, triptona, etc. (MISHRA et al., 2020). Por isso, o substrato afeta o desempenho de bactérias eletroativas na superfície de um ânodo. Fornecem elétrons, nutrientes, como minerais, aminoácidos, sais e recursos energéticos para sua sobrevivência (DWIVEDI et al., 2022; YAQOOB et al., 2020).

Alguns dos substratos amplamente empregados em BEF's incluem acetato de sódio, glicose, biomassa lignocelulósica, águas residuais de síntese, águas residuais de processamento de amido, lixiviados de aterros sanitários, efluentes têxteis, bem como substratos inorgânicos. No entanto, estudos recentes mostraram que o acetato e a glicose são os substratos mais usados (OBILEKE et al., 2021). O acetato tem sido o tipo de substrato amplamente utilizado para geração de eletricidade. É uma fonte rica em carbono e tende a promover microrganismos eletroativos. Os íons acetato contidos no ácido acético são também o produto final de várias vias metabólicas para fontes de carbono de ordem superior (BIFFINGER et al., 2008). De acordo com a literatura, o acetato como substrato geralmente resulta em maior EC em comparação com outros compostos orgânicos (PANT et al., 2010). O acetato, sendo um composto simples, é mais fácil de degradar, o que tende a melhorar a potência em relação ao substrato complexo favorecido por diversas comunidades de bactérias eletrogênicas (PANT et al., 2010). No estudo de Malyan; Mongia; Kumar (2022) foi alcançada uma EC de 25,29% para a amostra com acetato, enquanto, sem acetato, foi calculada como 9,71%. Além disso, foi observada uma DP máxima de águas residuais de 0,017 mW m^{-2}. No entanto, para águas residuais com acetato, a DP aumentou consideravelmente para 0,546 mW m^{-2} em 1000 Ω R_{ext}. Da mesma forma, o desempenho de quatro substratos diferentes foi investigado em termos de sua EC e potência de saída. Foi revelado que o reator alimentado com acetato apresentou maior EC de 72,3%, seguido por butirato (43,0%), propionato (36,0%) e glicose (15,0%) (CHAE et al., 2009).

Normalmente, quando os sistemas são alimentados com glicose apresentam baixa EC devido à perda de elétrons por bactérias concorrentes. No entanto, a estrutura bacteriana relativamente diversa permite uma utilização de substrato muito mais ampla e maior DP. Outra razão para a baixa EC associada com alimentação via glicose, é a presença da propriedade fermentável do substrato, que consome diversos metabolismos concorrentes, como fermentação e metanogênese, que não podem produzir eletricidade (CHAE et al., 2009; FADZLI; BHAWANI; MOHAMMAD, 2021). Entretanto, como o objetivo principal do BEF é a produção de H_2O_2, no estudo de Wang et al. (2017) uma maior densidade de corrente foi alcançada quando o compartimento anódico foi alimentado com glicose. Consequentemente, a concentração máxima de H_2O_2 foi de 0,36 mg L^{-1} usando haste de grafite como eletrodo. Em contraste, a concentração correspondente de H_2O_2 quando alimentada com acetato foi de 0,08 mg L^{-1}. Isso pode ser atribuído à maior diversidade da comunidade microbiana quando alimentada com glicose (CHAE et al., 2009; LOGAN, 2004). No estudo de Sim et al. (2015), devido as diferentes densidades de corrente, a taxa máxima de produção de H_2O_2 foi de 141 mg L^{-1} h^{-1} quando alimentado com glicose, mas tornou-se baixa em 6 mg H_2O_2 L^{-1} h^{-1} quando alimentado com água residuária. A presença de consórcios mistos mais complexos ou bactérias sintróficas devido à produção de diversos subprodutos da fermentação da glicose, como acetato e butirato, resultam na geração rápida de corrente elétrica (MUNOZ-CUPA et al., 2021; OBILEKE et al., 2021).

A geração de energia pode aumentar com o incremento das taxas de carga de substrato. As razões subjacentes a esta crescente geração de energia são relatadas como (i) aumento na atividade biológica microbiana (ii) geração e disponibilidade de força iônica adequada que está envolvida na diminuição da resistividade interna (NAWAZ et al., 2020). Quando o BEF foi alimentado com 5 g L^{-1} de glicose, Jafary; Ghoreyshi; Najafpour (2010) obtiveram resultados de tensão, DP e corrente elétrica de 905 mV, 39,3 mW m^{-2} e 85,1 mA m^{-2}, respectivamente. Soltani et al. (2021) obtiveram o melhor desempenho do sistema BEF na concentração de substrato de 2 g L^{-1}, resultado devido à decomposição da concentração adequada de H_2O_2 na presença de íons ferrosos para geração de •OH. Por outro lado, houve diminuição da eficiência de degradação quando o aumento da concentração de substrato passou de 2 para 10 g L^{-1}. Além disso, no estudo de Rahmani et al. (2022) o pH diminuiu severamente na câmara do ânodo ao usar alta concentração de substrato. Os resultados de Wen et al. (2010) mostraram que o aumento da concentração de substrato de 614 a 2062 mg L^{-1} DQO teve um efeito positivo no desempenho eletroquímico com densidades de corrente mais altas. Eles também relataram que a maior concentração de substrato, em termos de DQO, criou condições adequadas para o crescimento do biofilme no ânodo além de um aumento considerável na DPV, alcançando até 42,6 W m^{-3}. Em outro estudo semelhante, González del Campo et al. (2013) relataram que o aumento do substrato (em termos de DQO do efluente de 0,1 para 3,0 g L^{-1}) melhorou a atividade dos microrganismos e, como resultado, a corrente elétrica gerada no sistema aumentou gradativamente. Portanto, a capacidade de geração de energia sem o uso de fonte externa de energia é a vantagem mais positiva e significativa do processo BEF.

Além disso, a DP do BEF pode ser incrementada com um valor ideal de DQO. Entretanto, quando a concentração de substrato é alta pode causar incrustação do eletrodo, levando à restrição e acúmulo de sais e precipitados (MAQSOOD et al., 2022). Em termos de DQO, os resultados de Rahmani et al. (2022) mostraram que a eficiência de remoção de DQO aumentou em altas concentrações de matéria orgânica. De modo que na concentração de DQO de 2,0 g L^{-1} obteve-se a maior eficiência de remoção de DQO (84%), mas com o aumento da concentração inicial de substrato para 10,0 g L^{-1} a eficiência diminuiu para 79%. O estudo de Ye et al. (2019) teve como objetivo avaliar os impactos da taxa de carga orgânica (taxa de DQO de 435–870 mg O_2 L^{-1} d^{-1}) na degradação de matéria orgânica. A DP máxima alcançada no ânodo foi de 253,84 mW m^{-2} para uma taxa de DQO de 435 mg O_2 L^{-1} d^{-1}. O mesmo padrão foi observado para a EC, onde seu maior valor foi de 25% para uma taxa de DQO de 435 mg O_2 L^{-1} d^{-1}. Portanto, a alimentação com um substrato pode afetar a produção de energia, mas apenas aumentar a concentração do substrato não aumentará a produção de energia se o desempenho for limitado pela solução tampão (ROSSI et al., 2021).

Sun et al. (2009) investigaram o efeito do co-substrato na descoloração de ABRX3 e geração de eletricidade usando concentração idêntica de glicose, sacarose e acetato em compartimentos anódicos de câmara única de cátodo exposto ao ar. Seus resultados mostraram que a taxa máxima de descoloração de ABRX3 foi obtida com glicose, seguida de sacarose. O acetato foi considerado um co-substrato pobre com uma taxa mínima de descoloração. Isso pode ser atribuído ao fato de que o acetato e outros ácidos graxos voláteis são normalmente pobres doadores de elétrons, enquanto a glicose é um doador de elétrons mais eficaz para a redução de azo-corante (SANTOS et al., 2005). Tan et al. (2022) chegaram à conclusão de que o incremento na concentração do verde reativo 19 também aumentou o desempenho geral do processo. No entanto, a DP diminuiu com a adição na concentração de corante. O aumento adicional da carga de substrato em 3 vezes (2,43 g L^{-1}) melhorou a eficiência de descoloração em aproximadamente 7%, mas deteriorou a DP em 42%, para 63,40 ± 0,07 mW m^{-2}. No estudo de Ravinuthala et al. (2022) a presença de glicose produziu a maior tensão e corrente (0,123 V; 0,012A) em comparação com os valores obtidos sem qualquer co-substrato (0,077 V; 0,001A) em uma concentração de corante vermelho Congo (50 mg L^{-1}). Cao et al. (2010) também estudaram o efeito da DP para diferentes CCM's alimentadas com co-substratos durante a descoloração do vermelho do Congo. A DP foi maior para glicose>acetato>etanol, respectivamente, 103, 85,9 e 63,2 mW m^{-2}. Uma taxa média de carga de 1 g L^{-1} d^{-1} de glicose em reator de câmara dupla, resultou em 4,31 W m^{-2} e correspondeu a 81% da EC (RABAEY et al., 2004). Em uma pilha de CCM's (composta por quatro unidades e operada em modo contínuo), 30 g L^{-1} de glicose pura, 200 µmol L^{-1} de corante vermelho natural e *Saccharomyces cerevisiae* como biocatalisador ativo no ânodo, resultou em 6,447 A m^{-2} e 2,0 W m^{-2} (RAHIMNEJAD et al., 2012).

2.5.3 Síntese de H_2O_2

O H_2O_2 é um agente oxidante muito utilizado em POA's. A concentração inicial de H_2O_2 desempenha um papel importante no processo EF (FANG; ZHOU; DIONYSIOU, 2013). Ele fornece o meio para a formação do radical •OH, enquanto os outros processos de oxidação fornecem a energia para facilitar a formação do agente oxidante (M'ARIMI et al., 2020).

Por isso, vários parâmetros operacionais podem influenciar a produção de H_2O_2 no sistema BEF. Em questão, a R_{ext} pode interferir diretamente na produção *in situ* de H_2O_2 (APOLLON et al., 2022; DWIVEDI et al., 2022). Especificamente, foi demonstrado que a concentração de H_2O_2 aumenta em consonância com a diminuição da R_{ext} (WANG et al., 2017). A razão para o aumento na concentração de H_2O_2 é dado pelo aumento no fluxo de corrente do ânodo para o cátodo. Além disso, o efeito de uma R_{ext} aplicada ao BEF recentemente recebeu atenção, pois o crescimento de bactérias eletroativas pode ser controlado alterando a R_{ext} (DO et al., 2020). Ao variar a R_{ext} a corrente produzida pelo reator muda e, portanto, densidades de corrente mais altas podem ser obtidas em R_{ext} mais baixas. Espera-se que, com a diminuição da R_{ext}, mais elétrons passem pelo circuito, resultando em um aumento na taxa cinética da reação de eletro-oxidação do corante, e consequentemente, uma maior remoção de cor (SUN et al., 2009).

No estudo de Rossi; Logan (2020) a redução de R_{ext} durante a aclimatação do BEF diminuiu a transferência de carga e de difusão. Com R_{ext} de 20 Ω as resistências de transferência de carga e difusão foram menores em relação àquelas obtidas com 50 Ω. Zhang et al. (2017) descobriram que as R_{ext} tiveram um efeito significativo na etapa de aclimatação do biofilme. Para isso, quatro reatores de câmara dupla com campos de fluxo serpentino no ânodo e no cátodo foram conduzidos no experimento com 10, 50, 250 e 1000 Ω. Os autores indicaram que os reatores com maior R_{ext} teriam um processo de inicialização mais rápido. Com o aumento de 10 para 1000 Ω, o período de latência diminuiu de aproximadamente 3 para 0,6 dias. A CCM-1000 Ω atingiu um pico de tensão de 0,74 V no 2,5 dia. O pico de tensão para CCM-250Ω, CCM-50Ω e CCM-10Ω foi observado nos dias 3,2, 4 e 5, respectivamente. Portanto, é possível inicializar a CCM com uma R_{ext} mais alta e, em seguida, alternar gradualmente para uma R_{ext} mais baixa para obter uma corrente alta. No estudo de Mu et al. (2009), quando a R_{ext} foi aumentada de 3,2 para 100 Ω, a eficiência de descoloração do corante diminuiu de 83,1 ± 0,5% para 34,5 ± 0,8%. Fu et al. (2010b) também observaram uma taxa de degradação ligeiramente maior para resistências menores. Em uma CCM de câmara única com cátodo de ar, Sun et al. (2009) obtiveram uma curva de DP variando a R_{ext}. Uma taxa de descoloração mais rápida foi alcançada com uma R_{ext} mais baixa em comparação com uma resistência mais alta. Com 50 Ω, mais de 90% da cor foi removida em 24 h, enquanto o mesmo processo levou 36 h a 500 Ω. Com 5.000 Ω, 85% de descoloração foi observada em 48 h.

Quando se aumenta a DP e o tempo de operação, pode-se favorecer a remoção de cor. Keyikoglu; Can (2021) obtiveram uma taxa de remoção de cor de até 98,8% quando a densidade de corrente foi mais alta em um tempo de 20 min. No estudo de Tao et al. (2015) as tensões máximas, EC's e DP's da CCM de câmara única e dupla foram 443 e 524 mV, 35% e 51% e 560 e 528 mW m^{-2}, respectivamente. Ou seja, a DP foi ligeiramente menor em reator de câmara dupla. Isso pode afetar a geração *in situ* de H_2O_2 no compartimento catódico. Zou et al. (2021) alcançaram uma taxa máxima de produção de H_2O_2 de 10,82 mg L^{-1} h^{-1} e a concentração cumulativa de H_2O_2 de 454,44 mg L^{-1} em 42 h foram obtidas com uma tensão de entrada de 0,6 V, velocidade de aeração catódica de 0,045 mL min^{-1}, Na_2SO_4 50 mM e pH inicial de 3,0.

O material do cátodo também tem um impacto significativo no BEF, pois a reação de redução terminal combina elétrons, prótons e oxigênio para produzir H_2O_2 no compartimento catódico (MAQSOOD et al., 2022; YADAV et al., 2022). Por isso, o grafite é considerado um material catódico promissor por causa de sua boa condutividade elétrica, baixo custo e alta biocompatibilidade (CHEN; PATIL; SCHRÖDER, 2018; QIU et al., 2021). Chen et al. (2014) investigaram o desempenho de três eletrodos catódicos de carbono ativado, inclusive, eletrodos de partículas de grafite. Entre os três tipos diferentes de eletrodos, suas descobertas indicaram que o eletrodo de partícula de grafite favoreceu reações de dois elétrons para redução de oxigênio em comparação com os demais. Assim, o grafite foi relatado como um eletrodo ótimo para a síntese de H_2O_2. Wang et al. (2022b) utilizaram escova de fibra de grafite como eletrodo catódico e obtiveram tensão de 0,96 V e densidade de potência 1,99 W m^{-3}. Por consequência, a concentração de H_2O_2 alcançou 20,18 mg L^{-1} com degradação do AM na ordem de 93,5%. Ademais, o impacto da adição de grânulos de grafite nas câmaras catódicas foi explorado por Wang et al. (2017). Seu estudo relatou que a adição de grânulos de grafite aumentou a densidade de corrente, alcançando um aumento na geração de H_2O_2. Em outro estudo, Li et al. (2018a) realizaram o pré-tratamento ácido em cátodos de grafite tridimensionais para aumentar ainda mais a geração de H_2O_2. Com isso, a taxa de H_2O_2 aumentou em 46,9% após o pré-tratamento com ácido. A alta área de superfície de microporos do cátodo de grafite pré-tratado com ácido aumentou as reações de oxirredução no eletrodo. Wang et al. (2013a) usaram feltros de grafite dopados com Fe^{2+} como cátodo no BEF. O sistema alcançou uma DP máxima 3 vezes maior do que de um eletrodo não modificado (925 vs. 288 mW m^{-3}). As diferentes formações de Fe, como Fe_2O_3, FeOOH e óxidos de Fe^{3+} foram confirmadas como sendo responsáveis pela redução da resistência interna e melhoria da atividade eletroquímica do feltro de grafite.

Uma abordagem eficaz para aumentar a produção de H_2O_2 no sistema BEF é o controle do pH. Na câmara catódica, o pH alto reduz a geração de corrente. Já o pH baixo permite a redução do oxigênio, bem como alcança maior corrente elétrica (KUMAR; SINGH; ZULARISAM, 2016; NIESSEN; SCHRODER; SCHOLZ, 2004; PHUNG et al., 2004). Ou seja, um pH ácido pode favorecer a produção de H_2O_2, enquanto o consumo contínuo de prótons pode incrementar o valor do pH (CHUNG et al., 2020; MARTÍNEZ-HUITLE; PANIZZA, 2018). Como um fator indispensável para o acúmulo de H_2O_2, o pH controlado entre 1 e 3 pode promover a evolução do íon H^+. Entretanto, um pH alto causa a decomposição do H_2O_2 em H_2O (NIDHEESH; GANDHIMATHI, 2012). Zhang et al. (2015a) provaram que o pH ácido do católito pode levar a um aumento nas concentrações residuais de H_2O_2 (até ~ 150 mg H_2O_2 L^{-1} em pH 1,5) durante a descoloração catódica e a degradação de corantes têxteis. No estudo de Wang et al. (2017) após 6 h, a concentração média de H_2O_2 estava acima de 1,5 mg L^{-1}. O valor máximo atingiu 2,75 mg L^{-1} quando teve o controle do pH. Isso indica que o pH é um parâmetro crítico para a geração de H_2O_2.

A temperatura também tem uma influência significativa em quase todos os processos químicos, físicos e biológicos. Estudos relataram um desempenho eficiente do BEF em termos de DP e remoção da DQO em uma temperatura mais alta. Ou seja, para aumentar a potência de saída do BEF a temperatura deve ser aumentada, o que resultará no aumento das atividades bacterianas (JAFARY; GHOREYSHI; NAJAFPOUR, 2010; OBILEKE et al., 2021). Yong et al. (2013) revelaram que temperaturas ≥ 30˚C tendem a serem mais benéficas para a operação do compartimento anódico. Isso se deve ao biofilme de bactérias que apresentam atividade catalítica máxima entre temperaturas mais altas. No compartimento catódico, a alta temperatura promove a geração eficiente de H_2O_2 na faixa de 20-33 °C. No entanto, devido à natureza instável do H_2O_2, temperaturas mais altas (> 33°C) levam à sua decomposição (LING et al., 2016).

Apenas a redução de dois elétrons do oxigênio pode gerar H_2O_2 (Eq. 9), em tanto que a redução de quatro elétrons do oxigênio favorece à geração de H_2O (Eq. 10).

$$O_2 + 2H^+ + 2e^- \rightarrow H_2O_2 \quad (9)$$

$$O_2 + 4H^+ + 4e^- \rightarrow 2H_2O \quad (10)$$

Assim, o suprimento de ar adequado pode promover a produção de H_2O_2 por meio da redução de dois elétrons do oxigênio. No estudo de Zhao; Zhang (2021) a concentração de H_2O_2 aumentou com o aumento da intensidade de aeração na faixa de 50-200 mL min^{-1} e começou a diminuir quando a intensidade da aeração tornou-se superior a ~ 200 mL min^{-1}. Isso demonstrou que o suprimento de ar excessivo ou inadequado interromperia o equilíbrio estequiométrico desse processo. Sim et al. (2015) investigaram como diferentes métodos de aeração influenciam a síntese de H_2O_2 em uma célula eletroquímica convencional. Em seu estudo, uma CCM com um cátodo de eletrodo de difusão de gás (EDG) foi montada para determinar a diferença entre a aplicação de aeração ativa (a uma taxa de fluxo de 860 mL min^{-1} usando um soprador de ar) e aeração passiva (expondo gás O_2 no cátodo). As densidades de corrente produzidas usando aeração ativa variaram de 3,5 a 42,6 A m^{-2}, o que foi significativamente maior do que a configuração de aeração passiva (0,07 a 1,1 A m^{-2}). Além disso, com o método de aeração ativa foi alcançada uma taxa de produção máxima de H_2O_2 de 7,32 kg m^{-3} d^{-1}, que superou a taxa de produção de H_2O_2 de 2,50 kg m^{-3} d^{-1} na configuração de aeração passiva.

2.5.4 Tempo de detenção hidráulica (TDH)

O tempo de detenção hidráulica (TDH) desempenha um papel significativo no tratamento biológico de efluentes, incluindo o tratamento via CCM e EF (SOBIESZUK; ZAMOJSKA-JAROSZEWICZ; MAKOWSKI, 2017). O TDH afeta a concentração de oxigênio dissolvido presente no reator e a concentração de substrato restante. A taxa de carregamento orgânico também depende do TDH, o que resulta em uma saída de potência variável. Em TDH mais baixo, a taxa de carregamento de substrato aumenta, o que consequentemente leva a um aumento na taxa de consumo do substrato. O consumo geral de substrato resulta em potência e tensão de saída aprimorados. Em baixo TDH a bioincrustação pode ser controlada, enquanto gera maior potência de saída. Por outro lado, se o afluente tiver uma grande quantidade de oxigênio dissolvido, ocorre um aumento no potencial de oxirredução resultando em menor potência e saída de tensão (MANSOORIAN et al., 2016; VERMA et al., 2021b). Além disso, tempos curtos não permitem o metabolismo completo da matéria orgânica pela comunidade microbiana anódica. Já o aumento no TDH leva a um aumento na geração de energia de sistemas contínuos, favorecendo a remoção de matéria orgânica (TRAPERO et al., 2017). Entretanto, tem consequências negativas para a potência de saída devido ao esgotamento do substrato, que pode induzir uma reversão de tensão se os níveis forem muito baixos (MALEKMOHAMMADI; MIRBAGHERI, 2021; TABASSUM; ISLAM; AHMED, 2021).

Li et al. (2010) estudaram a influência do TDH na DP em relação ao substrato (em termos de DQO) e a remoção do Vermelho do Congo. Os resultados mostraram que a DP máxima foi alcançada quando o TDH era de 14,8 h. O aumento do TDH de 14,8 para 44,4 h diminuiu a concentração de substrato na câmara anódica, o que aumentou o potencial de circuito aberto do ânodo de -431 para -238,8 mV. A diminuição do TDH para 7,4 h aumentou a concentração do substrato na câmara catódica, o que causou uma diminuição na DP. Liu et al. (2009) também avaliaram os efeitos do TDH na remoção de cor. A remoção total de cor aumentou de 68% para 96%; e a remoção de cor em câmara anódica aumentou de 35% para 82% com o aumento do TDH de 7,5 para 45 h. Por outro lado, Mu et al. (2009) investigaram o efeito do TDH catódico nas descolorações de laranja de metila 7 (LM7) na faixa de 0,31-3,75 h. Com o aumento do TDH catódico, a eficiência de descoloração LM7 foi de 34,6 ± 1,8% para 90,0 ± 1,5%, demonstrando uma relação positiva entre o TDH e a remoção de cor. Entretanto, a taxa de descoloração do LM7 diminuiu com o prolongamento do TDH, de 5,05 ± 0,27 para 1,10 ± 0,02 mol m^{-3} d^{-1} no sistema BEF.

No estudo de Ye et al. (2020), as taxas de remoção de DQO foram influenciadas de forma insignificante pela variação do TDH de 0,35 a 0,69 d, que foram superiores a 92%. Em contraste, a geração máxima de potência diminuiu quando o TDH aumentou, provavelmente pela escassez de substrato. Em Haavisto et al. (2017) o TDH foi otimizado para a DP máxima diminuindo gradualmente de 3,5 d para 0,17

d. A maior DP (430 mW m^{-2}) foi obtida em 1 d. A EC diminuiu de 30% para 0,6% com TDH's de 3,5 d e 0,17 d, respectivamente. As taxas de remoção de DQO em TDH's 13, 14 e 20 d foram 71, 73 e 83%, enquanto as EC's foram 7,1; 2,4 e 0,3%, respectivamente. A DP máxima em TDH 13 e 14 d foram semelhantes, 12 mW m^{-2} e 13 mW m^{-2}, que foram 26 vezes maiores do que TDH em 20 d (0,5 mW m^{-2}). O efeito de diferentes TDH's na diminuição do conteúdo orgânico por biocatálise leva a baixa disponibilidade de material orgânico para geração de eletricidade, resultando em menor geração de corrente elétrica (MA et al., 2016). De acordo com Oon et al. (2017), a eficiência de remoção de DQO e a descoloração do azo-corante aumentaram de 70 para 77% e de 88 para 93%, respectivamente, quando a TDH se estendeu de 1 para 2 dias. Portanto, um TDH ótimo contribui com um período suficiente para o biofilme degradar o substrato, a fim de melhorar a produção de energia. Para o tratamento em larga escala de efluentes têxteis, um alto TDH seria um fator limitante para o tratamento de grande volume de efluentes, o que demanda um tratamento mais rápido (YADAV et al., 2022).

No estudo de Wang et al. (2017), o objetivo original do BEF alimentado continuamente era atingir o acúmulo de H_2O_2, mas o resultado não foi tão alto quanto o esperado ocorrendo rápido declínio da concentração de H_2O_2. No modo contínuo, a corrente é diretamente proporcional à taxa de carga orgânica. A densidade de corrente obtida pelo processo BEF contínuo pode ser considerada 2 vezes maior que a obtida operando em batelada (RAFAQAT et al., 2022). A taxa de produção de H_2O_2 é muito menor e variável, o que pode ser estabilizado operando o sistema de modo contínuo que resultaria em um fornecimento regular de substrato fresco ao biofilme anódico (SATHE et al., 2022a).

Em contraste, no modo batelada-alimentada, o aumento da concentração de substrato aumenta a corrente até certo ponto, mas subsequentemente, a densidade de corrente diminui. A EC permanece estável no modo contínuo, enquanto diminui ao longo do tempo em batelada-alimentada. Comparado ao modo de alimentação descontínua, o modo de alimentação contínua favorece a abundância de bactérias eletrogênicas e reduz as metanogênicas e outras não eletroativas. Neste sentido, a abundância de elétrons tem sido considerada como o principal fator que governa o número de elétrons liberados, que aumentam a clivagem redutiva do azo-corante e a geração de elétrons. No entanto, no modo batelada-alimentada, o pH da câmara do ânodo geralmente diminui, o que inibe o crescimento microbiano e afeta adversamente a descoloração do corante e o potencial de geração de eletricidade. Assim, o modo contínuo parece aumentar a produção de energia devido ao seu efeito na formação de biofilme que garante o transporte de elétrons (FANG et al., 2015; YADAV et al., 2022).

Rossi et al. (2019) afirmaram que a recirculação do anólito melhorou ainda mais o desempenho em 17% (0,118 ± 0,006 W m^{-2}) para um TDH de 22 min, em comparação com as condições de fluxo estático. Para Lay; Kokko e Puhakka (2015) o desempenho da geração de energia aumentou para 372 ±20 mW m^{-2} em TDH de 1,7 d em modo contínuo com taxa de recirculação de 4,8 reator-volume/h, enquanto a EC caiu para 13,4 ± 0,5%. Portanto, em operação contínua, diminuir o TDH pode melhorar o desempenho elétrico do BEF.

2.6 METODOLOGIA DA PESQUISA

No quadro 1 está apresentado o diagrama metodológico das fases da pesquisa desenvolvida. Em resumo, o trabalho foi organizado em três fases, (1) inoculação e aclimatação; (2) processo BEF; e (3) sistema híbrido – CCM+BEF, de maneira que cada fase, além de corresponder a um artigo, cumpre a cada um dos objetivos específicos da pesquisa.

A pesquisa experimental foi desenvolvida no Laboratório Integrado de Meio Ambiente (LIMA) e no Laboratório de Reúso das Águas (LaRA) do departamento de Engenharia Sanitária e Ambiental da Universidade Federal de Santa Catarina (UFSC). O reator proposto foi operado em todas as fases experimentais em regime de batelada e em duplicata. A alimentação da câmara anódica da CCM foi dada por um efluente sintético em pH = 7,0, rico em matéria orgânica, vitaminas e micronutrientes. Para a câmara catódica, a alimentação do azo-corante VBR-5R foi dada em pH = 3,0 com adição pré-estabelecida de eletrólito e de fonte de ferro para reação de Fenton.

Quadro 1 – Diagrama representativo das fases metodológicas da pesquisa

FASE 1	FASE 2	FASE 3
INOCULAÇÃO E ACLIMATAÇÃO **Aspectos operacionais** Inóculo: lodo anaeróbio ETE Alimentação: 1 g L^{-1} acetato; 50 mM PBS; 12,5 mL L^{-1} minerais; 5 mL L^{-1} vitaminas Ânodo: escova de fibra de carbono Cátodo: feltro de grafite R_{ext}: 1000 Ω pH 7,0 Batelada-alimentada (24h) Temperatura 35 ± 2˚C **Monitoramento** Curva de polarização Tensão, corrente e potência [DQO] e [H_2O_2] Eficiência de Coulomb (EC) Eficiência de Faraday (EF) Biofilme anódico	**BIO-ELETRO-FENTON (BEF)** **Câmara anódica** Biofilme formado – escova fibra de carbono; Alimentação em batelada sem adição de inóculo (1 g L^{-1} acetato de sódio) $CH_3COOH + 2H_2O \rightarrow 2CO_2 + 8H^+ + 8e^-$ **Câmara catódica** Avaliação da eficiência de degradação do azo-corante Feltro de grafite; pH 3,0; 68,0 mg $FeSO_4.7H_2O$; 1,77 g Na_2SO_4; TDH (12 h) $O_2 + 2H^+ + 2e^- \rightarrow H_2O_2$ **Variáveis operacionais** Corante (mg L^{-1}): 5,0; 10,0; e 20,0 R_{ext} (Ω): 1000, 100 e 10 **Monitoramento** Curva de polarização Tensão, corrente e potência EC e EF [DQO], pH, cor, grupos aromáticos e [H_2O_2]	**SISTEMA HÍBRIDO (CCM+BEF)** **Câmara anódica** Biofilme formado – escova fibra de carbono; **Variáveis operacionais** Corante/Acetato (mg L^{-1}/g L^{-1}) 5,0/0,75; 10,0/0,50; 20,0/0,25 TDH (h) (CCM/EF): 2/2; 4/4; 6/6 TDH (h) (CCM/EF): 2/12; 4/12; 6/12 **Câmara catódica** Pós-tratamento oxidativo do azo-corante $O_2 + 2H^+ + 2e^- \rightarrow H_2O_2$ Feltro de grafite; pH 3,0; 34,25 mg $FeSO_4.7H_2O$; 1,77 g Na_2SO_4 **Monitoramento** Curva de polarização Tensão, corrente, potência EC e EF [DQO], pH, cor, grupos aromáticos e [H_2O_2] Biofilme anódico

De acordo com a proposta metodológica, a seguir será apresentada em capítulos cada fase experimental da pesquisa

3 CAPÍTULO 3 - EXPLORING MICROBIAL COMMUNITY DYNAMICS IN MICROBIAL FUEL CELL (MFC) ACCLIMATION FOR HYDROGEN PEROXIDE (H_2O_2) SYNTHESIS

ABSTRACT

Hydrogen peroxide (H_2O_2) is a critical intermediate in microbial fuel cells (MFCs) and can play a vital role in the degradation of many organic pollutants. However, the H_2O_2 synthesis rate is often limited by the low activity of the two-electron oxygen reduction reaction (2e-ORR). The bacterial acclimation process can enhance MFC performance by promoting the augmentation of electrogenic bacteria in the anodic biofilm. For this reason, a microbial consortium was employed to investigate the H_2O_2 synthesis approach through microbial electrosynthesis in a two-chamber MFC. After achieving stability in the electric current density (day 15), the H_2O_2 concentration reached 15.17 mg L^{-1}. The polarization curve results showed that the MFC acclimation process after 20 days generated a maximum power density of 60.6 mW m^{-2}, corresponding to 607 mA m^{-2} of current density. Principal coordinate analysis (PCoA) and canonical coordinate analysis (CCA) confirmed changes in the MFC microbial structure. The substrate and pH control had more influence than the temperature during electrogenic biofilm development in the MFC-1000 Ω R_{ext} acclimation process. After acclimation, there was a notable increase in the relative abundance of the predominant phyla in the MFC, indicating 28.1% to 62% for Proteobacteria and 7% to 19.6% for Firmicutes. Among the genera identified in this study, Kerstersia (42%), Pandoraea (1%), Petrimonas (6%), and C10-SB1A (1%) showed a positive correlation ($r > 0.85$) in substrate conversion into electric current and consequent H_2O_2 synthesis. The findings highlight the potential of using microbial electrosynthesis as a sustainable and efficient method for H_2O_2 synthesis on a laboratory scale. These results suggest that the acclimation process can significantly improve the H_2O_2 synthesis rate in the MFC and provide insights into the microbial community dynamics and bioelectrochemical process.

Keywords: microbial fuel cell; microbial consortium; H_2O_2 synthesis; 16S rRNA sequencing; microbial electroactive community.

RESUMO

O peróxido de hidrogênio (H_2O_2) é um intermediário crítico na célula a combustível microbiana (CCM), que pode desempenhar um papel vital na degradação de vários poluentes orgânicos. No entanto, a taxa de síntese de H_2O_2 é frequentemente limitada pela baixa atividade da reação de redução de oxigênio de dois elétrons (2e-ORR). O processo de aclimatação bacteriana pode melhorar o desempenho da CCM por promover o aumento de bactérias eletrogênicas no biofilme anódico. Por esta razão, um consórcio microbiano foi empregado para investigar a abordagem de síntese de H_2O_2 através da eletrossíntese microbiana em uma CCM de câmara dupla. Após alcançar estabilidade na densidade de corrente elétrica (dia 15), a concentração de H_2O_2 atingiu 15,17 mg L^{-1}. Os resultados da curva de polarização mostraram que o processo de aclimatação da CCM, após 20 dias, gerou uma densidade de potência máxima de 60,6 mW m^{-2}, correspondendo a 607 mA m^{-2} de densidade de corrente. Análises de coordenadas principais (ACP) e coordenadas canônicas (ACC) confirmaram mudanças na estrutura microbiana da CCM. O controle do substrato e do pH influenciou mais do que a temperatura no desenvolvimento do biofilme eletrogênico no processo de aclimatação MFC-1000Ω R_{ext}. Após a aclimatação, houve um notável aumento na abundância relativa dos filos predominantes na MFC, indicando 28,1% a 62% para Proteobacteria e 7% a 19,6% para Firmicutes. Dentre os gêneros identificados neste estudo, Kerstersia (42%), Pandoraea (1%), Petrimonas (6%) e C10-SB1A (1%) apresentaram correlação positiva (r > 0,85) na conversão do substrato em corrente elétrica e consequente síntese de H_2O_2. Os resultados destacam o potencial do uso da eletrossíntese microbiana como uma maneira sustentável e eficiente para a síntese de H_2O_2 em escala de laboratório. Estes resultados sugerem que o processo de aclimatação pode melhorar significativamente a taxa de síntese de H_2O_2 na CCM e fornecer informações sobre a dinâmica da comunidade microbiana e o processo bioeletroquímico.

Palavras-chave: célula a combustível microbiana; consórcio microbiano; síntese de H_2O_2; sequenciamento 16S rRNA; comunidade microbiana eletroativa.

3.1 INTRODUCTION

Hydrogen peroxide (H_2O_2) is an environmentally friendly reagent often used in water and wastewater treatment (DENG; BRILLAS, 2023). However, it is commercially produced through toxic and costly anthraquinone processes (CHUNG et al., 2020). The synthesis and use of H_2O_2 in situ are found to be more appealing for a variety of applications. A possible environmentally favorable technique for ongoing H_2O_2 synthesis is the cathodic reduction of dissolved oxygen (KHATAEE et al., 2017; LI; ANGELIDAKI; ZHANG, 2017). An innovative method for H_2O_2 synthesis from wastewater is through a two-electron oxygen reduction reaction (2e-ORR) in bioelectrochemical systems (BES), where a cathode catalyst is a crucial component impacting oxygen reduction reaction (ORR) performance. For this, a microbial fuel cell (MFC) may provide a cost-effective method for H_2O_2 synthesis at the cathode (SONG et al., 2019).

The MFC is a potential system that uses microorganisms and electrochemistry for H_2O_2 synthesis, which can degrade pollutants (FAJARDO-PUERTO et al., 2023). Organic compounds in wastewater are oxidized by electrogenic bacteria using the anode as an electron acceptor. A bioelectrochemical reactor for H_2O_2 synthesis consists of two chambers separated by a proton exchange membrane (PEM). The solution containing dissolved organic matter (e.g., acetate) is fed to the anode compartment, where microorganisms oxidize the organics and use the anode as an electron acceptor (Eq. 11). The electrons flow through an external electric circuit to the cathode, where O_2 is reduced to H_2O_2 (Eq. 12) or H_2O (Eq. 13) (MODIN; FUKUSHI, 2013; PERAZZOLI; DE SANTANA NETO; SOARES, 2018).

$$CH_3COOH + 2H_2O \rightarrow 2CO_2 + 8H^+ + 8e^- \ (E^0_{anode} = -0.300 \text{ V}) \tag{11}$$

$$O_2 + 2e^- + 2H^+ \rightarrow H_2O_2 \ (E^0_{cathode} = +0.280 \text{ V}) \tag{12}$$

$$O_2 + 4e^- + 4H^+ \rightarrow 2H_2O \ (E^0_{cathode} = +0.805 \text{ V}) \tag{13}$$

H_2O_2 can be a critical intermediate vital in degrading organic pollutants in MFCs. H_2O_2 is the primordial reagent for the Fenton reaction at acidic pH. In the cathode chamber, the reaction between Fe^{2+} and H_2O_2 promotes the generation of hydroxyl radicals (•OH) with high oxidative power (E_0 = 2.8 V) (MACHADO; TEIXEIRA; RUOTOLO, 2023). However, the H_2O_2 synthesis rate is often limited by the low activity of the 2e-ORR (Eq. 12) in the cathode chamber, due to the more favorable reduction of O_2 to H_2O (4e-ORR) (Eq. 13) (FAJARDO-PUERTO et al., 2023). The ORR activity is influenced by various factors, such as the cathode material, electrode surface area, and anodic microbial community composition (GAO; LU; LI, 2020). The fundamental principles of the acclimation process have yet to be fully understood, and it is yet to be discovered how different acclimation procedures would affect the makeup of the microbial community and electrochemical performance. The development of ORR-active microorganisms on the anode surface can be encouraged by acclimation to increase metabolic activity and boost H_2O_2 synthesis. According to Chen et al. (2020; 2018), acclimation occurs in response to environmental factors such as nutrient availability, pH, temperature, and substrate concentration changes. Acclimation can accelerate H_2O_2 synthesis in the MFC by promoting 2e-ORR-active microorganism colonization on the anode surface and improving the electron transmission efficiency between the anode and cathode chambers (ZHANG et al., 2020). The microbial community significantly impacts the ability of the MFC microbial consortium to generate energy. Islam et al. (2018) noted that the most highly potentiated electrogenic bacteria are primarily found within the phyla Bacteroidota, Clostridium, Proteobacteria, and Firmicutes.

Several studies have investigated the influence of acclimation on the efficacy of MFCs (MA et al., 2023; PARK et al., 2017; ROSSI; LOGAN, 2020; ULLERY; LOGAN, 2015; ZHANG et al., 2019a). The acclimation strategy, according to Wang et al. (2022b), significantly increased the H_2O_2 synthesis rate in the MFC by employing an activated carbon fiber felt cathode. The cause of enhancement is attributed to an increased microbial diversity and an abundance of ORR-active microorganisms, along with the use of an adequate cathodic electrode. Similarly, Wu et al. (2020a) demonstrated that by using a graphite-felt cathode, the acclimation process speeds up contaminant breakdown in the MFC cathode chamber. They suggested that developing a biofilm on the anode surface caused an increase in 2e-ORR activity, which promoted electron transport and consequently accelerated H_2O_2 synthesis. Zhang et al. (2019a) revealed that acclimated inoculum for MFC startup can be reduced to 43 h, yielding a decrease of 63.2% compared to MFCs using non-acclimated inoculums.

MFC acclimation for H_2O_2 synthesis has emerged as an interesting method that has produced promising outcomes in recent studies. Although challenges remain, such as low energy efficiency and scalability, appropriate microbial consortia and operating conditions can boost H_2O_2. As research and development improve, MFC-based H_2O_2 synthesis may become a viable and sustainable option for large-scale production of this critical oxidant. This study investigated using an acclimated microbial consortium to synthesize H_2O_2 via microbial electrosynthesis without potential energy input. Acclimation time and the corresponding evolution of power density, current density, Coulomb and Faraday efficiencies, COD, and H_2O_2 synthesis were analyzed. Performance statistics were individually analyzed to identify and correlate possible microbial genera responsible for bioelectrochemical process efficiency.

3.2 MATERIAL AND METHODS

3.2.1 MFC setup

All experiments were conducted on H-type glass MFC reactor with an effective volume of 250 mL for each chamber, according to Fig. 4. A proton exchange membrane (PEM) separated the two chambers of the reactor (Nafion 117, DuPont Co., USA). Nafion 117 was previously treated with H_2O_2 5%, H_2SO_4 5% w/w, and deionized water. The anodic electrode was a carbon fiber brush (MiliRose, USA) pretreated at 450 °C for 20 min (YANG et al., 2022). The cathodic electrode was graphite felt (3.10^{-3} m^2) (MIRONG, China). A titanium wire of 0.8 mm diameter was connected to the electrical circuit with external resistance. A data acquisition system (HM-2030, Hikari) was connected to the MFC to monitor voltage and electrical current output. A small air pump (SC-7500, Boyu) was coupled to the system for aeration of the cathode chamber.

Figure 4 - Schematic MFC reactor setup

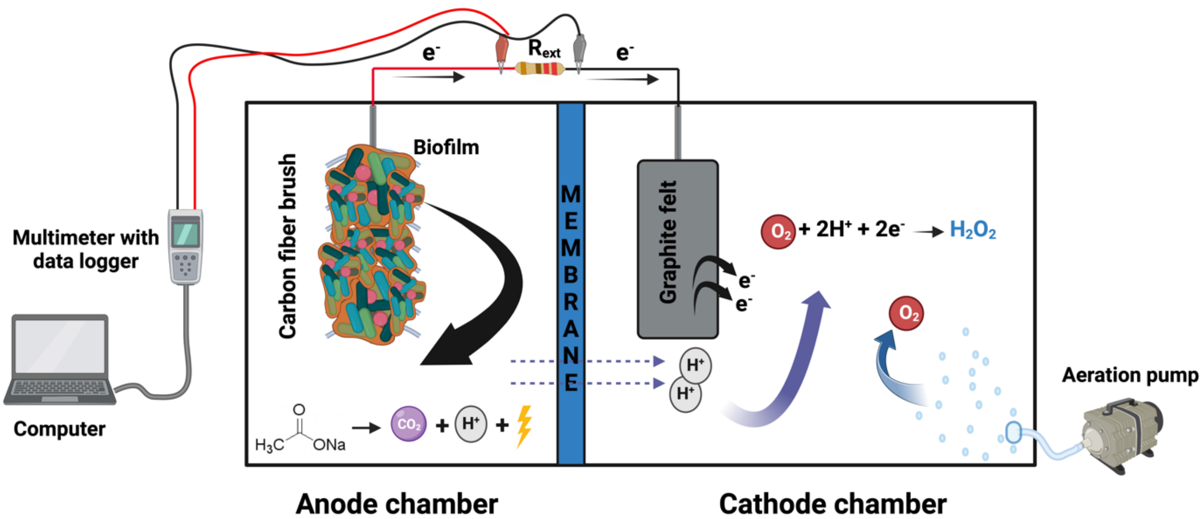

Source: Author (2023)

3.2.2 Inoculum and acclimation

The inoculum consisted of a microbial consortium collected from an anaerobic tank in a domestic wastewater treatment plant (Florianópolis, Brazil). Acclimation was performed by feeding the anodic chamber with sludge and growth medium (1:1) every

24 hours until maximum voltage output was achieved. The growth medium was composed of the following (in g L^{-1}): sodium acetate – $C_2H_3NaO_2$ (1.0); phosphate buffer solution (PBS): $Na_2HPO_4 \cdot H_2O$ (4.28), NaH_2PO_4 (2.74), NH_4Cl (0.31); and KCl (0.13); 12.5 ml L^{-1} of minerals (mg L^{-1}): $MgSO_4.7H_2O$ (10.0), $MnCl_2.4H_2O$ (3.0), $MgCl_2 \cdot 6H_2O$ (10.0), $CoCl_2.6H_2O$ (1.0), $NiCl_2.6H_2O$ (2.0), $NaMoO_4.7H_2O$ (3.0), H_3BO_3 (30.0) and $CuCl_2.2H_2O$ (1.0) e $CaCl_2 \cdot 2H_2O$ (1.0); and 5 ml L^{-1} of vitamin solution (IQBAL et al., 2022; ROSSI et al., 2019; TAN et al., 2022; YU et al., 2020). Nitrogen gas was applied before each feeding cycle to obtain an anaerobic environment in the anodic chamber (ALMEIDA et al., 2021).

The MFC anode chamber was fed during each operation cycle until the voltage dropped to < 50 mV, considering a full-cycle operation. After many full-cycle operations achieved 250 mV, the MFC was fed only with PBS, sodium acetate (1.0 g L^{-1}), mineral solution, and vitamins. The cathode chamber was fed with deionized water containing 50 mM Na_2SO_4 to maintain an adequate ionic force and continually subjected to aeration with an air pump. The pH was adjusted to 3.0 with 0.5 M H_2SO_4. In the start-up, an external resistor (R_{ext}) of 1000 Ω was connected to the MFC circuit (VICARI et al., 2018). The acclimation was conducted at 35 ± 2 °C in a controlled biochemical incubator.

3.2.3 Analysis and calculation

The voltage was measured using a digital multimeter with a data logger. The current, I [mA], was calculated according to Ohm's law (Eq. 14), where U is the voltage [mV], and R_{ext} is the external resistance (Ω). Current densities (mA m^{-2}) (Eq. 15) and power densities (mW m^{-2}) (Eq. 16) were normalized to the total exposed cathode projected area (3.10^{-3} m^{-2}).

$$I\ (mA) = \frac{U}{R_{ext}} \tag{14}$$

$$j\ (mA\ m^{-2}) = \frac{I}{A} \tag{15}$$

$$PD\ (mW\ m^{-2}) = \frac{U^2}{R_{ext}\ A} \tag{16}$$

The polarization curve was generated by varying the external resistance, setting the MFC to open the circuit until a stable voltage was observed. The applied external resistance was varied from 1000 to 500, 200, 100, 55, 20, and 10 Ω in ten-minute intervals. Moreover, the MFC performance was evaluated regarding the anodic COD and cathodic H_2O_2 concentration. All samples collected in the anode chamber for COD determination were filtered through a 0.45 μm membrane. The COD was measured by spectrophotometry (Hach DR3900) according to the procedure described in Hach 8000, based on the dichromate oxidation method (APHA, 2018). Cathodic samples were collected when the maximum voltage reached a plateau, and the H_2O_2 concentration was measured by the iodine (I_3^-) method (WANG et al., 2022b). Coulomb efficiency (CE), defined as the fractional recovery of electrons from the substrate, was calculated according to Eq. (17). Faraday efficiency (FE) is the ratio of the electricity consumed by the electrode reaction to produce H_2O_2 and the total electricity of the reaction system. The value was obtained according to Eq. (18).

$$CE\ (\%) = \frac{8\ \int_0^t I\ dt}{F\ V\ \Delta COD}\ .\ 100 \tag{17}$$

$$FE\ (\%) = \frac{n\ F\ C_{H_2O_2}\ V}{\int_0^t I\ dt}\ .\ 100 \tag{18}$$

where I is the average current (mA), t is the hydraulic retention time (HRT) (s), F is Faraday's constant (96485 C mol^{-1}), n is the number of electrons exchanged per mole of oxygen (2 mol e^- mol^{-1}), V is the MFC volume chamber (L), ΔCOD is the change in COD (g L^{-1}) over time t, and $C_{H_2O_2}$ represents the measured H_2O_2 concentration (mg L^{-1}) (BOAS et al., 2022; SIM et al., 2015). The internal resistance (R_{int}) was calculated from the slope of the polarization curves using Eq. (19):

$$U = OCV - j.R_{int} \tag{19}$$

where U represents MFC voltage in a determinate current intensity; OCV, the open circuit voltage; j, the current density; and R_{int}, the internal resistance (CHENG; LIU; LOGAN, 2006).

3.2.4 Microbial community analysis

16S rRNA sequencing was conducted to assess and determine the microbial community structure. Microbial community sampling was performed by scraping the anode biofilm and storing it in an Eppendorf 5 mL microtube at -4.0 °C until analysis. For each sample, 250 µL was mechanically lysed through disruption with the aid of the L-BEADER HT disruptor (Loccus) using zirconium beads. DNA extraction from the lysate samples was performed using a modification of the DNeasy® 96 PowerSoil® Pro QIAcube® HT kit. The QiaCube HT robot performed the extraction (Qiagen, Germany). The variable V3-V4 regions of the 16S ribosomal RNA gene (16S rRNA) were amplified using the universal primers 341F 5′-CCTACGGGRSGCAGCAG-3′ (WANG; QIAN, 2009) 806R 5′-GGACTACHVGGGTWTCTAAT-3′ (CAPORASO et al., 2010) The PCR products were sequenced in an Illumina MiSeq with 2x300 (Forward) and 2x250 (Reverse) reads.

Fastq files were demultiplexed with MiSeq software according to their index and analyzed using QIIME 2, version 2 (2021.11) (BOLYEN et al., 2019) on VirtualBox (7.1 version). Sequencing reads were filtered, denoised, and merged, and chimeras were removed using DADA2 (CALLAHAN et al., 2016) for quality control. Subsequently, sequences were taxonomically classified using the SILVA database (QUAST et al., 2012), and mitochondria or chloroplast-related features were removed. The median frequency was 23,562 (min: 20,605 – max: 29,469) reads, so the number of sequences was rarefied to 20,000 for each sample for further diversity analyses. The align-to-tree-MAFFT-fast tree pipeline from q2-phylogeny was used for phylogenetic-dependent analyses. Alpha diversity (α) analyses were performed to assess the complexity of microbial diversity for each sample, including the operational taxonomic unit (OTU) to measure observed species richness and the Shannon index to identify community diversity.

The percent of reads in each sample matching the top 20 abundant genera were plotted and compared among samples in a heatmap using an average Bray–

Curtis metric. All alpha diversity indices and beta diversity analyses were performed using QIIME 2 software (2021.11).

3.2.5 Data analysis

Prism 9 (GraphPad, version 9.2) was used for statistical analysis of the physicochemical parameters. ANOVA was performed, and the collected data are represented as the mean value. A p value ≤ 0.05 indicated statistically significant differences between values. Canonical coordinate analysis (CCA) correlated the main microbial genera with the MFC reactor feeding operational variables (pH, substrate, and temperature). Principal coordinate analysis (PCoA) was performed from the genera relative abundance dataset to compare differences in microbial communities between inoculum and MFC acclimated. Pearson's correlation analysis was performed to examine the significant relationships between the relative abundances of the microbial community and the different MFC metrics (CE, FE, COD removal, current, and H_2O_2). CCA, PCoA, and Pearson correlation tests were performed using the statistical software XLSTAT Pro® (XLSTAT, Paris, France), and $p < 0.05$ was considered significant.

3.3 RESULTS AND DISCUSSION

3.3.1 Current density output and H_2O_2 synthesis

The development of an electroactive biofilm is a crucial factor for the performance of an MFC system. A startup time is needed to produce considerable current output. According to the generation of electric current measured MFC-1000 Ω (Fig. 5A), a latency phase was observed during the first eight days, followed by a significant increase in current density between days 9 and 14. The current generation reached a plateau of approximately 65 mA m^{-2} from day 15. Previous studies found similar results (HALFELD et al., 2022; KAMAU et al., 2017; MALYAN; MONGIA; KUMAR, 2022; UDDIN et al., 2019). As the biofilm develops, the transfer of electrons between the bacteria and the electrode becomes more efficient, generating more electrical current (ANGELAALINCY et al., 2018; JIN et al., 2022).

On day 8, the electric current did not show a significant increase (Fig. 5A). Biofouling emerged on the proton exchange membrane (PEM) surface and probably obstructed the active membrane sites responsible for H^+ transfer (H_2O_2 synthesis), preventing the effective transfer of electrons and protons to the cathode chamber. According to Hemdan et al. (2023), the leading cause of these occurrences can be attributed to the gradual decline in the electrogenicity of the mature biofilm due to the continuous growth of the dead cell layer on the surface of the PEM and the nutritional restrictions brought about by the prolonged use of the batch mode. Furthermore, Flimban et al. (2020) state that biofouling affects the CE and power density in the bioelectrochemical system. In critical cases, the observed long-term energy performance can fall by more than 90% (KOLAJO et al., 2022; PASTERNAK et al., 2022). For this reason, in this study, on operational day 9 (Fig. 5A), the PEM was exchanged for a new one. From this, the electric current density reached 53.7 mA m^{-2}, and the addition of sludge was suspended from there. Then, the anodic chamber was fed only PBS, acetate, vitamin, and mineral solution.

Figure 5 - Development of MFC acclimation: (A) relation of the increase in electric current density (mA m^{-2}) with H_2O_2 (mg L^{-1}) for R_{ext}=1000 Ω; (B) polarization curve

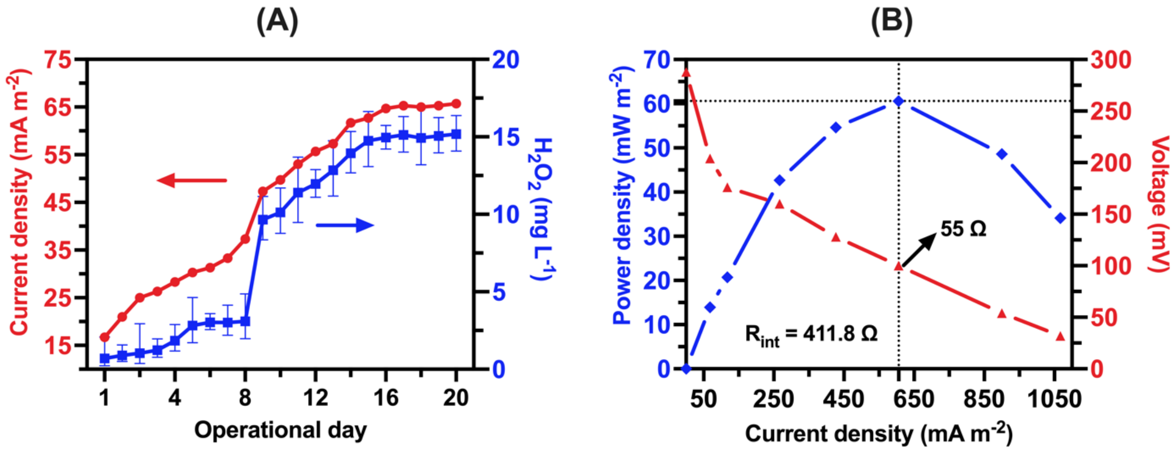

After the new PEM, the H_2O_2 concentration increased positively and gradually with each cycle of operation. On operating day 20, the H_2O_2 synthesis in the MFC-1000 Ω reached 15.18 ± 0.10 mg L^{-1} at 65.7 mA m^{-2} (Fig. 5A). The cumulative H_2O_2 concentration on the 20 acclimation days was 125.9 ± 0.2 mg L^{-1}. In an MFC, H_2O_2 synthesis gradually increases as the electroactive biofilm develops on the anode electrode (SUN et al., 2016). However, after a certain point, the H_2O_2 concentration reached a plateau and remained relatively constant, even if the applied electric current was kept constant (FAJARDO-PUERTO et al., 2023; ZHANG; TAO, 2018). This can be explained because the synthesis rate of H_2O_2 begins to balance with the speed of degradation so that the concentration of H_2O_2 reaches a stable and constant concentration (ASGHAR; RAMAN; DAUD, 2014; KAHOUSH et al., 2018). Similar results can be compared to those of this study. A graphite cathode electrode reached 78.85 mg H_2O_2 L^{-1} after 12 h with an external resistance of only 20 Ω (6.57 mg L^{-1} h^{-1}) (FU et al., 2010a). In the study of Sim et al. (2018) the maximum cumulative concentration of H_2O_2 was only 98 mg L^{-1} in 20 days with 7.2% conversion efficiency, indicating significant losses of H_2O_2 in any further reduction in the cathode or decomposition in the medium.

On operational day 20, the polarization curve was performed with R_{ext} from 10 to 1000 Ω. According to Fig. 5(B), the MFC inoculated with mixed culture reached a maximum power density of 60.6 mW $m^{-2,}$ corresponding to a current density of 607 mA m^{-2} with 55 Ω R_{ext}. Similar results for power density and maximum current were found in previous studies (CHOUDHURY et al., 2021; GHASEMI et al., 2013; MANI et al., 2020; SHABANGU et al., 2023; SHANG et al., 2023; VICARI et al., 2018). However, internal resistance in the MFC could contribute to the low power density primarily affected by membrane biofouling. In the polarization curve (Fig. 5B), on operational day 20, the internal resistance (R_{int}) was 411.8 Ω for the MFC dual chamber with an electrode spacing of 25 cm. Zavala and Gutiérrez (2023) obtained 28.23 mW m^{-2} with a high R_{int} between 2 and 5 kΩ on average in their MFC dual chamber. In the study by Tan et al. (2020), the low power density of 44.27 mW m^{-2} was attributed to 200 Ω R_{int} in the MFC dual chamber with an electrode spacing of 11 cm. For Malyan et al. (2022), the low power density value (0.546 mW m^{-2}) was attributed to a high R_{int} of 9.5 kΩ. Karamzadeh et al. (2023) achieved only 47.9 mW m^{-2} due to 332 Ω R_{int}.

According to our results, the high R_{int} (411.8 Ω) value may have contributed significantly to the low power density. As the electric current passes through the MFC, the internal resistance causes an internal voltage to drop. This voltage drop consumes a portion of the energy produced by the MFC. The loss of internal voltage increases with increasing internal resistance. A decreased power density results from less voltage to push the electric current through the external electric circuit (LOGAN et al., 2018). This is because the distance between the electrodes influences the ohmic resistance, while their respective geometries or configurations determine the resistance of the anode and cathode. Therefore, each modification in the electrode spacing or MFC setup impacts the internal resistance (MALYAN; MONGIA; KUMAR, 2022; NASRUDDIN; BAKAR, 2021). This, in turn, affects the operational efficiency of the MFC.

3.3.2 Coulomb and Faraday efficiency

Coulomb (CE) and Faraday (FE) efficiencies are essential to available H_2O_2 synthesis. In general, they are affected by several factors, including operating conditions, the composition of the bacterial consortium, and the geometry of the reactor, among others. Table 5 presents the COD removal, CE, FE, and power density generated in the MFC during the operation time. A noticeable increase in CE and FE was observed during 20 days of acclimation. This performance can be attributed to the inactivation of methanogenic and fermentative bacteria due to the selectivity and adaptation of electroactive bacteria in the development of the biofilm (see section 3.3.3).

Table 5 - COD removal and electrochemical parameters in MFC-1000 Ω R_{ext} during the acclimation

Operational day	**COD removal (%)**	**CE (%)**	**FE (%)**	**Power density (mW m^{-2})**
1	12.9	0.52	0.85	0.4
5	25.1	1.06	1.37	4.8
10	36.3	2.67	3.66	24.8
20	67.2	4.88	4.47	60.6

After 20 days of operation, significant results were obtained in converting the substrate into power density output (Table 5). The COD removal, CE, FE, and power density values achieved were 67.2%, 4.88%, 4.47%, and 60.6 mW m^{-2}, respectively. Similar results were found in the study by Mani et al. (2020), where the MFC-acclimated biofilm produced a maximum power density of 64,6 ± 3,5 mW m^{-2}. In the study of Capodaglio et al. (2013), the MFC produced an average power density of 0.369 mW m^{-2} with a CE ranging from 0.8 to 1.9%. Viccari et al. (2018) achieved a power density of 47.1 mW m^{-2} with 1.48% CE. For Khater et al. (2017), the MFC successfully revealed a maximum power density of 86.1 mW m^{-2} with 65% CE after five days.

Fermentative bacteria can restrict the viability of mixed cultures as inoculum in MFCs, which are apparent competitors of electrogenic bacteria, leading to a decrease in power density and CE (HOLMES et al., 2019; PRÉVOTEAU et al., 2020). Therefore, the loss of performance of the MFC inoculated with the microbial consortium is often associated with the ineffective conversion of the substrate into electrons and H^+ ions, consequently, in the low power density generated in the reactor (JADHAV et al., 2019; NATH; CHAKRABORTY; GHANGREKAR, 2021). The low CE values found in this study suggest that bioelectrogenesis and anaerobic transformation competed fiercely for the substrate. Different COD availability may have impacted the current produced through a concentration of overpotentials in the mass and electron transport (SANTORO et al., 2021). Furthermore, the COD removal with low CE could be related to MFC impacted by additional factors such as the consumption of electrons by microbes for growth, other electron acceptors (O_2, SO_4^{-2}, and CO_2), or concurrent reactions of methanogenesis and fermentation (YANG et al., 2022).

Furthermore, the temperature also has a significant influence on MFCs. Studies report that efficient power density output performance occurs between 30 °C and 45 °C (SURANSH et al., 2023). In this study, the MFC was acclimated in a biochemical incubator at 35 ± 2 °C, resulting in 60.6 mW m^{-2}. This can be explained by the fact that bacteria have maximized metabolic activities, while lower and higher temperatures lead to biofilm decomposition and inactivation of bacterial metabolic activities (JAFARY; GHOREYSHI; NAJAFPOUR, 2010; OBILEKE et al., 2021). Michie et al. (2013) also noted that the performance was much more significant when operated at 35 °C than at 10 °C, 7.2 W m^{-3} and 1.07 W m^{-3}. The elevated temperature also accelerates bacterial growth, reducing the time to onset. Patil et al. (2010) reported that the time needed for biofilm formation decreased from 40 to 3.5 days when the temperature increased from 15 to 35 °C. When applied at 40 °C, Oliot et al. (2017) observed that the biofilm formation time was reduced by 50%, from 40 to 20 days. The CEs were 47.4 ± 9.4% and 42.9 ± 11.9% at 40 °C and 25 °C, respectively. The efficiency of the MFC in converting the chemical energy of microbial degradation into electricity can be improved at higher temperatures since there is often an increase in the rate of electron transfer at the electrode (SAVLA et al., 2022).

In the MFC-1000Ω, a significant increase in operational efficiency was observed from day 1 to 20 (Table 5). The CE increased from 0.52% to 4.88%. Furthermore, the increase higher than 99% (0.4 to 60.6 mW m^{-2}) in generating power density in the MFC-1000Ω can also be directly related to the selection and augmentation of the electrogenic bacterial community (section 3.3.3 - Fig. 7). On day 20, the FE achieved a 4.47% conversion to a fixed 1000 Ω R_{ext}. One of how acclimation can favor the increase in FE of an MFC is by improving the electrochemical adhesion between the electrons produced during microbial oxidation and the cell's electrode. In addition, the rate of electron transport to the electrode can also be accelerated by acclimation, which can increase the enzymatic activity of microbial cells. The cell can release more electrons from the substrate, controlling microbial oxidation enzymes to make it more effective (GUO et al., 2021; JIN et al., 2022; THAPA et al., 2022).

3.3.3 Microbial community analysis

The role of MFC in the generation of electrical current and H_2O_2 synthesis requires an understanding of the microbial community. Organic matter-degrading microorganisms, electrogenic and fermentative bacteria, and other types of microorganisms with specific functions can work together to decide the overall performance of the MFC. The 16S rRNA sequencing was used to evaluate the diversity and structure of the microbial community of the biofilm acclimated for 20 days in the MFC-1000Ω. The alpha diversity results, as presented in Table 6, indicated a notable change in the microbial community structure when comparing the inoculum with the MFC. This highlights the considerable impact of MFC-induced conditions (substrate, temperature, and pH) on microbial diversity and richness.

Table 6 - Numbers of rRNA sequences analyzed and alpha diversity indices for the microbial communities in the inoculum and MFC biofilm after 20 days of acclimation

Samples	Raw reads	Effective reads	Microbial richness (OTU)	Microbial diversity (Shannon)
Inoculum	105,049	29,469	181	6.51
MFC	128,777	23,185	119	5.87

The Shannon index, representing diversity in the microbial community in a sample, revealed a decrease in MFC compared to the inoculum (Shannon index 5.87 vs. 6.51, respectively, Table 6). Furthermore, the microbial richness, as indicated by the number of unique species (OTUs) in a sample, was lower in the MFC (119 OTUs) than in the inoculum (181 OTUs). These results showed that the MFC reactor operated with the same anaerobic sludge inoculum, but the microbial community structure differed for the inoculum and the MFC. Recent research has demonstrated that the most energy-efficient bacteria can selectively suppress less adaptable microorganisms in the MFC (PRATHIBA; KUMAR; VO, 2022). These findings support that bioelectrochemical circumstances may promote suppression of the metabolic diversity of the system. A lower Shannon index and OTU in the MFC indicated that the operational conditions favored the enrichment of specific microorganisms involved in H_2O_2 synthesis through electrosynthesis, potentially enhancing the efficiency. For an MFC system Lesnik et al. (2019) and Rossi; Logan (2020), reducing microbial diversity and richness can make the system more stable, less susceptible to environmental changes, and, consequently, more predictable for the H_2O_2 concentration.

Principal coordinates analysis (PCoA) was used to investigate the microbial structural patterns of the top 20 genera identified (Fig. 6). The principal coordinates described PCo1 (41.28%) and PCo2 (35.76%) of the normalized data variance. Through the PCoA diagram, the beta diversity analysis supported the alpha diversity results, showing the difference in the microbial community structure between the samples. Similar results found in MFCs have been reported in recent studies (HEMDAN et al., 2023; MILLS et al., 2022).

Figure 6 - PCoA ordination using the genera abundance data to represent the differences between the investigated microbial communities

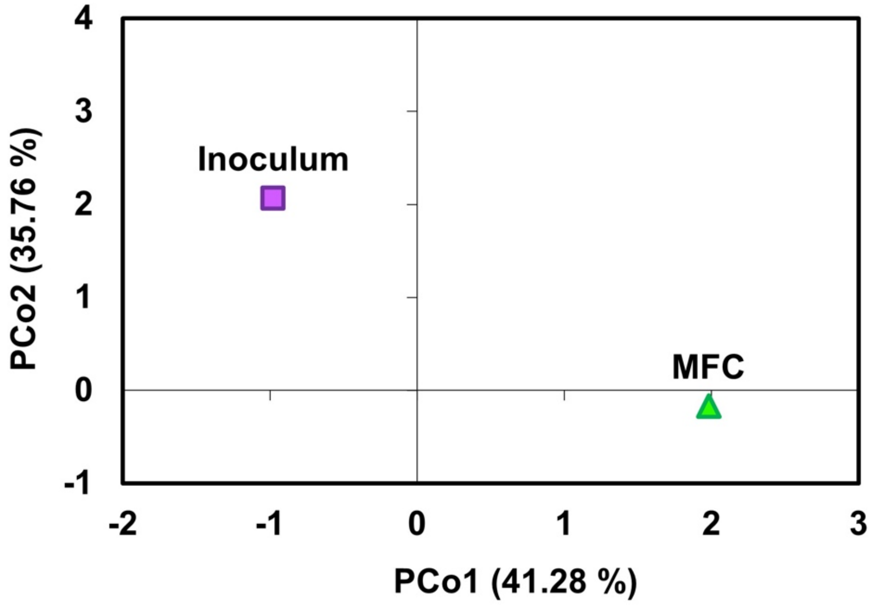

According to Fig. 7(A), the two large groups formed and represented by the two large clusters of dendrograms show the structural differences between the bacterial genera identified in the inoculum and MFC. The operational conditions in the MFC acclimation process favored the development of electrogenic bacteria belonging to the phyla Proteobacteria (genera Kerstersia, Chelatococcus, and Ochrobactrum), Firmicutes (genera Acetoanaerobium and Clostridium_sensu_stricto_9), and Bacteroidota (genus Petrimonas). Proteobacteria was the phylum with the highest abundance compared to the other microbial groups in the MFC, corresponding to 62% of the relative abundance (Fig. 7B). Most of the electrogenic bacteria in MFCs are identified as gram-negative bacteria affiliated with the phylum Proteobacteria (ZHI et al., 2014). Comparing the MFC with the inoculum, the relative abundance of microbial communities from the phyla Proteobacteria and Firmicutes increased by 54.7% and 64.3%, respectively, in the MFC. In contrast, the abundances of Chloroflexi, Actinobacteriota, and Desulfobacterota decreased by 89.8%, 84.5%, and 84.4%, respectively, in the MFC. However, in a smaller proportion, the following phyla were also identified only in the inoculum (Fig. 7B): Synergistota, Caldisericota, Halobacterota, Acidobacteriota, SAR324, Bdellovibrionota, Myxococcota, Campilobacterota, and Patescibacteria, corresponding to 4.5%. For the MFC, the minority diversity was more selective, with only 1.8% corresponding to the phyla

Cyanobacteria, Synergistota, Caldisericota, and Campilobacterota. Previous studies found similar results (CAO et al., 2021; LONG et al., 2019a; ZHANG et al., 2019c).

Figure 7 - (A) Taxonomy of the most prevalent genera in the Inoculum and MFC samples; and (B) The 20 top phyla's relative abundance in percentage according to inoculum and MFC-acclimated biofilm

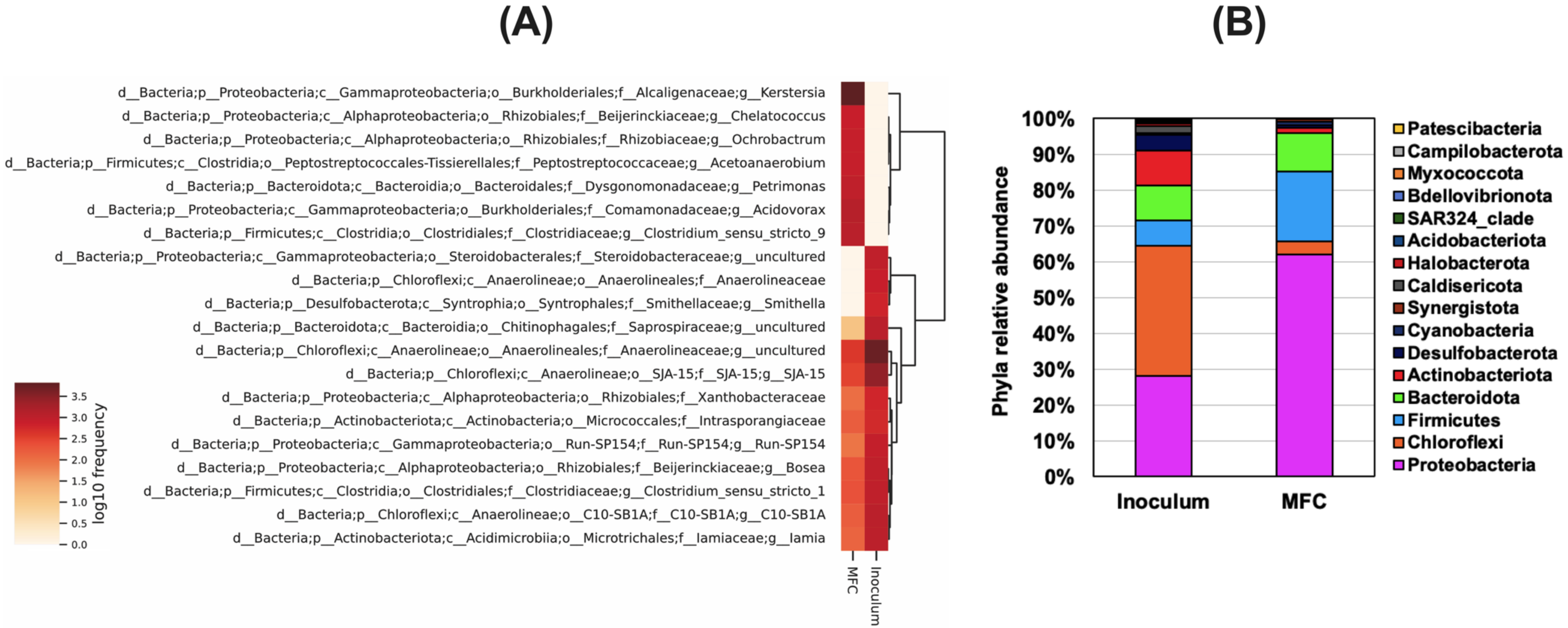

Microorganisms are grouped based on their relative abundance, as shown in the dendrogram on the right.

The darker the color on the frequency scale, the more abundant the genus in the sample (d: Domain; p: Phylum; c: Class; o: Order; f: Family; g: Genus)

Fig. 7(A) shows the microbial community composition according to taxonomic classification (domain, phylum, class, order, family, and genus). In the inoculum, the communities were composed mainly of uncultured genera of the family Anaerolineaceae (39%); SJA-15 (20%); C10-SB1A, Lamia, and uncultured of the family Saprospiraceae (8%); Clostridium and Bosea (7%); and Rhizobiaceae (2%). Anaerolineaceae is the predominant proportion of anaerobic digestive systems in wastewater treatment plants (OWUSU-AGYEMAN et al., 2019). This strain has been considered a typical fermentative population within the microbial community that has also been reported in the MFC (LU; XING; REN, 2015; SIEBER; MCINERNEY; GUNSALUS, 2012; XIA et al., 2016). For proper electricity generation in a MFC, fermentable substrates must be degraded into acetate (PARK et al., 2017). These vast populations of fermentative bacteria are thought to thrive in conjunction with the anaerobic electroactive biofilm at the anode, which is volume-facing, where oxygen bioavailability is feasible if the anolyte is not fully anaerobic. The oxygen that enters the anode is rapidly depleted by its potential synergistic involvement in the anaerobic microbial composition (SANTORO et al., 2021).

Figure 7 (A) shows that the two clusters represent the microbial genera influenced by the MFC acclimation process. The relative abundance of uncultivated genera of the Anaerolineaceae family was suppressed by approximately 92.3% in the MFC. Furthermore, the relative abundance of the genus Kerstersia was 42%, the highest among all identified genera. Kerstersia comprises *K. gyiorum* and *K. similis* belonging to the Proteobacteria phylum, known for their direct electron transfer capacity (KHAN et al., 2021; SUN et al., 2023). Given the lack of data on its electron transfer capacity, Petrimonas (Bacteroidota family) emerged as one of the leading genera in this study. It is a fermentative acidogenic bacterial genus that can transfer and, at the same time, use electrons to produce hydrogen (H^+) (DAI et al., 2020b; DINH et al., 2021). Pandoraea and Petrimonas are fermentative bacteria and have been reported in MFCs (SUN et al., 2012; TABATABAEI; DASTBARSAR; MOSLEHI, 2019). According to Schröder (2007), some metabolic byproducts of fermentation can be oxidized on the electrode surface. These substances can serve as intermediates for electron transfers, absorbing electrons from electron-transporting cellular networks and diffusing them to the electrode surface, known as direct interspecies electron transfer (DIET)-based syntrophic metabolism

(GRABOWSKI et al., 2005; ZHAO; ZHANG, 2021). Another genus in the MFC cluster was Clostridium, considered a significant producer of caproate for chain elongation in the microbial consortium fermentations (QIAN et al., 2020; VASSILEV et al., 2021). It has generally been shown that redox pairs, outer membrane cytochromes (OMCs), or pili are responsible for extracellular electron transport (GU et al., 2021). In addition, the genera of the family Rhizobiaceae have been shown to express unipolar polysaccharide adhesion, which, as extracellular polymeric substances, can promote irreversible fusion under the anode electrode (KOKKO et al., 2015). Therefore, the increasing number of Rhizobiales should be another significant factor for the faster onset of the acclimated inoculum of the MFC. The synergistic impact of Rhizobiales and conductive bacterial nanowires can be responsible for good electrochemical performance (FRITTS et al., 2017; ZHANG et al., 2019a).

In extracellular anaerobic respiration via MFC, effective electron transfer has been hindered by the thickness and composition of the cell walls of gram-positive bacteria (CHENG et al., 2023). They have a more direct chemical composition with 10% teichoic acid and 90% peptidoglycan (JUANG et al., 2011). This explains why gram-negative bacteria make up the majority of documented electrogenic bacteria. The genera Kerstersia, Chelatococcus, Ochrobactrum, Pandoreae, and Petrimonas identified in the MFC are considered gram-negative bacteria (DEBBARMA et al., 2023; VAYENAS, 2011; WHITBY, 2022). They have thin cell walls with cell membranes composed of only approximately 10% peptidoglycan and the rest of the protein. This facilitates the transfer of electrons but makes them more susceptible to environmental stress (SONG et al., 2019).

For a more comprehensive analysis of microbial community dynamics in the MFC acclimation process, including pH, substrate, and temperature as the main operational variables, a canonical correspondence analysis diagram (CCA) (Fig. 8) was used to represent these interactions. The CCA indicated that the genera Pandoraea (1%) and Kerstersia (42%) were strongly related to temperature in their abundances. Temperature directly influences the performance of an MFC, such as the metabolic activity of microbes, extracellular electron transfer, and decrease of ohmic resistances with the formation of a stable biofilm (SIDDIQUI et al., 2023; VERMA et al., 2021b). In this study, the MFC reactor was operated in an environment with a controllable temperature of 35 ± 2 °C. Furthermore, pH control did not direct the development of microorganisms correlated with the conversion of the substrate into electrical current. For example, the genera Panninobacter and Acidovorax showed a favorable relationship with pH. However, these genera were negatively correlated with MFC operational metrics (CE and H_2O_2) (Fig. 9). The low proton transport rate between the anode and cathode can alter the pH and affect the MFC performance. Acidification at the anode due to the accumulation of H^+ decreases the pH, and low pH can inhibit the growth of electrogenic microorganisms (MUNOZ-CUPA et al., 2021).

Figure 8 - CCA diagram showing relationships of 20 dominant genera associated with the variables highlighted in red color (pH, substrate, and temperature)

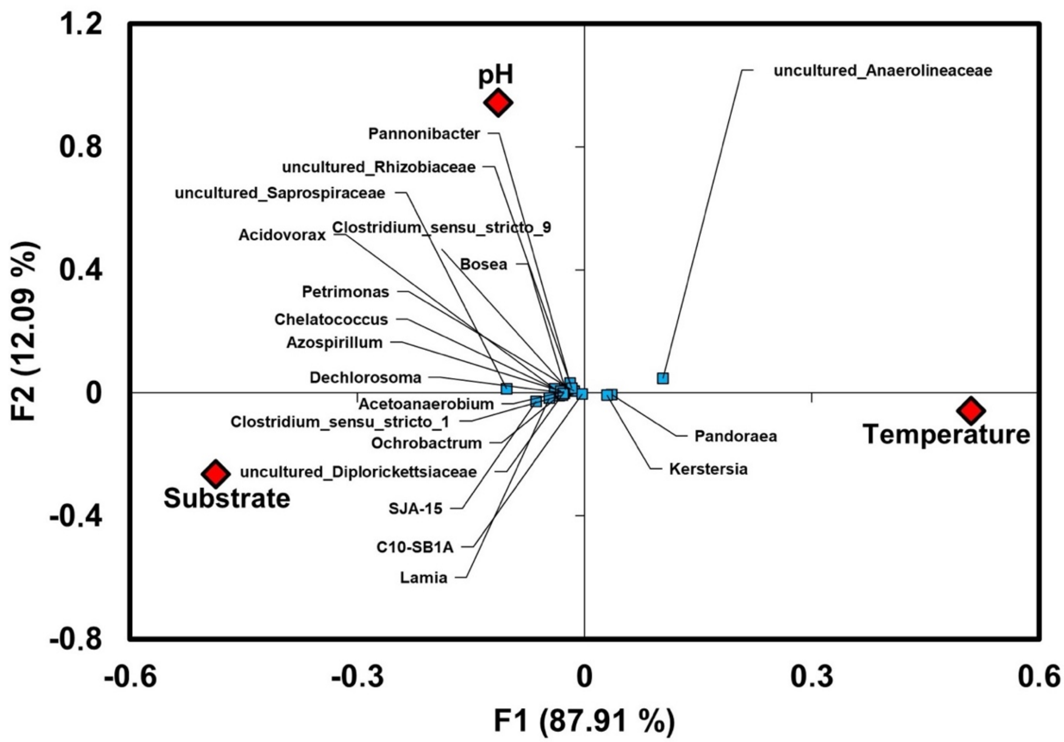

Furthermore, the substrate affected the performance of electroactive bacteria on the surface of the anode. According to the CCA (Fig. 8), the specific substrate (sodium acetate) impacted some microbial groups that were loaded with this variable; that is, the substrate impacted the relative abundance of these genera, which influenced their structure. This findings agree with the results found by previous studies (ISHII et al., 2017;

SANTORO et al., 2021). The development of bacteria belonging to the phylum Proteobacteria (Dechlorosoma, Chelatococcus, and Ochrobactrum, for example) and Firmicutes (Clostridium and C10-SB1A, for example) was promoted by the substrate. Given that the operation of MFC imposed a constant selective pressure on the microbial processes of extracellular electron transfer, it can be inferred that the taxonomic differences between the microbial communities of the inoculum and MFC were mainly due to the specific feeding system and pH control. This indicates that comparing microbial populations as a function of different operational conditions allows an understanding of the specific taxonomic groups associated with electricity generation in MFC reactors.

According to Fig. 9, several significant correlations were identified among the top 20 genera abundant in MFC related to performance metrics (CE, FE, COD removal, current, and H_2O_2). The Pearson correlation coefficient (r) was interpreted as a strong correlation when $r \geq 0.9$ and a moderate correlation when $0.5 \leq r < 0.7$ (COHEN; COOLEY, 1988; MILTON; BULL; BAUMAN, 2011). Overall, 10 genera highlighted significant impacts on the positive correlation between the performance results of the MFC acclimation process. Pandoraea, Kerstersia, and C10-SB1 significantly impacted the conversion of the organic substrate into an electric current and H_2O_2 synthesis ($r > 0.7$). These genera belonging to the phyla Proteobacteria and Chloroflexi are considered partially electrogenic microorganisms. Our findings agree with the results of recently published studies (CAI et al., 2021; LONG et al., 2019a; WANG et al., 2022b). Pandoraea and Petrimonas, for example, are gram-negative and fermentative bacteria considered pathogenic to humans and some animals (AMBROSE et al., 2016; PITHER et al., 2021). However, in studies aimed at H_2O_2 synthesis or production of green hydrogen in MFCs, these bacteria have been reported due to their contributions to the production of H^+ (CHEN et al., 2021; WANG et al., 2018). The positive correlations of the genera Pandoraea and Petrimonas ($r > 0.700$) shown in Fig. 9 significantly impacted the overall efficiency of the MFC. However, the electron transfer mechanisms and metabolic behavior of these genera in MFCs are still unknown.

The genera predominantly belonging to the phylum Proteobacteria highlighted in red (Fig. 9) were negatively correlated ($r < 0$) with the performance metrics of the investigated MFC. Most bioelectricity generation systems are limited by their ability to generate electric current because complex natural electroactive communities have poorly defined microbial species that can interact positively (mutualism, symbiosis) or negatively (parasitism, antagonism) (AJUNWA et al., 2021).

Figure 9 - Pearson's correlation analysis (r) between the 20 dominant microbial genera in the MFC and the efficiencies of substrate conversion into electric current and H_2O_2

Genus	CE	FE	COD removal	Current	H_2O_2
Pandoraea	0.804	0.920	0.756	0.894	**0.952**
Kerstersia	0.757	0.843	0.691	0.819	0.893
uncultured_Anaerolineaceae	0.498	0.811	0.458	0.718	0.815
Petrimonas	0.610	0.831	0.553	0.765	0.859
SJA-15	0.080	-0.297	0.147	-0.161	-0.314
Ochrobactrum	0.474	0.221	0.560	0.336	0.178
Dechlorosoma	0.180	-0.057	0.068	-0.012	0.061
Pannonibacter	-0.433	-0.169	-0.519	-0.286	-0.126
Clostridium_sensu_stricto_9	-0.078	0.258	-0.157	0.132	0.289
Acidovorax	-0.728	-0.604	-0.804	-0.684	-0.558
Acetoanaerobium	0.576	0.774	0.507	0.710	0.815
Clostridium_sensu_stricto_1	0.721	0.316	0.733	0.463	0.350
Bosea	0.431	0.540	0.533	0.548	0.447
C10-SB1A	0.853	0.913	0.803	0.904	**0.952**
uncultured_Rhizobiaceae	0.455	0.614	0.549	0.606	0.522
Chelatococcus	0.948	0.679	0.935	0.784	0.722
Lamia	0.030	-0.436	0.050	-0.288	-0.406
Azospirillum	-0.316	-0.081	-0.206	-0.130	-0.198
uncultured_Diplorickettsiaceae	0.842	0.481	0.825	0.609	0.536
uncultured_Saprospiraceae	-0.576	-0.695	-0.490	-0.651	-0.757

Scale
1
0.5
0
-0.5
-1

Strong correlation when r ≥ |0.9|; moderate correlation when |0.5| ≤ r < |0.7|). Colors: red - negative correlation; blue - positive correlation. The black line indicates which microbial group had trends in the parameters. Values in bold differ from 0 with a significance level (alpha=0.05)

According to the results, several metabolic abilities are believed to be related to the diversity of the microbial population in the biofilm. The most abundant bacterial genera identified in the MFC correlated satisfactorily with operational efficiency metrics. Pearson coefficients showed that the acclimation process may have promoted microorganisms of interest for generating electrical current and synthesizing H_2O_2 in the MFC. This is because MFC can stimulate the development and metabolic adaptation of electroactive microorganisms and other communities capable of creating synergies between microbial populations. This approach aims to understand and control the MFC for H_2O_2 synthesis, paving the way for practical applications that benefit sectors such as sustainable energy and pollutant treatment.

3.4 CONCLUSION

The acclimation process of a microbial consortium from a domestic effluent treatment plant was carried out in an MFC to synthesize H_2O_2. After 20 days of operation, the MFC increased the CE, FE, power density, and H_2O_2 concentration by 4.88%, 4.47%, 60.6 mW m^{-2}, and 15.17 mg L^{-1}, respectively. According to the microbial community analysis, developing a biofilm composed predominantly of electrogenic bacteria during the acclimation process was responsible for the MFC performance.

The predominant phyla in the MFC were Proteobacteria (62%) and Firmicutes (19.6%). However, the phyla Proteobacteria (62%) and Chloroflexi (3.7%) showed a significant relationship ($p < 0.05$) in all MFC operational metrics. Although it is known that temperature influences electrogenic bacterial development, in this study, it was observed through CCA that the substrate and pH variables had more influence on the microbial community than temperature. Kerstersia (42%) and Pandoraea (1%) were the only genera that showed a correlation with temperature among the entire MFC microbial community. The low OTU (119) and Shannon index (5.87) for MFC indicated that the control and feeding operating conditions imposed during the biofilm acclimation process may have promoted the development of electrogenic bacteria of different synergies. It is essential to highlight that more studies are still needed to improve and optimize the acclimation process and evaluate its economic and environmental viability compared with conventional H_2O_2 synthesis and effluent treatment methods. The ability to synthesize H_2O_2, the next step will be to direct efforts toward its application in treating organic pollutants through the MFC-Fenton association.

4 CAPÍTULO 4 - EVALUATING THE BIO-ELECTRO-FENTON (BEF) PROCESS FOR REMOVAL OF THE REMAZOL BRILLIANT VIOLET-5R (RBV-5R) AZO DYE

ABSTRACT

Given the environmental challenges arising from pollution caused by azo dyes, this study aimed to evaluate the application of the bio-electro-Fenton (BEF) process for Remazol Brilliant Violet – 5R (RBV-5R) removal. In this study, three operational strategies were applied with different RBV-5R concentrations (5, 10, and 20 mg L^{-1}) and external resistances (R_{ext}) (10, 100, and 1000 Ω) for a hydraulic retention time (HRT) of 12 h. According to the results, the strategy using 20 mg RBV-5R L^{-1} and 10 Ω R_{ext}, in general, presented the best efficiencies of color removal, aromatic group degradation, and COD removal, 95.5 ± 0.25%, 73.6 ± 0.4%, and 82.4 ± 0.3%, respectively. The system synthesized 12.25 mg H_2O_2 L^{-1} at a maximum power density of 69.4 mW m^{-2} for a 7.2 ± 0.4% CE and a 5.81 ± 0.1% FE. However, the phytotoxicity analysis showed that after an HRT of 12 h, the germination index (GI) (concentration of 100%) increased from 6.1 ± 1.4% to 39.0 ± 1.4% for *Lactuca sativa* and from 6.8 ± 1.7% to 39.3 ± 1.0% for *Raphanus sativus*. The GIs were low (< 80%) for the operational strategy, indicating the persistence of a posttreatment toxic character. Therefore, this study contributes to understanding the potential of BEF as a promising technology in treating effluents contaminated with azo dyes. However, it also underscores the relevance of additional approaches to completely mitigate residual toxicity. These results provide essential insights for future research and efforts toward sustainable textile pollutant management in industrial settings.

Keywords: microbial fuel cell; bio-electro-Fenton; azo dye; COD removal; phytotoxicity.

RESUMO

Tendo em vista os desafios ambientais decorrentes da poluição causada por azo-corantes, este estudo teve como objetivo avaliar a aplicação do processo bio-eletro-Fenton (BEF) para degradação do Violeta Brilhante de Remazol – 5R (VBR-5R). Neste estudo, três estratégias operacionais foram aplicadas com diferentes concentrações de VBR-5R (5, 10 e 20 mg L^{-1}) e resistências externas (R_{ext}) (10, 100 e 1000 Ω) para um tempo de detenção hidráulica (TDH) de 12 h. De acordo com os resultados obtidos, a estratégia utilizando 20 mg VBR-5R L^{-1} e 10 Ω R_{ext}, em geral, apresentou as melhores eficiências de remoção de cor, grupos aromáticos e DQO, respectivamente, 95,5 ± 0,25%, 73,6 ± 0,4% e 82,4 ± 0,3%. O sistema foi capaz de sintetizar 12,25 mg H_2O_2 L^{-1} a uma densidade de potência máxima de 69,4 mW m^{-2}, para uma EC de 7,2 ± 0,4% e EF de 5,81 ± 0,1%. Entretanto, análise de fitotoxicidade mostrou que após 12 h de TDH o índice de germinação (IG) (concentração de 100%) aumentou de 6,1 ± 1,4% a 39,0 ± 1,4% para *Lactuca sativa* e de 6,8 ± 1,7% a 39,3 ± 1,0% para *Raphanus sativus*. Os IGs foram baixos (< 80%) para a estratégia operacional, indicando a persistência de um caráter tóxico pós-tratamento. Portanto, este estudo contribui para o entendimento do

potencial do BEF como uma tecnologia promissora no tratamento de efluentes contaminados com azo-corantes, embora também ressalte a relevância de abordagens adicionais para mitigar completamente a toxicidade residual. Esses resultados fornecem insights essenciais para futuras pesquisas e esforços voltados para a gestão sustentável de poluentes têxteis em ambientes industriais.

Palavras-chave: célula a combustível microbiana; bio-eletro-Fenton; azo-corante; remoção de DQO; fitotoxicidade.

4.1 INTRODUCTION

Azo dyes are well known for their variety and extensive use in the textile industry (SELVARAJ et al., 2021). They are considered the most important and largest class of commercial dyes, representing between 65% and 75% of all textile dye products (CASTRO et al., 2021; HASHEMI; KAYKHAII, 2022; RAFAQAT et al., 2022). They have resistance to degradation, as they are characterized by aromatic rings joined by one or more azo bonds (N=N) (CHAUHAN; GAUTAM; KANWAR, 2022; ESKANDARI; SHAHNAVAZ; MASHREGHI, 2019). The effluents of textile dyes can be recalcitrant to biodegradation, causing acute toxicity to water bodies due to the presence of several toxic degradation byproducts (GARG; TRIPATHI, 2017; LEKHAK, 2023). Furthermore, a body of water with a low concentration (in ppm) of dye has a reduced aesthetic value. It impacts the photosynthetic process, with less sunlight penetration and a low dissolved oxygen concentration (LEKHAK, 2023).

Over the past several years, the need for effective dyeing effluent decontamination techniques has grown. Advanced oxidative process-based technologies (AOPs) have proven to be highly efficient for treating water with dyes (DENG; BRILLAS, 2023). Electro-Fenton (EF) oxidation, which is one of the most influential and progressive oxidation processes, has been widely used to treat various recalcitrant contaminants (RAJARAMAN; GANDHI; PARIKH, 2021; SARAVANAN et al., 2022). AOPs, such as electro-oxidation, photo-Fenton, and conventional Fenton, are the most effective in reducing the color (> 90%) and organic matter (>78%) of these effluents (ZHANG et al., 2021). However, the main disadvantage of this method is the relatively high cost due to energy consumption (0.98 kWh m^{-3}) and the need for a substantial amount of H_2O_2 when complete degradation is needed. Therefore, new Fenton processes capable of synthesizing H_2O_2 in situ, with low energy consumption and in a sustainable way, have attracted much attention (MONTEIL et al., 2019; ZHAO; ZHANG, 2021). The coupling of Fenton oxidation with microbial fuel cells (MFCs) offers benefits, such as low cost, minimal external energy requirements, and in situ generation of oxidizing agents (SATHE et al., 2022a).

Recently, one of the emerging methods of POAs that has gained attention is the bio-electro-Fenton (BEF) (YANG et al., 2021). The popularity of BEF systems is based on the fact that the hydrogen ions (H^+) needed to synthesize H_2O_2 are generated in the anode by oxidation of organic substrates by electrogenic bacteria, also releasing electrons and CO_2 (OLVERA-VARGAS et al., 2017; SATHE et al., 2022a). This generation and transfer of H^+ and electrons through the mass solution and an external circuit, respectively, is a spontaneous process without any input from the external energy (ZHAO; ZHANG, 2021). H_2O_2 can be generated in a BEF system without external energy input if acetate, for example, is used as an anode substrate (Eq. 20). Then, a two-electron oxygen reduction reaction (2e-ORR) at the cathode can synthetase H_2O_2 (Eq. 21). Iron (Fe^{2+}) is the most widely used catalyst to activate H_2O_2. Then, H_2O_2 interacts with Fe^{2+} to generate hydroxyl radicals (•OH) (Eq. 22). The •OH is very effective in the degradation of highly toxic and persistent pollutants, as it is among the most powerful oxidants, with a very high standard oxidation potential (E = 2.80 V) (NAJAFINEJAD et al., 2023). The Fe^{3+} produced in Eq. 22 is reduced by $1e^-$ to Fe^{2+} (Eq. 23), which is again oxidized in Eq. 22.

$$CH_3COOH + H_2O \rightarrow 2CO_2 + 8H^+ + 8e^- \tag{20}$$

$$O_2 + 2e^- + 2H^+ \rightarrow H_2O_2 \tag{21}$$

$$Fe^{2+} + H_2O_2 \rightarrow Fe^{3+} + OH^- + \bullet OH \tag{22}$$

$$Fe^{3+} + e^- \rightarrow Fe^{2+} \tag{23}$$

Therefore, the BEF process can be used to treat different types of contaminants, such as triphenyl-tin chloride (YONG et al., 2017), anti-inflammatory compounds drugs (NADAIS et al., 2018), surfactants (SATHE et al., 2022b), sulfonated polyethylenes

(GHATGE et al., 2022), medicinal herbs (BIRJANDI et al., 2020), metropolol (YANG et al., 2021), arsenic (WANG et al., 2014), mesotrione (ZHAO; ZHANG, 2021), landfill leachate ((HASSAN et al., 2017; LINH; HO, 2020; YANG et al., 2022), antibiotics (LI et al., 2022), biological nitrogen removal (NGUYEN; BABEL, 2022), hydroponic crop effluent ((BRYSZEWSKI; RODZIEWICZ; JANCZUKOWICZ, 2022), sulfates (DAI et al., 2022), effluents from beverage industries (AFOLABI; ADEKALU; OKUNADE, 2022), p-nitrophenol (WANG et al., 2022c), and textile azo dyes (FENG et al., 2010b; LIU et al., 2012; WANG et al., 2022b; XU et al., 2020b; YUAN et al., 2017; ZHANG; WANG; ANGELIDAKI, 2015a). Considering the success of the Fenton-based process in the treatment of textile dyes, the BEF coupled system has high potential energy generation potential in the treatment of dyes in the textile effluents (WANG et al., 2023). Applying BEF, Wang et al. (2022b) achieved 93.5% methylene blue (MB) decolorization with 20.18 mg H_2O_2 L^{-1} and a power density of 1.99 W m^{-3}. Ling et al. (2016) obtained 86.7% removal of methyl orange (MO) with only 88.63 mmol H_2O_2 L^{-1}. In the study by Dios et al. (2014), the removal efficiencies of green lissamine B, carmine indigo, crystal violet, and reactive black 5 were 98.2%, 97.2%, 96.2%, and 88.2%, respectively, in just 15 minutes. Yang et al. (2016) obtained a corresponding 94.90 ± 0.01% decolorization efficiency with a constant reaction rate of 0.503 ± 0.001 h^{-1}. Although these studies evaluated the BEF for dye removal, the focus remains more on energy generation and decolorization than on the COD removal and detoxification of waters with textile azo dyes after BEF treatment (FATIMA et al., 2017; ILAMATHI; JAYAPRIYA, 2018; SABA et al., 2018; SINGH; DAHIYA; MISHRA, 2021; SOLANKI; SUBRAMANIAN; BASU, 2013).

Therefore, this study aimed to evaluate the RBV-5R dye removal efficiency regarding color and COD removal, aromatic group degradation, and phytotoxicity assessment. In this study, three operational strategies were used using different azo dye concentrations (5, 10, and 20 mg L^{-1}) with different external resistances (R_{ext}) values (1000, 100, and 10 Ω) for a hydraulic retention time (HRT) of 12 h. Furthermore, phytotoxicity analyses were carried out with raw samples at time t=0 h and samples collected from BEF after t=12 h of treatment.

4.2 MATERIALS AND METHODS

4.2.1 Azo dye

The azo dye Remazol Brilliant Violet 5R (RBV-5R) was obtained from Dystar® Brazil with a high laboratory grade. The textile industry has used this dye for dyeing and printing cotton, silk, and linen. As a reactive dye, it is used to dye cellulosic fibers (RÁPÓ et al., 2020). The physicochemical characteristics of the dye are shown in Table 7. The 1.0 g L^{-1} stock solution was prepared with deionized water by dissolving the dark violet powder. The solution was used without any further purification.

Table 7 - Chemical structure of the reactive azo dye

Dye name	Remazol Brilliant Violet-5R (RBV-5R)
Chemical structure	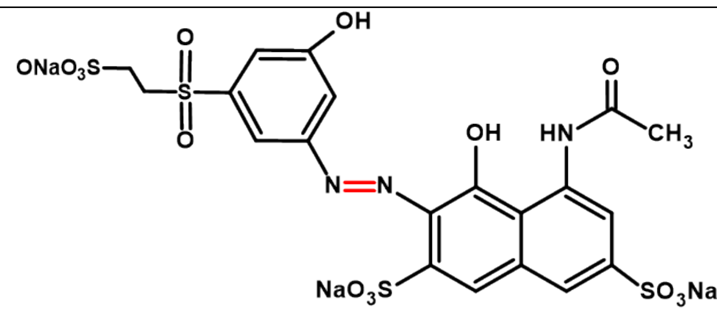
Molecular formula	$C_{20}H_{16}N_3Na_3O_{15}S_4$
Molecular weight	735.58 g mol^{-1}
Color Index	18097
CAS number	12226-38-9
Purity	≤ 95%
Melting point	~ 360 °C
λ max	554 nm

Source: Adapted from Lai (2021)

4.2.2 BEF setup

The MFC reactor was a dual chamber H-type glass apparatus (Fig. 9) with an effective volume of 250 mL. A proton exchange membrane (PEM) separated the two chambers (Nafion 117, DuPont Co., USA). Nafion 117 was previously treated with H_2O_2 5%, H_2SO_4 5% w/w, and deionized water. The anodic electrode was a carbon fiber brush (MiliRose, USA) pretreated at 450 °C for 20 min (YANG et al., 2022). The cathode electrode was graphite felt (A_{cat} = 3.10^{-3} m^2) (MIRONG, China). A titanium wire 0.8 mm in diameter was connected to the electrical circuit with R_{ext}. A data acquisition system (HM-2030, Hikari) was connected to the MFC to monitor voltage and electrical current output. A small air pump (SC-7500, Boyu) was coupled to the system for aeration in the cathode chamber.

Figure 10 - The BEF reactor configuration with the data acquisition system

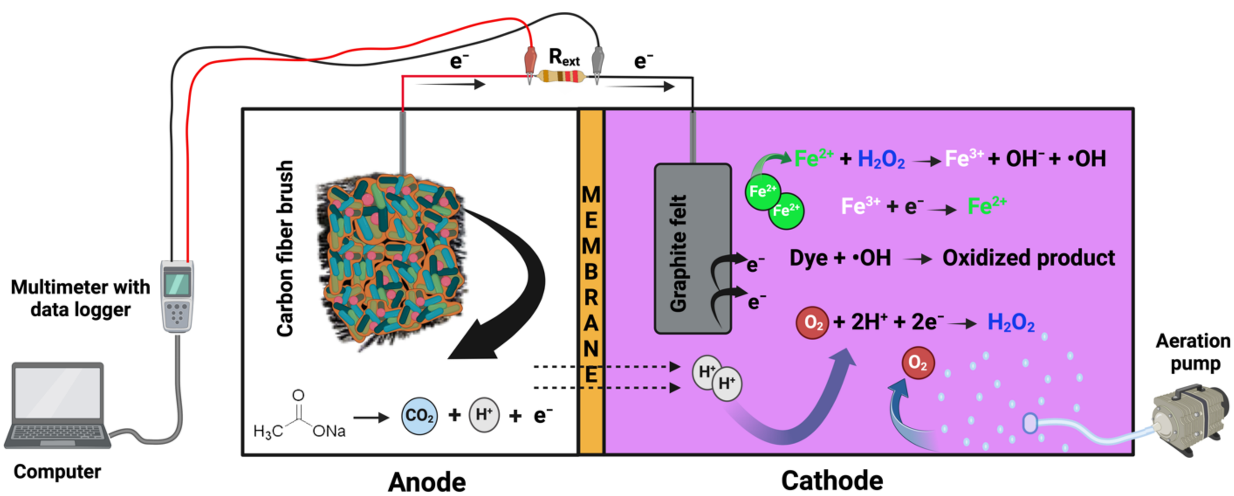

Source: Author (2023)

4.2.3 Operational strategies

Serial acclimation was implemented to develop a stable biofilm. The inoculum consisted of a mixed consortium of bacteria collected from an anaerobic tank in a domestic wastewater treatment plant (Florianópolis, Brazil). Acclimation was performed by feeding the reactors with sludge and growth medium (1:1) every 24 hours until maximum voltage output was achieved. The growth medium was composed of the following in g L^{-1}: sodium acetate – $C_2H_3NaO_2$ (1.0); phosphate buffer solution (PBS): $Na_2HPO_4 \cdot H_2O$ (4.28), NaH_2PO_4 (2.74), NH_4Cl (0.31); e KCl (0.13); 12.5 ml L^{-1} of minerals (mg L^{-1}): $MgSO_4.7H_2O$ (10.0), $MnCl_2.4H_2O$ (3.0), $MgCl_2 \cdot 6H_2O$ (10.0), $CoCl_2.6H_2O$ (1.0), $NiCl_2.6H_2O$ (2.0), $NaMoO_4.7H_2O$ (3.0), H_3BO_3 (30.0) and $CuCl_2.2H_2O$ (1.0) e $CaCl_2 \cdot 2H_2O$ (1.0); and 5 ml L^{-1} of vitamin solution (IQBAL et al., 2022; ROSSI et al., 2019; TAN et al., 2022; YU et al., 2020). Nitrogen gas was applied before each feeding cycle to obtain an anaerobic environment in the anodic chamber (ALMEIDA et al., 2021). The MFC anode chamber was fed during each operation cycle until the voltage dropped to < 50 mV, considering a full-cycle operation. Acclimation was completed at 35 ± 2 °C, with 1000 Ω R_{ext} (VICARI et al., 2018).

During acclimation, the cathodic solution consisted of H_2O and 50 mM sodium sulfate (Na_2SO_4) at pH 3.0, enabling ideal conditions for the BEF start-up process. After many full-cycle operations achieved 250 mV, the MFC was fed only PBS, sodium acetate (1.0 g L^{-1}), mineral solution, and vitamins. The BEF reached stable operation in 20 days. In the cathode chamber, for a volume of 250 mL, the electro-Fenton (EF) reagents (68.5 mg $FeSO_4.7H_2O$ and 1.77 g Na_2SO_4) and the different RBV-5R concentrations (5, 10 and 20 mg L^{-1}) were introduced in the batch-feeding system at pH 3.0. The pH adjustment was performed with 0.1 M NaOH and 0.1 M H_2SO_4. The BEF performance was investigated using three operational strategies with a continuum HRT of 12 h (Table 8). The temperature was maintained at 35 ± 2 °C during the operation in a biochemical incubator.

Table 8 - Operational strategies applied in the BEF for HRT = 12 h

Parameter	**Strategy**		
	S1	**S2**	**S3**
RBV-5R (mg L^{-1})	5.0	10.0	20.0
R_{ext} (Ω)	1000	100	10

4.2.4 Analytical procedures

The BEF system performance was evaluated regarding RBV-5R decolorization, aromatic group degradation, COD removal, and H_2O_2 concentration. All samples were collected in the cathode chamber and filtered through a 0.45 µm membrane before analysis. The operational strategies were conducted in duplicate. The COD was measured by spectrophotometry (Hach DR3900) according to the procedure described in Hach 8000, based on oxidation by the dichromate method (APHA, 2018). The pH was measured with a multiparameter probe (AK88, Akson). RBV-5R decolorization (λ = 554 nm) and aromatic group degradation (λ = 318 nm) were measured by scanning analysis ranging from 190 to 1100 nm with a UV–Vis spectrophotometer (BEL Photonics, UV - M51). The determination of H_2O_2 concentration followed the methodology proposed by Wang et al. (2022b). The method is known as iodine (I_3^-), where a 2 mL sample is added to 1 mL of iodide reagent containing 0.40 mol L^{-1} KI, 0.06 mol L^{-1} NaOH, 10^{-4} mol L^{-1} $(NH_4)_2MoO_4$ and 1 mL of $KHC_8H_4O_4$ (0.10 mol L^{-1}). Reagents were used to measure absorbance at λ = 352 nm.

4.2.5 Calculation

The voltage was measured using a digital multimeter with a data logger. The current, I [mA], was calculated according to Ohm's law (Eq. 24), where U is the voltage [mV], and R_{ext} is the external resistance (Ω). Current densities (j, mA m^{-2}) (Eq. 25) and power densities (PD, mW m^{-2}) (Eq. 26) were normalized to the total exposed cathode projected area (3.10^{-3} m^{-2}).

$$I\ (\text{mA}) = \frac{U}{R_{ext}} \tag{24}$$

$$j\ (\text{mA m}^{-2}) = \frac{I}{A} \tag{25}$$

$$PD\ (\text{mW m}^{-2}) = \frac{U^2}{R_{ext}\ A} \tag{26}$$

The polarization curve was generated by varying the external resistance, setting the MFC to open the circuit for at least 10 min or until a stable voltage was observed, and lowering the external resistance from 1000, 500, 200, 100, 55, 20, and 10 Ω at 10 min intervals. Moreover, the MFC performance was evaluated regarding COD and H_2O_2 conversion efficiency. Coulomb efficiency (CE), defined as the fractional recovery of electrons from the substrate, was calculated according to Eq. (27). Faraday efficiency (FE) is defined as the ratio of the electricity consumed by the electrode reaction to produce H_2O_2 and the total electricity of the reaction system. The value can be obtained according to Eq. (28).

$$\mathrm{CE}\ (\%) = \frac{8\ \int_0^t \mathrm{I}\ dt}{\mathrm{F\ V}\ \Delta\mathrm{COD}}\ .\ 100 \tag{27}$$

$$\mathrm{FE}\ (\%) = \frac{\mathrm{n\ F\ C_{H_2O_2}\ V}}{\int_0^t \mathrm{I}\ dt}\ .\ 100 \tag{28}$$

where I is the average current (mA), t is the hydraulic retention time (s), F is Faraday's constant (96485 C mol^{-1}), n is the number of electrons exchanged per mole of oxygen (2 mol e^{-} mol^{-1}), V is the cathode chamber volume (L), ΔCOD is the change in COD over time t (g L^{-1}), and $C_{H_2O_2}$ represents the measured concentration of H_2O_2 (mg L^{-1}) (BOAS et al., 2022; HASSAN et al., 2019; SIM et al., 2015).

4.2.6 Phytotoxicity assessment

The toxicity evaluation will be performed through phytotoxicity analysis with samples collected before and after treatment via BEF using *Lactuca sativa* (lettuce) and *Raphanus sativus* (radish) seeds (ISLA PRO). The assay involves exposing ten seeds of each plant in Petri dishes lined with filter paper. Before revealing the seeds, the filter paper was soaked in 4 mL of samples in different concentrations of each sample (100, 75, 50, and 25%). The Petri dishes were isolated with parafilm to avoid moisture loss and incubated for 120 h under a temperature-controlled environment (25 °C) and without light. Deionized water was used as the positive control, and 0.5 M $ZnSO_4$ was used as the negative control. The radicle length and seed germination percentage in the treated sample vs. the control results were used to determine the germination index (GI) (LUO et al., 2018). Phytotoxicity was determined by calculating the GI, according to Eq. (29) (DE ARAÚJO et al., 2022; SHARIFI et al., 2022).

$$\text{GI (\%)} = \frac{\text{GSS x RLS}}{\text{GSC x RLC}} \text{ x } 100 \tag{29}$$

where GSS represents the number of germinated seeds in the sample, GSC represents the number of germinated seeds in the control, RLS represents the radicle length in the sample, and RLC represents the radicle length in the control.

4.2.7 Data analysis

Prism9 software (GraphPad, version 9.2) was used to reveal the effects of the mean and standard deviation of RBV-5R concentration on color removal efficiency, COD, H_2O_2 concentration, and phytotoxicity in the treatment via BEF. ANOVA was applied to test differences between means of data with normal distribution, followed by the Tukey test. The difference was considered significant when $p < 0.05$. All operational strategies were carried out in duplicate.

4.3 RESULTS AND DISCUSSION

4.3.1 RBV-5R removal

Fig. 10 shows the UV–visible spectrum evolution as a function of the reaction time for different concentrations of RBV-5R and external resistances applied in the BEF, according to each operational strategy (Table 8). Before treatment (t = 0 h), the dye UV–Vis spectrum shows an absorption broadband at λ = 554 nm, which characterizes the azo chromophore group (N=N), and another band at λ = 318 nm characteristic of aromatic groups. A gradual reduction in the absorbance of the absorption bands was observed over time, indicating that the large conjugation system formed by the aromatic rings (benzene and naphthalene) linked to the N=N bond, responsible for the emitted color, was gradually destroyed, thus promoting RBV-5R removal.

Figure 11 - UV-vis spectra evolution as a function of reaction time for (A) S1, (B) S2, (C) S3 strategies, and (D) RBV-5R removal rate

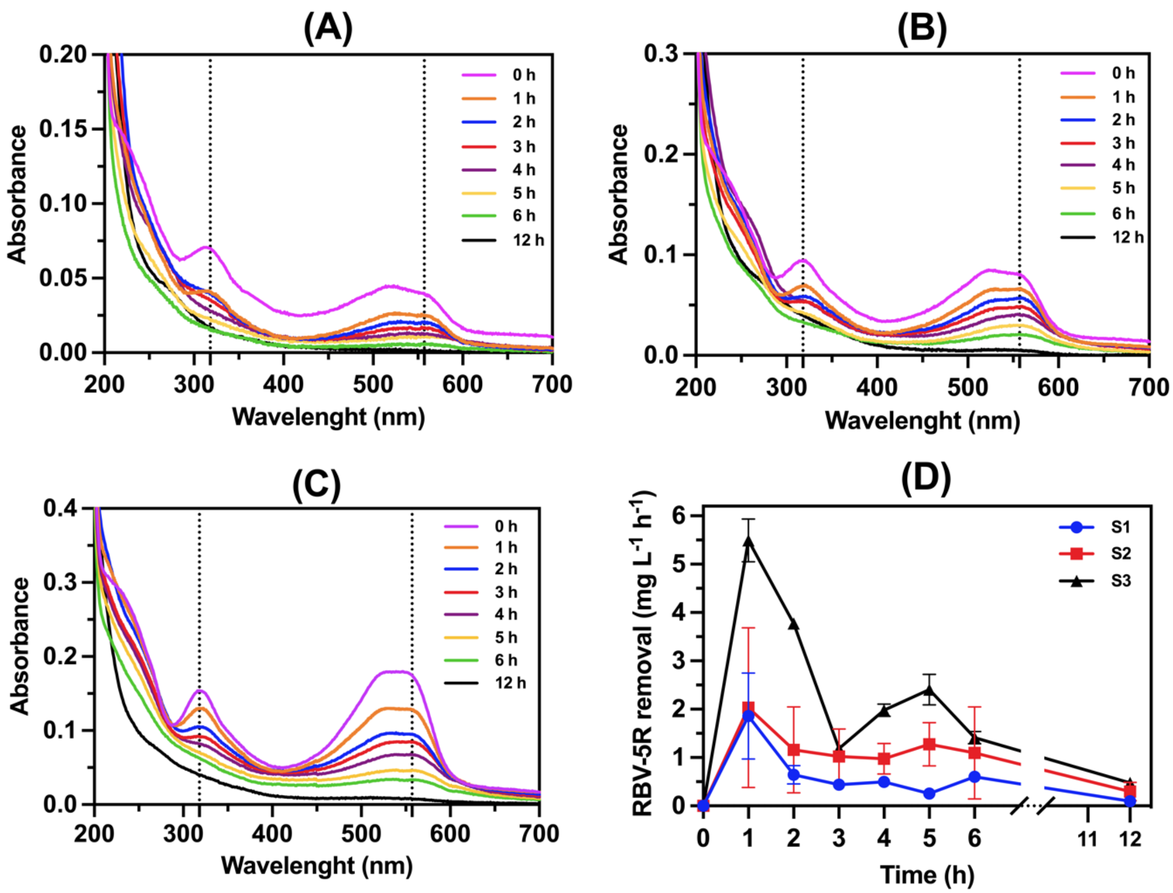

In strategy S1 (Fig. 10A), the highest RBV-5R removal rate occurred at t = 1 h (Fig. 10D), with a value of 1.86 ± 0.01 mg RBV-5R L^{-1} h^{-1} and an approximately 37.2% removal efficiency. However, at 2 h, the BEF reached only 0.64 ± 0.070 mg RBV-5R L^{-1} h^{-1}. As the reaction time increased, rates followed a decline in RBV-5R removal, and after 12 h, the removal rate was 0.09 ± 0.02 mg RBV-5R L^{-1} h^{-1}. However, after a 12 h reaction time, the color removal was almost total, reaching 96.75 ± 0.35%. The low RBV-5R concentration (5 mg L^{-1}) may have increased removal efficiency because more reactive oxidant species were present per dye unit. Reduced competition for reagents and greater availability of reactive species to oxidize aromatic groups may be two reasons for the observed removal efficiency (ADACHI et al., 2022; SURESH et al., 2022). In S2 (Fig. 10B), a similar behavior was observed in RBV-5R removal. Operating the BEF with 100 Ω R_{ext}, a maximum decolorization rate of 2.03 ± 0.20 mg RBV-5R L^{-1} h^{-1} was achieved in 1 h. However, from 2 h onwards, the rate declined to 1.16 ± 0.30 mg RBV-5R L^{-1} h^{-1}. At 12 h, a rate of 0.29 ± 0.05 mg RBV-5R L^{-1} h^{-1} was obtained, slightly higher than in S1 operating the BEF with 1000 Ω R_{ext}. Decolorization in the S2 strategy was 93.13 ± 0.51% after 12 h (Table 9), slightly lower than that in S1.

The RBV-5R removal rate via BEF can decrease over time for many reasons. The high Fe^{2+} concentration during the early stages of oxidation causes an increase in the formation of •OH species due to the interaction between the Fe^{2+} ions and H_2O_2 synthesized at the cathode (Eq. 22). Due to the formation of iron hydroxides, the concentration of Fe^{2+} decreases over time, which causes the efficiency of the Fenton process to decrease (KULEYIN; GÖK; AKBAL, 2021; WU et al., 2015). In addition, the synthesis and consumption of H_2O_2 in the Fenton reaction may have interfered. The rate of azo dye removal decreases when •OH is reduced (BENASSI et al., 2021). Furthermore, the generation of degradation byproducts or the adsorption of organic compounds on the cathode electrode or other system surfaces may have interfered with removal rates over time. This matter accumulation can prevent the interaction between •OH and the azo dye (ZHANG et al., 2021).

For the S3 strategy at 10 Ω (Fig. 10C), the decolorization rates were much more pronounced than those of S1 and S2. In just 1 h, S3 reached 5.49 ± 0.052 mg RBV-5R L^{-1} h^{-1}, corresponding to 27.45% decolorization efficiency for an initial concentration of 20 mg RBV-5R L^{-1}. According to Olvera-Vargas et al. (2017), the decolorization rate increases as the azo dye concentration increases. The increased number of dye molecules exposed to the Fenton reaction may cause this. In addition, this improves dye decolorization rates and employs •OH species in the intended processes (KAHOUSH et al., 2018). For several reasons, the rate of azo dye removal through BEF increases as the R_{ext} applied to the system decreases. Because there is more electron transport when there is less R_{ext}, more •OH species are generated (SATHE et al., 2022a). More effective binding with azo dye is made possible by reducing R_{ext}, improving the diffusion of reactive species in the solution. Because of this, removing azo dye is more successful, as these elements work together (SURESH et al., 2022). However, according to S3 (Fig. 10D), between time 1 and 3 h, there was a sharp reduction in the removal rate to 1.18 ± 0.050 mg RBV-5R L^{-1} h^{-1}. However, between 3 and 5 h, a new peak in the rate with a value of 2.38 ± 0.048 mg RBV-5R L^{-1} h^{-1} was observed. After t=12 h, the rate approached the values obtained in the previous strategies by approximately 0.48 ± 0.051 mg RBV-5R L^{-1} h^{-1}. This may be related to the competition of degradation intermediates with the RBV-5R molecule by •OH radicals, i.e., strong adsorption decreased the number of functional active sites on the cathode surface, slowing the removal rate. In the S3 strategy, after 12 h, decolorization was 95.49 ± 0.26%, close to S1, thus indicating the highest degradation of dye compared to S1 and S2. Similar results can be compared with this study through Table 9, applying different textile azo dyes.

Table 9 - Maximum decolorization efficiency applying the BEF system for different azo dyes

Azo dye	Concentration (mg L^{-1})	Decolorization (%)	R_{ext} (Ω)	HRT (h)	Reference
Congo red	20	90.0	1000	72	(YUAN et al., 2017)
Rhodamine B	10	95.0 ± 3.5	120	24	(XU et al., 2020b)
Orange G	400	99.6	10	16	(LI et al., 2017)
Acid Orange	35	90.0	5	10	(LE et al., 2016a)
Methyl orange	5	73.9	100	2	(LING et al., 2016)
Methyl blue	50	97.0	5	8	(ZHANG; WANG; ANGELIDAKI, 2015a)
Methyl blue	30	93.5	100	5	(WANG et al., 2022b)
RBV-5R	5 10 20	96.8 ± 0.35 93.1 ± 0.51 95.5 ± 0.26	1000 100 10	12	This study

The degradation efficiency of aromatic groups was also evaluated with BEF application. S1 (Fig. 10A) showed the best degradation efficiency, 75.7 ± 0.3%. A similar result was found for S3 (Fig. 10C), operating with 10 Ω R_{ext} and 20 mg RBV-5R L^{-1}. For this strategy (S1), the removal of aromatic groups was 73.6 ± 0.35% in 12 h. This result may be related to the higher electric current generated when R_{ext} was lower. To increase H_2O_2 synthesis and promote RBV-5R degradation, additional electrons were transmitted from the anode through the external electrical circuit. Similar results were found by Xu et al. (2020b) with rhodamine B degradation.

However, S2 (Fig. 10B) with 100 Ω R_{ext} showed the worst performance compared to the other strategies. The efficiency of aromatic group removal was only 56.9 ± 0.34% for 12 h. Due to the effects of saturation, reactant competition, restricted reaction kinetics, and the impact of R_{ext}, removing aromatic groups may have been ineffective at moderate concentrations of RBV-5R even when operating at 100 Ω R_{ext}. According to Teymore et al. (2020), the system's ability to produce reactive species may be limited at moderate azo dye concentrations, reducing the effectiveness of aromatic group removal. In addition, •OH species and aromatic groups may react only at a certain rate, which may also slow the removal of more complex compounds (MANNA; SEN, 2023; YANG, 2020).

4.3.2 H_2O_2 synthesis

In the Fenton reaction, the H_2O_2 consumption is necessary for RBV-5R degradation. However, in this study, the H_2O_2 concentration values may have been low estimates because H_2O_2 synthesis and consumption by the Fenton reaction co-occurred. Therefore, in this study, residual H_2O_2 was quantified during the first 6 h and after 12 h for each operational strategy. Fig. 12 shows the electric current (mA m^{-2}) generation with the residual H_2O_2 concentration (mg L^{-1}) according to the reaction time (h) for each operational strategy.

Figure 12 - Relationship between the electric current generation and H_2O_2 synthesis in the BEF system applying different R_{ext}: (A) S1, 1000 Ω; (B) S2, 100 Ω; and (C) S3, 10 Ω

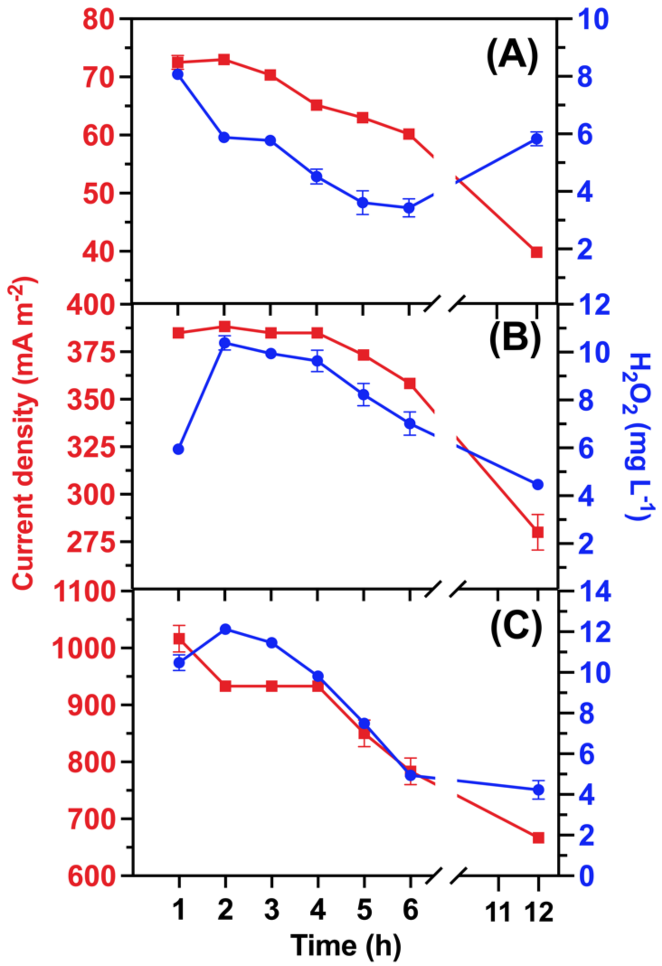

In S1 (Fig. 12A), during the first 2 h of BEF operation, electric current generation reached a maximum peak of 73.0 ± 0.47 mA m^{-2} with 8.08 ± 0.11 mg H_2O_2 L^{-1}. However, after 12 h, there was a decay of approximately 45.5% in the electric current and 27.8% in the H_2O_2 concentration. The decay of the electric current generation may be related to the consumption of the substrate (sodium acetate), which decreased the availability of feed for electrogenic bacteria. As a result, H_2O_2 synthesis is limited as the migration of protons (H^+) to the cathode chamber is reduced. On the other hand, in S1 (Fig. 12A), it was observed that the final H_2O_2 concentration (t=12 h) showed an increase compared to t = 6 h. Due to the very low RBV-5R concentration at t=12 h, the probability of collision between the RBV-5R molecule and •OH radicals decreased. Then, the two •OH radicals may have reacted with each other to regenerate H_2O_2, which may explain the increase in H_2O_2 concentration between 6 and 12 h.

Furthermore, applying a higher R_{ext} (1000 Ω) in this study may have contributed to limiting the flow of electrons necessary for H_2O_2 synthesis and favored the rapid decay of the system's electric current. In the study by Mu et al. (2009), when R_{ext} was increased from 3.2 to 100 Ω, the dye decolorization efficiency decreased from 83.1 ± 0.5% to 34.5 ± 0.8% to the initial Acid orange 7 (AO7) concentration of 224 mg L^{-1}. Fu et al. (2010b) also observed a slightly higher degradation rate for smaller resistances. In the study by Sun et al. (2009), a faster decolorization rate was achieved with a lower R_{ext}. At 50 Ω, more than 90% of the MB color was removed within 24 h, while the same process took 36 h with 500 Ω. At 5000 Ω, 85% decolorization was observed within 48 h.

According to Fig. 12(B), in S2 at 2 h of reaction, the system reached a maximum electric current (388.33 ± 2.36 mA m^{-2}) and 10.39 ± 0.30 mg H_2O_2 L^{-1}, considerably higher values than S1. A 100 Ω R_{ext} was applied in S2, i.e., 10 times lower than S1. The R_{ext} reduction (S1 for S2) may have favored the flow of electrons released by the electrogenic bacteria. At t=12 h, S2 (Fig. 12B) generated only 280 ± 9.43 mA m^{-2} and 4.47 ± 0.08 mg H_2O_2 L^{-1}. This can be explained through sodium acetate consumption by the electrogenic biofilm, which may have promoted the decay of the electric current. However, the H_2O_2 concentration at t=12 h was higher in S1 than in S2. On the other hand, in S2, a substantial amount of RBV-5R was degraded, and the Fenton process performed very well.

After 24h of system stabilization, the S3 (Fig. 12C) showed the best operational conditions for H_2O_2 synthesis and fast RBV-5R removal. At t=1 h, BEF generated 1016.67 ± 23.57 mA m^{-2} and 10.49 ± 0.39 mg H_2O_2 L^{-1} operating at 10 Ω. This made the flow of electrons easy to reach the cathode electrode due to the low R_{ext}. According to S3 (Fig. 12C), from 2 h onwards, a maximum peak of 12.13 ± 0.17 mg H_2O_2 L^{-1} was observed. Zhang et al. (2015a) observed that when operating the BEF at 0 Ω, a maximum current density of 2.7 A m^{-2} was found; however, when R_{ext} increased, the current density decreased. Zhang et al. (2017) also observed that H_2O_2 synthesis decreased with increasing R_{ext}. Thus, the BEF achieved a higher H_2O_2 yield by applying 10 Ω.

Figure 13 - Proton exchange membrane (PEM) with fouling characteristics

Fig. 13 shows that the PEM on the cathode side showed a strong yellow-orange coloration, probably due to the deposition of Fe^{3+} on the membrane surface. This study found the BEF limitation regarding electric current generation and output power density. Lower voltage generation caused by alternative electron acceptors (O_2), saturation kinetics, and competitive reactions may have implied significant systemic losses, including ohmic, metabolic, and concentration losses. However, according to the operational strategies in this study, a high RBV-5R removal efficiency and sufficient H_2O_2 synthesis for dye degradation were achieved. Therefore, BEF was efficient for RBV-5R degradation despite these limitations, according to the results shown in Table 9.

4.3.3 Coulomb and Faraday efficiency

For H_2O_2 synthesis, Coulomb (CE) and Faraday (FE) efficiencies are crucial factors to consider. The amount of energy that flows through the external circuit when a device is operating compared to the amount of energy that would theoretically be transformed by the oxidative organic matter degradation at the anode is known as the CE (WANG et al., 2022b). The ratio of the energy used by the electrode reaction to synthesize H_2O_2 to the total electricity used by the reaction system is known as the FE (HASSAN et al., 2019; LOGAN et al., 2006). Fig. 14 shows the values for CE and FE in the different operational strategies at an HRT of 12 h and the maximum output power densities.

Figure 14 - (A) Increased CE and FE values in the BEF system fed 1 g L^{-1} sodium acetate with an HRT = 12 h; (B) polarization curve for each operational strategy

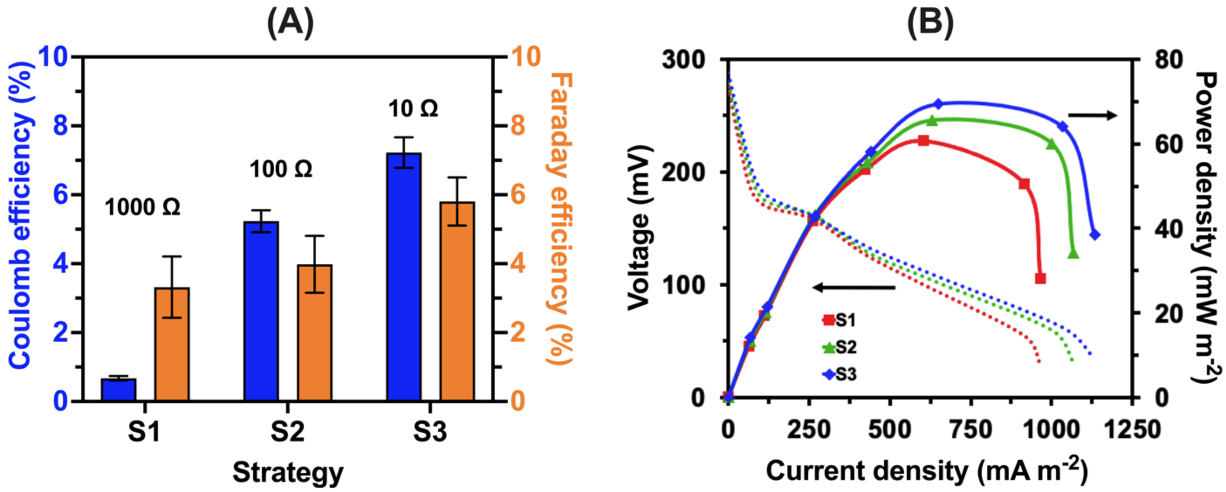

According to Fig. 14(A), the CE and FE values positively impacted each strategy by applying different R_{ext}. For S1, operating the BEF system with 1000 Ω, CE and FE were 0.67 ± 0.1% and 3.32 ± 0.1%, respectively. When R_{ext} increases during BEF operation, CE decreases dramatically. Logan et al. (2018) explain the causes for this by the effects of electrode polarization, lower current density, insufficient application of the applied potential, and limits in the transport of electrons through the external electrical circuit. This is because a higher R_{ext} impedes the effective transfer of electrons, decreases the oxidation kinetics of organic matter, and decreases the potential available for the desired processes (LI et al., 2020a).

However, when R_{ext} decreased to 100 Ω at S2 (Fig. 14A), the efficiencies showed a positive increase. After 12 h of operation, S2 obtained a CE and FE of 5.24 ± 0.32% and 3.98 ± 0.1%, respectively. The same was observed in S3, where CE (7.22 ± 0.44%) and FE (5.81 ± 0.09%) had a higher increase for a 10 Ω R_{ext}. The BEF operation with low R_{ext} is advantageous to increase CE and FE. This is because the greater transfer of electrons is possible due to the lower resistance of the system, which increases the CE, allowing more electrons to participate in the necessary processes (ROSSI; LOGAN, 2020). The system also develops a higher current density, accelerating reaction kinetics and increasing FE. The low R_{ext} also optimizes the use of the applied potential, increasing the efficiency in electron transport and reaction. In addition, the effects of electrode polarization are reduced. Overall, the use of a low R_{ext} in BEF encourages better process efficiency, which helps the treatment work more effectively (WANG et al., 2017).

In this study, the highest RBV-5R removal was given by S3 (19.1 mg RBV-5R removed), where the CE and FE values and dye concentration were the highest compared to the other operational strategies. The BEF operation by an HRT of 12 h with 10 Ω R_{ext} is believed to have contributed to the CE and FE. In the study by Wang et al. (2022b), the CE and FE were 1.26% and 74.25%, respectively, when operating the BEF system at pH 3.0 with 100 Ω R_{ext}. Suransh et al. (2023) achieved 93.52% COD removal. However, the CE was only 3%. According to the BEF proposed by Xu et al. (2020b), the CE value was 12.2 ± 3.2% for a reactor inoculated with an acclimated microbial consortium. For Li et al. (2017), the CE was 15.56 ± 0.76% with 81.16 ± 1.85% COD removal. Lv et al. (2023) achieved approximately 37.14% COD removal with a 12.87% CE in 10 h. Therefore, according to the results of this study, despite the low values of CE and FE achieved compared to the literature, RBV-5R degradation was very efficient. Similar results were found and can be compared.

According to Fig. 14(B), polarization curves positively impacted the output power density with decreased R_{ext}. These differences may also help explain the BEF performance concerning the power density generated for H_2O_2 synthesis and consequent RBV-5R degradation. S3 (Fig. 14B) was the best-performing strategy, reaching a 69.4 mW m^{-2} maximum power density. For S2 at 100 Ω, the BEF achieved 65.6 mW m^{-2}, a reduction of only 5.48% in output power compared to S3. However, when the system was operated with 1000 Ω (S1), the power density dropped slightly to 60.6 mW m^{-2}, corresponding to a 12.7% reduction compared to S3. This shows that BEF operation with lower R_{ext} increases the power density and improves the electrical current. The BEF biofilm operated with low R_{ext} for a long period can become accustomed to releasing electrons more easily. This allows a more robust electrical current to pass through the biofilm and boost microbial metabolism. As a result, microorganisms can modify their metabolic behaviors to increase the release of electrons and cope with environments with high electrical charge (ROSSI; LOGAN, 2020; ZHANG et al., 2017). Consequently, H_2O_2 synthesis is optimized at a higher power density in the lower R_{ext}.

4.3.4 COD removal

For the BEF context, COD is an essential indicator for assessing a sample's organic load. The amount of oxidizable organic molecules in a sample that can be degraded during BEF can be quantified in COD. This study obtained COD removal efficiencies, as shown in Fig. 15. The BEF achieved COD removal efficiencies of over 70% for all operational strategies.

Figure 15 - COD removal according to operational strategies compared to RBV-5R and aromatic group removal efficiencies after HRT = 12 h

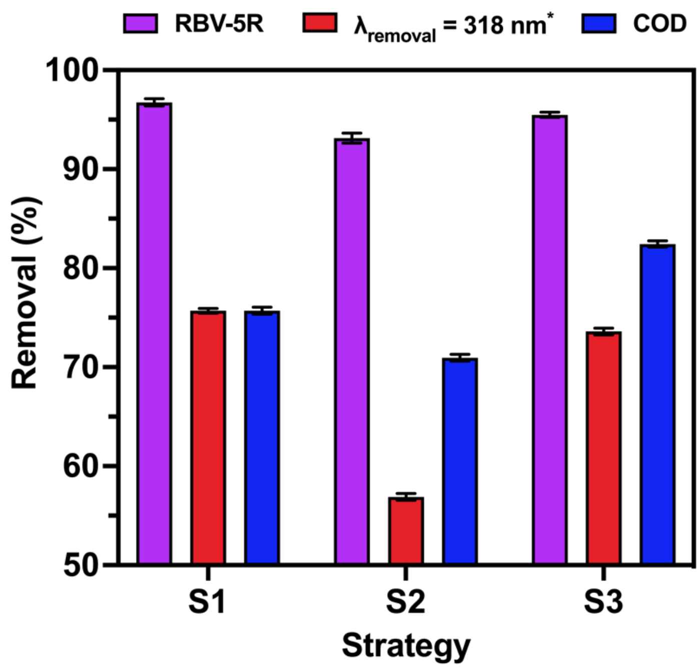

*Absorbance removal at λ=318 nm (aromatic group)

According to Fig. 15, for S1, the COD removal reached 75.71 ± 0.36% with 75.70 ± 0.23% aromatic group degradation. The operation was performed with the lowest concentration of azo dye (5.0 mg RBV-5R L^{-1}) and the highest R_{ext} (1000 Ω). In S2, operating the BEF for 12 h with 10 mg RBV-5R L^{-1} and 100 Ω R_{ext} removed 70.96 ± 0.35% of COD. The decrease in COD removal efficiency for S2 compared to S1 can be attributed to a lower removal of aromatic groups (56.90 ± 0.34%) in S2. Low degradation efficiency requires a longer degradation time and is caused by the high concentration of recalcitrant compounds and COD values (LI et al., 2018b). Similar results can be found in the literature. Zhuang et al. (2010) achieved 95% rhodamine B removal with a 12 h HRT, with 90% COD removal. Benhadji and Ahmed (2020) achieved 85% COD removal during yellow 2G degradation. In a cathode chamber with pH 3.0 and 0.8 g of $FeVO_4$ powder, Luo et al. (2011) obtained 89% acid orange 7 (AO7) removal and 81% COD. In the study by Xu et al. (2020b), the removal efficiency of 10 mg RhB L^{-1} was 95.0 ± 3.5% at 120 Ω R_{ext} and pH 3.0. After 24 h, the COD removal was 75.1 ± 3.1%. COD removal increases as current generation and substrate oxidation increase with decreasing R_{ext} (CAI et al., 2018).

According to Fig. 15, S3 presented a higher COD removal efficiency than S1 and S2. After 12 h of the Fenton reaction, it removed 82.44 ± 0.32% COD. The removal of aromatic groups in S3 was close to the values found for S1, approximately 73.60 ± 0.35%. Significant effects on COD removal and aromatic group degradation in azo dyes result from the low R_{ext} applied to the BEF process. The R_{ext} reduction increases the electrodes' ability to transfer electrons, which increases the electric current density and, consequently, •OH generation (BRILLAS; MARTÍNEZ-HUITLE, 2015). Similar results were found by Zou et al. (2020); for 20 mg MB $L^{-1,}$ they obtained a 99% decolorization efficiency ($k = 0.68\ h^{-1}$) and 74% COD removal with a 28 h HRT. In the study by Wang et al. (2022b) for 40 mg MB L^{-1}, the BEF system achieved only 31.58% COD removal efficiency. Oxidation via •OH was mainly responsible for MB degradation. However, the degradation rate was reduced by 45.19% when •OH was extinguished in the reaction.

Therefore, in terms of COD removal, BEF was able to partially degrade the RBV-5R aromatic groups at an HRT of 12 h. Because of their complex structures and large molecular weight, azo dyes are more difficult to degrade than to decolorize quickly and easily. The concentration of Fenton's reagents can theoretically be increased to increase the RBV-5R advanced oxidation. However, according to Zhang and Tao (2018), a too high reagent concentration could cause H_2O_2 to function as a strong oxidant (•OH) with a free radical to recombine, impairing the overall decolorization process.

4.3.5 Phytotoxicity assessment

The first stage of plant growth, seed germination, has limitations in growth, especially sensitivity to toxic pollutants (LUO et al., 2018). According to Table 10, the control assays in deionized water showed average radicle lengths of 2.6 ± 0.4 cm and 4.5 ± 0.7 cm for *L. sativa* and *R. sativus*, respectively. In the phytotoxicity assays, all samples showed toxicity. However, all the samples after 12 h of treatment showed a lower toxicity than the initial RBV-5R solution (t= 0 h), as the less toxic samples were those from the S3 strategy (highest initial dye concentration and lowest R_{ext}). In all cases, toxicity decreased as the sample dilution increased. The treated samples (t=12 h) positively impacted the average root growth, i.e., the samples treated in the BEF were less toxic than the raw effluent (t=0 h).

Table 10 - Effects of phytotoxicity on the average root length (cm) of *L. sativa* and *R. sativus* for the different operational strategies according to the raw sample (t=0 h) and after oxidative treatment (t=12 h)

***Lactuca sativa* (lettuce)**							
Concentration (%)	**S1**		**S2**		**S3**		**Control**
	0 h	**12 h**	**0 h**	**12 h**	**0 h**	**12 h**	
100	0.37 ± 0.2	0.69 ± 0.3	0.33 ± 0.1	0.47 ± 0.2	0.21 ± 0.2	0.97 ± 0.2	2.6 ± 0.4
75	0.60 ± 0.2	0.93 ± 0.2	0.55 ± 0.2	0.68 ± 0.2	0.33 ± 0.2	1.13 ± 0.1	
50	0.92 ± 0.2	1.42 ± 0.3	0.84 ± 0.2	1.10 ± 0.3	0.57 ± 0.2	2.0 ± 0.2	
25	1.23 ± 0.4	1.95 ± 0.1	1.04 ± 0.1	1.68 ± 0.3	0.86 ± 0.3	2.23 ± 0.2	
***Raphanus sativus* (radish)**							
Concentration (%)	**S1**		**S2**		**S3**		**Control**
	0 h	**12 h**	**0 h**	**12 h**	**0 h**	**12 h**	
100	0.61 ± 0.3	1.23 ± 0.5	0.50 ± 0.3	0.78 ± 0.3	0.40 ± 0.2	1.81 ± 0.1	4.5 ± 0.7
75	1.41 ± 0.3	1.89 ± 0.3	0.79 ± 0.3	1.66 ± 0.3	0.61 ± 0.3	2.84 ± 0.5	
50	2.09 ± 0.3	2.64 ± 0.4	1.25 ± 0.3	2.19 ± 0.4	0.91 ± 0.2	3.58 ± 0.4	
25	2.47 ± 0.3	3.41 ± 0.5	1.77 ± 0.3	2.87 ± 0.3	1.62 ± 0.3	4.27 ± 0.2	

The germination index (GI) of *L. sativa* and *R. sativus* were 100% in the control experiments. In this study, according to Fig. 16(A);(C), the GI of *L. sativa* (lettuce) and *R. sativus* (radish) seeds exposed to raw samples (t = 0 h, 100% concentration) was less than 20% for all operational strategies. According to Fig. 16(B);(D), after 12 h HRT, all operational strategies showed a slight reduction in the phytotoxicity of the treated effluent for all sample concentrations (100, 75, 50, and 25%). However, the results indicated that raw and treated effluents are still phytotoxic, as the GI < 80% (LEIVA et al., 2019). The *L. sativa* seeds were slightly more sensitive than the *R. sativus* seeds. Due to genetic, structural, and physiological variations, lettuce seeds in phytotoxicity studies are more susceptible to weathering at germination than radish seeds. The reaction of seeds to harmful chemicals is influenced by the genetic makeup of a plant, and lettuce and radish have different genetic characteristics (PEDUTO; JESUS; KOHATSU, 2019). Furthermore, compared to radish seeds, lettuce seeds have thinner and more porous integuments, allowing greater contact with the sample (ARAÚJO; EL-DEIR; TAVARES, 2021; ROMERO et al., 2014).

Figure 16 - GI of *L. sativa* and *R. sativus* seeds for raw azo dye wastewater (A and C, t = 0 h) and the treated effluent (B and D, t = 12 h) for the different operational strategies

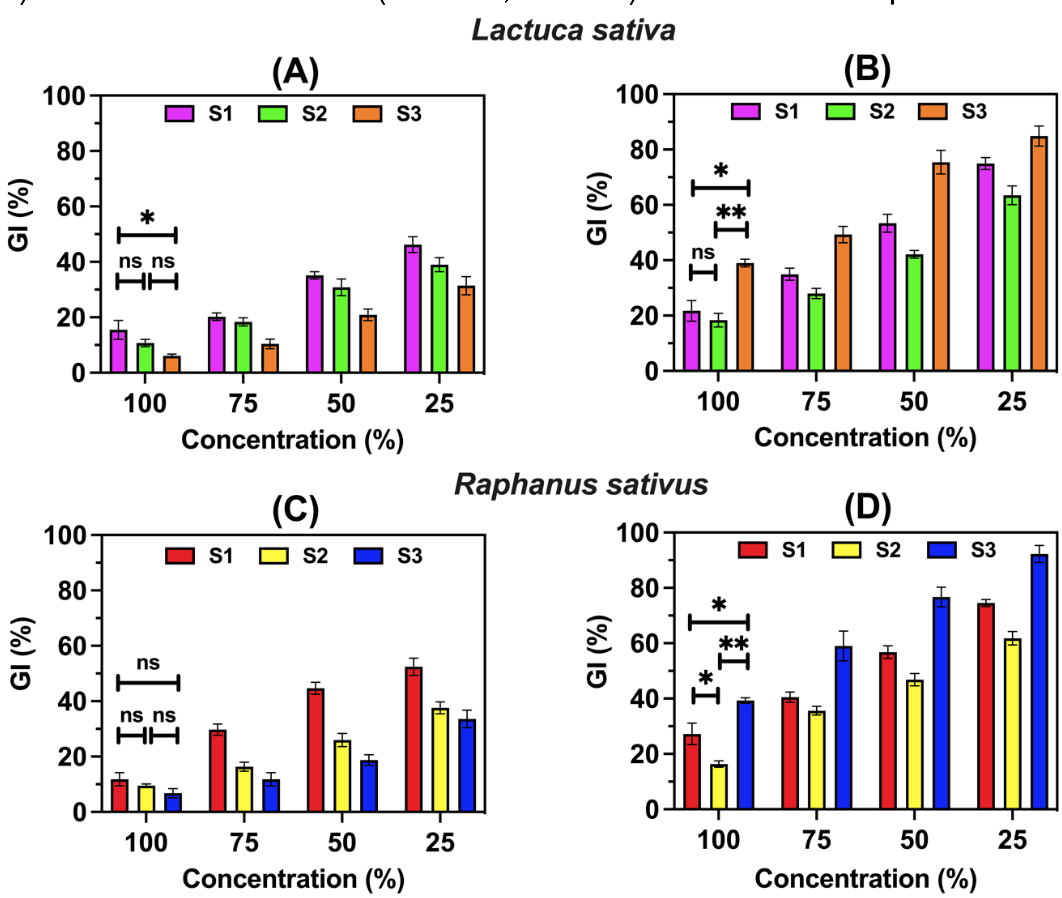

Tukey’s test was performed and described: (ns) no significance; (*) p < 0.05; (**) p < 0.005

In Fig. 16(B); (D), it can be observed that S3 had a significant reduction in phytotoxicity relative to the other operational strategies (S1-S3, $p < 0.05$) (S2-S3, $p < 0.005$). For the treated effluent after 12 h (100% concentration), the sample presented a GI for *L. sativa* and *R. sativus* seeds of 39.02 ± 1.38% and 39.32 ± 1.02%, respectively. However, for S1 and S2, phytotoxicity was persistent even after 12 h of treatment. In these strategies, a higher R_{ext} with lower RBV-5R concentrations was applied. The R_{ext} effect was believed to be one of the main reasons for the low toxicity reduction of the samples evaluated. In S1 (Fig. 16 B and D), operating with 1000 Ω R_{ext} and 5 mg RBV-5R L^{-1}, the GI values for *L. sativa* and *R. sativus* seeds were 21.73 ± 3.71% and 27.25 ± 3.90%, respectively. The worst results were found in S2 when 100 Ω R_{ext} and 10 mg RBV-5R L^{-1} were applied. For this strategy (S2) (Fig. 16 B and D), GI values of 18.35 ± 2.48% and 16.37 ± 1.18% were obtained for *L. sativa* and *R. sativus* seeds, respectively. These results indicate that harmful degradation byproducts may have been generated constantly, even during the short oxidative reactions. In addition, textile azo dyes are chemically complex and resistant to degradation. As a result, as a dye degrades, intermediate degradation byproducts are generated, some of which may even be more toxic than the initial dye solution itself (FERNANDES et al., 2018; SULTANA et al., 2015). By targeting the •OH produced during the BEF process, some of these byproducts can compete with the azo dye and decrease the degradation effectiveness (BELBEL et al., 2022; NIE et al., 2017).

In the study by Le et al. (2016b), the increased toxicity of the AO7 solution, which reached 100% during the first 100 minutes of Fenton treatment, was related to the early synthesis of hazardous aromatic groups such as 1,2-naphthoquinone or 1,4-benzoquinone. However, the subsequent attack of •OH caused by the Fenton reaction may have produced short-chain carboxylic acids, significantly decreasing the toxicity of the treated effluent. The same was observed in the study by Singh et al. (2022). After Reactive Yellow 145 treatment, the *Cicer arietinum* and *Vigna mungo* seeds showed 100% and 90% germination, respectively, for samples with initial concentrations of 50 and 100 mg L^{-1}. As a result, new functional groups, such as hydroxyl, amine, carboxyl, carbonyl, and sulfonate groups, were formed, a sign of dye degradation. Similar results were found by Santana et al. (2018), applied the Fenton process to direct orange 26 degradation. The GI for *L. sativa* was only 44.98%, causing a delay in the development of the plant due to the toxic character of the sample evaluated.

Therefore, according to the results found in this study, all GI values were lower than 80%, and the treatment allowed a slightly significant reduction in toxicity in all strategies, showing S3 the best results. The BEF application has potential in the detoxification of textile effluents. Thus, with the phytotoxicity test with *L. sativa* and *R. sativus,* it was possible to affirm that applying a lower R_{ext} (10 Ω) can be considered an adequate operational strategy for treating waters containing azo textile dyes.

4.4 CONCLUSION

This study evaluated the BEF operational efficiency for RBV-5R removal with simultaneous electric current production and H_2O_2 synthesis. The results demonstrated that S3 (20 mg RBV-5R L^{-1} and 10 Ω R_{ext}) showed the best results in decolorization, aromatic group degradation and COD removal, 95.5 ± 0.3%, 73.6 ± 0.4%, and 82.4 ± 0.3%, respectively. The S3 highlight relative to the other operational strategies can be given by applying the lower R_{ext}. A lower R_{ext} may have facilitated the flow of electrons from the anode chamber to the cathode electrode; consequently, H_2O_2 synthesis may be promoted. Phytotoxicity analysis revealed variations in RBV-5R concentrations, and R_{ext} affected the rootlet lengths and GIs of *L. sativa* and *R. sativus* seeds. For S3, the GIs for *L. sativa* and *R. sativus* were the highest compared to the other operational strategies, 39.0 ± 1.4% and 39.3 ± 1.0% (100% concentration), respectively. The R_{ext} is believed to play an important role in reducing the toxicity of the samples evaluated.

Therefore, this study highlights the BEF potential as an effective approach for RBV-5R removal, with simultaneous electric current generation and H_2O_2 synthesis. However, it is essential to consider the effects of R_{ext} and their impacts on sample phytotoxicity when applying this technology in practical and environmental contexts. The findings here may contribute to future investigations and more effective applications in treating azo dye effluents.

5 CAPÍTULO 5 - HYBRID BIOELECTROCHEMICAL PROCESS MFC ANODIC BIOFILM AND CATHODIC BEF (MFC+BEF) FOR RBV-5R DYE REMOVAL WITH SIMULTANEOUS ELECTRIC CURRENT GENERATION AND H_2O_2 SYNTHESIS

ABSTRACT

The performance of a hybrid MFC anodic biofilm and cathodic BEF (MFC+BEF) to remove the azo dye Remazol Brilliant Violet – 5R (RBV-5R) was investigated, aiming to remove color, aromatic group and COD from solution while generating current electricity and H_2O_2 in situ. Three operational strategies were adopted with different concentrations of RBV-5R/cosubstrate (5/0.75; 10/0.5; 20/0.25) (mg L^{-1}/g L^{-1}) and hydraulic retention times (HRTs) (MFC/BEF - 2h/2h, 4h/4h, and 6h/6h). To compare, prolonged HRTs were adopted for BEF (MFC/BEF - 2h/12h; 4h/12h; and 6h/12h). The results showed that applying 20 mg RBV-5R L^{-1}/0.25 g L^{-1} sodium acetate and HRT 6h/12h (MFC/BEF) presented the best operational metrics. The system achieved a maximum power density of 73.3 mW m^{-2} and 12.3 ± 0.2 mg H_2O_2 L^{-1} for Coulomb efficiency (CE) of 8.34 ± 0.23% and Faraday efficiency (FE) of 6.03 ± 0.20%. The color, COD, and aromatic group removals reached 99.8 ± 0.1%, 79.58 ± 0.30%, and 78.68 ± 1.0%, respectively. The phytotoxicity analysis revealed that the effluent treated with acidic pH harmed the germination index (GI). However, with a pH adjustment to 7.0, the seeds of *L. sativa* (30.1 ± 1.5% GI) and *R. sativus* (43.8 ± 1.6% GI) showed lower toxicity than the raw effluent. The genera of the uncultivated family_Rhizobiaceae (r = 0.9475), Soehngenia (r = 0.9750), and Pandoraea (r = 0.8307) showed a positive correlation since the RBV-5R degradation stage, conversion into current electrical and H_2O_2 synthesis. Therefore, an acclimated bioelectrochemical system performed well in RBV-5R degrading with simultaneous generation of electric current and H_2O_2 synthesis. The promising findings from this hybrid approach could be a viable and effective alternative for treating wastewater contaminated with recalcitrant organic compounds, providing potential for future environmental and industrial applications.

Keywords: microbial fuel cell; hybrid treatment; azo dye; 16S rRNA sequencing; electroactive microbial community

RESUMO

O desempenho do sistema híbrido de biofilme anódico CCM e BEF catódico (CCM+BEF) para remover o azo-corante Violeta Brilhante de Remazol – 5R (VBR-5R) foi investigado, visando remover cor, grupo aromático e DQO da solução enquanto gerava corrente elétrica e H_2O_2 in situ. Foram adotadas três estratégias operacionais com diferentes concentrações de VBR-5R/cosubstrato (5/0,75; 10/0,5; 20/0,25) (mg L^{-1}/g L^{-1}) e tempos de detenção hidráulica (TDH's) (CCM/BEF - 2h/2h, 4h/4h e 6h/6h). Para comparação, foram adotados TRH prolongados para BEF (CCM/BEF - 2h/12h, 4h/12h e 6h/12h). Os resultados mostraram que a aplicação de 20 mg VBR-5R L^{-1}/0,25 g L^{-1} de acetato de sódio e TDH de 6h/12h (CCM/BEF) apresentou as melhores métricas operacionais. O sistema alcançou densidade de potência máxima de 73,3 mW m^{-2} e 12,3 ± 0,2 mg H_2O_2 L^{-1} para eficiência de Coulomb (EC) de 8,34 ± 0,23% e eficiência de Faraday (EF) de 6,03 ± 0,20%. As remoções de cor, DQO e grupo aromático atingiram 99,8 ± 0,1%, 79,58 ± 0,30% e 78,68 ± 1,0%, respectivamente. A análise de fitotoxicidade revelou que o efluente tratado com pH ácido prejudicou o índice de germinação (IG). Porém, com ajuste de pH para 7,0, as sementes de *L. sativa* (30,1 ± 1,5% IG) e *R. sativus* (43,8 ± 1,6% IG) apresentaram menor toxicidade que o efluente bruto. Os gêneros da família não cultivada_Rhizobiaceae (r = 0,9475), Soehngenia (r = 0,9750) e Pandoraea (r = 0,8307) apresentaram correlação positiva desde a fase de degradação do VBR-5R, conversão em corrente elétrica até a síntese de H_2O_2. Portanto, o sistema bioeletroquímico aclimatado teve um bom desempenho na degradação do VBR-5R com geração simultânea de corrente elétrica e síntese de H_2O_2. As descobertas promissoras desta abordagem híbrida podem ser uma alternativa viável e eficaz para o tratamento de águas contaminadas com compostos orgânicos recalcitrantes, proporcionando potencial para futuras aplicações ambientais e industriais.

Palavras-chave: célula a combustível microbiana; tratamento híbrido; azo-corante; sequenciamento 16S rRNA; comunidade microbiana eletroativa.

5.1 INTRODUCTION

Reactive dyes are the most widely used among all other types, accounting for 30% of the total dyes used in the textile industry (UJIIE, 2015). The classification of dyes is based on the chromophore group. On an industrial scale, more than 70% of these substances are azo-dyes, which have hydroxyl (^-OH) or sulfonate ($^-SO_3$) groups - that improve solubility - bound to aromatic portions (benzene, naphthalene, etc.) linked to one or more azo groups (N=N) (DENG; BRILLAS, 2023). Azo dyes have at least one chromophore, which is an extended conjugated system of π-electrons containing an N=N group, which causes absorption at visible wavelengths (λ = 400-800 nm) (JOKSIMOVIĆ et al., 2022). Due to these characteristics, solubility in water and color, azo-dyes threaten aquatic and human life when introduced into the environment through textile effluents (AJAZ; SHAKEEL; REHMAN, 2020). A series of environmental issues, such as direct damage to natural aesthetics, limitation of air-water oxygen exchange, low photosynthesis, and decreasing in aquatic flora and fauna, are caused by the discharge of azo dyes (HUANG et al., 2018; JOSHI; HINSU; KOTHARI, 2022). Textile effluents are responsible for 17 to 20% of the world's freshwater contamination. Because they include a variety of toxic dyes that are difficult to remove, these effluents are resistant to biodegradation and highly harmful to water bodies (BHARATHI et al., 2022; LEKHAK, 2023).

Wastewater remediation of textile dyes is being thoroughly researched using a variety of hybrid bioelectrochemical systems (BESs), including the constructed wetland microbial fuel cell (CW-MFC) (FANG et al., 2017; KESARWANI et al., 2022), floating treatment wetland-MFC (ROY et al., 2023), hybrid aerobic or anaerobic bioreactor-MFC (DAS; MISHRA, 2019; SULTANA et al., 2015), membrane bioreactor-MFC (LIU et al., 2018; MENG et al., 2017), MFC-Fenton system, photoelectrocatalytic-MFC system (PEC-MFC) (LONG et al., 2017) and other hybrid BESs. This makes sense for the energy-effective remediation of textile dye wastewater using bioelectrochemical systems (BESs). In BESs, biological oxidation-reduction processes eliminate textile dyes in wastewater and provide clean energy for bioelectricity (PATEL et al., 2023a). Although they are still in the early stages of development, hybrid systems that combine traditional treatment techniques can provide an excellent way to process large amounts of wastewater (ZHANG et al., 2022). A high degradation efficiency can be achieved by advanced oxidation techniques (95 and 97% in synthetic or real effluents, respectively) (CASTILLO-SUÁREZ et al., 2023). Combining the electro-Fenton (EF) process with a biological technique can reduce the extended time needed for a complete dye degradation (ROSHINI et al., 2017). Partial or complete mineralization of organic molecules is one of the main benefits of the EF method (WAKRIM et al., 2022). The main characteristic of all these advanced oxidative processes (AOPs) is the in situ generation of intensely oxidizing radicals, such as the hydroxyl radical (•OH), the second strongest known oxidant with a very high standard reduction potential (E = 2.8 V) and capable of degrading most organic contaminants in water (CASADO, 2019; DENG; BRILLAS, 2023).

Microbial fuel cells (MFCs) can degrade textile dyes and turn them into electrical energy. The oxidation of biodegradable organic matter (e.g., acetate) (Eq. 30) by electrogenic bacteria in an anaerobic environment and the reduction of oxygen with aeration are key processes in this technology, which generates bioelectricity as a source of green and clean energy to meet the demand of an AOP in a hybrid treatment system (PANDIT et al., 2023). Fenton oxidation, which is one of the most effective and advanced oxidation processes, has been widely used to treat various recalcitrant contaminants (RAJARAMAN; GANDHI; PARIKH, 2021; SARAVANAN et al., 2022). H_2O_2 can be synthesized via a two-electron oxygen reduction reaction (2e-ORR) on the cathodic electrode surface through biological electrons generated in an MFC without the need for external power (Eq. 31) (APOLLON et al., 2022; SOLTANI; NAVIDJOUY; RAHIMNEJAD, 2022). Iron is the most widely used catalyst to activate H_2O_2. Then, H_2O_2 interacts with Fe^{2+} (Eq. 32) to generate hydroxyl radical (•OH) (DENG; ZHAO, 2015). The •OH radicals oxidize the azo dye, ideally until its degradation.

$$CH_3COO^- + 4H_2O \rightarrow 2HCO_3^- + 9H^+ + 8e^- \quad (30)$$

$$O_2 + 2H^+ + 2e^- \rightarrow H_2O_2 \quad (31)$$

$$Fe^{2+} + H_2O_2 \rightarrow Fe^{3+} + OH^- + \bullet OH \quad (32)$$

Recently, Reyes et al. (2021) used a microbial consortium to degrade four anthraquinone dyes in a MFC. Dye removal efficiencies varied, with higher complexity dyes showing lower removal rates. Similarly, in another study, Saba et al. (2018) found that a reactive black 5 azo dye (RB5) was 90% decolorized at different time points and concentrations. A reactive blue 4 anthraquinone dye (RB4) required longer times for decolorization, and it was not removed. RB4 contains the dichloro-triazine group, which, together with the C=O chromophore group, makes the dye more stable, making it difficult to degrade. In the study by Oon et al. (2017), the discoloration rates of mono-azo dyes were approximately 50% higher than those of diazo dyes. The results revealed that the dye structure influenced the decolorization and energy performance of the MFC. Despite the excellent decolorization, incomplete degradation and low power density limit the application of full-scale MFCs (SINGH; DAHIYA; MISHRA, 2021; SIVASANKAR et al., 2019). In addition, the toxicity of a dye can cause microorganisms to take longer to adapt to biofilm formation (SABA; KJELLERUP; CHRISTY, 2021; ZHONG et al., 2018). Integrating microorganisms with a physicochemical strategy resulted in better performance and greater economic viability. Therefore, it can be stated that a single treatment technique cannot efficiently remove azo dyes.

It is known that AOPs based on •OH production can degrade a wide range of complex organic compounds that are naturally resistant to microbiological attack in simple low molecular weight species. Therefore, this study aims to evaluate the efficiency of the textile azo-dye (RBV-5R) treatment by applying a primary treatment via MFC anodic biofilm and an oxidative posttreatment via cathodic BEF with H_2O_2 synthesis (MFC+BEF). In this study were applied different concentrations of RBV-5R/cosubstrate (5/0.75; 10/0.5; 20/0.25) (mg L^{-1}/g L^{-1}) and hydraulic retention times (HRTs) (MFC/BEF - 2h/2h, 4h/4h, and 6h/6h). Furthermore, the efficiency of the BEF process was investigated until a 12-h HRT was achieved. The phytotoxicity analysis with seeds of *Lactuca sativa* and *Raphanus sativus* was related to the operational efficiencies of each strategy applying the proposed hybrid system. 16S rRNA sequencing enabled the identification of the microorganisms responsible for the system performance, improving the biological RBV-5R removal while concurrently generating electric current for the H_2O_2 synthesis.

5.2 MATERIALS AND METHODS

5.2.1 Azo dye

The azo dye Remazol Brilliant Violet 5R (RBV-5R) was obtained from Dystar® Brazil with a high laboratory grade. The textile industry has used this dye for dyeing and printing cotton, silk, and linen. As a reactive dye, it is used to dye cellulosic fibers (RÁPÓ et al., 2020). The physicochemical characteristics of the dye are shown in Table 11. The 1.0 g L^{-1} stock solution was prepared with deionized water by dissolving the dark violet powder. The solution was used without any further purification.

Tabela 11 - Chemical structure of the reactive azo dye

Dye name	**Remazol Brilliant Violet-5R (RBV-5R)**
Molecular formula	$C_{20}H_{16}N_3Na_3O_{15}S_4$
Molecular weight	735.58 g mol^{-1}
CAS number	12226-38-9
Chemical structure	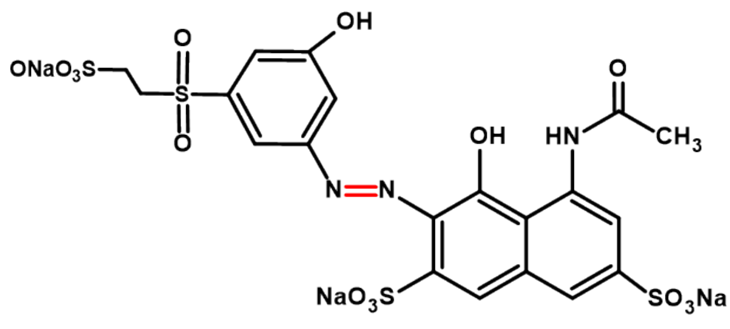

Source: Adapted from Lai (2021); Rapó et al. (2019)

5.2.2 Hybrid system setup

All experiments were conducted in H-type glass MFC reactor with an effective volume of 250 mL, according to Fig. 17. A proton exchange membrane (PEM) separated the double-chamber reactor (Nafion 117, DuPont, USA). The Nafion 117 membrane was treated with H_2O_2 5%, H_2SO_4 5% w/w, and deionized water. The anodic electrode was a carbon fiber brush (MiliRose, USA) pretreated at 450 °C for 20 min (YANG et al., 2022). The cathode electrode was graphite felt (3.10^{-3} m^2) (MIRONG, China). A titanium wire of 0.8 mm was used to connect the electrical circuit with external resistance. The digital multimeter (HM-2030, Hikari) was connected to the system to monitor voltage and electrical current output. A small aeration pump (SC-7500, Boyu) was coupled for O_2 supply in the cathode chamber.

Figure 17 - Schematic representation of the MFC+BEF reactor with the data acquisition system

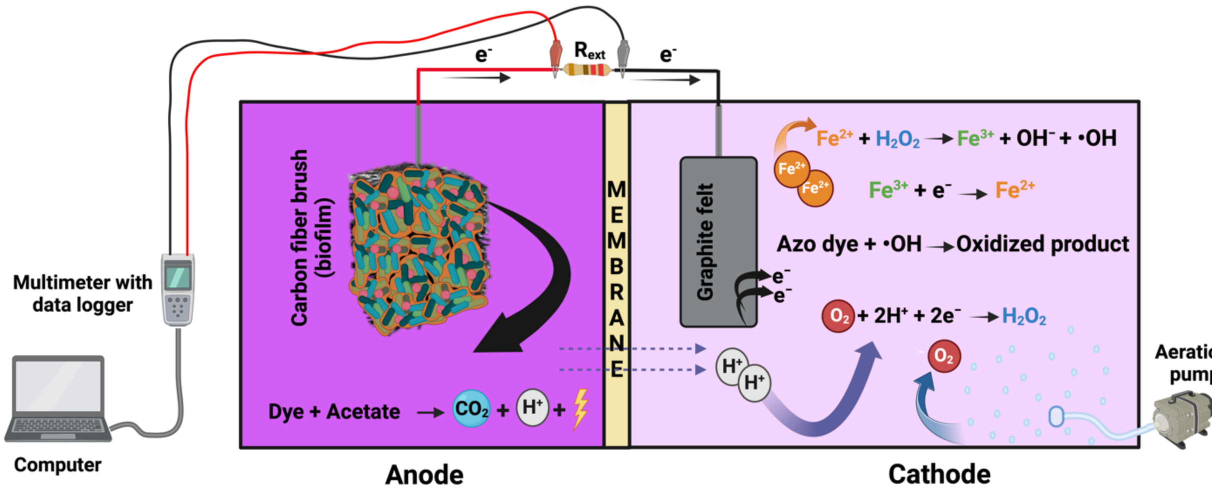

Source: Author (2023)

5.2.3 Operational strategies

The MFC was acclimated for 2 months from an anaerobic inoculum of a wastewater treatment plant collected in Florianópolis (Brazil) until the development of a stable biofilm on the anodic electrode. The growth medium was composed of (g L^{-1}): sodium acetate – $C_2H_3NaO_2$ (1.0); phosphate buffer solution (PBS): $Na_2HPO_4 \cdot H_2O$ (4.28), NaH_2PO_4 (2.74), NH_4Cl (0.31); e KCl (0.13); 12.5 ml L^{-1} mineral solution (mg L^{-1}): $MgSO_4.7H_2O$ (10.0), $MnCl_2.4H_2O$ (3.0), $MgCl_2 \cdot 6H_2O$ (10.0), $CoCl_2.6H_2O$ (1.0), $NiCl_2.6H_2O$ (2.0), $NaMoO_4.7H_2O$ (3.0), H_3BO_3 (30.0) e $CuCl_2.2H_2O$ (1.0) e $CaCl_2 \cdot 2H_2O$ (1.0); and 5 ml L^{-1} vitamin solution (IQBAL et al., 2022; ROSSI et al., 2019; TAN et al., 2022; YU et al., 2020).

The cathodic solution (250 mL) consisted of H_2O and 1.77 g of sodium sulfate (Na_2SO_4) at pH 3.0, enabling ideal conditions for H_2O_2 synthesis. Na_2SO_4 improves the conductivity of the solution and accelerates the electron transfer. According to each operational strategy, the MFC anodic chamber was fed with vitamins, minerals, PBS, and azo dye. After reaching the given HRT in the MFC, the EF reagents (34.8 mg $FeSO_4.7H_2O$ and 1.77 g Na_2SO_4) and the partially treated azo dye solution in the anaerobic environment (250 mL) were introduced into the batch feed condition at pH 3.0 into the cathodic chamber. The pH adjustment was performed with 0.1 M NaOH and 0.1 M H_2SO_4. The MFC+BEF performance was investigated using different operational strategies with 10 Ω R_{ext}. To evaluate the effect of different HRT values, an extended HRT was also applied to the BEF process (Table 12). The temperature was controlled at 35 ± 2 °C during all operations in a biochemical incubator.

Table 12 - Operational strategies applied in the MFC+BEF hybrid treatment system

Parameter	**Strategy**		
	S1	**S2**	**S3**
RBV-5R/Acetate (mg L^{-1}/g L^{-1})	5.0/0.75	10.0/0.50	20.0/0.25
HRT (h/h) (MFC/BEF)	2/2	4/4	6/6
HRT (h/h) (MFC/BEF)	2/12	4/12	6/12

5.2.4 Analytical methods

The performance of MFC+BEF was evaluated regarding color, COD removals, and residual H_2O_2. For this, cathodic and anodic chamber samples were collected at the beginning and end of each cycle. The experimental trials were conducted in duplicate and followed the recommendations of the Standard Methods for the Examination of Water and Wastewater – APHA. The COD was measured by spectrophotometry (Hach DR3900) according to the procedure described in Hach 8000, based on oxidation by the dichromate method (APHA, 2018). The pH was measured with a multiparameter probe (AK88, Akson). All solution samples were filtered using a 0.45 μm membrane filter before analysis. The RBV-5R decolorization was measured by colorimetry at λ = 560 nm and aromatic group degradation (λ = 248 nm). The RBV-5R decolorization and degradation were measured by scanning analysis ranging from 190 to 1100 nm with a UV–Vis spectrophotometer (BEL Photonics, UV - M51). The H_2O_2 concentration followed the methodology proposed by Wang et al. (2022b). The method is known as iodine (I_3^-), where a 2 mL sample is added to 1 mL of iodine reagent containing 0.40 mol L^{-1} KI, 0.06 mol L^{-1} NaOH, 10^{-4} mol L^{-1} $(NH_4)_2MoO_4$ and 1 mL of $KHC_8H_4O_4$ (0.10 mol L^{-1}). Reagents were used to measure absorbance at λ = 352 nm.

5.2.5 Calculations and measurements

The voltage was measured using a digital multimeter with a data logger. The current, I [mA], was calculated according to Ohm's law Eq. (33), where U is the voltage [mV], and R_{ext} is the external resistance (Ω). Current densities (j, mA m^{-2}) and power densities (PD, mW m^{-2}) were normalized to the total exposed cathode projected area (3.10^{-3} m^{-2}), Eq. (34), and (35), respectively (ROSSI et al., 2018).

$$I\ (mA) = \frac{U}{R_{ext}} \tag{33}$$

$$j\ (mA\ m^{-2}) = \frac{I}{A} \tag{34}$$

$$PD\ (mW\ m^{-2}) = \frac{U^2}{R_{ext}\ A} \tag{35}$$

The polarization curve was generated by varying the external resistance, setting the MFC to open the circuit for at least 10 min or until a stable voltage was observed, and lowering the external resistance from 1000, 500, 200, 100, 55, 20, and 10 Ω at 10 min intervals. Moreover, the MFC performance was evaluated in terms of COD and H_2O_2. Coulomb efficiency (CE), defined as the fractional recovery of electrons from the substrate, was calculated according to Eq. 36. Faraday efficiency (FE) is defined as the ratio of the electricity consumed by the electrode reaction to produce H_2O_2 and the total electricity of the reaction system. The value can be obtained according to Eq. 37.

$$CE\ (\%) = \frac{8\ \int_0^t I\ dt}{F\ V\ \Delta COD}\ .\ 100 \tag{36}$$

$$FE\ (\%) = \frac{n\ F\ C_{H_2O_2}\ V}{\int_0^t I\ dt}\ .\ 100 \tag{37}$$

where I is the average current (mA), t is the hydraulic retention time (s), F is Faraday's constant (96485 C mol^{-1}), n is the number of electrons exchanged per mole of oxygen (2 mol e^- mol^{-1}), V is the cathode chamber volume (L), ΔCOD is the change in COD over time t (g L^{-1}), and $C_{H_2O_2}$ represents the measured concentration of H_2O_2 (mg L^{-1}) (BOAS et al., 2022; HASSAN et al., 2019; SIM et al., 2015).

5.2.6 Bioassay assessment

The toxicity evaluation was performed through phytotoxicity analysis with samples collected before and after treatment via MFC+BEF using *Lactuca sativa* (lettuce) seeds and *Raphanus sativus* (radish) (ISLA PRO). The assay involved exposing 10 seeds of each plant in Petri dishes lined with filter paper. Before revealing the seeds, the filter paper was soaked in 4 mL of each sample. The Petri dishes were isolated with parafilm to avoid moisture loss and incubated for 120 h under a temperature-controlled environment (25°C) and without light. Deionized water was used as the positive control, and 0.5 M $ZnSO_4$ was used as the negative control. The radicle length and seed germination percentage in the treated sample vs. the control were used to determine the germination index (GI) (LUO et al., 2018). Phytotoxicity was determined by calculating the GI, according to Eq. (38) (DE ARAÚJO et al., 2022; SHARIFI et al., 2022).

$$GI\ (\%) = \frac{GSS \times RLS}{GSC \times RLC} \times 100 \tag{38}$$

where GSS is the number of germinated seeds in the sample; GSC is the number of germinated seeds in the control; RLS is the radicle length in the sample; RLC is the radicle length in the control. According to the validation criterion, 80% of the seeds should germinate. The results were compared to each other (treated and raw) at the same concentrations and with the control (YOUNG et al., 2012).

5.2.7 Microbial community analysis

16S rRNA sequencing was conducted to assess and determine the microbial community structure. Microbial community sampling was performed by scraping the anode biofilm and storing it in an Eppendorf 5 mL microtube at -4.0 °C until analysis. For each sample, 250 µL was mechanically lysed through disruption with the aid of the L-BEADER HT disruptor (Loccus) using zirconium beads. DNA extraction from the lysate samples was performed using a modification of the DNeasy® 96 PowerSoil® Pro QIAcube® HT kit. The QiaCube HT robot performed the extraction (Qiagen, Germany). The variable V3-V4 regions of the 16S ribosomal RNA gene (16S rRNA) were amplified using the universal primers 341F 5′-CCTACGGGRSGCAGCAG-3′ (WANG; QIAN, 2009) 806R 5′-GGACTACHVGGGTWTCTAAT-3′ (CAPORASO et al., 2010). The PCR products were sequenced on an Illumina MiSeq with 2x300 (forward) and 2x250 (reverse) reads.

Fastq files were demultiplexed with MiSeq software according to their index and analyzed using QIIME 2, version 2 (2021.11) (BOLYEN et al., 2019) on VirtualBox (7.1 version). Sequencing reads were filtered, denoised, and merged, and chimeras were removed using DADA2 (CALLAHAN et al., 2016) for quality control. Subsequently, sequences were taxonomically classified using the SILVA database (QUAST et al., 2012), and mitochondria or chloroplast-related features were removed. The median frequency was 23,562 (min: 20,605 – max: 29,469) reads, so the number of sequences was rarefied to 20,000 for each sample for further diversity analyses. The align-to-tree-MAFFT-fast tree pipeline from q2-phylogeny was used for phylogenetic-dependent analyses. Alpha diversity (α) analyses were performed to assess the complexity of microbial diversity for each sample, including the operational taxonomic unit (OTU) to measure observed species richness and the Shannon index to identify community diversity.

The percent of reads in each sample matching the top 20 abundant genera were plotted and compared among samples. All alpha diversity indices and beta diversity analyses were performed using QIIME 2 software (2021.11).

5.2.8 Data analysis

Prism9 software (GraphPad, version 9.2) was used to reveal the effects of the mean and standard deviation of the dye and substrate concentrations on the color removal efficiency, COD, and phytotoxicity. ANOVA was applied to test differences between means of data with normal distribution, followed by the Tukey test. The difference was considered significant when $p < 0.05$. All operational strategies were carried out in duplicate.

Canonical coordinate analysis (CCA) correlated the main microbial genera with the MFC reactor feeding operational variables (temperature azo dye RBV-5R). Principal coordinate analysis (PCoA) was performed from the genera relative abundance dataset to compare differences in microbial communities between inoculum, MFC – acetate, and MFC – RBV-5R+acetate. Pearson's correlation analysis was performed to examine the significant relationships between the relative abundances of the microbial community and the different MFC metrics (CE, FE, COD, RBV-5R removal, electric current, and H_2O_2) to the MFC – RBV-5R+acetate. The CCA, PCoA, and Pearson correlation tests were performed using the statistical software XLSTAT Pro® (XLSTAT, Paris, France), and $p < 0.05$ was considered significant.

5.3 RESULTS AND DISCUSSION

5.3.1 MFC anodic biofilm: color and aromatic group removals

To evaluate the RBV-5R removal, samples were collected from the influent and effluent from the anodic and cathodic chambers. The evolution of the UV–visible spectra of the RBV-5R solution as a function of reaction time for different initial concentrations and hydraulic retention times (HRT) can be seen in Fig. 18. Before MFC+BEF treatment, the RBV-5R spectrum showed an absorption broad band centered at $\lambda = 554$ nm that characterizes the azo chromophore group and another band at $\lambda = 248$ nm characteristic of benzenic rings. The spectra in Figs. 18A, 18B, and 18C showed a band at $\lambda = 318$ nm, which may correspond to the naphthalene group. It is known that under anaerobic conditions, azo dyes easily undergo reducing biotransformation into the corresponding aromatic amines, with the consequent loss of color (JOKSIMOVIĆ et al., 2022). During the primary treatment in the anodic chamber via MFC bacterial biofilm, a decrease over time of the band at λ = 554 nm was observed for all operational strategies (Figs. 18A, 18B, and 18C).

Figure 18 - UV–visible spectra evolution for (A) S1, (B) S2, and (C) S3 in primary treatment via MFC anodic biofilm and (D) S1, (E) S2, and (F) S3 in oxidative posttreatment via cathodic BEF for the different operational strategies

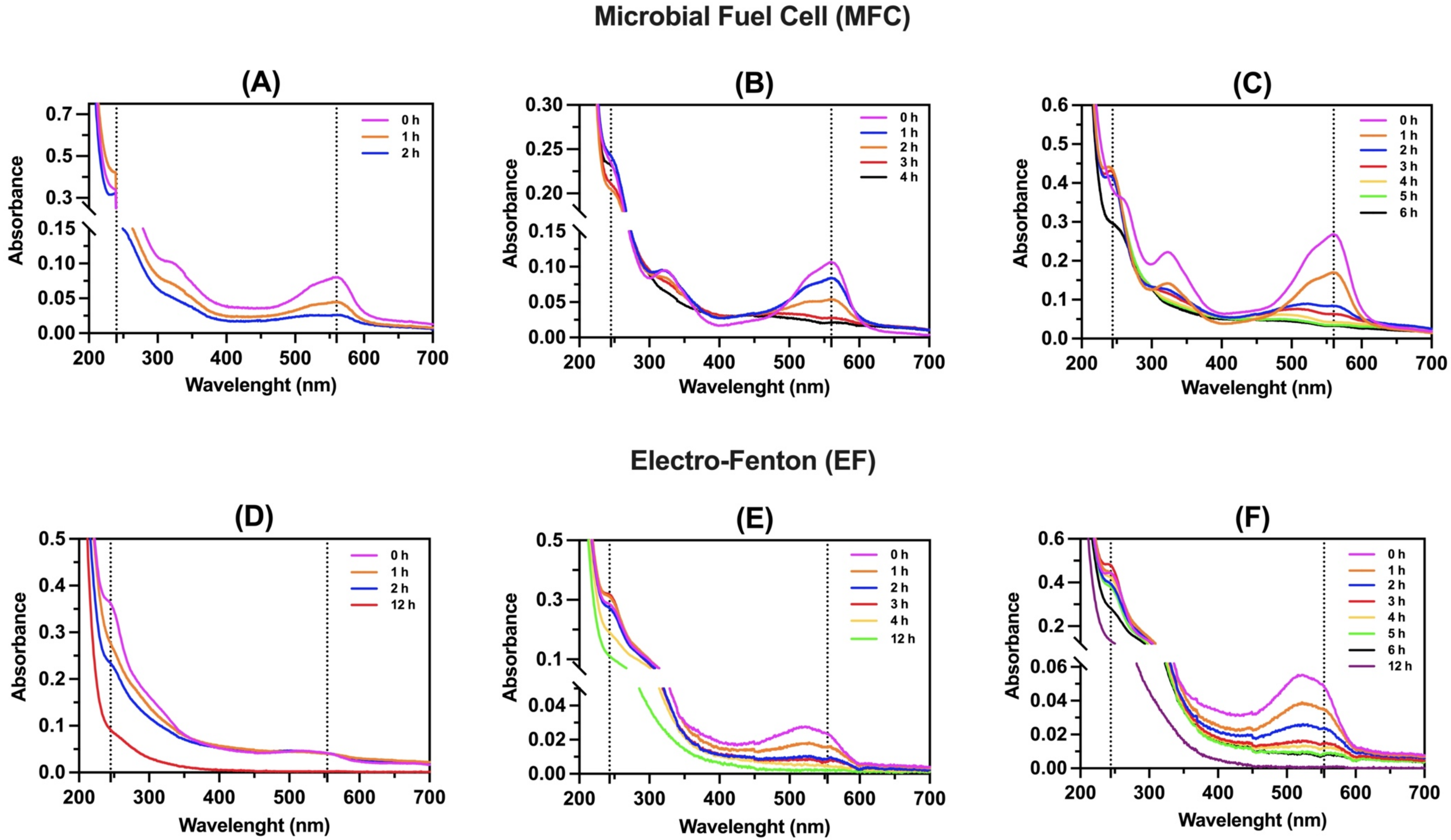

According to Table 13, a fast RBV-5R decolorization was observed after 2-h HRT for S1 (Fig. 18A), with an efficiency of 67.97 ± 0.21%. Similar results were found for S2 (Fig. 18B), with 80.17 ± 0.10% RBV-5R removal in 4 h HRT. When the HRT increased to 6 h in S3 (Fig. 18C), the RBV-5R removal efficiency was increased to 87.70 ± 0.07%. So, it can be deduced that the decolorization increases with the HRT increasing. Similar results were found by Li et al. (2016a) and Liu et al. (2009). During anaerobic decolorization, the dye can act as an electron acceptor via the electron transport chain transporters (ZAFAR; BUKHARI; REHMAN, 2022). Bacteria create azoreductases that reductively break the electrophilic N=N bond itself at the expense of a reducing agent, usually NADPH (JAYAPRAKASH; PARTHASARATHY; VIRARAGHAVAN, 2016). In addition, anodic biofilm-catalyzed oxidation of the biodegradable substrate may be the bioelectrochemical pathway that reduces azo bonds. It can be understood that electrogenic bacteria provide electrons by donating them outside their cell membrane (MITTAL et al., 2022; SRIVASTAVA et al., 2019).

Table 13 - Color and aromatic groups removal efficiency for each stage of the hybrid treatment system

Parameter	Strategy	Treatment stage		
		MFC	**BEF**	**BEF (HRT=12 h)**
RBV-5R removal (%)	S1	67.97 ± 0.21	72.22 ± 0.25	95.56 ± 0.57
	S2	80.17 ± 0.11	81.10 ± 0.10	92.56 ± 0.46
	S3	87.70 ± 0.10	84.88 ± 0.37	98.58 ± 0.83
Aromatic group removal (%)	S1	1.71 ± 0.25	35.30 ± 0.10	74.63 ± 0.24
	S2	1.27 ± 0.24	33.86 ± 0.54	61.70 ± 0.34
	S3	7.95 ± 0.74	37.17 ± 0.30	70.73 ± 0.24

The degradation of benzenic compounds by the MFC anodic biofilm was slow with batch feeding and varying dye concentrations, as shown by the evolution of the band at λ = 248 nm (Figs., 18A, 18B, and 18C). This can be due to short HRT, low substrate availability, and the need for microbial adaptation. The chemical composition of the dye can also impact how quickly microorganisms can access and breakdown the dye (WANG et al., 2019a). Thus, removal efficiencies of benzenic compounds in the MFC (Table 13) were only 1.71 ± 0.25%, 1.27 ± 0.24%, and 7.95 ± 0.74% for S1, S2, and S3, respectively. It is to note a significant increase in the intermediary times in the intensity of the band at λ = 248 nm. This fact can be due to the accumulation of the sulfonate derivative of aniline caused by the cleavage of the N=N group. However, the intensity of the band assigned to the naphthalenic group decreases over time in all the operational strategies, indicating an easier degradation by the bacterial biofilm.

The results obtained from the initial treatment of the RBV-5R dye in the MFC anodic chamber indicated partial decolorization and partial degradation of benzenic compounds, highlighting the need for additional treatment. So, the effluents from the primary treatment were treated by EF in the cathodic chamber.

5.3.2 Cathodic BEF: color and aromatic group removals

In the secondary treatment of the RBV-5R dye via BEF, the absorbance of the band at λ = 554 nm decreased with time from 0 to 12 h (Figs. 18D, 18E, 18F), showing that RBV-5R was further decolorized. According to Table 13, S1 did not show significant results in color removal after 2 h for BEF posttreatment (67.97 ± 0.21% to 72.22 ± 0.25%). However, with only a 2 h HRT, the aromatic group degradation was 35.30 ± 0.1%. More satisfactory results were found when the HRT was increased to 12 h, with 74.63 ± 0.24% for aromatic group removal and 95.56 ± 0.57% for RBV-5R removal (Table 13). For S2 (Fig. 18E), the RBV-5R removal was 81.10 ± 0.1% and 33.86 ± 0.54% for aromatic compounds. However, when the HRT reached 12 h, the values increased to 92.56 ± 0.46% and 61.70 ± 0.34%, respectively.

The more significant efficiency was observed in S3 (Fig. 18F), operated with a 6-h HRT. In this strategy (S3), the RBV-5R removal efficiency was 84.88 ± 0.37% and 37.17 ± 0.30% for the aromatic group. Extending the HRT to 12 h (Table 13), the BEF process achieved 98.58 ± 0.83% and 70.73 ± 0.24%, respectively. Even at high azo dye concentrations, the BEF method's ability to remove color and aromatic compounds is enhanced by increasing the HRT. The longer HRT allows for greater interaction between the target chemicals and the reactive oxygen species (ROS) produced during the EF, such as •OH. Consequently, the chemicals are oxidized and degraded more effectively, improving color and aromatic group removal. In addition, extended HRT stimulates improved reactor mixing, ensuring uniform dispersion of ROS and increasing the degradation efficacy (DERAKHSHANI et al., 2021). Extended HRT increases total removal efficiency by allowing the breakdown of stable intermediates created during azo dye degradation. In addition, longer HRTs give more chances for secondary reactions, reducing unfavorable interactions between ROS and other components of the solution (ROY et al., 2023).

Aromatic amines are known to be susceptible to further degradation in an oxidative environment (YADAV et al., 2022). In this study, when the biodegraded samples were subjected to the BEF process in the cathodic chamber, a significant drop in the absorbance of the RBV-5R absorption spectra was observed (Figs. 18D, 18E, 18F), indicating, as expected, a further degradation. These results support the widely held belief that derivatives of type aromatic amines can only be decomposed in an environment with high oxidative potential (BAÊTA et al., 2015; CHEN et al., 2012).

In this study, was applied the 10 Ω R_{ext} for all operational strategies. This parameter may also have contributed to the RBV-5R removal. Thus, a high decolorization efficiency was often recorded when MFCs were operated with a low R_{ext} (DAS; MISHRA, 2019). The low R_{ext} makes effective electron transfer possible, which increases the current flow and the reactive oxygen species (ROS) generation, such as •OH radicals at the cathode chamber (WANG et al., 2019b). A low R_{ext} also stimulates greater mass transfer, which increases the interaction between bacteria and azo dyes at the anode. Improved electrochemical processes and decreased electronic competition also help improve efficiency (NAWAZ et al., 2022; OBILEKE et al., 2021). Therefore, the obtained results in this study show the effectiveness of the MFC+BEF hybrid treatment in the degradation of the aromatic rings and RBV-5R decolorization.

5.3.3 COD removal

The removal efficiency of the organic load from RBV-5R and the decrease in organic pollution in the sample were evaluated by COD in the MFC+BEF hybrid system. The initial COD for feeding the MFC ranged between 893.0 ± 2.83 mg L^{-1} and 1481.0 ± 9.90 mg L^{-1} for the three operational strategies. The COD values were derived from the azo dye and the co-substrate, referred to as RBV-5R and sodium acetate. According to Fig. 19, the COD removal efficiencies as a function of HRT are shown for the different operational strategies.

Figure 19 - COD removal as a function of HRT (1) according to the operational strategy for the study and (2) an extended 12-h HRT for BEF. The results in graph (A) correspond to MFC decolorization, (B) BEF oxidative treatment, and (C) represent the overall removal efficiency with joint MFC+BEF

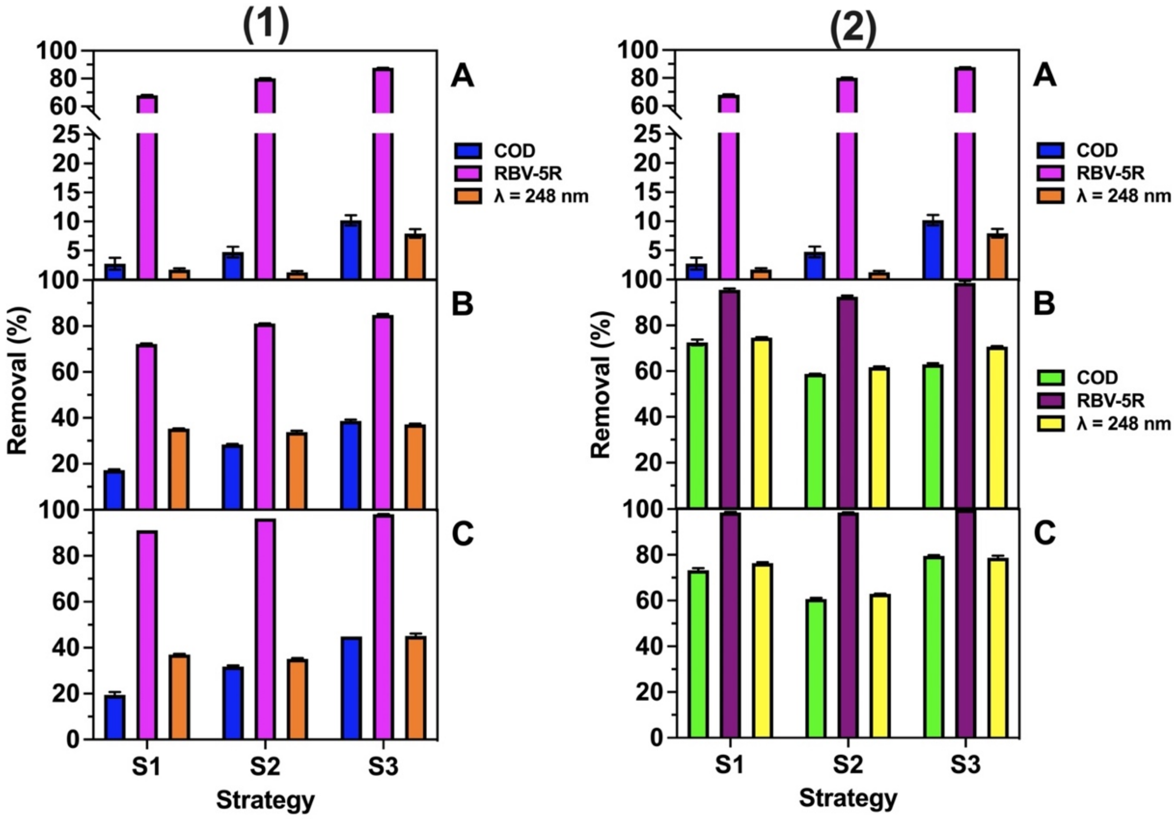

Graphs (1) – According to the HRTs (h) (MFC/BEF): S1 (2 h/2 h); S2 (4 h/4 h); and S3 (6 h/6 h)
Graphs (2) – According to the extended HRTs (h) for the BEF process (B and C) (MFC/BEF): S1 (2 h/12 h); S2 (4 h/12 h); and S3 (6 h/12 h)

According to Fig. 19 (1A), the COD removal via MFC showed more significant results for higher HRTs. In S1 for a 2-h HRT, the removal was only 2.74 ± 1.02%. However, when the HRTs of S2 and S3 were 4 h and 6 h, respectively, COD removal reached 4.75 ± 0.90% and 10.20 ± 0.89%. Similar results were found by Prajapati and Yelamarthi (2020) through 700 ppm of Congo Red via MFC from HRT 18 to 54 h, and 80.95 ± 2.08% decolorization and 73.96 ± 1.76% COD removal were achieved. This can be explained by the HRT increase encouraging COD removal from azo dye. In short HRTs, acetate is more easily removed by bacteria than dye. This happens due to the extended interaction between the bacteria and the dye, which increases substrate availability and improves biofilm function. As a result, COD is removed from the dye in the MFC more effectively (TRAPERO et al., 2017). In addition, the ability of anaerobic heterotrophic microorganisms to use azo dye and sodium acetate for growth, metabolism, and as an energy source favored the incremental formation of biofilms that may be responsible for the gradual increase in COD removal (GUPTA; SRIVASTAVA; YADAV, 2020; MITTAL et al., 2022). This study hypothesized that the azo bond was removed using electrons, accelerating COD removal at the anode.

After MFC treatment, the BEF was more incisive in COD removal. According to the results in Fig. 19 (1B), the COD removal was higher for S3 > S2 > S1, at 38.65 ± 0.61%, 28.42 ± 0.19%, and 17.21 ± 0.37%, respectively. The HRT increase may have improved the RBV-5R degradation more effectively, increasing COD removal throughout the BEF. In this study, the COD input values for the BEF were between 868.50 ± 6.36 and 1330 ± 4.24 mg COD L^{-1}. This COD load may have impacted BEF's ability to remove contaminants. This happens due to the competition for •OH, accumulation of residues, and difficulties in pH control. Due to the high COD load, there is more competition for •OH because pollutants wait impatiently for their release to oxidize completely (PIETRUK; PIĄTKOWSKA; OLEJNIK, 2019). In addition, the accumulation of toxic or persistent byproducts can reduce the effectiveness. H_2O_2 synthesis can be threatened by significant pH fluctuations (MACHADO; TEIXEIRA; RUOTOLO, 2023).

When the HRT was extended to 12 h for BEF (Fig. 19 (2B)), the COD removal efficiencies increased notably. All the COD removal efficiency values found were ≥ 58%. The EF efficiency for COD removal was given by an increase in the aromatic group removal, reaching efficiencies between 60 and 75%. Since aromatic groups often account for most of the COD, removing aromatic groups using EF increases the degradation. Similar results were found by Roshini et al. (2017), where achieved 63% color removal, and 48% COD removal. The system proposed by Suhan et al. (2020) achieved more than 76% and 94% COD and color removal, respectively. Similar results were also found by Belal et al. (2022) for basic yellow 28 (BY28) removal. The color and COD removal were 94.3% and 72.1%, respectively.

A comparison between the overall COD removal efficiencies in Fig. 19 (1C) and (2C) indicates that the increase in HRT for BEF showed the best results. Overall, the COD removal efficiencies (Fig. 19 (2C)) were approximately 73.29 ± 0.95%, 60.74 ± 0.49%, and 79.60 ± 0.30% for S1, S2, and S3, respectively. It was also observed that the increase in the organic matter load between the operational strategies had a significant impact, mainly on the BEF and, consequently, on the overall efficiency of the MFC+BEF system. Therefore, according to the results of this study, the best operational strategy was S3. Even with a higher RBV-5R concentration (20 mg L^{-1}) and extended HRT (MFC/BEF – 6 h/12 h), it removed 79.60 ± 0.3% of COD. The excellent efficiency of the hybrid process for COD removal can be attributed to 99.8 ± 0.1% of RBV-5R removal and 78.7 ± 1.0% of the aromatic group degradation.

5.3.4 Coulomb and Faraday efficiency

The Coulomb efficiency (CE) is the ratio between the actual and theoretical electricity conversion. A lower CE implies that more organic matter is used for metabolic processes and byproduct synthesis by bacteria, and only a small portion is used for electrical energy production (SARATALE et al., 2017). On the other hand, the fraction of electrons that are transferred to the electrode can be estimated by Faraday's efficiency (FE). The CE and FE values obtained during the hybrid system operation can be found in Fig. 20. The results show that the conversions of organic matter into electric current and, consequently, into H_2O_2 were optimized with increasing HRT and azo dye concentration.

Figure 20 - An increase in Coulomb and Faraday efficiency values for an MFC+BEF system fed with azo dye and sodium acetate for different HRTs

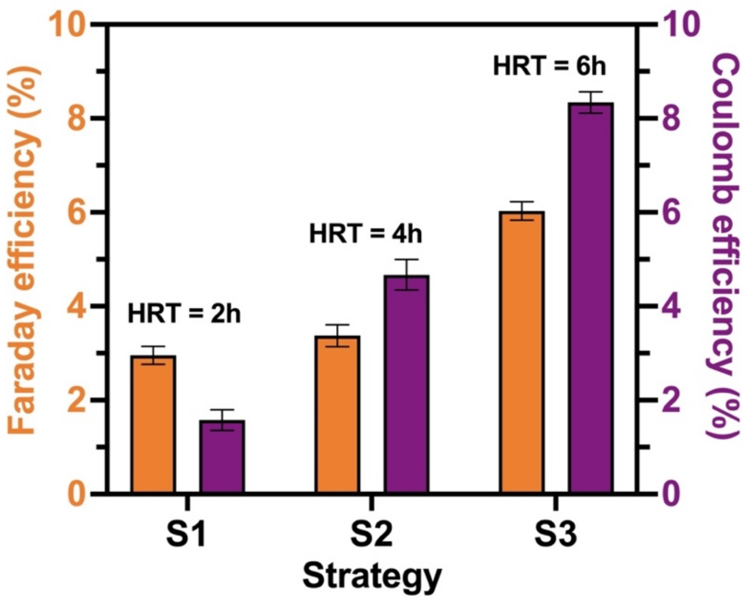

According to Fig. 20, S1 presented the lowest values of CE and FE among the other strategies, with values of 1.58 ± 0.22% and 2.96 ± 0.20%, respectively. The low values found can be explained by several reasons, especially the low HRT adopted in the strategy. Low HRTs can restrict the access of these bacteria to substrates, originating slow bioelectrochemical processes and decreasing the CE (MALYAN; MONGIA; KUMAR, 2022). In addition, a low HRT can also result in an excess supply of protons around the electrode or protons competing with the electrons on the electrode surface, responsible for limiting the FE (NAWAZ et al., 2022).

For S2 and S3, the increase in HRT and dye concentration resulted in more significant CE and FE values than S1. According to S2, the CE and FE values achieved 4.67 ± 0.33% and 3.38 ± 0.23%, respectively. For the S3, the values were even higher, with CE 8.34 ± 0.22% and FE 6.03 ± 0.20%. Similar results were found by Haavisto et al. (2017), where the decrease in HRT from 3.5 d to 0.17 d decreased from 30% to 0.6% CE, respectively. At HRTs of 13, 14, and 20 d, the COD removal efficiency was 71, 73, and 83%, respectively, while the CEs were 7.1, 2.4, and 0.3%, respectively. High COD, equivalent to highly saturated anodic surface conditions, can aid in competition between electrogenic bacteria and other types of microorganisms, leading to a more significant removal of organic matter, which is not associated with the generation of electric current (FAN; SHARBROUGH; LIU, 2008; VELVIZHI; VENKATA MOHAN, 2012).

The increased availability of substrates for oxidation and electron generation by the bacteria present in the MFC is made possible by a higher HRT, which allows for a more complete breakdown of the azo dye and acetate. This improves the CE by increasing the electron transport efficiency to the electrode (OON et al., 2017; TRAPERO et al., 2017). In addition, an increase in HRT stimulates the development of biofilms and microbial adhesion to the electrodes, resulting in increased bioelectrochemical activity (TABASSUM; ISLAM; AHMED, 2021). In addition, the system's stability is increased, allowing for more complete chemical decomposition and preventing the accumulation of inhibitors or dangerous byproducts that can impede microbial action (RAFAQAT et al., 2022). However, mass transfer constraints in the cathode chamber can affect the electron acceptance process (KAHOUSH et al., 2018).

Applying a 10 Ω R_{ext} may have contributed to the CE and FE values of this study. Previous results found by Ren et al. (2011) confirmed that the average CE for MFCs with a 10 Ω was 45%, while for MFCs with a 5000 Ω, it was only 6%. This is because the low electron recovery at high resistances was mainly due to the long batch duration. This resulted in more electron loss for non-electricity reactions such as aerobic respiration and perhaps methanogenesis (XIA et al., 2019). In some circumstances, however, the loss of systematic stability at higher current density due to kinetic or mass transfer limitations can sometimes lead to a substantially unstable voltage output. This can lead to a decrease in CE for an MFC operated at a low external load, particularly in the case of a non-catalyzed cathode (YOU et al., 2009).

However, the MFC activity is affected by overpotentials, and other losses caused by cathode reduction. In this study, significant fouling was observed on the surface of the proton exchange membrane. This may be due to the accumulation of Fe^{3+} precipitates from the Fenton reaction in the cathode compartment and biological material in the anode chamber. In addition, when the substrate concentration is high, it can cause electrode fouling, leading to restriction and accumulation of salts and precipitates (KOLAJO et al., 2022; MAQSOOD et al., 2022). That is, it interrupts the functioning of the material on which they accumulate, thus inhibiting the efficiency of the materials.

5.3.5 H_2O_2 synthesis

H_2O_2 is a crucial component of the BEF process because it provides the essential oxidizing species for the RBV-5R degradation. In this study, it was observed that adopting different HRTs showed significant impacts on H_2O_2 synthesis and consequent interference in RBV-5R decolorization and degradation capacity. Fig. 21 shows the electric current generation (mA m^{-2}) with H_2O_2 synthesis (mg L^{-1}) according to the reaction time (h) for each operational strategy.

Figure 21 - Relationship between electric current generation and H_2O_2 synthesis in the MFC+BEF hybrid system to (A) S1, (B) S2 and (C) S3 applying 10 Ω R_{ext}

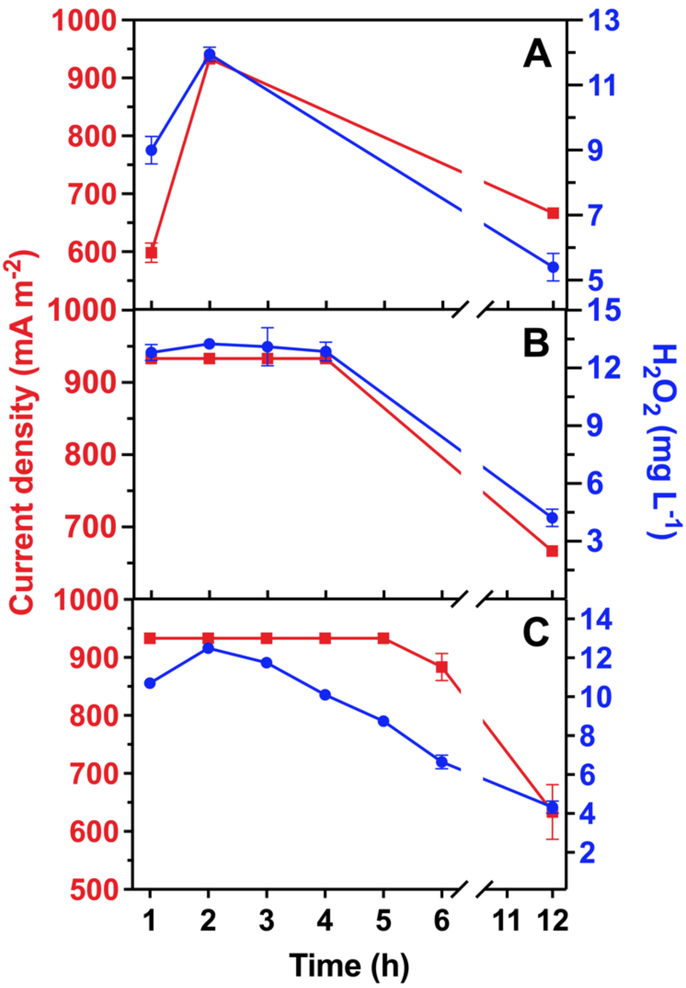

According to S1 (Fig. 21A), in the first two hours, the electric current generation reached a maximum peak of 933.4 mA m^{-2} with 11.95 ± 0.21 mg H_2O_2 L^{-1}. However, with the increase in HRT for 12 h, there was a decay of approximately 28.6% in the electric current and 54.8% in the H_2O_2 concentration. The decay of the current generation may have been related to the consumption of the substrate, which decreases the availability of food for the anodic biofilm. As a result, H_2O_2 synthesis is limited as the migration of protons (H^+) from the anode chamber is reduced. The same results were observed in S2 (Fig. 21B) and S3 (Fig. 21C). For S2, the current density presented constant values (933.33 mA m^{-2}) for the first four hours. However, H_2O_2 showed a small increase in the two hours, with a mean of 13.25 ± 0.21 mg H_2O_2 L^{-1}. After reaching a 12-h HRT, the H_2O_2 concentration decreased to 4.23 ± 0.46 mg L^{-1}, corresponding to a decrease of approximately 68%. In S3, the maximum peak was observed at two hours with 12.50 ± 0.28 mg H_2O_2 L^{-1} and 933.33 mA m^{-2}. After reaching the HRT of 12 h, there was a sharp reduction of approximately 65.36% and 32.14% for the H_2O_2 concentration and electric current density, respectively.

These results show that the BEF reaction suffers a drop in electric current, slowing the H_2O_2 synthesis. This is because the electrons supplied by the electric current accelerate the redox processes involved in H_2O_2 breakdown. Fewer electrons are given when the electric current is decreased, which causes less H_2O_2 to decay. As a result, less H_2O_2 is used during the reaction, which decreases its concentration at the end of the process (DAS et al., 2020; ZHOU et al., 2019). For Fu et al. (2010a), the H_2O_2 synthesis rate in the MFC was 6.50 mg L^{-1} h^{-1} during the first 12 h and 0.74 mg L^{-1} h^{-1} during the past 12 h. When the MFC was operated at high current densities, the substrate degradation rate at the anode was higher than that at low current densities. Therefore, the current densities decreased rapidly in the second stage. In addition, an extended HRT allows for a reaction period between the azo dye and reactive species produced during BEF to increase the oxidation potential and removal effectiveness.

5.3.6 Output power density

Output power density measures how well the microorganisms in the system breakdown the substrate to produce energy. Therefore, the effects of HRT on the MFC output power were investigated during periods of 2, 4, and 6 h. The COD influent concentration was scaled between initial concentrations of 893 ± 2.83 and 1372 ± 5.67 mg COD L^{-1}. Fig. 22 shows the results obtained in the polarization curve for the different operational strategies of the study, according to the HRT of the posttreatment by BEF.

Figure 22 - Polarization curve performed after the operating HRT: (S1) 2 h; (S2) 4 h; and (S3) 6 h

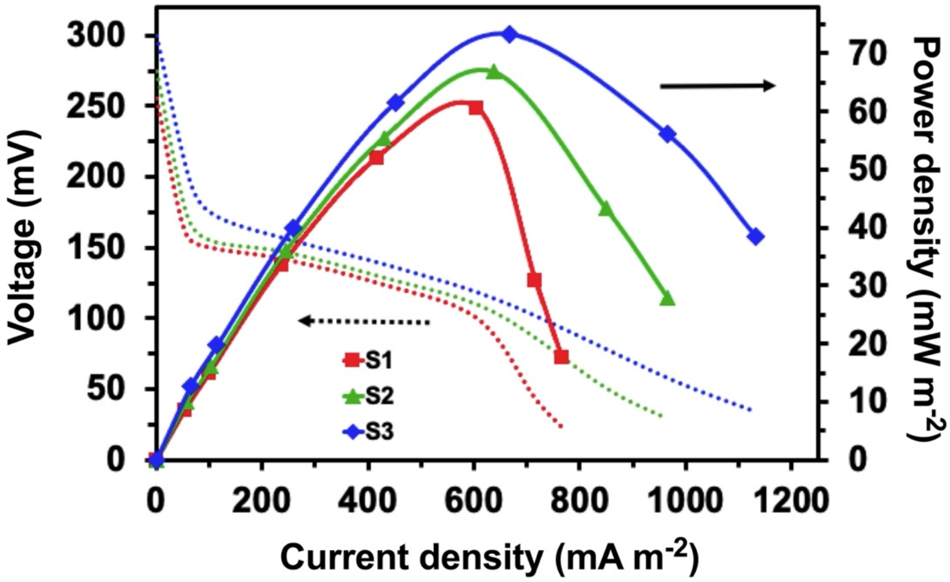

According to Fig. 22, the MFC showed significant results for different HRTs. S1 was the strategy that presented the lowest maximum power density (60.6 mW m^{-2}) with S1 < S2 < S3. In S3, after reaching a 6-h HRT, the system obtained a maximum power density of 73.3 mW m^{-2}. The MFC output power is influenced by ohmic behavior, activation potential, concentration potential, bacterial metabolism, and pH (GUL et al., 2021; JANNELLI et al., 2017). The increase in HRT has shown a significant impact on the system. This can be explained by the fact that a longer HRT promotes better microbial growth, biofilm formation, and electron transfer efficiency. Higher energy production and total energy density are the observed effects (SIDDIQUI et al., 2023). Similar results were found and can be compared to this study (CRUZ-NORIEGA et al., 2023; HAAVISTO et al., 2017; MA et al., 2016; YE et al., 2020).

Moreover, the MFC power density can be increased by increasing the azo dye concentration. This is due to the system's improved substrate availability, more significant electron transport, and favorable redox potential. More organic substrate is available for microbial oxidation at higher dye concentrations, which increases substrate utilization and energy production. Consequently, more electrons are produced as the azo dye is oxidized, which increases the effectiveness of electron transfer and, as a result, increases the electric current generation (ADELAJA; KESHAVARZ; KYAZZE, 2015; ULLAH; ZESHAN, 2020). In this study (S3), the increasing azo dye concentration showed significant results for color removal (87.7 ±

0.1%) and aromatic compounds (7.95 ± 0.74%) with increased HRT and consequent power density. Tan et al. (2022) concluded that the reactive green 19 concentration increased the performance. The additional 3-fold increase in substrate loading (2.43 g L^{-1}) improved decolorization efficiency by approximately 7% with a 42% increase in power density (63.40 ± 0.07 mW m^{-2}).

However, one of the hypotheses responsible for the low density of power and electric current produced by the system proposed in this study compared to the literature can be explained by the affinity of the dye with the electrons produced during the oxidation reaction of organic matter. Jayaprakash et al. (2016) observed that the different chemical structures of methyl orange and reactive blue 172 (RB172) dyes reduced the power density by approximately half (41 mW m^{-2}), even though 92% of RB172 was decolorated. This can be explained by the competition between the anode and the azo dye for electrons produced by the substrate oxidation. This can cause destabilization of the dye and have a detrimental effect on the electrical current density that the MFC generates. When the redox potential of the dye is greater than that of the MFC working electrode, electron sequestration occurs because the electrons are diverted to the dye instead of the electrode. However, this hypothesis needs to be investigated in future work.

5.3.7 Phytotoxicity assessment

Assessing phytotoxicity in MFC+BEF effluent samples is crucial to determine their potential environmental impact and locate hazardous substances that may harm the ecosystem. Plant growth bioassays and seed germination methods are excellent ways to assess phytotoxicity (LEIVA et al., 2019). At this stage, the phytotoxicity analysis was performed with *L. sativa* and *R. sativus* for the raw samples, partially MFC treated, and MFC+BEF treated with the HRT extended to 12 h. According to Table 14, the germination index (GI) of *L. sativa* and *R. sativus* was relatively sensitive to the initial and treated RBV-5R solutions. In deionized water, *L. sativa* and *R. sativus* used as controls showed 100% GI with average radicle lengths of 3.62 ± 0.49 cm and 2.44 ± 0.41 cm, respectively. The variations in radicle lengths and GIs were noticeable with the application of different RBV-5R concentrations and HRTs. The samples treated with the MFC+BEF hybrid system significantly impacted seeds. These data indicated that treated RBV-5R samples were less toxic than raw effluent. However, a decrease in the toxicity of the treated effluent (after 12 h BEF) was observed when the low pH was neutralized.

Table 14 - Phytotoxicity effects on the mean root length (cm) of *L. sativa* and *R. sativus*

Lactuca sativa					
Strategy	**HRT (h)**				**Control**
	0	**Xn**	**12 (pH 3.0)**	**12 (pH 7.0)**	
S1	0.19 ±0.10	0.13 ± 0.10	0.45 ± 0.24	1.95 ± 0.14	
S2	0.14 ± 0.10	0.10 ± 0.09	0.37 ± 0.21	1.68 ± 0.32	3.32 ± 0.50
S3	0.10 ± 0.10	0.07 ± 0.06	0.29 ± 0.17	1.13 ± 0.13	
Raphanus sativus					
Strategy	**HRT (h)**				**Control**
	0	**Xn**	**12 (pH 3.0)**	**12 (pH 7.0)**	
S1	0.26 ± 0.14	0.18 ± 0.12	0.40 ± 0.14	1.47 ± 0.20	
S2	0.20 ± 0.12	0.15 ± 0.09	0.40 ± 0.25	1.23 ± 0.30	2.44 ± 0.41
S3	0.11 ± 0.10	0.07 ± 0.10	0.34 ± 0.22	1.04 ± 0.20	

According to Fig. 23, the results showed that the initial RBV-5R solution was extremely toxic for all strategies. At t = 0 h (Fig. 23A), the GIs for *L. sativa* at S1, S2, and S3 were 5.16 ± 0.57%, 3.87 ± 0.64%, and 1.90 ± 0.16%, respectively. The values of *R. sativus* (Fig. 23B) were less sensitive than *L. sativa*, with GIs of 9.15 ± 0.63%, 6.89 ± 0.69%, and 3.08 ± 0.40%, respectively. However, after reaching the HRT for each operational strategy, the effluent proved much more toxic for both seeds. At S1, after 2 h HRT, the *L. sativa* and *R. sativus* GIs were 3.66 ± 0.63% and 5.82 ± 1.01%, respectively. The 10 mg RBV-5R L^{-1} and 4 h HRT values in S2 were 3.03 ± 0.81% and 6.16 ± 1.05%, respectively. The GI values worsened when the RBV-5R concentration was increased at 6-h HRT (S3). The strategy S3 (Fig. 23) achieved only 1.39 ± 0.74% (*L. sativa*) and 3.38 ± 0.60% (*R. sativus*). According to the results, *L. sativa* seeds were more sensitive to germination in the presence of the sample compared to *R. sativus*. The N=N bond cleavage, which produces aromatic amines, is believed to cause some toxicity of the azo dye. After hydroxylation or acetylation, aromatic amines, often the byproduct of the reaction, become compounds with more mutagenic and carcinogenic characteristics than the initial sample (NGO; TISCHLER, 2022). Toxicity tests revealed that dyes breakdown can release carcinogenic compounds, such as 1-amino-2-naphthalenol (MANI et al., 2019).

Figure 23 - Germination index (GI) of (A) *L. sativa* and (B) *R. sativus* seeds for azo dye solution in the different operational strategies

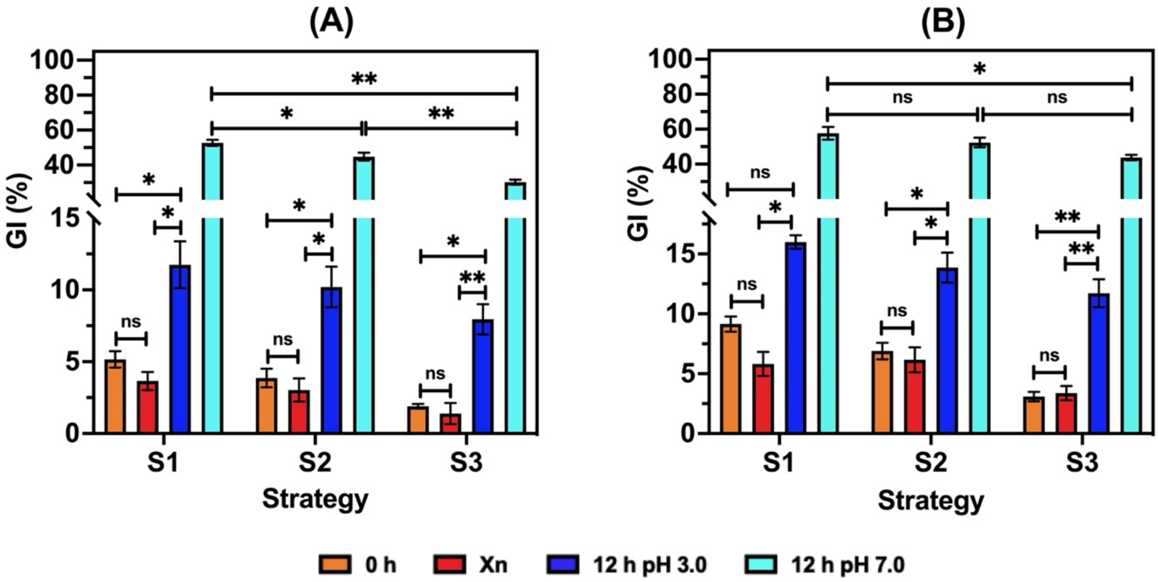

"Xn" represents the HRT: (S1) Xn = 2 h; (S2) Xn = 4 h; (S3) Xn = 6 h
Tukey's test was performed and described: (ns) no significance; (*) $p < 0.05$; (**) $p < 0.005$

In the study by Fang et al. (2016), for example, 1,4-benzenediamine, N-methyl- and p-phenylenediamine (PPD) were produced due to the inability of the hybrid treatment system to completely breakdown methyl orange. Similar to the bright red reactive X-3B, which has been only partially decomposed into aniline and sulfonated aromatic amines. However, even in an aerobic cathode environment, the volume of the cathode layer was insufficient to convert all byproducts into H_2O and CO_2 (FANG et al., 2013). Olvera-Vargas et al. (2017) examined the efficacy of coupled BEF and aerobic biological processes to mineralize metoprolol from real wastewater. The BOD/COD ratio increased from 0.012 to 0.44 after 1 h of electrolysis, with a 47% reduction in TOC. Like the current investigation, the toxicity of the solution was significantly reduced. Therefore, it has been found that dye decolorization does not result in its full degradation; instead, only a small portion of it is fully oxidized to H_2O and CO_2, and some of its amino groups are partially degraded.

When the BEF process started operating at 12-h HRT, the GIs were higher than those of the samples at t = 0 h (Fig. 23). S1 presented the best results for both seeds because it was the strategy with the lowest initial RBV-5R concentration.

However, S3 presented the worst GIs, even though it slightly reduced the phytotoxicity of the raw effluent. When evaluated through *L. sativa*, the GIs for S1, S2, and S3 were 11.75 ± 1.63%, 10.20 ± 1.41%, and 7.96 ± 1.05%, respectively. After the 12-h HRT, *R. sativus* was 16 ± 0.56%, 13.87 ± 1.25%, and 11.72 ± 1.16%, respectively. An extended HRT, the proposed hybrid system achieved up to a 26.6% GI increase for the S1. This proves that HRT impacts the final phytotoxicological quality of the MFC+BEF hybrid treatment process. Similar results of rootlet germination and growth were found by Roshini et al. (2017). The treated wastewater showed less phytotoxicity (19 mm; GI = 100%) than untreated wastewater (0 mm; IG = 0%). This is because the treated and untreated wastewater showed that the complex chemical bonds present in the dyes were cleaved into simpler components.

This study observed a low GI value for the seeds evaluated. Supposedly, the effects observed on germination could be related to the acidic pH of the treated solution and the generation of toxic byproducts from the RBV-5R degradation. Therefore, according to Fig. 23, the GI of the seeds increased after neutralizing the treated RBV-5R solution. The maximum GIs reached were in S1, at approximately 52.65 ± 1.77% and 57.68 ± 3.64%, respectively, in *L. sativa* and *R. sativus*. Several reasons may explain this considerable increase. EF may have produced intermediate, final toxic, or harmful byproducts to the seeds, some of which may be more toxic in an acidic environment. This is because chemicals are more likely to damage seeds when they take on a chemical state caused by a mismatched pH (RAWAT et al., 2018). Acidity also affects the activity of enzymes necessary for seed germination, which can cause problems in early development and the root system (GUARI et al., 2015; OLIVEIRA et al., 2018). Therefore, neutralizing the solution can stop unwanted chemical reactions between the seed chemicals and the acidic environment, allowing the seeds to germinate undisturbed.

5.3.8 Microbial community analysis

Numerous microorganisms are known to be electrochemically active, and certain biofilms develop distinct electron transfer mechanisms to establish electrical communication with the electrode (CHEN et al., 2020; LUO et al., 2023). These microorganisms are usually evaluated based on their surface structure and biochemical properties, confirmed by a 16S rDNA sequence experiment (CHIARELLO et al., 2022; IDRIS et al., 2022). To obtain insights into how MFC communities differed taxonomically, we assigned an identity to each operational taxonomic unit (OTU) and phylogenetic diversity (Shannon index) to biofilm samples collected from MFC. According to Table 15, the results showed that the structure of the microbial community changed significantly from the inoculum and that MFC feeding strongly impacted the microbial diversity and richness.

Table 15 - The number of rRNA sequences analyzed and alpha diversity indices for the microbial communities in the inoculum and MFC-acclimated

Sample	Raw reads	Effective reads	Microbial richness (OTU)	Microbial diversity (Shannon)
Inoculum	105,049	29,469	181	6.51
MFC - Acetate	119,219	21,258	115	6.10
MFC - RBV-5R + acetate	105,737	24,522	75	4.24

The Shannon index calculates the variety and variation within a sample of a species' population, i.e., the diversity of the microbial community in a sample. A higher Shannon value indicates greater community diversity (Table 15). As a result, in this investigation, MFC- RBV-5R+acetate showed lower microbial diversity than MFC - acetate (Shannon index 4.42 vs. 6.10, respectively). In addition, the microbial density, indicated by the number of unique species (OTUs), was lower in the MFC-RBV-5R+acetate sample (75 OTUs) than in the MFC-acetate sample (115 OTUs). Although the MFCs operated with the same anaerobic sludge inoculum, the microbial communities differed. As the objective of this study was to evaluate the efficiency of RBV-5R degradation and the simultaneous H_2O_2 synthesis, the lower microbial richness and diversity also decrease the range of microorganisms that can help remove even various forms of co-metabolites. However, fewer species of microorganisms competing for resources may have resulted in more efficient use of available substrates.

Principal coordinate analysis (PCoA) was used to investigate the effect of the relative abundance of the 20 main genera on the diversity of the microbial community for inoculum, MFC - acetate, and MFC - RBV-5R + acetate (Fig. 24). The principal coordinates described PCo1 (41.48%) and PCo2 (35.18%) of the normalized data variance. The analysis of beta diversity through the PCoA plot, which provides information on the dissimilarity in the microbial community structure between the samples evaluated, indicates that the community structure of the anodic biofilm of the MFCs was statistically divergent from the inoculum. Similar results found in MFCs have been reported in previous studies (HU et al., 2023; LONG et al., 2019b).

Figure 24 - PCoA ordering using overall abundance data to represent differences between the investigated microbial communities

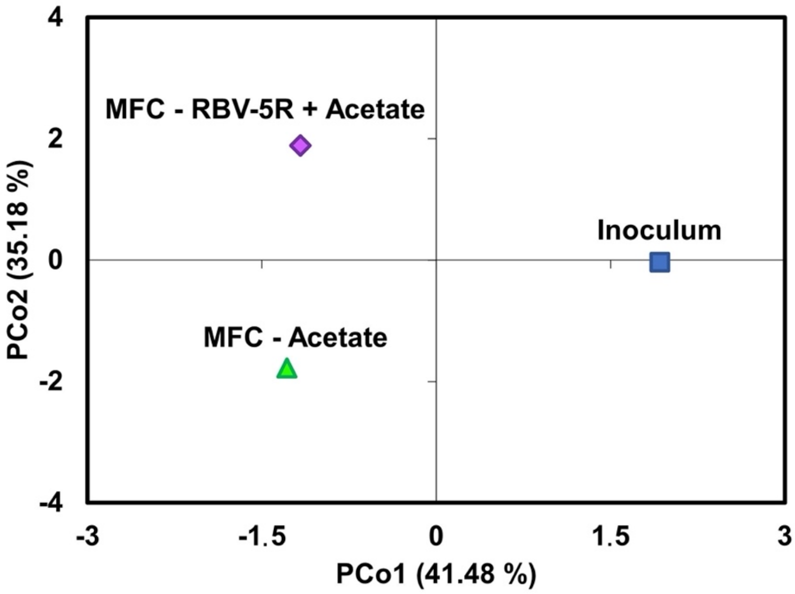

Textile azo dyes often have complex chemical structures and are refractory, defying biological decomposition. The bacterial that breakdown azo dye compete for the substrate. As a result, the composition of the microbial community may change (BAYINENI, 2022; UDUMA et al., 2023). Azo dye can cause microorganisms with specific enzymes and metabolic capacities to destroy this compound (PATEL et al., 2023b). Because they are not competitive in this selective environment, the number of microorganisms that cannot use the dye as a carbon source may decrease. Although cooperation between microorganisms can occur, competition is still a significant component (MITTAL; KUMAR, 2022; YADAV et al., 2022). Different microbial species can cooperate to break down azo dye in some microbial communities, allowing the application of metabolic synergies to increase degradation efficiency (ALZAIN; KALIMUGOGO; HUSSEIN, 2023). Azo dye can cause genetic changes in microbial populations over time, increasing their ability to break down dye. As organisms adapt to the new substrate, the microbial community can change significantly (CAO et al., 2021; JOKSIMOVIĆ et al., 2022; PANDE et al., 2019).

According to Fig. 25, canonical coordinate analysis (CCA) was performed for a more comprehensive investigation of the structure of the microbial community in the MFC+EF hybrid process. For CCA, temperature and RBV-5R were used as operational variables. The CCA indicated that RBV-5R development influenced the genus with the highest relative abundance (Pandoraea 69%) in the electrogenic biofilm. However, the CCA (Fig. 25) showed that temperature had a greater influence on the microbial structure of MFC+BEF, positively affecting the development or selection of electrogenic bacteria. The anodic chamber is entirely anaerobic; substrate decomposition occurs, and mesophilic temperatures ranging between 35 and 40°C are generally used for microbial development and activity (PATWARDHAN et al., 2021; SAVLA et al., 2022). Therefore, the results found in this study can be related to the constant temperature of 35 ± 2°C applied in the hybrid system. The temperature variation in the performance of MFC+BEF can be reflected in the evolution of the nature and distribution of the microbial community, the increase in the mass/electron transport rate, and the high nutrient/raw material activity in the microorganisms (DANGE et al., 2021; KHAN et al., 2014; REBEQUI et al., 2023).

Figure 25 - CCA diagram showing the relationships of 20 dominant genera associated with the variables highlighted in red (temperature and RBV-5R azo dye)

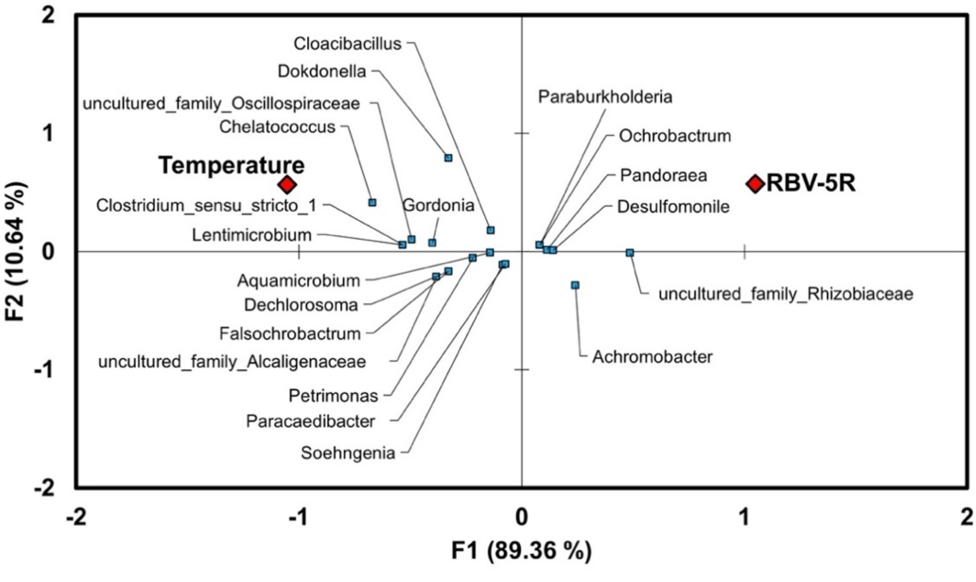

Figure 26 shows the relative abundance of the 20 genera of bacteria identified in the MFC anodic biofilm. In the MFC - RBV-5R + acetate, the development of the Proteobacteria and Synergistota phyla was increased by approximately 32% and 71%, respectively, compared to MFC - acetate. The Proteobacteria phylum consisted of the following genera: Pandoraea (69%), uncultured_family_Rhizobiaceae (3%), non-uncultured_family_Alcaligenaceae (2%), Achromobacter (2%), Paracaedibacter (2%), Aquamicrobium (1%), Ochrobactrum (1%), Falsochrobactrum (1%), Paraburkholderia (1%), Dechlorosoma (1%), Dokdonella (0.5%) and Chelatococcus (0.5%). In this study, an increase of approximately 97% in the genus Pandoraea (Proteobacteria phylum) was observed in the MFC - RBV-5R+acetate. This genus belongs to the β subclass of Proteobacteria, which contains a group of gram-negative bacilli that are aerobic or facultative anaerobes (JEONG et al., 2016; LIN et al., 2019). Some studies show that soil and water represent the natural habitats of Pandoraea bacteria, where they can be part of rhizosphere communities (ANANDHAM et al., 2010; JEONG et al., 2016). *P. faecigallinarum, P. oxalativorans, P. terrae, P. thiooxydans,* and *P. vervacti* were isolated from environmental samples (SEE-TOO et al., 2019). These free-living Pandoraea bacteria are often enriched in polluted soils and participate in the biodegradation of complex organic substances (PEETERS et al., 2019). Little is known about its metabolic activity and bioelectrochemical behavior in MFCs. The results from previous studies have demonstrated the predominant identification of Pandoraea in MFCs for the degradation of complex organic compounds (CHEN et al., 2022; LI et al., 2020b; LUO et al., 2021). In addition to the genus Pandoraea, the genus Petrimonas (Bacteroidota phyla) emerged as one of the leading genera in this study. Both are genera of fermentative acidogenic bacteria that can transfer and simultaneously use electrons to produce hydrogen (H^+) ((DAI et al., 2020b; DINH et al., 2021).

Figure 26 - The 20 top genera's relative abundance in percentage according to MFC-acetate and MFC-RBV-5R+acetate

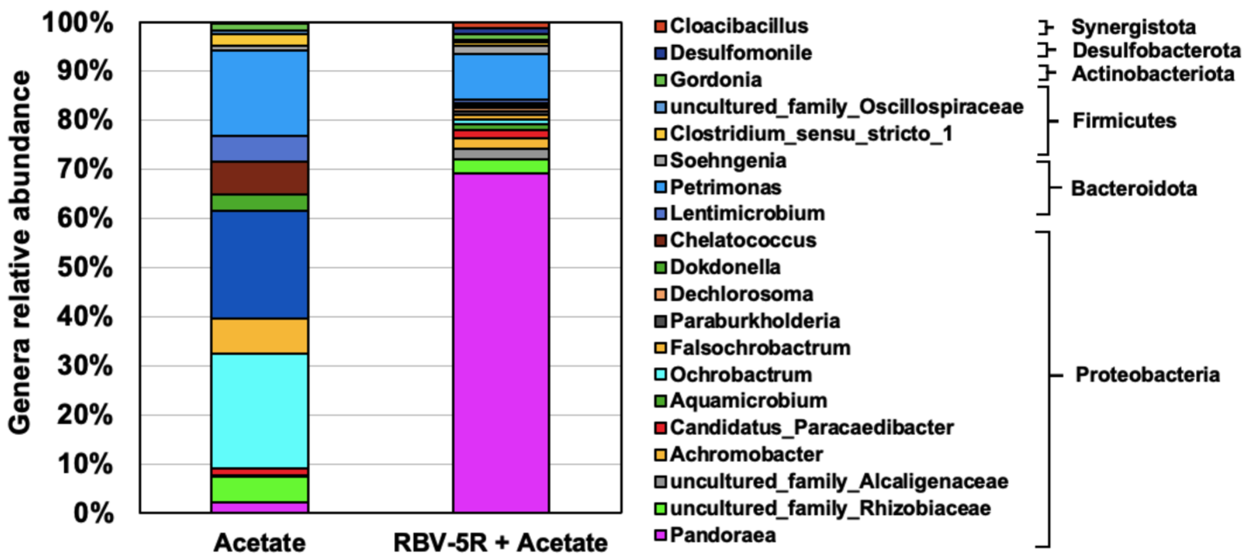

According to Fig. 26, the Bacteroidota phylum comprised bacteria of the genera Petrimonas (10%) and Lentimicrobium (1%). The Firmicutes phylum included the genera Clostridium_sensu_stricto_1 (1%), uncultured_family_Oscillospiraceae (1%), and Soehngenia (2%). The Desulfobacterota phylum with the genus Desulfomonile (1%). The Synergistota phylum with the genus Cloabacillus (1%). The Actinobacteria phylum with the genus Gordonia (1%). Although it is difficult to track the activities of these genera of microorganisms and their events, mixed cultures are considered more efficient for generating bioelectricity. The symbiosis of microorganisms, the recovery of microbial electrons, and collaboration in using the substrate help the microbial consortium to be more effective (KUMAR et al., 2017). In addition, a mixed microbial community is more resilient to process instability, such as overload, anodic air contamination, and toxic compounds (LOGAN et al., 2006). In general, it is important to state that the metabolic enhancement part has yet to be explored in the literature in an optimized way to generate bioelectricity. Most bioelectricity generation systems are limited by their ability to generate large amounts of energy because complex natural electroactive communities have poorly defined microbial species that can interact in various positive and negative ways (AHMED et al., 2022; AJUNWA et al., 2021; HALFELD et al., 2022; PRATHIBA; KUMAR; VO, 2022).

Correlation analysis helps identify relationships and associations between different groups of microorganisms and can show how microbial structure responds to changes in the MFC with operational efficiency metrics. In this study, the predominant bacterial genera were correlated with the MFC+BEF operational parameter efficiency (Fig. 27). Notably, the RBV-5R removal efficiency, electric current generation, and H_2O_2 synthesis could be correlated with the microbial community effect.

Figure 27 - Pearson's correlation analysis (r) between the 20 dominant microbial genera in the MFC and the efficiencies of RBV-5R+acetate conversion into electric current and H_2O_2

Genus	RBV-5R removal	COD removal	CE	Current	FE	H_2O_2	Scale
Pandoraea	-0.2036	-0.3510	-0.3685	-0.1105	0.3929	0.8307	1
Petrimonas	-0.8667	-0.5773	-0.0970	0.4644	0.7294	0.3056	
uncultured_family_Rhizobiaceae	0.9475	0.7534	0.3291	-0.2706	-0.8525	-0.4517	0.5
uncultured_family_Alcaligenaceae	-0.3896	-0.5114	-0.5481	-0.4688	0.3228	-0.1466	
Achromobacter	-0.6968	-0.5227	-0.2107	0.1513	0.5447	0	0
Soehngenia	-0.2611	0.2217	0.7086	**0.9750**	0.0838	-0.0999	
Candidatus_Paracaedibacter	-0.3050	-0.5362	-0.6857	-0.6674	0.2908	-0.0869	-0.5
Desulfomonile	0.3306	-0.0663	-0.5288	-0.9143	-0.2629	-0.3463	
Cloacibacillus	-0.4216	-0.7496	-0.9291	-0.7956	0.4958	0.2871	-1
Aquamicrobium	-0.1691	-0.4498	-0.6798	-0.7559	0.1735	-0.1520	
Gordonia	-0.5130	-0.7831	-0.8909	-0.7001	0.5562	0.2746	
Ochrobactrum	0.3934	-0.0618	-0.5467	-0.8389	-0.1850	0.1729	
Falsochrobactrum	0.5962	0.3048	-0.0801	-0.4079	-0.4031	0.1313	
Paraburkholderia	-0.1860	-0.4108	-0.5929	-0.6611	0.1578	-0.2269	
Clostridium_sensu_stricto_1	-0.8205	-0.5433	-0.0481	0.6049	0.7888	0.7283	
Dechlorosoma	0.4199	0.0268	-0.3997	-0.6543	-0.2009	0.2656	
uncultured_family_Oscillospiraceae	0.3306	-0.0663	-0.5288	-0.9143	-0.2629	-0.3463	
Lentimicrobium	0.6067	0.2514	-0.2534	-0.8007	-0.5543	-0.5663	
Dokdonella	-0.4199	-0.0268	0.3997	0.6543	0.2009	-0.2656	
Chelatococcus	-0.5962	-0.3048	0.0801	0.4079	0.4031	-0.1313	

Strong correlation when r ≥ |0.9|; moderate correlation when |0.5| ≤ r < |0.7|). Colors: red - negative correlation; blue - positive correlation

The genus uncultured_family_Rhizobiaceae was positively correlated with the proportion of microorganisms responsible for RBV-5R removal (r = 0.9475) and COD removal (r = 0.7534). Further research demonstrates that acclimation can increase the bacterial species belonging to the Rhizobiaceae family and produce conductive bacterial nanowires (ZHANG et al., 2019b). As a result, we believe that metabolically adaptive conductive bacterial nanowires can work together to accelerate startup, helping bacteria irreversibly connect and build a stable, specific biofilm. Therefore, in anaerobic situations, these bacteria can cleave the azo bond of the dye molecule, apparently through the action of cytoplasmic azoreductases of short specificity, to produce colorless aromatic amines (AJAZ; SHAKEEL; REHMAN, 2020; SHABIR et al., 2022). Regarding electron transfer efficiency and H_2O_2 synthesis, the genera Petrimonas, Clostridium_sensu_stricto_1, and Pandoraea were significantly positively correlated with the MFC metrics. The findings demonstrate the ability of these microbial genera in the RBV-5R removal relationship with H_2O_2 synthesis. Previous studies identified these genera in MFC biofilms (CAO et al., 2018, 2019; YING et al., 2021; YOU et al., 2023). Meanwhile, the genus Soehgenia (Bacteroidota phylum) was significantly positively correlated with the efficiency of substrate conversion in voltage (CE) (r = 0.7086) and consequently in electric current (r = 0.9750). Soehngenia is a genus of lactic acid bacteria known for their ability to ferment a variety of organic substrates (NAZINA et al., 2020; TRABLY et al., 2008). However, it is important to note that despite its metabolic efficiency, a detailed understanding of its bioelectrochemical behavior still requires further investigation.

According to the results, due to the complexity of the dynamics of microbial interactions, the association between bacterial genera and MFC operational metrics was difficult to establish. As a result of factors such as adaptability, competition, and changes in operational circumstances, MFC bacterial populations may have varied over the time of operation. Bacteria often cooperate, and one species' actions can immediately impact another. This can result in synergies that are difficult to associate with a specific genus.

5.4 CONCLUSION

This study demonstrated that the MFC+BEF hybrid treatment system promoted rapid discoloration mainly due to oxidative post-treatment. The best operational strategy was to apply 20 mg RBV-5R L^{-1} for a 6-h HRT for MFC and 12-h HRT for BEF. The color, COD removal, and aromatic group degradation reached 99.8 ± 0.10%, 79.58 ± 0.30% and 78.68 ± 1.0%, respectively, after BEF 12-h HRT. An extended HRT allows for a longer reaction time between the azo dye and the oxidizing agents generated in the BEF process. Furthermore, phytotoxicity analysis revealed that adjusting the pH from 3.0 to 7.0 resulted in lower phytotoxicity for *L. sativa* (GI = 30.1%) and *R. sativus* (GI = 43.8%) seeds compared to raw effluent.

The PCoA and CCA showed substantial changes when feeding the system with RBV-5R compared to sodium acetate and the inoculum feeding. The genera of the uncultured_family_Rhizobiaceae (r = 0.9475), Soehngenia (r = 0.9750), and Pandoraea (r = 0.8307) showed positive correlations, from the RBV-5R degradation stage, conversion into electrical current and H_2O_2 synthesis. This study provides insights into the microbial dynamics regulating the effectiveness of the MFC+BEF system, highlighting the system's great potential for sustainable and effective wastewater treatment.

6 CAPÍTULO 6 – CONCLUSÕES GERAIS E RECOMENDAÇÕES

6.1 CONCLUSÃO

A primeira fase da pesquisa proporcionou insights fundamentais sobre o processo de aclimatação de uma CCM de câmara dupla para a síntese de H_2O_2 por meio de eletrossíntese microbiana. Após 20 dias de aclimatação, a CCM demonstrou um desempenho notável, atingindo uma densidade de potência máxima de 60,6 mW m^{-2} e uma concentração de 15,17 mg H_2O_2 L^{-1}. A análise da estrutura microbiana revelou mudanças significativas, com um aumento substancial de bactérias eletrogênicas pertencentes aos filos Proteobacteria e Firmicutes. Além disso, os gêneros Kerstersia e Pandoraea apresentaram correlações positivas ($r > 0,850$) entre a conversão de substrato em corrente elétrica e a subsequente síntese de H_2O_2. Esses resultados fornecem uma base robusta para a continuidade da pesquisa, validando a eficácia das adaptações metabólicas impostas pela CCM. Devido à complexidade da dinâmica das interações microbianas, a associação entre gêneros bacterianos e as métricas operacionais da CCM foram difíceis de se estabelecerem. Como resultado de fatores como adaptabilidade, competição e mudanças nas circunstâncias operacionais, as populações bacterianas da CCM podem ter variado ao longo do tempo. Isso porque as bactérias cooperam frequentemente e as ações de uma espécie podem ter um impacto imediato nas outras.

A segunda fase da pesquisa foi dedicada à avaliação do processo BEF na remoção do VBR-5R. A aplicação de 10 Ω R_{ext} apresentou os melhores resultados. A taxa de remoção do VBR-5R foi incrementada à medida que a R_{ext} aplicada ao sistema diminuiu. Por haver maior transporte de elétrons quando aplicado menor R_{ext}, mais espécies •OH podem terem sido geradas. Uma ligação mais eficaz com o VBR-5R foi promovida reduzindo a R_{ext}, melhorando a difusão do •OH na solução. No entanto, a persistência da toxicidade, embora menor que na solução inicial de corante, pode ter sido promovida pela degradação parcial dos grupos aromáticos e subprodutos da reação de oxidação formados durante o tratamento via BEF. Apesar do desafio de reduzir a toxicidade do efluente, a eficiência operacional sugere que o BEF pode ter aplicações práticas em escala industrial para o tratamento de efluentes contendo azo-corantes, desde que técnicas complementares de tratamento possam ser combinadas para obtenção de efluente de saída com melhor qualidade e segurança ambiental.

A implementação do sistema híbrido CCM+BEF alcançou eficientemente uma eficiência global de remoção do VBR-5R superior a 99,8 ± 0,1% e degradação de grupos aromáticos de 78,7 ± 1,0%. A CCM fortaleceu significativamente o reator acoplado, levando à rápida descoloração e degradação parcial de VBR-5R. O sistema acoplado ao BEF possivelmente obteve melhor eficiência de tratamento devido ao biofilme e ao ataque cortante do •OH na estrutura química do VBR-5R. Mesmo em altas concentrações de VBR-5R, a capacidade do processo BEF de remover cor e compostos aromáticos foi incrementada pelo aumento do TDH. Além disso, o ajuste de pH final reduziu significativamente a toxicidade do efluente tratado, indicando a importância das condições operacionais. Alguns gêneros de bactérias eletrogênicas presentes no biofilme anódico apresentaram correlações positivas ($r > 0,900$), sugerindo que esses microrganismos desempenharam papéis cruciais na degradação do VBR-5R, na conversão em corrente elétrica e na síntese de H_2O_2. A correlação entre a mudança na estrutura microbiana e o incremento na síntese de H_2O_2 sugere uma resposta específica da comunidade aos estímulos eletroquímicos, destacando a importância dessas interações para o desempenho do sistema.

Ao comparar as técnicas de tratamento entre BEF e o sistema híbrido CCM+BEF, a aplicação do BEF mostrou-se a abordagem mais eficaz para degradar o VBR-5R. Isso se deve as remoções superiores de DQO no BEF, enquanto as remoções de cor e compostos aromáticos foram muito próximas às observadas no CCM+BEF. Considerando o efluente tratado com pH final ácido (sem ajuste do pH), as diferenças entre os índices de germinação do BEF e do sistema híbrido CCM+BEF foram significativamente superiores para os efluentes tratados via BEF. Os valores de IG foram superiores em cerca de 79,6% para *L. sativa* e 70,2% para *R. sativus* no efluente tratado via BEF em comparação ao sistema híbrido. Ou seja, o processo de tratamento via BEF eliminou a toxicidade de forma mais incisiva e eficaz em comparação ao sistema híbrido proposto. A hipótese é que no sistema híbrido CCM+BEF, pode ter ocorrido uma maior geração de subprodutos da degradação do

VBR-5R, que possivelmente eram tóxicos. Essa ocorrência pode estar relacionada aos maiores TDH’s e as altas concentrações de DQO de entrada aplicados no sistema híbrido, o que potencialmente pode ter prejudicado a toxicidade no efluente tratado.

Em resumo, a pesquisa apresentou avanços importantes na compreensão e aplicação de sistemas híbridos de tratamento, oferecendo contribuições valiosas para a comunidade científica e proporcionando potenciais soluções práticas para desafios ambientais associados à contaminação por azo-corantes têxteis. Com base nas conclusões obtidas em cada fase da pesquisa, é possível afirmar que o sistema bioeletroquímico de eletrossíntese microbiana aplicado à remoção de azo-corantes apresentou resultados promissores. A investigação detalhada das fases permitiu obter insights significativos, respondendo de maneira afirmativa às questões de pesquisa e validando parcialmente as hipóteses estabelecidas.

6.2 RECOMENDAÇÕES

- Explorar alternativas para minimizar impactos ambientais adversos, especialmente em relação à toxicidade do efluente pós-tratamento, considerando diferentes estratégias operacionais e ajustes na configuração do reator.
- Conduzir estudos de longo prazo para avaliar a estabilidade do sistema ao longo do tempo, considerando possíveis mudanças na comunidade microbiana e eficiência do tratamento.
- Testar a eficiência dos processos BEF e CCM+BEF com efluentes têxteis reais.
- O uso da oxidação de Fenton acionada pela CCM ainda está em escala de laboratório, com o volume dos sistemas na faixa de algumas centenas de mililitros. A replicabilidade de tais sistemas para configurações maiores devem ser avaliada para entender as dificuldades práticas que podem surgir durante o *upscaling*.
- Deve ser realizado estudo de viabilidade em termos de operação em modo contínuo com tratamento de efluentes fortemente contaminados, ou seja, mais próximos possíveis das circunstâncias reais de operação;
- Para melhorar o desempenho da operação a longo prazo e reduzir o custo da CCM, é necessário estudar e desenvolver eletrodos, catalisadores e materiais separadores sustentáveis, de baixo custo e alto desempenho.

REFERÊNCIAS

ABNT. **Materiais têxteis — Segurança química em têxteis — Requisitos e métodos de ensaio.** Rio de Janeiro, 2019.

ADACHI, A. et al. Decolorization and degradation of methyl orange azo dye in aqueous solution by the electro-Fenton process: application of optimization. **Catalysts**, v. 12, n. 6, p. 1–12, 2022.

ADELAJA, O.; KESHAVARZ, T.; KYAZZE, G. The effect of salinity, redox mediators and temperature on anaerobic biodegradation of petroleum hydrocarbons in microbial fuel cells. **Journal of Hazardous Materials**, v. 283, p. 211–217, fev. 2015.

AFOLABI, O. A.; ADEKALU, K. O.; OKUNADE, D. A. Electro-Fenton treatment process for brewery wastewater: effects of oxidant concentration and reaction time on BOD and COD removal efficiency. **Journal of Engineering and Applied Science**, v. 69, n. 1, p. 1–14, 2022.

AGRAWAL, K. et al. Microbial fuel cell: a boon in bioremediation of wastes. In: **Microbial Wastewater Treatment**. [s.l.] Elsevier Inc., 2019. p. 175–194.

AHMED, S. F. et al. Insights into the development of microbial fuel cells for generating biohydrogen, bioelectricity, and treating wastewater. **Energy**, v. 254, p. 1–24, 2022.

AIYER, K. S. Synergistic effects in a microbial fuel cell between co-cultures and a photosynthetic alga Chlorella vulgaris improve performance. **Heliyon**, v. 7, n. 1, p. 1–7, jan. 2021.

AIYER, K. S.; VIJAYAKUMAR, B. S. A selection strategy for enhancing exoelectrogenic consortium towards improved power generation in microbial fuel cells. **International Journal of Energy Research**, v. 45, n. 4, p. 5318–5324, 2021.

AJAZ, M.; SHAKEEL, S.; REHMAN, A. Microbial use for azo dye degradation—a strategy for dye bioremediation. **International Microbiology**, v. 23, n. 2, p. 149–159, 2020.

AJUNWA, O. M. et al. Influence of enhanced electrogenicity on anodic biofilm and bioelectricity production by a novel microbial consortium. **Process Biochemistry**, v. 104, p. 27–38, 2021.

AL-TOHAMY, R. et al. A critical review on the treatment of dye-containing wastewater: ecotoxicological and health concerns of textile dyes and possible remediation approaches for environmental safety. **Ecotoxicology and**

Environmental Safety, v. 231, p. 1–17, 2022.

ALBARRACIN-ARIAS, J. A. et al. Microbial community dynamics and electricity generation in MFCs inoculated with POME sludges and pure electrogenic culture. **International Journal of Hydrogen Energy**, v. 46, n. 74, p. 36903–36916, 2021.

ALMEIDA, E. J. R. DE et al. Azo dyes degradation and mutagenicity evaluation with a combination of microbiological and oxidative discoloration treatments. **Ecotoxicology and Environmental Safety**, v. 183, p. 1–10, 2019.

ALMEIDA, E. J. R. DE et al. Simultaneous energy generation, decolorization, and detoxification of the azo dye Procion Red MX-5B in a microbial fuel cell. **Journal of Environmental Chemical Engineering**, v. 9, n. 5, p. 1–10, 2021.

ALZAIN, H.; KALIMUGOGO, V.; HUSSEIN, K. A review of bacterial degradation of azo dyes. **International Journal of Research and Review**, v. 10, n. 6, p. 443–462, 20 jun. 2023.

AMBROSE, M. et al. Pandoraea pnomenusa Isolated from an australian patient with cystic fibrosis. **Frontiers in Microbiology**, v. 7, p. 1–9, 11 maio 2016.

ANANDHAM, R. et al. Pandoraea thiooxydans sp. nov., a facultatively chemolithotrophic, thiosulfate-oxidizing bacterium isolated from rhizosphere soils of sesame (Sesamum indicum L.). **International Journal of Systematic and Evolutionary Microbiology**, v. 60, n. 1, p. 21–26, 1 jan. 2010.

ANDREIDES, M.; DOLEJŠ, P.; BARTÁČEK, J. The prediction of WWTP influent characteristics: good practices and challenges. **Journal of Water Process Engineering**, v. 49, p. 1–13, out. 2022.

ANGELAALINCY, M. J. et al. Biofilm engineering approaches for improving the performance of microbial fuel cells and bioelectrochemical systems. **Frontiers in Energy Research**, v. 6, p. 1–12, 2018.

APHA. **Standard methods for the examination of water and wastewater (3ed.)American Public Health Association**, 2018. Disponível em: <http://dl.mozh.org/upload/StandardMetods23RD.pdf>

APOLLON, W. et al. Improvement of zero waste sustainable recovery using microbial energy generation systems: a comprehensive review. **Science of the Total Environment**, v. 817, n. 153055, p. 1–22, 2022.

ARAÚJO, M. P. DE; EL-DEIR, S. G.; TAVARES, R. G. Lactuca sativa as bioindicator of aluminum contamination in water treatment plant sludge. **S & G**

Journal, v. 16, n. 2, p. 178–186, 2021.

ARENDS, J. B. A. et al. Principles and technology of microbial fuel cells. In: **Fuel Cell Science and Engineering: Materials, Processes, Systems and Technology**. [s.l: s.n.]. v. 1p. 147–184.

ASGHAR, A.; RAMAN, A. A. A.; DAUD, W. M. A. W. Recent advances, challenges and prospects of in situ production of hydrogen peroxide for textile wastewater treatment in microbial fuel cells. **Journal of Chemical Technology and Biotechnology**, v. 89, n. 10, p. 1466–1480, 2014.

BAÊTA, B. E. L. et al. Evaluation of soluble microbial products and aromatic amines accumulation during a combined anaerobic/aerobic treatment of a model azo dye. **Chemical Engineering Journal**, v. 259, p. 936–944, 2015.

BAGHERZADEH, F. et al. Prediction of energy consumption and evaluation of affecting factors in a full-scale WWTP using a machine learning approach. **Process Safety and Environmental Protection**, v. 154, p. 458–466, out. 2021.

BANERJEE, A.; CALAY, R. K.; MUSTAFA, M. Review on material and design of anode for microbial fuel cell. **Energies**, v. 15, n. 2283, p. 1–18, 2022.

BAYINENI, V. K. Bioremediation of toxic dyes for zero waste. In: **Biotechnology for Zero Waste**. [s.l.] Wiley, 2022. p. 47–66.

BEHERA, C. R. et al. A process synthesis tool for WWTP: an application to design sustainable energy recovery facilities. **Chemical Engineering Research and Design**, v. 156, p. 353–370, abr. 2020.

BEHERA, M. et al. A review on the treatment of textile industry waste effluents towards the development of efficient mitigation strategy: an integrated system design approach. **Journal of Environmental Chemical Engineering**, v. 9, n. 4, p. 1–21, 2021.

BELAL, R. M. et al. Electrochemical degradation and degree of mineralization of the BY28 dye in a supporting Electrolyte mixture using an expanded dimensionally stable anode. **Electrocatalysis**, v. 13, n. 1, p. 26–36, 2022.

BELBEL, H. et al. Use of metallurgical waste as a catalyst in electro-Fenton process for degradation of dyes from aqueous solution. **Desalination and Water Treatment**, v. 273, p. 261–269, 2022.

BENASSI, J. C. et al. Evaluation of color removal efficiencies and kinetic parameters of Fenton (H2O2/Fe2+) and photo-Fenton (H2O2/Fe2+/UV) processes in the treatment of a textile wastewater containing indigo blue. **Brazilian Journal of**

Development, v. 7, n. 11, p. 102327–102347, 2021.

BENHADJI, A.; AHMED, M. T. Yellow 2G dye degradation by electro-Fenton process using steel electrode as catalysis and its phytotoxicity effect. **Water Science and Technology**, v. 82, n. 3, p. 565–576, 2020.

BENKHAYA, S.; RABET, S.; EL HARFI, A. A review on classifications, recent synthesis and applications of textile dyes. **Inorganic Chemistry Communications**, v. 115, p. 1–35, 2020.

BHAGAT, S. K. et al. Comprehensive review on machine learning methodologies for modeling dye removal processes in wastewater. **Journal of Cleaner Production**, v. 45, p. 1–177, dez. 2022.

BHARATHI, D. et al. Microbial approaches for sustainable remediation of dye-contaminated wastewater: a review. **Archives of Microbiology**, v. 204, n. 3, p. 1–11, 2022.

BIFFINGER, J. C. et al. Oxygen exposure promotes fuel diversity for Shewanella oneidensis microbial fuel cells. **Biosensors and Bioelectronics**, v. 23, n. 6, p. 820–826, 2008.

BIRJANDI, N. et al. Enhanced medicinal herbs wastewater treatment in continuous flow bio-electro-Fenton operations along with power generation. **Renewable Energy**, v. 155, p. 1079–1090, ago. 2020.

BOAS, J. V. et al. Review on microbial fuel cells applications, developments and costs. **Journal of Environmental Management**, v. 307, p. 1–19, 2022.

BOLYEN, E. et al. Reproducible, interactive, scalable and extensible microbiome data science using QIIME 2. **Nature Biotechnology**, v. 37, n. 8, p. 852–857, 24 ago. 2019.

BORJA-MALDONADO, F.; ZAVALA, M. Á. L. Contribution of configurations, electrode and membrane materials, electron transfer mechanisms, and cost of components on the current and future development of microbial fuel cells. **Heliyon**, v. 8, n. 9849, p. 1–25, 2022.

BRILLAS, E.; MARTÍNEZ-HUITLE, C. A. Decontamination of wastewater containing synthetic organic dyes by electrochemical methods: an updated review. **Applied Catalysis B: Environmental**, v. 166–167, p. 603–643, 2015.

BRYSZEWSKI, K. Ł.; RODZIEWICZ, J.; JANCZUKOWICZ, W. Effect of bio-electrochemical treatment of hydroponic effluent on the nutrient content. **Applied Sciences**, v. 12, n. 19, p. 1–11, 2022.

CAI, J. et al. Insights into microbial community in microbial fuel cells simultaneously treating sulfide and nitrate under external resistance. **Biodegradation**, v. 32, n. 1, p. 73–85, 13 fev. 2021.

CAI, W. F. et al. Investigation of a two-dimensional model on microbial fuel cell with different biofilm porosities and external resistances. **Chemical Engineering Journal**, v. 333, p. 572–582, 2018.

CALLAHAN, B. J. et al. DADA2: high-resolution sample inference from Illumina amplicon data. **Nat. Methods**, v. 13, n. 7, p. 581, 2016.

CAO, X. et al. Azo dye degradation pathway and bacterial community structure in biofilm electrode reactors. **Chemosphere**, v. 208, p. 219–225, 2018.

CAO, X. et al. Azo dye as part of co-substrate in a biofilm electrode reactor–microbial fuel cell coupled system and an analysis of the relevant microorganisms. **Chemosphere**, v. 216, p. 742–748, 2019.

CAO, X. et al. Limitation of voltage reversal in the degradation of azo dye by a stacked double-anode microbial fuel cell and characterization of the microbial community structure. **Science of the Total Environment**, v. 754, p. 1–7, 2021.

CAO, Y. et al. Explore various co-substrates for simultaneous electricity generation and Congo red degradation in air-cathode single-chamber microbial fuel cell. **Bioelectrochemistry**, v. 79, n. 1, p. 71–76, 2010.

CAPODAGLIO, A. G. et al. Microbial fuel cells for direct electrical energy recovery from urban wastewaters. **The Scientific World Journal**, p. 1–9, 2013.

CAPORASO, J. G. et al. QIIME allows analysis of high-throughput community sequencing data. **Nat. Methods**, v. 7, n. 5, p. 335, 2010.

CASADO, J. Towards industrial implementation of electro-Fenton and derived technologies for wastewater treatment: a review. **Journal of Environmental Chemical Engineering**, v. 7, n. 1, p. 1–15, 2019.

CASTILLO-SUÁREZ, L. A. et al. A critical review of textile industry wastewater: green technologies for the removal of indigo dyes. **International Journal of Environmental Science and Technology**, p. 1–38, 2023.

CASTRO, F. D. et al. Reactive Orange 16 dye degradation in anaerobic and aerobic MBBR coupled with ozonation: addressing pathways and performance. **International Journal of Environmental Science and Technology**, v. 18, n. 7, p. 1991–2010, 2021.

CETINKAYA, A. Y. et al. Electricity production and characterization of high-strength industrial wastewaters in microbial fuel cell. **Applied Biochemistry and Biotechnology**, v. 182, n. 2, p. 468–481, 2017.

CHAE, K.-J. et al. Effect of different substrates on the performance, bacterial diversity, and bacterial viability in microbial fuel cells. **Bioresource Technology**, v. 100, n. 14, p. 3518–3525, jul. 2009.

CHANKHANITTHA, T. et al. Performance of solvothermally grown Bi2MoO6 photocatalyst toward degradation of organic azo dyes and fluoroquinolone antibiotics. **Materials Letters**, v. 258, p. 1–13, jan. 2020.

CHATURVEDI, V.; VERMA, P. Microbial fuel cell: a green approach for the utilization of waste for the generation of bioelectricity. **Bioresources and Bioprocessing**, v. 3, n. 1, p. 1–14, 17 dez. 2016.

CHAUHAN, V.; GAUTAM, P.; KANWAR, S. S. Azo dyes: a notorious class of water pollutant, and role of enzymes to decolorize and degrade them. In: **Development in Wastewater Treatment Research and Processes**. [s.l.] Elsevier, 2022. p. 433–448.

CHAVAN, R. B. Environmentally friendly dyes. In: **Handbook of Textile and Industrial Dyeing**. [s.l.] Elsevier, 2011. p. 515–561.

CHEN, B.-Y. et al. Assessment upon azo dye decolorization and bioelectricity generation by Proteus hauseri. **Bioresource Technology**, v. 101, n. 12, p. 4737–4741, jun. 2010.

CHEN, G. et al. Aerobic degradation of sulfanilic acid using activated sludge. **Water Research**, v. 46, n. 1, p. 145–151, 2012.

CHEN, H. et al. Fundamentals, applications, and future directions of bioelectrocatalysis. **Chemical Reviews**, v. 120, n. 23, p. 12903–12993, 2020.

CHEN, J. et al. The fate of antibiotic resistance genes (ARGs) and mobile genetic elements (MGEs) from livestock wastewater (dominated by quinolone antibiotics) treated by microbial fuel cell (MFC). **Ecotoxicology and Environmental Safety**, v. 218, p. 1–9, jul. 2021.

CHEN, J. et al. Reduction and control of antibiotic-resistance genes and mobile genetic elements in tetracycline livestock wastewater treated by microbial fuel cell. **Journal of Environmental Engineering**, v. 148, n. 8, p. 1–11, 2022.

CHEN, J.; LI, N.; ZHAO, L. Three-dimensional electrode microbial fuel cell for hydrogen peroxide synthesis coupled to wastewater treatment. **Journal of Power Sources**, v. 254, p. 316–322, maio 2014.

CHEN, S.; PATIL, S. A.; SCHRÖDER, U. A high-performance rotating graphite fiber brush air-cathode for microbial fuel cells. **Applied Energy**, v. 211, p. 1089–1094, fev. 2018.

CHENG, P. et al. Degradation efficiency of antibiotics by the sewage-fed microbial fuel cells depends on gram-staining property of exoelectrogens. **Process Safety and Environmental Protection**, v. 176, p. 421–429, 2023.

CHENG, S.; LIU, H.; LOGAN, B. E. Increased power generation in a continuous flow MFC with advective flow through the porous anode and reduced electrode spacing. **Environmental Science & Technology**, v. 40, n. 7, p. 2426–2432, 1 abr. 2006.

CHENGALROYEN, M. D.; DABBS, E. R. The microbial degradation of azo dyes: minireview. **World Journal of Microbiology and Biotechnology**, v. 29, n. 3, p. 389–399, 30 mar. 2013.

CHIARELLO, M. et al. Ranking the biases: the choice of OTUs vs. ASVs in 16S rRNA amplicon data analysis has stronger effects on diversity measures than rarefaction and OTU identity threshold. **PLoS ONE**, v. 17, p. 1–19, 2022.

CHIRANJEEVI, P.; PATIL, S. A. Strategies for improving the electroactivity and specific metabolic functionality of microorganisms for various microbial electrochemical technologies. **Biotechnology Advances**, v. 39, n. 107468, p. 1–16, 2020.

CHOUDHURY, P. et al. Performance improvement of microbial fuel cell (MFC) using suitable electrode and bioengineered organisms: a review. **Bioengineered**, v. 8, n. 5, p. 471–487, 2017.

CHOUDHURY, P. et al. The overall performance improvement of microbial fuel cells connected in series with dairy wastewater treatment. **Journal of Electrochemical Science and Technology**, v. 12, n. 1, p. 101–111, 28 fev. 2021.

CHUNG, T. H. et al. Microbial electrochemical systems for hydrogen peroxide synthesis: critical review of process optimization, prospective environmental applications, and challenges. **Bioresource Technology**, v. 313, p. 1–15, 2020.

COHEN, O.; COOLEY, M. The aim of production. **Computerised Manufacturing**, v. 1988, n. 2, p. 20, 1988.

CRUZ-NORIEGA, M. D. LA et al. Use of wastewater and electrogenic bacteria to generate eco-friendly electricity through microbial fuel cells. **Sustainability**, v. 15, n. 13, 2023.

CUI, D. et al. The comparative study on the rapid decolorization of azo, anthraquinone and triphenylmethane dyes by anaerobic sludge. **International Journal of Environmental Research and Public Health**, v. 13, n. 11, p. 1–18, 2016.

DAI, Q. et al. Sulfide-mediated azo dye degradation and microbial community analysis in a single-chamber air cathode microbial fuel cell. **Bioelectrochemistry**, v. 131, p. 1–11, fev. 2020a.

DAI, Q. et al. Sulfide-mediated azo dye degradation and microbial community analysis in a single-chamber air cathode microbial fuel cell. **Bioelectrochemistry**, v. 131, p. 1–12, fev. 2020b.

DAI, S. et al. Improving the performance of bioelectrochemical sulfate removal by applying flow mode. **Microbial Biotechnology**, p. 1–10, 2022.

DALARI, B. L. S. K. **Utilização de esferas de quitosana no processo foto-fenton heterogêneo no tratamento de efluente têxtil**. [s.l.] Universidade Federal de Santa Catarina, 2018.

DANGE, P. et al. Recent developments in microbial electrolysis cell-based biohydrogen production utilizing wastewater as a feedstock. **Sustainability**, v. 13, n. 16, p. 1–12, 6 ago. 2021.

DAS, A.; MISHRA, S. Complete biodegradation of azo dye in an integrated microbial fuel cell-aerobic system using novel bacterial consortium. **International Journal of Environmental Science and Technology**, v. 16, n. 2, p. 1069–1078, 2019.

DAS, S. et al. Microbial electrosynthesis: a way towards the production of electro-commodities through carbon sequestration with microbes as biocatalysts. **Journal of The Electrochemical Society**, v. 167, n. 155510, p. 1–10, 2020.

DE ARAÚJO, J. L. et al. Decontamination of real urban sewage—comparison between Fenton and electrochemical oxidation. **Environmental Science and Pollution Research**, v. 29, n. 23, p. 35061–35072, 2022.

DEBBARMA, P. et al. Microbial consortia and their application for environmental sustainability. In: **Advanced Microbial Techniques in Agriculture, Environment, and Health Management**. [s.l.] Elsevier, 2023. p. 205–222.

DEKA, R. et al. A techno-economic approach for eliminating dye pollutants from industrial effluent employing microalgae through microbial fuel cells: barriers and perspectives. **Environmental Research**, v. 212, p. 1–13, 2022.

DENG, F.; BRILLAS, E. Advances in the decontamination of wastewaters with synthetic organic dyes by electrochemical Fenton-based processes. **Separation and Purification Technology**, v. 316, p. 1–42, 2023.

DENG, Y.; ZHAO, R. Advanced oxidation processes (AOPs) in wastewater treatment. **Current Pollution Reports**, v. 1, n. 3, p. 167–176, set. 2015.

DERAKHSHANI, E. et al. Electro-fenton process efficiency for decolourization of aqueous solutions: study of reaction kinetics. **Desalination and Water Treatment**, v. 211, p. 296–303, 2021.

DEWIL, R. et al. New perspectives for advanced oxidation processes. **Journal of Environmental Management**, v. 195, p. 93–99, 2017.

DI FRAIA, S.; MASSAROTTI, N.; VANOLI, L. A novel energy assessment of urban wastewater treatment plants. **Energy Conversion and Management**, v. 163, p. 304–313, 2018.

DINH, H. T. T. et al. Bioelectrical methane production with an ammonium oxidative reaction under the no organic substance condition. **Microbes and Environments**, v. 36, n. 2, p. 1–8, 2021.

DIOS, M. A. F. DE et al. Application of benthonic microbial fuel cells and electro-Fenton process to dye decolourisation. **Journal of Industrial and Engineering Chemistry**, v. 20, n. 5, p. 3754–3760, set. 2014.

DO, M. H. et al. Microbial fuel cell-based biosensor for online monitoring wastewater quality: a critical review. **Science of the Total Environment**, v. 712, p. 1–11, 2020.

DWIVEDI, K. A. et al. Fundamental understanding of microbial fuel cell technology: recent development and challenges. **Chemosphere**, v. 288, p. 1–22, 2022.

EASHW. **Regulation (EC) No 1272/2008 - classification, labelling and packaging of substances and mixtures (CLP)**. Disponível em: <https://osha.europa.eu/en/legislation/directives/regulation-ec-no-1272-2008-classification-labelling-and-packaging-of-substances-and-mixtures>.

ESKANDARI, F.; SHAHNAVAZ, B.; MASHREGHI, M. Optimization of complete RB-5 azo dye decolorization using novel cold-adapted and mesophilic bacterial consortia. **Journal of Environmental Management**, v. 241, p. 91–98, 2019.

FADZLI, F. S.; BHAWANI, S. A.; MOHAMMAD, R. E. A. Microbial fuel cell: recent developments in organic substrate use and bacterial electrode interaction. **Journal of Chemistry**, p. 1–16, 2021.

FAJARDO-PUERTO, E. et al. From Fenton and ORR 2e - type catalysts to bifunctional electrodes for environmental remediation using the electro-Fenton process. **Catalysts**, v. 13, n. 674, p. 1–39, 2023.

FAN, Y.; SHARBROUGH, E.; LIU, H. Quantification of the internal resistance distribution of microbial fuel cells. **Environmental Science & Technology**, v. 42, n. 21, p. 8101–8107, 1 nov. 2008.

FANG, G.-D.; ZHOU, D.-M.; DIONYSIOU, D. D. Superoxide mediated production of hydroxyl radicals by magnetite nanoparticles: demonstration in the degradation of 2-chlorobiphenyl. **Journal of Hazardous Materials**, v. 250–251, p. 68–75, abr. 2013.

FANG, Z. et al. Performance of microbial fuel cell coupled constructed wetland system for decolorization of azo dye and bioelectricity generation. **Bioresource Technology**, v. 144, p. 165–171, set. 2013.

FANG, Z. et al. Electricity production from azo dye wastewater using a microbial fuel cell coupled constructed wetland operating under different operating conditions. **Biosensors and Bioelectronics**, v. 68, p. 135–141, 2015.

FANG, Z. et al. A microbial fuel cell-coupled constructed wetland promotes degradation of azo dye decolorization products. **Ecological Engineering**, v. 94, p. 455–463, set. 2016.

FANG, Z. et al. Electrode and azo dye decolorization performance in microbial-fuel-cell-coupled constructed wetlands with different electrode size during long-term wastewater treatment. **Bioresource Technology**, v. 238, p. 450–460, ago. 2017.

FATIMA, M. et al. A review on biocatalytic decomposition of azo dyes and electrons recovery. **Journal of Molecular Liquids**, v. 246, p. 275–281, 2017.

FENG, C. et al. A polypyrrole/anthraquinone-2,6-disulphonic disodium salt (PPy/AQDS)-modified anode to improve performance of microbial fuel cells. **Biosensors and Bioelectronics**, v. 25, n. 6, p. 1516–1520, fev. 2010a.

FENG, C. H. et al. Bioelectro-Fenton process driven by microbial fuel cell for wastewater treatment. **Environmental Science and Technology**, v. 44, n. 5, p. 1875–1880, 2010b.

FERNANDES, N. C. et al. Removal of azo dye using Fenton and Fenton-like processes: evaluation of process factors by Box–Behnken design and ecotoxicity tests. **Chemico-Biological Interactions**, v. 291, n. June, p. 47–54, 2018.

FERNANDO, E.; KESHAVARZ, T.; KYAZZE, G. Enhanced bio-decolourisation of acid orange 7 by Shewanella oneidensis through co-metabolism in a microbial fuel cell. **International Biodeterioration & Biodegradation**, v. 72, p. 1–9, ago. 2012.

FLIMBAN, S. G. A. et al. Overview of microbial fuel cell (MFC) recent advacement from fundamentals of application: MFC designs, major elements, and scalabilty. **Energy & Fuel Technology**, n. 2018100763, p. 1–48, 2018.

FLIMBAN, S. G. A. et al. The effect of Nafion membrane fouling on the power generation of a microbial fuel cell. **International Journal of Hydrogen Energy**, v. 45, n. 25, p. 13643–13651, maio 2020.

FRITTS, R. K. et al. A Rhizobiales-specific unipolar polysaccharide adhesin contributes to Rhodopseudomonas palustris biofilm formation across diverse photoheterotrophic conditions. **Applied and Environmental Microbiology**, v. 83, n. 4, p. 1–14, 15 fev. 2017.

FU, L. et al. Synthesis of hydrogen peroxide in microbial fuel cell. **Journal of Chemical Technology and Biotechnology**, v. 85, n. 5, p. 715–719, 2010a.

FU, L. et al. Degradation of azo dyes using in-situ Fenton reaction incorporated into H2O2-producing microbial fuel cell. **Chemical Engineering Journal**, v. 160, n. 1, p. 164–169, 15 maio 2010b.

GADEKAR, M. R.; AHAMMED, M. M. Modelling dye removal by adsorption onto water treatment residuals using combined response surface methodology-artificial neural network approach. **Journal of Environmental Management**, v. 231, p. 241–248, fev. 2019.

GAJDA, I.; GREENMAN, J.; IEROPOULOS, I. A. Recent advancements in real-world microbial fuel cell applications. **Current Opinion in Electrochemistry**, v. 11, p. 78–83, out. 2018.

GANDIGLIO, M. et al. Enhancing the energy efficiency of wastewater treatment plants through co-digestion and fuel cell systems. **Frontiers in Environmental Science**, v. 5, p. 1–21, 2017.

GANTA, A.; BASHIR, Y.; DAS, S. Dairy wastewater as a potential feedstock for valuable production with concurrent wastewater treatment through microbial electrochemical technologies. **Energies**, v. 15, n. 9084, p. 1–34, 2022.

GAO, M.; LU, J. Y.; LI, W. W. Oxygen reduction reaction electrocatalysts for microbial fuel cells. In: SINGH, ET AL. (Ed.). . **Novel catalyst materials for bioelectrochemical systems: fundamentals and applications**. Washington, DC: American Chemical Society, 2020. v. 1342p. 73–96.

GARG, S. K.; TRIPATHI, M. Microbial strategies for discoloration and detoxification of azo dyes from textile effluents. **Research Journal of Microbiology**, v. 12, n. 1, p. 1–19, 15 dez. 2017.

GHASEMI, M. et al. Effect of pre-treatment and biofouling of proton exchange membrane on microbial fuel cell performance. **International Journal of Hydrogen Energy**, v. 38, n. 13, p. 5480–5484, 2013.

GHATGE, S. et al. Degradation of sulfonated polyethylene by a bio-photo-fenton approach using glucose oxidase immobilized on titanium dioxide. **Journal of Hazardous Materials**, v. 423, p. 1–13, fev. 2022.

GOMAA, O. M. et al. The role of riboflavin in decolourisation of Congo red and bioelectricity production using Shewanella oneidensis-MR1 under MFC and non-MFC conditions. **World Journal of Microbiology and Biotechnology**, v. 33, n. 3, p. 1–10, 2017.

GONZALEZ DEL CAMPO, A. et al. Short-term effects of temperature and COD in a microbial fuel cell. **Applied Energy**, v. 101, p. 213–217, jan. 2013.

GOYAL, R. N.; MINOCHA, A. Electrochemical behaviour of the bisazo dye, Direct Red-81. **Journal of Electroanalytical Chemistry and Interfacial Electrochemistry**, v. 193, n. 1–2, p. 231–240, out. 1985.

GRABOWSKI, A. et al. Petrimonas sulfuriphila gen. nov., sp. nov., a mesophilic fermentative bacterium isolated from a biodegraded oil reservoir. **International Journal of Systematic and Evolutionary Microbiology**, v. 55, n. 3, p. 1113–1121, 1 maio 2005.

GU, T. et al. Extracellular electron transfer in microbial biocorrosion. **Current Opinion in Electrochemistry**, v. 29, p. 1–10, out. 2021.

GUARI, E. B. et al. Azo dye Acid Blue 29: biosorption and phytotoxicity test. **Water, Air, and Soil Pollution**, v. 226, n. 11, p. 1–7, 2015.

GUL, H. et al. Progress in microbial fuel cell technology for wastewater treatment and energy harvesting. **Chemosphere**, v. 281, p. 1–14, out. 2021.

GUO, J. et al. Redox potential-induced regulation of extracellular polymeric substances in an electroactive mixed community biofilm. **Science of the Total Environment**, v. 797, p. 1–8, 2021.

GUPTA, S.; SRIVASTAVA, P.; YADAV, A. K. Simultaneous removal of organic matters and nutrients from high-strength wastewater in constructed wetlands followed by entrapped algal systems. **Environmental Science and Pollution Research**, v. 27,

n. 1, p. 1112–1117, 9 jan. 2020.

GURIKAR, C. et al. Microbial fuel cells: an alternate approach for bioelectricity generation and waste management. **Journal of Pure and Applied Microbiology**, v. 15, n. 4, p. 1833–1845, 2021.

HAAVISTO, J. M. et al. Effect of hydraulic retention time on continuous electricity production from xylose in up-flow microbial fuel cell. **International Journal of Hydrogen Energy**, v. 42, n. 45, p. 27494–27501, 2017.

HALFELD, G. G. et al. Acclimatization of a microbial consortium into a stable biofilm to produce energy and 1,3-propanediol from glycerol in a microbial fuel cell. **International Journal of Hydrogen Energy**, v. 47, n. 49, p. 21241–21252, 2022.

HASHEMI, S. H.; KAYKHAII, M. Azo dyes: sources, occurrence, toxicity, sampling, analysis, and their removal methods. In: **Emerging Freshwater Pollutants**. [s.l.] Elsevier, 2022. p. 267–287.

HASSAN, M. et al. Influence of iron species on integrated microbial fuel cell and electro-Fenton process treating landfill leachate. **Chemical Engineering Journal**, v. 328, p. 57–65, 2017.

HASSAN, M. et al. Microbial electro-Fenton: an emerging and energy-efficient platform for environmental remediation. **Journal of Power Sources**, v. 424, p. 220–244, 2019.

HEMDAN, B. A. et al. Bacterial community structure of electrogenic biofilm developed on modified graphite anode in microbial fuel cell. **Scientific Reports**, v. 13, n. 1, p. 1–14, 2023.

HOLMES, D. E. et al. A membrane-bound cytochrome enables methanosarcina acetivorans to conserve energy from extracellular electron transfer. **MBio**, v. 10, n. 4, p. 789–819, 27 ago. 2019.

HORCIU, I. L. et al. Biosorption of reactive dyes from aqueous media using the Bacillus sp. residual biomass. **Desalination and Water Treatment**, v. 195, p. 353–360, 2020.

HU, L. et al. Performance and response of coupled microbial fuel cells for enhanced anaerobic treatment of azo dye wastewater with simultaneous recovery of electrical energy. **Environmental Science and Pollution Research**, v. 30, p. 89495–89509, 2023.

HUANG, T. et al. Microbial fuel cells coupling with the three-dimensional electro-Fenton technique enhances the degradation of methyl orange in the wastewater. **Environmental Science and Pollution Research**, v. 25, n. 18, p. 17989–18000, 2018.

IDRIS, M. O. et al. Exploring the effectiveness of microbial fuel cell for the degradation of organic pollutants coupled with bio-energy generation. **Sustainable Energy Technologies and Assessments**, v. 52, p. 1–15, 2022.

IEA, I. E. A. **Water-Energy Nexus**.

ILAMATHI, R.; JAYAPRIYA, J. Microbial fuel cells for dye decolorization. **Environmental Chemistry Letters**, v. 16, n. 1, p. 239–250, 2018.

IMMICH, A. P. S.; ULSON DE SOUZA, A. A.; ULSON DE SOUZA, S. M. DE A. G. Removal of Remazol Blue RR dye from aqueous solutions with Neem leaves and evaluation of their acute toxicity with Daphnia magna. **Journal of Hazardous Materials**, v. 164, n. 2–3, p. 1580–1585, 2009.

IMRAN, M. et al. Microbial biotechnology for decolorization of textile wastewaters. **Reviews in Environmental Science and Bio Technology**, v. 14, n. 1, p. 73–92, 19 mar. 2015.

IQBAL, A. et al. Decolorization and toxicity evaluation of simulated textile effluent via natural microbial consortia in attached growth reactors. **Environmental Technology and Innovation**, v. 26, p. 1–14, 2022.

ISHII, S. et al. Population dynamics of electrogenic microbial communities in microbial fuel cells started with three different inoculum sources. **Bioelectrochemistry**, v. 117, p. 74–82, 2017.

ISLAM, M. A. et al. Enhanced current generation using mutualistic interaction of yeast-bacterial coculture in dual chamber microbial fuel cell. **Industrial & Engineering Chemistry Research**, v. 57, n. 3, p. 813–821, 24 jan. 2018.

JADHAV, D. A. et al. Suppressing methanogens and enriching electrogens in bioelectrochemical systems. **Bioresource Technology**, v. 277, p. 148–156, 2019.

JADHAV, D. A.; GHANGREKAR, M. M. Optimising the proportion of pure and mixed culture in inoculum to enhance the performance of microbial fuel cells. **International Journal of Environmental Technology and Management**, v. 23, n. 1, p. 50–67, 2020.

JAFARY, T.; GHOREYSHI, A. A.; NAJAFPOUR, G. D. **The effect of substrate concentration on the electrical performance of MFC**. International Conference on Environment. **Anais**...2010

JAHAN, N. et al. A comprehensive review on the sustainable treatment of textile wastewater: zero liquid discharge and resource recovery perspectives. **Sustainability**, v. 14, n. 22, p. 1–38, 2022.

JANNELLI, N. et al. Low pH, high salinity: too much for microbial fuel cells? **Applied Energy**, v. 192, p. 543–550, abr. 2017.

JAYAPRAKASH, J.; PARTHASARATHY, A.; VIRARAGHAVAN, R. Decolorization and degradation of mono azo and diazo dyes in Pseudomonas catalyzed microbial fuel cell. **Environmental Progress & Sustainable Energy**, v. 35, n. 6, p. 1623–1628, nov. 2016.

JEONG, S. E. et al. Pandoraea terrae sp. nov., isolated from forest soil, and emended description of the genus Pandoraea Coenye et al. 2000. **International Journal of Systematic and Evolutionary Microbiology**, v. 66, n. 9, p. 3524–3530, 1 set. 2016.

JIN, J. et al. Electrochemical responses and microbial community shift of electroactive biofilm to acidity stress in microbial fuel cells. **Minerals**, v. 12, n. 10, p. 1–16, 2022.

JOKSIMOVIĆ, K. et al. Microbial fuel cells as an electrical energy source for degradation followed by decolorization of Reactive Black 5 azo dye. **Bioelectrochemistry**, v. 145, n. November, p. 1–9, 2022.

JOSHI, A.; HINSU, A.; KOTHARI, R. Evaluating the efficacy of bacterial consortium for decolorization of diazo dye mixture. **Archives of Microbiology**, v. 204, n. 8, p. 1–8, 2022.

JUANG, D. F. et al. Electrogenic capabilities of gram negative and gram positive bacteria in microbial fuel cell combined with biological wastewater treatment. **International Journal of Environmental Science & Technology**, v. 8, n. 4, p. 781–792, 1 set. 2011.

JUSTINO, N. M. **Processo foto-fenton solar mediador por ferrioxalato (FeOx/H2O2/UV) aplicado ao tratamento de efluente têxtil**. [s.l.] Universidade Federal de Santa Catarina, 2016.

KABUTEY, F. T. et al. An overview of plant microbial fuel cells (PMFCs): configurations and applications. **Renewable and Sustainable Energy Reviews**, v. 110, p. 402–414, 2019.

KADHOM, M. et al. Removal of dyes by agricultural waste. **Sustainable Chemistry and Pharmacy**, v. 16, p. 1–9, 2020.

KAHOUSH, M. et al. Bio-Fenton and Bio-electro-Fenton as sustainable methods for degrading organic pollutants in wastewater. **Process Biochemistry**, v. 64, p. 237–247, jan. 2018.

KAMAU, J. et al. Microbial fuel cells: influence of external resistors on power, current and power density. **Journal of Thermodynamics & Catalysis**, v. 8, n. 1, p. 1–5, 2017.

KARAMZADEH, M. et al. Modeling and experimental investigation of the effect of carbon source on the performance of tubular microbial fuel cell. **Scientific Reports**, v. 13, n. 1, p. 1–8, 2023.

KESARWANI, S. et al. Constructed wetland coupled microbial fuel cell: a clean technology for sustainable treatment of wastewater and bioelectricity generation. **Fermentation**, v. 9, n. 1, p. 6, 22 dez. 2022.

KEYIKOGLU, R.; CAN, O. T. The role of dye molecular weight on the decolorization performance of the electrocoagulation. **Environment, Development and Sustainability**, v. 23, n. 3, p. 3917–3928, 2021.

KHAJEH, R. T. et al. Treatment of mixed dairy and dye wastewater in anode of microbial fuel cell with simultaneous electricity generation. **Environmental Science and Pollution Research**, v. 27, n. 35, p. 43711–43723, 2020.

KHALID, S. et al. Dye degradation and electricity generation using microbial fuel cell with graphene oxide modified anode. **Materials Letters**, v. 220, p. 272–276, jun. 2018.

KHAN, M. D. et al. Bioelectricity generation and bioremediation of an azo-dye in a microbial fuel cell coupled activated sludge process. **PLoS ONE**, v. 10, p. 1–18, 23 out. 2015.

KHAN, M. D. et al. Integrated air cathode microbial fuel cell-aerobic bioreactor set-up for enhanced bioelectrodegradation of azo dye Acid Blue 29. **Science of the Total Environment**, v. 756, p. 1–11, 2021.

KHAN, M. Z. et al. Feasibility study on anaerobic biodegradation of azo dye reactive orange 16. **RSC Advances**, v. 4, n. 87, p. 46851–46859, 2014.

KHAN, R.; BHAWANA, P.; FULEKAR, M. H. Microbial decolorization and degradation of synthetic dyes: a review. **Reviews in Environmental Science and Biotechnology**, v. 12, n. 1, p. 75–97, 8 mar. 2013.

KHAN, R.; PATEL, V.; KHAN, Z. Bioremediation of dyes from textile and dye manufacturing industry effluent. In: **Abatement of Environmental Pollutants: Trends and Strategies**. [s.l.] Elsevier Inc, 2020. p. 107–125.

KHANDAKER, S. et al. Sustainable energy generation from textile biowaste and its challenges: a comprehensive review. **Renewable and Sustainable Energy Reviews**, v. 157, p. 1–16, 2022.

KHATAEE, A. et al. A comparative study on electrogeneration of hydrogen peroxide through oxygen reduction over various plasma-treated graphite electrodes. **Electrochimica Acta**, v. 244, p. 38–46, 2017.

KHATER, D. Z.; EL-KHATIB, K. M.; HASSAN, H. M. Microbial diversity structure in acetate single chamber microbial fuel cell for electricity generation. **Journal of Genetic Engineering and Biotechnology**, v. 15, n. 1, p. 127–137, 2017.

KISHOR, R. et al. Ecotoxicological and health concerns of persistent coloring pollutants of textile industry wastewater and treatment approaches for environmental safety. **Journal of Environmental Chemical Engineering**, v. 9, n. 2, p. 1–18, 2021.

KITAFA, B. A.; AL-SANED, A. J. O. A review on microbial fuel cells. **Engineering and Technology Journal**, v. 39, n. 1, p. 1–8, 2021.

KOKKO, M. E. et al. Effects of anode potentials on bioelectrogenic conversion of xylose and microbial community compositions. **Biochemical Engineering Journal**, v. 101, p. 248–252, set. 2015.

KOLAJO, O. O. et al. Impact of cathode biofouling in microbial fuel cells and mitigation techniques. **Biocatalysis and Agricultural Biotechnology**, v. 43, p. 1–18, 2022.

KULEYIN, A.; GÖK, A.; AKBAL, F. Treatment of textile industry wastewater by electro-Fenton process using graphite electrodes in batch and continuous mode. **Journal of Environmental Chemical Engineering**, v. 9, p. 1–9, 2021.

KUMAR, M. Optimisation and modeling approaches for the textile industry water treatment plants. In: **Industrial Wastewater Treatment**. [s.l: s.n.]. p. 285–307.

KUMAR, R.; SINGH, L.; ZULARISAM, A. W. Exoelectrogens: recent advances in molecular drivers involved in extracellular electron transfer and strategies used to improve it for microbial fuel cell applications. **Renewable and Sustainable Energy Reviews**, v. 56, p. 1322–1336, abr. 2016.

KUMAR, S. S. et al. Syntrophic association and performance of Clostridium, Desulfovibrio, Aeromonas and Tetrathiobacter as anodic biocatalysts for bioelectricity generation in dual chamber microbial fuel cell. **Environmental Science and Pollution Research**, v. 24, n. 19, p. 16019–16030, 2017.

KUMAR, S. S. et al. Microbial fuel cells as a sustainable platform technology for bioenergy, biosensing, environmental monitoring, and other low power device applications. **Fuel**, v. 255, p. 1–16, 2019a.

KUMAR, S. S. et al. Microbial fuel cells (MFC’s) for bioelectrochemical treatment of different wastewater streams. **Fuel**, v. 254, n. May, p. 1–17, 2019b.

LAI, H. J. Adsorption of remazol brilliant violet 5R (RBV-5R) and remazol brilliant blue R (RBBR) from aqueous solution by using agriculture waste. **Tropical Aquatic and Soil Pollution**, v. 1, n. 1, p. 11–23, 2021.

LAY, C. H.; KOKKO, M. E.; PUHAKKA, J. A. Power generation in fed-batch and continuous up-flow microbial fuel cell from synthetic wastewater. **Energy**, v. 91, p. 235–241, 2015.

LE, T. X. H. et al. Design of a novel fuel cell-Fenton system: a smart approach to zero energy depollution. **Journal of Materials Chemistry A**, v. 4, n. 45, p. 17686–17693, 2016a.

LE, T. X. H. et al. Toxicity removal assessments related to degradation pathways of azo dyes: toward an optimization of Electro-Fenton treatment. **Chemosphere**, v. 161, p. 308–318, 2016b.

LEIVA, A. M. et al. Evaluation of phytotoxicity of effluents from activated sludge and constructed wetland system for wastewater reuse. **Water Science and Technology**, v. 79, n. 4, p. 656–667, 2019.

LEKHAK, U. M. Ecotoxicity of synthetic dyes. In: **Current Developments in Bioengineering and Biotechnology**. [s.l.] Elsevier, 2023. p. 45–67.

LELLIS, B. et al. Effects of textile dyes on health and the environment and bioremediation potential of living organisms. **Biotechnology Research and Innovation**, v. 3, n. 2, p. 275–290, 2019.

LESNIK, K. L.; CAI, W.; LIU, H. Microbial community predicts functional stability of microbial fuel cells. **Environmental Science and Technology**, v. 54, p. 427–436, 2019.

LI, B. et al. A hybrid subnano cluster electrocatalysis process for recalcitrant wastewater treatment. **Separation and Purification Technology**, v. 304, p. 1–9, jan. 2023.

LI, N. et al. Acid pretreatment of three-dimensional graphite cathodes enhances the hydrogen peroxide synthesis in bioelectrochemical systems. **Science of the Total Environment**, v. 630, p. 308–313, 2018a.

LI, S. et al. Bio-electro-Fenton systems for sustainable wastewater treatment:

mechanisms, novel configurations, recent advances, LCA and challenges - an updated review. **Journal of Chemical Technology and Biotechnology**, v. 95, n. 8, p. 2083–2097, 2020a.

LI, S. et al. Deciphering the fate of antibiotic resistance genes in norfloxacin wastewater treated by a bio-electro-Fenton system. **Bioresource Technology**, v. 364, p. 1–8, nov. 2022.

LI, T. et al. The performance of the microbial fuel cell-coupled constructed wetland system and the influence of the anode bacterial community. **Environmental Technology**, v. 37, n. 13, p. 1683–1692, 2 jul. 2016a.

LI, X. et al. Novel bio-electro-Fenton technology for azo dye wastewater treatment using microbial reverse-electrodialysis electrolysis cell. **Bioresource Technology**, v. 228, p. 322–329, mar. 2017.

LI, X. et al. Bio-electro-Fenton processes for wastewater treatment: advances and prospects. **Chemical Engineering Journal**, v. 354, p. 492–506, 2018b.

LI, X. et al. Isolation of oxytetracycline-degrading bacteria and its application in improving the removal performance of aerobic granular sludge. **Journal of Environmental Management**, v. 272, p. 1–15, out. 2020b.

LI, X.; ANGELIDAKI, I.; ZHANG, Y. Salinity-gradient energy driven microbial electrosynthesis of hydrogen peroxide. **Journal of Power Sources**, v. 341, p. 357–365, 2017.

LI, Y. et al. Enhancement of azo dye decolourization in a MFC-MEC coupled system. **Bioresource Technology**, v. 202, p. 93–100, 2016b.

LI, Z. et al. Azo dye treatment with simultaneous electricity production in an anaerobic-aerobic sequential reactor and microbial fuel cell coupled system. **Bioresource Technology**, v. 101, n. 12, p. 4440–4445, 2010.

LIN, C. et al. Pneumonia due to Pandoraea Apista after evacuation of traumatic intracranial hematomas:a case report and literature review. **BMC Infectious Diseases**, v. 19, n. 1, p. 1–9, 2019.

LING, T. et al. Repeated oxidative degradation of methyl orange through bio-electro-Fenton in bioelectrochemical system (BES). **Bioresource Technology**, v. 203, p. 89–95, mar. 2016.

LINH, H. N.; HO, H. T. N. Bio-electro-Fenton: a novel method for treating leachate in Da Phuoc Landfill, Vietnam. **Science and Technology Development Journal**, v. 23, n. 1, p. 461–469, 19 mar. 2020.

LIU, L. et al. Microbial fuel cell with an azo-dye-feeding cathode. **Applied Microbiology and Biotechnology**, v. 85, n. 1, p. 175–183, 2009.

LIU, W. et al. Microbial fuel cell and membrane bioreactor coupling system: recent trends. **Environmental Science and Pollution Research**, v. 25, n. 24, p. 23631–23644, 3 ago. 2018.

LIU, X.-W. et al. Anodic Fenton process assisted by a microbial fuel cell for enhanced degradation of organic pollutants. **Water Research**, v. 46, n. 14, p. 4371–4378, set. 2012.

LIU, Y. et al. Degradation of azo dyes with different functional groups in simulated wastewater by electrocoagulation. **Water**, v. 14, n. 1, p. 1–13, 5 jan. 2022.

LOGAN, B. E. Peer reviewed: extracting hydrogen and electricity from renewable resources. **Environmental Science & Technology**, v. 38, n. 9, p. 160–167, 1 maio 2004.

LOGAN, B. E. et al. Microbial fuel cells: methodology and technology. **Environmental Science and Technology**, v. 40, n. 17, p. 5181–5192, 2006.

LOGAN, B. E. et al. Impact of ohmic resistance on measured electrode potentials and maximum power production in microbial fuel cells. **Environmental Science and Technology**, v. 52, n. 15, p. 8977–8985, 2018.

LOGROÑO, W. et al. Single chamber microbial fuel cell (SCMFC) with a cathodic microalgal biofilm: a preliminary assessment of the generation of bioelectricity and biodegradation of real dye textile wastewater. **Chemosphere**, v. 176, p. 378–388, jun. 2017.

LONG, X. et al. Microbial fuel cell-photoelectrocatalytic cell combined system for the removal of azo dye wastewater. **Bioresource Technology**, v. 244, p. 182–191, nov. 2017.

LONG, X. et al. Characterization of electricity generation and microbial community structure over long-term operation of a microbial fuel cell. **Bioresource Technology**, v. 285, p. 1–5, 2019a.

LONG, X. et al. The azo dye degradation and differences between the two anodes on the microbial community in a double-anode microbial fuel cell. **Water, Air, and Soil Pollution**, v. 230, p. 1–11, 2019b.

LU, L. et al. Active harvesting enhances energy recovery and function of electroactive microbiomes in microbial fuel cells. **Applied Energy**, v. 247, p. 492–502, 2019.

LU, L.; XING, D.; REN, Z. J. Microbial community structure accompanied with electricity production in a constructed wetland plant microbial fuel cell. **Bioresource Technology**, v. 195, p. 115–121, nov. 2015.

LUO, J. et al. Coupled biodegradation of p-nitrophenol and p-aminophenol in bioelectrochemical system: mechanism and microbial functional diversity. **Journal of Environmental Sciences**, v. 108, p. 134–144, out. 2021.

LUO, J. et al. Recent advances in microbial fuel cells: a review on the identification technology, molecular tool and improvement strategy of electricigens. **Current Opinion in Electrochemistry**, v. 37, p. 1–15, fev. 2023.

LUO, Y. et al. Simultaneous degradation of refractory contaminants in both the anode and cathode chambers of the microbial fuel cell. **Bioresource Technology**, v. 102, n. 4, p. 3827–3832, fev. 2011.

LUO, Y. et al. Seed germination test for toxicity evaluation of compost: its roles, problems and prospects. **Waste Management**, v. 71, p. 109–114, 2018.

LV, J. et al. Bioelectrochemical performance of microbial fuel cell powered electro-Fenton system (MFC℗EFs) with composite PANI-Mn/CF anode. **Environmental Engineering Research**, v. 28, n. 4, p. 1–14, 2023.

M'ARIMI, M. M. et al. Recent trends in applications of advanced oxidation processes (AOPs) in bioenergy production: Review. **Renewable and Sustainable Energy Reviews**, v. 121, p. 1–18, 2020.

MA, D. et al. Electricity generation from swine wastewater in microbial fuel cell: hydraulic reaction time effect. **International Journal of Hydrogen Energy**, v. 41, n. 46, p. 21820–21826, 2016.

MA, H. et al. Acclimation of electroactive biofilms under different operating conditions: comprehensive analysis from architecture, composition, and metabolic activity. **Environmental Science and Pollution Research**, p. 1–12, 2023.

MACHADO, F.; TEIXEIRA, A. C. S. C.; RUOTOLO, L. A. M. Critical review of Fenton and photo-Fenton wastewater treatment processes over the last two decades. **International Journal of Environmental Science and Technology**, p. 1–38, 2023.

MAHMUD, I.; KAISER, S. Recent progress in waterless textile dyeing. v. 10, n. 6, p. 1–3, 2020.

MAJUMDAR, R. et al. A review on microbial potential of toxic azo dyes bioremediation in aquatic system. In: **Microbial Biodegradation and Bioremediation**. [s.l.] Elsevier, 2022. p. 241–261.

MALEKMOHAMMADI, S.; MIRBAGHERI, S. A. A review of the operating parameters on the microbial fuel cell for wastewater treatment and electricity generation. **Water Science and Technology**, v. 84, n. 6, p. 1309–1323, 2021.

MALYAN, A.; MONGIA, G.; KUMAR, S. Catalytic effect of acetate (C2H3O2) on coulombic efficiency and bio-electricity generation from wastewater sample prepared from domestic kitchen waste using dual chamber microbial fuel cell technology. **Journal of Applied and Natural Science**, v. 14, n. 2, p. 652–659, 2022.

MANCÍLIO, L. B. K. et al. Biocatalysts in electrofermentation systems. In: **Bioelectrochemical Systems**. Singapore: Springer Singapore, 2020. p. 239–276.

MANI, P. et al. Degradation of azo dye (Acid Orange 7) in a microbial fuel cell: comparison between anodic microbial-mediated reduction and cathodic laccase-mediated oxidation. **Frontiers in Energy Research**, v. 7, p. 1–12, 18 set. 2019.

MANI, P. et al. Development of an electroactive aerobic biocathode for microbial fuel cell applications. **Environmental Microbiology Reports**, v. 12, n. 5, p. 607–612, 2020.

MANNA, M.; SEN, S. Advanced oxidation process: a sustainable technology for treating refractory organic compounds present in industrial wastewater. **Environmental Science and Pollution Research**, v. 30, p. 25477–25505, 2023.

MANSOORIAN, H. J. et al. Evaluation of dairy industry wastewater treatment and simultaneous bioelectricity generation in a catalyst-less and mediator-less membrane microbial fuel cell. **Journal of Saudi Chemical Society**, v. 20, n. 1, p. 88–100, jan. 2016.

MAQSOOD, Q. et al. Applications of microbial fuel cell technology and strategies to boost bioreactor performance. **Nature Environment and Pollution Technology**, v. 21, n. 3, p. 1191–1199, 2022.

MARAMI, H. et al. Going beyond conventional wastewater treatment plants within circular bioeconomy concept - a sustainability assessment study. **Water Science and Technology**, v. 85, n. 6, p. 1878–1903, 2022.

MARTÍNEZ-HUITLE, C. A.; PANIZZA, M. Electrochemical oxidation of organic pollutants for wastewater treatment. **Current Opinion in Electrochemistry**, v. 11, p. 62–71, out. 2018.

MAULIK, S. R. et al. Reactive dye and its advancements. In: **Textile Dyes and Pigments**. [s.l.] Wiley, 2022. p. 17–44.

MENEK, N.; KARAMAN, Y. Polarographic and voltammetric investigation of 8-

hydroxy-7-(4-sulfo-1-naphthylazo)-5-quinoline sulfonic acid. **Dyes and Pigments**, v. 67, n. 1, p. 9–14, 2005.

MENG, F. et al. Fouling in membrane bioreactors: An updated review. **Water Research**, v. 114, p. 151–180, maio 2017.

MICHIE, I. S. et al. Factors affecting microbial fuel cell acclimation and operation in temperate climates. **Water Science and Technology**, v. 67, n. 11, p. 2568–2575, 2013.

MIKLOS, D. B. et al. Evaluation of advanced oxidation processes for water and wastewater treatment – a critical review. **Water Research**, v. 139, p. 118–131, ago. 2018.

MILLS, S. et al. A meta-analysis of acetogenic and methanogenic microbiomes in microbial electrosynthesis. **NPJ Biofilms and Microbiomes**, v. 8, n. 1, p. 1–11, 2022.

MILTON, K.; BULL, F. C.; BAUMAN, A. Reliability and validity testing of a single-item physical activity measure. **British Journal of Sports Medicine**, v. 45, n. 3, p. 203–208, 1 mar. 2011.

MIRAN, W. et al. Sulfate-reducing mixed communities with the ability to generate bioelectricity and degrade textile diazo dye in microbial fuel cells. **Journal of Hazardous Materials**, v. 352, p. 70–79, 2018.

MISHRA, B. et al. Insights into Interdisciplinary approaches for bioremediation of organic pollutants: innovations, challenges and perspectives. **Proceedings of the National Academy of Sciences India Section B - Biological Sciences**, v. 90, n. 5, p. 951–958, 2020.

MITTAL, N.; KUMAR, A. Microbial fuel cell as water-energy-environment nexus: a relevant strategy for treating streamlined effluents. **Energy Nexus**, v. 7, p. 1–12, 2022.

MITTAL, Y. et al. Azo dye containing wastewater treatment in earthen membrane based unplanted two chambered constructed wetlands-microbial fuel cells: A new design for enhanced performance. **Chemical Engineering Journal**, v. 427, p. 1–12, 2022.

MODIN, O.; FUKUSHI, K. Production of high concentrations of H2O2 in a bioelectrochemical reactor fed with real municipal wastewater. **Environmental Technology**, v. 34, n. 19, p. 2737–2742, 2013.

MOHANTY, S. S.; KUMAR, A. Enhanced degradation of anthraquinone dyes by microbial monoculture and developed consortium through the production of specific enzymes. **Scientific Reports**, v. 11, n. 1, p. 1–15, 2021.

MONTEIL, H. et al. A review on efficiency and cost effectiveness of electro and bio-electro-Fenton processes: application to the treatment of pharmaceutical pollutants in water. **Chemical Engineering Journal**, v. 376, n. 119577, p. 1–30, 2019.

MOYO, S.; MAKHANYA, B. P.; ZWANE, P. E. Use of bacterial isolates in the treatment of textile dye wastewater: a review. **Heliyon**, v. 8, n. 6, p. 1–13, 2022.

MU, Y. et al. Decolorization of azo dyes in bioelectrochemical systems. **Environmental Science and Technology**, v. 43, n. 13, p. 5137–5143, 2009.

MUNOZ-CUPA, C. et al. An overview of microbial fuel cell usage in wastewater treatment, resource recovery and energy production. **Science of the Total Environment**, v. 754, p. 1–21, 2021.

MURALI, V. et al. Comprehensive review and compilation of treatment for azo dyes using microbial fuel cells. **Water Environment Research**, v. 85, n. 3, p. 270–277, 1 mar. 2013.

NADAIS, H. et al. Bio-electro-Fenton process for the degradation of non-steroidal anti-onflammatory drugs in wastewater. **Chemical Engineering Journal**, v. 338, p. 401–410, abr. 2018.

NAJAFINEJAD, M. S. et al. Application of electrochemical oxidation for water and wastewater treatment: an overview. **Molecules**, v. 28, n. 10, p. 1–25, 2023.

NARAYANASAMY, S.; JAYAPRAKASH, J. Improved performance of seudomonas aeruginosa catalyzed MFCs with graphite/polyester composite electrodes doped with metal ions for azo dye degradation. **Chemical Engineering Journal**, v. 343, p. 258–269, 2018.

NASRUDDIN, N. I. S. M.; BAKAR, M. H. A. Mitigating membrane biofouling in biofuel cell system - a review. **Open Chemistry**, v. 19, n. 1, p. 1202–1215, 2021.

NATH, D.; CHAKRABORTY, I.; GHANGREKAR, M. M. Methanogenesis inhibitors used in bio-electrochemical systems: a review revealing reality to decide future direction and applications. **Bioresource Technology**, v. 319, p. 1–13, 2021.

NAWAZ, A. et al. A state of the art review on electron transfer mechanisms, characteristics, applications and recent advancements in microbial fuel cells technology. **Green Chemistry Letters and Reviews**, v. 13, n. 4, p. 101–117, 2020.

NAWAZ, A. et al. Microbial fuel cells: insight into simultaneous wastewater treatment and bioelectricity generation. **Process Safety and Environmental**

Protection, v. 161, p. 357–373, 2022.

NAZINA, T. N. et al. Soehngenia longivitae sp. nov., a fermenting bacterium isolated from a petroleum reservoir in Azerbaijan, and emended description of the genus Soehngenia. **Microorganisms**, v. 8, n. 12, p. 1967, 11 dez. 2020.

NGO, A. C. R.; TISCHLER, D. Microbial degradation of azo dyes: approaches and prospects for a hazard-free conversion by microorganisms. **International Journal of Environmental Research and Public Health**, v. 19, n. 8, p. 1–24, 2022.

NGUYEN, H. D.; BABEL, S. Insights on microbial fuel cells for sustainable biological nitrogen removal from wastewater: a review. **Environmental Research**, v. 204, p. 1–8, 2022.

NIDHEESH, P. V.; GANDHIMATHI, R. Trends in electro-Fenton process for water and wastewater treatment: an overview. **Desalination**, v. 299, p. 1–15, 2012.

NIE, C. et al. An efficient strategy for full mineralization of an azo dye in wastewater: a synergistic combination of solar thermo and electrochemistry plus photocatalysis. **RSC Advances**, v. 7, n. 58, p. 36246–36255, 2017.

NIESSEN, J.; SCHRODER, U.; SCHOLZ, F. Exploiting complex carbohydrates for microbial electricity generation a bacterial fuel cell operating on starch. **Electrochemistry Communications**, v. 6, n. 9, p. 955–958, 15 set. 2004.

OBILEKE, K. C. et al. Microbial fuel cells, a renewable energy technology for bio-electricity generation: a mini-review. **Electrochemistry Communications**, v. 125, p. 1–14, 2021.

OLIOT, M. et al. Increasing the temperature is a relevant strategy to form microbial anodes intended to work at room temperature. **Electrochimica Acta**, v. 258, p. 134–142, 2017.

OLIVEIRA, G. A. R. DE et al. A test battery for assessing the ecotoxic effects of textile dyes. **Chemico-Biological Interactions**, v. 291, p. 171–179, 2018.

OLVERA-VARGAS, H. et al. Bio-electro-Fenton: a new combined process – principles and applications. In: **The Handbook of Environmental Chemistry**. [s.l: s.n.]. p. 29–56.

OON, Y. S. et al. Microbial fuel cell operation using monoazo and diazo dyes as terminal electron acceptor for simultaneous decolourisation and bioelectricity generation. **Journal of Hazardous Materials**, v. 325, p. 170–177, 2017.

OWUSU-AGYEMAN, I. et al. The study of structure of anaerobic granules and methane producing pathways of pilot-scale UASB reactors treating municipal wastewater under sub-mesophilic conditions. **Bioresource Technology**, v. 290, p. 1–9, out. 2019.

PAL, P. Industry-specific water treatment. In: **Industrial Water Treatment Process Technology**. [s.l.] Elsevier, 2017. p. 243–511.

PALANISAMY, G. et al. A comprehensive review on microbial fuel cell technologies: processes, utilization, and advanced developments in electrodes and membranes. **Journal of Cleaner Production**, v. 221, p. 598–621, 2019.

PANDE, V. et al. Biodegradation of toxic dyes: a comparative study of enzyme action in a microbial system. In: **Smart Bioremediation Technologies**. [s.l.] Elsevier, 2019. p. 255–287.

PANDEY, A.; SINGH, P.; IYENGAR, L. Bacterial decolorization and degradation of azo dyes. **International Biodeterioration & Biodegradation**, v. 59, n. 2, p. 73–84, mar. 2007.

PANDEY, P. et al. Recent advances in the use of different substrates in microbial fuel cells toward wastewater treatment and simultaneous energy recovery. **Applied Energy**, v. 168, p. 706–723, 2016.

PANDIT, S. et al. Blue energy meets green energy in microbial reverse electrodialysis cells: Recent advancements and prospective. **Sustainable Energy Technologies and Assessments**, v. 57, p. 1–11, 2023.

PANEPINTO, D. et al. Evaluation of the energy efficiency of a large wastewater treatment plant in Italy. **Applied Energy**, v. 161, p. 404–411, jan. 2016.

PANT, D. et al. A review of the substrates used in microbial fuel cells (MFCs) for sustainable energy production. **Bioresource Technology**, v. 101, n. 6, p. 1533–1543, mar. 2010.

PARK, Y. et al. Response of microbial community structure to pre-acclimation strategies in microbial fuel cells for domestic wastewater treatment. **Bioresource Technology**, v. 233, p. 176–183, 2017.

PASTERNAK, G. et al. Prevention and removal of membrane and separator biofouling in bioelectrochemical systems: a comprehensive review. **iScience**, v. 25, n. 7, p. 1–21, 2022.

PATEL, D. et al. Bioelectrochemical systems for the treatment of textile dye wastewaters. In: **Current Developments in Bioengineering and Biotechnology**. [s.l.] Elsevier, 2023a. p. 649–678.

PATEL, J. N. et al. Bacterial enzymes for azo dye degradation: an insight.

Research Journal of Chemistry and Environment, v. 27, n. 4, p. 135–148, 15 mar. 2023b.

PATIL, S. A. et al. Electroactive mixed culture biofilms in microbial bioelectrochemical systems: the role of temperature for biofilm formation and performance. **Biosensors and Bioelectronics**, v. 26, n. 2, p. 803–808, out. 2010.

PATWARDHAN, S. B. et al. Microbial fuel cell united with other existing technologies for enhanced power generation and efficient wastewater treatment. **Applied Sciences**, v. 11, n. 22, p. 1–26, 2021.

PEDUTO, T. A. G.; JESUS, T. A. DE; KOHATSU, M. Y. Sensibilidade de diferentes sementes em ensaio de fitotoxicidade. **Revista Brasileira de Ciência, Tecnologia e Inovação**, v. 4, n. 2, p. 200–212, 2019.

PEETERS, C. et al. Comparative genomics of Pandoraea, a genus enriched in xenobiotic biodegradation and metabolism. **Frontiers in Microbiology**, v. 10, p. 1–21, 2019.

PERAZZOLI, S.; DE SANTANA NETO, J. P.; SOARES, H. M. Prospects in bioelectrochemical technologies for wastewater treatment. **Water Science and Technology**, v. 78, n. 6, p. 1237–1248, 2 nov. 2018.

PHUNG, N. T. et al. Analysis of microbial diversity in oligotrophic microbial fuel cells using 16S rDNA sequences. **FEMS Microbiology Letters**, v. 233, n. 1, p. 77–82, abr. 2004.

PIETRUK, K.; PIĄTKOWSKA, M.; OLEJNIK, M. Electrochemical reduction of azo dyes mimicking their biotransformation to more toxic products. **Journal of Veterinary Research**, v. 63, n. 3, p. 433–438, 2019.

PITHER, M. D. et al. A chronic strain of the cystic fibrosis pathogen Pandoraea pulmonicola expresses a heterogenous hypo-acylated lipid A. **Glycoconjugate Journal**, v. 38, n. 2, p. 135–144, 13 abr. 2021.

POPLI, S.; PATEL, U. D. Destruction of azo dyes by anaerobic-aerobic sequential biological treatment: a review. **International Journal of Environmental Science and Technology**, v. 12, n. 1, p. 405–420, 2015.

POTTER, M. C. Electrical effects accompanying the decomposition of organic compounds. **Proceedings of the Royal Society of London. Series B, Containing Papers of a Biological Character**, v. 84, n. 571, p. 260–276, 14 set. 1911.

PRAJAPATI, S.; YELAMARTHI, P. S. Microbial fuel cell-assisted Congo red dye decolorization using biowaste-derived anode material. **Asia-Pacific Journal of**

Chemical Engineering, v. 15, n. 5, p. 1–10, 2020.

PRATAP, B. et al. Wastewater generation and treatment by various eco-friendly technologies: Possible health hazards and further reuse for environmental safety. **Chemosphere**, v. 14, n. 137547, p. 1–59, 2022.

PRATHIBA, S.; KUMAR, P. S.; VO, D. V. N. Recent advancements in microbial fuel cells: a review on its electron transfer mechanisms, microbial community, types of substrates and design for bio-electrochemical treatment. **Chemosphere**, v. 286, p. 1–27, 2022.

PRÉVOTEAU, A. et al. Microbial electrosynthesis from CO2: forever a promise? **Current Opinion in Biotechnology**, v. 62, p. 48–57, 2020.

PRIYANKA, K.; SHEELA, C. A. M. Decolorization of congo red in microbial fuel cell. **Research Square**, p. 1–19, 2021.

PUNZI, M. et al. Combined anaerobic–ozonation process for treatment of textile wastewater: removal of acute toxicity and mutagenicity. **Journal of Hazardous Materials**, v. 292, p. 52–60, jul. 2015.

PUTHILIBAI, G.; JEYASHRI, R.; SANGAVI, T. **Power production by microbial fuel cell having conductive polymer electrode and bio catalysts**. ICPECTS 2020 - IEEE 2nd International Conference on Power, Energy, Control and Transmission Systems, Proceedings. **Anais**...2020

QI, J.; SCHLÖMANN, M.; TISCHLER, D. Biochemical characterization of an azoreductase from Rhodococcus opacus 1CP possessing methyl red degradation ability. **Journal of Molecular Catalysis B: Enzymatic**, v. 130, p. 9–17, ago. 2016.

QIAN, D.-K. et al. Caproate production from xylose by mesophilic mixed culture fermentation. **Bioresource Technology**, v. 308, p. 1–12, jul. 2020.

QIU, S. et al. An overview in the development of cathode materials for the improvement in power generation of microbial fuel cells. **Bioelectrochemistry**, v. 141, p. 1–13, 2021.

QIU, S. et al. Microbial fuel cell-based biosensor for simultaneous test of sodium acetate and glucose in a mixed solution. **International Journal of Environmental Research and Public Health**, v. 19, p. 1–12, 2022.

QUAST, C. et al. The SILVA ribosomal RNA gene database project: improved data processing and web-based tools. **Nucleic Acids Research**, v. 41, n. D1, p. D590–D596, 27 nov. 2012.

RABAEY, K. et al. Biofuel cells select for microbial consortia that self-mediate electron transfer. **Applied and Environmental Microbiology**, v. 70, n. 9, p. 5373–5382, set. 2004.

RAFAQAT, S. et al. Recent progress in treatment of dyes wastewater using microbial-electro-Fenton technology. **RSC Advances**, v. 12, n. 27, p. 17104–17137, 2022.

RAHIMNEJAD, M. et al. A novel microbial fuel cell stack for continuous production of clean energy. **International Journal of Hydrogen Energy**, v. 37, n. 7, p. 5992–6000, abr. 2012.

RAHMANI, A. R. et al. Effect of different concentrations of substrate in microbial fuel cells toward bioenergy recovery and simultaneous wastewater treatment. **Environmental Technology**, v. 43, n. 1, p. 1–9, 2022.

RAJARAMAN, T. S.; GANDHI, V.; PARIKH, S. P. Advanced oxidation processes for wastewater remediation: fundamental concepts to recent advances. In: GANDHI, V.; SHAH, K. (Eds.). . **Advances in Wastewater Treatment I**. Millersville, PA 17551, USA: Materials Research Forum LLC, 2021. p. 37–86.

RAMOS, M. D. N. et al. A critical analysis of the alternative treatments applied to effluents from Brazilian textile industries. **Journal of Water Process Engineering**, v. 43, p. 1–16, 2021.

RÁPÓ, E. et al. Adsorptive removal of remazol brilliant violet-5R dye from aqueous solutions using calcined eggshell as biosorbent. **Acta Chimica Slovenica**, v. 66, n. 3, p. 648–658, 2019.

RÁPÓ, E. et al. Adsorption of remazol brilliant violet-5R textile dye from aqueous solutions by using eggshell waste biosorbent. **Scientific Reports**, v. 10, n. 1, p. 1–12, 2020.

RATHER, L. J.; AKHTER, S.; HASSAN, Q. P. Bioremediation: green and sustainable technology for textile effluent treatment. In: **Sustainable Innovations in Textile Chemistry and Dyes**. [s.l: s.n.]. p. 75–91.

RAVINUTHALA, S. et al. Co-substrates’ influence on bioelectricity production in an azo dye-based microbial fuel cell. **Bioresource Technology Reports**, v. 18, n. March, p. 101012, 2022.

RAWAT, D. et al. Ecotoxic potential of a presumably non-toxic azo dye. **Ecotoxicology and Environmental Safety**, v. 148, p. 528–537, 2018.

REBEQUI, T. T. et al. Waste treatment and sustainable bioelectricity generation using microbial fuel cell. **Journal of Science & Sustainable Engineering**,

v. 1, p. 9–17, 2023.

REDDY, C. N.; MOHAN, S. V. Integrated bio-electrogenic process for bioelectricity production and cathodic nutrient recovery from azo dye wastewater. **Renewable Energy**, v. 98, p. 188–196, dez. 2016.

REN, J. et al. Study on the effect of synergy effect between the mixed cultures on the power generation of microbial fuel cells. **Bioengineered**, v. 12, n. 1, p. 844–854, 2021.

REN, Z. et al. Characterization of microbial fuel cells at microbially and electrochemically meaningful time scales. **Environmental Science and Technology**, v. 45, n. 6, p. 2435–2441, 2011.

REYES, K. R. E. et al. Biodegradation of anthraquinone dyes: interactive assessment upon biodecolorization, biosorption and biotoxicity using dual-chamber microbial fuel cells (MFCs). **Process Biochemistry**, v. 101, p. 111–127, fev. 2021.

ROBLEDO-PADILLA, F. et al. Evaluation and predictive modeling of removal condition for bioadsorption of indigo blue dye by Spirulina platensis. **Microorganisms**, v. 8, p. 1–12, 7 jan. 2020.

ROMERO, A. J. R. et al. Índices de germinación y elongación radical de calidad del agua del río Chalma. **Revista Internacional de Contaminacion del Ambiente**, v. 30, n. 3, p. 307–316, 2014.

ROSHINI, P. S. et al. Combined electro-Fenton and biological processes for the treatment of industrial textile effluent: mineralization and toxicity analysis. **Journal of Hazardous, Toxic, and Radioactive Waste**, v. 21, n. 4, p. 1–8, 2017.

ROSSI, R. et al. In situ biofilm removal from air cathodes in microbial fuel cells treating domestic wastewater. **Bioresource Technology**, v. 265, n. April, p. 200–206, 2018.

ROSSI, R. et al. Evaluation of electrode and solution area-based resistances enables quantitative comparisons of factors impacting microbial fuel cell performance. **Environmental Science and Technology**, v. 53, n. 7, p. 3977–3986, 2019.

ROSSI, R. et al. Continuous flow microbial flow cell with an anion exchange membrane for treating low conductivity and poorly buffered wastewater. **ACS Sustainable Chemistry and Engineering**, v. 9, n. 7, p. 2946–2954, 2021.

ROSSI, R.; EVANS, P. J.; LOGAN, B. E. Impact of flow recirculation and anode dimensions on performance of a large scale microbial fuel cell. **Journal of Power Sources**, v. 412, n. October 2018, p. 294–300, 2019.

ROSSI, R.; LOGAN, B. E. Impact of external resistance acclimation on charge transfer and diffusion resistance in bench-scale microbial fuel cells. **Bioresource Technology**, v. 318, p. 1–5, 2020.

ROY, S. V. et al. Elimination of pharmaceuticals from wastewater using microbial fuel cell-based bio-electro-Fenton process. **Environmental Science and Pollution Research**, v. 34, p. 1–13, 2023.

SABA, B. et al. Decolorization of reactive black 5 and reactive blue 4 dyes in microbial fuel cells. **Applied Biochemistry and Biotechnology**, v. 186, n. 4, p. 1017–1033, 2018.

SABA, B.; KJELLERUP, B. V.; CHRISTY, A. D. Eco-friendly bio-electro-degradation of textile dyes wastewater. **Bioresource Technology Reports**, v. 15, n. 5, p. 1–11, 2021.

SAHOO, A. K.; DAHIYA, A.; PATEL, B. K. Biological methods for textile dyes removal from wastewaters. In: **Development in Wastewater Treatment Research and Processes**. [s.l.] Elsevier, 2022. p. 127–151.

SANTANA, R. M. DA R. et al. Kinetic and ecotoxicological evaluation of the direct orange 26 dye degradation by Fenton and solar photo-Fenton processes. **Revista Eletrônica em Gestão, Educação e Tecnologia Ambiental**, v. 22, p. 1–20, 2018.

SANTORO, C. et al. How comparable are microbial electrochemical systems around the globe? An electrochemical and microbiological cross-laboratory study. **ChemSusChem**, v. 14, n. 11, p. 2313–2330, 2021.

SANTOS, A. B. DOS et al. Enhancing the electron transfer capacity and subsequent color removal in bioreactors by applying thermophilic anaerobic treatment and redox mediators. **Biotechnology and Bioengineering**, v. 89, n. 1, p. 42–52, 5 jan. 2005.

SARATALE, G. D. et al. A comprehensive overview on electro-active biofilms, role of exo-electrogens and their microbial niches in microbial fuel cells (MFCs). **Chemosphere**, v. 178, p. 534–547, 2017.

SARATALE, R. G. et al. Bacterial decolorization and degradation of azo dyes: a review. **Journal of the Taiwan Institute of Chemical Engineers**, v. 42, n. 1, p. 138–157, 2011.

SARAVANAN, A. et al. A detailed review on advanced oxidation process in treatment of wastewater: mechanism, challenges and future outlook. **Chemosphere**,

v. 308, p. 1–11, 2022.

SARKAR, S. et al. Degradation of synthetic azo dyes of textile industry: a sustainable approach using microbial enzymes. **Water Conservation Science and Engineering**, v. 2, n. 4, p. 121–131, 2017.

SATHE, S. M. et al. Microbial fuel cell coupled Fenton oxidation for the cathodic degradation of emerging contaminants from wastewater: applications and challenges. **Environmental Research**, v. 204, p. 1–12, 2022a.

SATHE, S. M. et al. Waste-derived iron catalyzed bio-electro-Fenton process for the cathodic degradation of surfactants. **Environmental Research**, v. 212, p. 1–9, set. 2022b.

SAVLA, N. et al. Recent advancements in the cathodic catalyst for the hydrogen evolution reaction in microbial electrolytic cells. **International Journal of Hydrogen Energy**, v. 47, n. 34, p. 15333–15356, 2022.

SCHRÖDER, U. Anodic electron transfer mechanisms in microbial fuel cells and their energy efficiency. **Phys. Chem. Chem. Phys.**, v. 9, n. 21, p. 2619–2629, 2007.

SEAN, W.-Y. et al. Energy consumption analysis in wastewater treatment plants using simulation and SCADA system: case study in northern Taiwan. **Journal of Cleaner Production**, v. 276, p. 1–9, dez. 2020.

SEE-TOO, W. S. et al. Pandoraea fibrosis sp. nov., a novel Pandoraea species isolated from clinical respiratory samples. **International Journal of Systematic and Evolutionary Microbiology**, v. 69, n. 3, p. 645–651, 1 mar. 2019.

SELVARAJ, V. et al. An over review on recently developed techniques, mechanisms and intermediate involved in the advanced azo dye degradation for industrial applications. **Journal of Molecular Structure**, v. 1224, p. 1–15, 2021.

SELVASEMBIAN, R. et al. Recent progress in microbial fuel cells for industrial effluent treatment and energy generation: fundamentals to scale-up application and challenges. **Bioresource Technology**, v. 346, p. 1–12, 2022.

SEN, S. K. et al. Fungal decolouration and degradation of azo dyes: a review. **Fungal Biology Reviews**, v. 30, n. 3, p. 112–133, jul. 2016.

SHABANGU, K. P. et al. Validation of RSM predicted optimum scaling-up factors for generating electricity in a DCMFC: MATLAB design and simulation model. **Fermentation**, v. 9, n. 9, p. 1–12, 19 set. 2023.

SHABIR, M. et al. A review on recent advances in the treatment of dye-polluted wastewater. **Journal of Industrial and Engineering Chemistry**, v. 112, p. 1–19, ago. 2022.

SHAHI, A.; RAI, B. N.; SINGH, R. S. Biodegradation of reactive orange 16 dye in microbial fuel cell: an innovative way to minimize waste along with electricity production. **Applied Biochemistry and Biotechnology**, v. 192, n. 1, p. 196–210, 2020.

SHAN, C. et al. Enhanced Fenton-like oxidation of As(III) over Ce–Ti binary oxide: a new strategy to tune catalytic activity via balancing bimolecular adsorption energies. **Environmental Science & Technology**, v. 54, n. 9, p. 5893–5901, 5 maio 2020.

SHANG, Y. et al. High storable power density of triboelectric nanogenerator within centimeter size. **Materials**, v. 16, n. 13, p. 1–15, 28 jun. 2023.

SHARIFI, N. et al. Synthesis of Fe3O4@activated carbon to treat metronidazole effluents by adsorption and heterogeneous Fenton with effluent bioassay. **Journal of Photochemistry and Photobiology A: Chemistry**, v. 427, p. 1–15, 2022.

SHOAIB, M. et al. Biological methods for degradation of textile dyes from textile effluent. In: **Development in Wastewater Treatment Research and Processes**. [s.l.] Elsevier, 2022. p. 329–353.

SHOKRI, A.; FARD, M. S. A critical review in Fenton-like approach for the removal of pollutants in the aqueous environment. **Environmental Challenges**, v. 7, n. 100534, p. 1–20, 2022.

SHU, Z. et al. Decolorization of Remazol Brilliant Blue R using a novel acyltransferase-ISCO (in situ chemical oxidation) coupled system. **Biochemical Engineering Journal**, v. 115, p. 56–63, nov. 2016.

SIDDIQUI, S. et al. Wastewater treatment and energy production by microbial fuel cells. **Biomass Conversion and Biorefinery**, v. 13, n. 5, p. 3569–3592, 2023.

SIEBER, J. R.; MCINERNEY, M. J.; GUNSALUS, R. P. Genomic Insights into syntrophy: the paradigm for anaerobic metabolic cooperation. **Annual Review of Microbiology**, v. 66, n. 1, p. 429–452, 13 out. 2012.

SILVA, E. Z. M. et al. The evaluation of reactive textile dyes regarding their potential to cause organ-specific cyto- and geno-toxicity. **Ecotoxicology and Environmental Contamination**, v. 17, n. 1, p. 60–66, 10 ago. 2022.

SIM, J. et al. Characterization and optimization of cathodic conditions for H2O2 synthesis in microbial electrochemical cells. **Bioresource Technology**, v. 195, p. 31–36, 2015.

SIM, J. et al. Hydrogen peroxide production in a pilot-scale microbial electrolysis cell. **Biotechnology Reports**, v. 19, p. 1–5, 2018.

SINGH, A.; DAHIYA, S.; MISHRA, B. K. Microbial fuel cell coupled hybrid systems for the treatment of dye wastewater: a review on synergistic mechanism and performance. **Journal of Environmental Chemical Engineering**, v. 9, n. 6, p. 1–16, 2021.

SINGH, A. L. et al. Biodegradation of Reactive Yellow-145 azo dye using bacterial consortium: a deterministic analysis based on degradable metabolite, phytotoxicity, and genotoxicity study. **Chemosphere**, v. 300, p. 1–11, 2022.

SINGH, R. L.; SINGH, P. K.; SINGH, R. L. Present status of biodegradation of textile dyes. **Current Trends in Biomedical Engineering & Biosciences**, v. 3, n. 4, p. 10–12, 2017.

SIVASANKAR, P. et al. Bioremediation of wastewater through a quorum sensing triggered MFC: a sustainable measure for waste to energy concept. **Journal of Environmental Management**, v. 237, n. June, p. 84–93, 2019.

SOBIESZUK, P.; ZAMOJSKA-JAROSZEWICZ, A.; MAKOWSKI, Ł. Influence of the operational parameters on bioelectricity generation in continuous microbial fuel cell, experimental and computational fluid dynamics modelling. **Journal of Power Sources**, v. 371, p. 178–187, 2017.

SOLANKI, K.; SUBRAMANIAN, S.; BASU, S. Microbial fuel cells for azo dye treatment with electricity generation: a review. **Bioresource Technology**, v. 131, p. 564–571, 2013.

SOLÍS, M. et al. Microbial decolouration of azo dyes: a review. **Process Biochemistry**, v. 47, n. 12, p. 1723–1748, 2012.

SOLTANI, F. et al. A novel bio-electro-Fenton system with dual application for the catalytic degradation of tetracycline antibiotic in wastewater and bioelectricity generation. **RSC Advances**, v. 11, n. 44, p. 27160–27173, 2021.

SOLTANI, F.; NAVIDJOUY, N.; RAHIMNEJAD, M. A review on bio-electro-Fenton systems as environmentally friendly methods for degradation of environmental organic pollutants in wastewater. **RSC Advances**, v. 12, n. 9, p. 5184–5213, 2022.

SONG, T. SHUN et al. Experimental evaluation of the influential factors of acetate production driven by a DC power system via CO2 reduction through microbial electrosynthesis. **Bioresources and Bioprocessing**, v. 6, n. 1, p. 1–10, 2019.

SORGATO, A. C. **Célula a combustível microbiana: operação em diferentes tempos de detenção hidráulica e extração de energia ativa**. [s.l.] Universidade Federal de Santa Catarina, 2022.

SOUZA, M. C. O. et al. Screening of regulated aromatic amines in clothing marketed in Brazil and Spain: assessment of human health risks. **Environmental Research**, p. 1–10, jan. 2023.

SRIVASTAVA, P. et al. Constructed wetland coupled microbial fuel cell technology. In: **Microbial Electrochemical Technology**. [s.l.] Elsevier, 2019. p. 1021–1036.

SUBRAMANIAM, R.; PONNUSAMY, S. K. Novel adsorbent from agricultural waste (cashew NUT shell) for methylene blue dye removal: optimization by response surface methodology. **Water Resources and Industry**, v. 11, p. 64–70, set. 2015.

SUHAN, M. B. K. et al. Comparative degradation study of remazol black B dye using electro-coagulation and electro-Fenton process: kinetics and cost analysis. **Environmental Nanotechnology, Monitoring and Management**, v. 14, p. 1–11, 2020.

SULTANA, S. et al. Bio-electro degradation of azo-dye in a combined anaerobic-aerobic process along with energy recovery. **New Journal of Chemistry**, v. 39, n. 12, p. 9461–9470, 2015.

SUN, J. et al. Simultaneous decolorization of azo dye and bioelectricity generation using a microfiltration membrane air-cathode single-chamber microbial fuel cell. **Bioresource Technology**, v. 100, n. 13, p. 3185–3192, 2009.

SUN, M. et al. Harvest and utilization of chemical energy in wastes by microbial fuel cells. **Chemical Society Reviews**, v. 45, n. 10, p. 2847–2870, 2016.

SUN, Y. et al. Microbial community analysis in biocathode microbial fuel cells packed with different materials. **AMB Express**, v. 2, n. 21, p. 1–8, 29 dez. 2012.

SUN, Y. et al. Kerstersia gyiorum isolated for the first time from two patients with neurodegenerative disease: report of two unusual cases and a review of the literature. **Journal of International Medical Research**, v. 51, n. 5, p. 1–9, 9 maio 2023.

SURANSH, J. et al. Scalable architecture of low-cost household microbial fuel cell for domestic wastewater treatment and simultaneous energy recovery. **Science of the Total Environment**, v. 857, n. 159671, p. 1–9, 2023.

SURESH, R. et al. Current advances in microbial fuel cell technology toward removal of organic contaminants – a review. **Chemosphere**, v. 287, p. 1–14, 2022.

TABASSUM, N.; ISLAM, N.; AHMED, S. Progress in microbial fuel cells for sustainable management of industrial effluents. **Process Biochemistry**, v. 106, p. 20–41, 2021.

TABATABAEI, M.; DASTBARSAR, M.; MOSLEHI, M. A. Isolation and identification of Pandoraea spp. From bronchoalveolar lavage of cystic fibrosis patients in Iran. **Italian Journal of Pediatrics**, v. 45, n. 1, p. 118, 2 dez. 2019.

TACAS, A. C. J. et al. Degradation and biotoxicity of azo dyes using indigenous bacteria-acclimated microbial fuel cells (MFCs). **Process Biochemistry**, v. 102, p. 59–71, 2021.

TAN, S. M. et al. The reaction of wastewater treatment and power generation of single chamber microbial fuel cell against substrate concentration and anode distributions. **Journal of Environmental Health Science and Engineering**, v. 18, n. 2, p. 793–807, 2020.

TAN, S. M. et al. Discerning the biodegradation of binary dyes in microbial fuel cell: interactive effects of dyes, electron transport behaviour, autocatalytic mechanism, and degradation pathways. **Journal of Environmental Chemical Engineering**, v. 10, n. 3, p. 1–16, 2022.

TAO, Q. et al. Nutrient removal and electricity production from wastewater using microbial fuel cell technique. **Desalination**, v. 365, p. 92–98, 2015.

TELKE, A. A.; KADAM, A. A.; GOVINDWAR, S. P. Bacterial enzymes and their role in decolorization of azo dyes. In: SINGH, S. N. (Ed.). . **Microbial Degradation of Synthetic Dyes in Wastewaters**. Environmen ed. [s.l.] Springer International Publishing Switzerland 2015, 2015. p. 149–168.

TEYMORI, M. et al. Electro-Fenton method for the removal of malachite green: effect of operational parameters. **Applied Water Science**, v. 10, n. 1, p. 1–14, 2020.

THAPA, B. SEN et al. Overview of electroactive microorganisms and electron transfer mechanisms in microbial electrochemistry. **Bioresource Technology**, v. 347, p. 1–14, 2022.

THUNG, W.-E. et al. A highly efficient single chambered up-flow membrane-less microbial fuel cell for treatment of azo dye acid orange 7-containing wastewater. **Bioresource Technology**, v. 197, p. 284–288, dez. 2015.

TKACH, O. et al. Performance of low temperature microbial fuel cells (MFCs) catalyzed by mixed bacterial consortia. **Journal of Environmental Sciences**, v. 52, p. 284–292, 2017.

TRABLY, E. et al. Microbial dynamics in anaerobic enrichment cultures degrading di-n-butyl phthalic acid ester. **FEMS Microbiology Ecology**, v. 66, n. 2, p. 472–483, nov. 2008.

TRAPERO, J. R. et al. Is microbial fuel cell technology ready? An economic answer towards industrial commercialization. **Applied Energy**, v. 185, p. 698–707, 2017.

UDDIN, S. S. et al. **Comparison of current density and power density obtained from a double chamber microbial fuel cell for different sludges**. 2019 International Conference on Robotics,Electrical and Signal Processing Techniques (ICREST). **Anais**...IEEE, jan. 2019Disponível em: <https://ieeexplore.ieee.org/document/8644198/>

UDUMA, R. C. et al. Bioelectrochemical technologies for simultaneous treatment of dye wastewater and electricity generation: a review. **International Journal of Environmental Science and Technology**, v. 20, n. 9, p. 10415–10434, 2023.

UJIIE, H. Fabric finishing. In: **Textiles and Fashion**. [s.l.] Elsevier, 2015. p. 507–529.

ULLAH, Z.; ZESHAN, S. Effect of substrate type and concentration on the performance of a double chamber microbial fuel cell. **Water Science and Technology**, v. 81, n. 7, p. 1336–1344, 1 abr. 2020.

ULLERY, M. L.; LOGAN, B. E. Anode acclimation methods and their impact on microbial electrolysis cells treating fermentation effluent. **International Journal of Hydrogen Energy**, v. 40, n. 21, p. 6782–6791, 2015.

VANMETER, K.; HUBERT, R. **Microbiology for the healthcare professional**. 3rd. ed. [s.l.] Evolve, 2021.

VASSILEV, I. et al. Anodic electro-fermentation: Empowering anaerobic production processes via anodic respiration. **Biotechnology Advances**, v. 48, p. 1–7, maio 2021.

VAYENAS, D. V. Attached growth biological systems in the treatment of potable water and wastewater. In: **Comprehensive Biotechnology**. [s.l.] Elsevier, 2011. p. 371–383.

VELVIZHI, G.; VENKATA MOHAN, S. Electrogenic activity and electron losses under increasing organic load of recalcitrant pharmaceutical wastewater. **International Journal of Hydrogen Energy**, v. 37, n. 7, p. 5969–5978, 2012.

VENKATACHALAM, C. D. et al. Biodegradation of azo dye using microbiological consortium. In: **Development in Wastewater Treatment Research and Processes**. [s.l.] Elsevier, 2022. p. 355–370.

VERMA, J. et al. Electricigens and microbial fuel cells for bioremediation and bioenergy production: a review. **Environmental Chemistry Letters**, v. 19, n. 3, p. 2091–2126, 2021a.

VERMA, P. et al. Microbial fuel cell – a sustainable approach for simultaneous wastewater treatment and energy recovery. **Journal of Water Process Engineering**, v. 40, p. 1–16, 2021b.

VICARI, F. et al. Effect of mode of operation, substrate and final electron acceptor on single-chamber membraneless microbial fuel cell operating with a mixed community. **Journal of Electroanalytical Chemistry**, v. 814, p. 104–110, 2018.

VIKRANT, K. et al. Recent advancements in bioremediation of dye: current status and challenges. **Bioresource Technology**, v. 253, p. 355–367, 2018.

WAKRIM, A. et al. Treatment and degradation of azo dye waste industry by electro-Fenton process. **Physical Chemistry Research**, v. 10, n. 4, p. 495–504, 2022.

WANG, B. et al. Renewable energy driving microbial electrochemistry toward carbon neutral. **Sustainable Horizons**, v. 4, n. 100031, p. 1–7, 2022a.

WANG, H. Y. A.; YANG, C. S.; LIN, C. H. A rapid quantification method for energy conversion efficiency of microbial fuel cells. **Journal of the Taiwan Institute of Chemical Engineers**, v. 109, p. 124–128, 2020.

WANG, J. et al. Degradation characterization and pathway analysis of chlortetracycline and oxytetracycline in a microbial fuel cell. **RSC Advances**, v. 8, n. 50, p. 28613–28624, 2018.

WANG, K. et al. Making cathode composites more efficient for electro-Fenton and bioelectro-Fenton systems: a review. **Separation and Purification Technology**, v. 304, p. 1–17, 2023.

WANG, P. et al. Deposition of Fe on graphite felt by thermal decomposition of Fe(CO)5 for effective cathodic preparation of microbial fuel cells. **Bioresource Technology**, v. 134, p. 30–35, abr. 2013a.

WANG, Q. et al. Sequential anaerobic and electro-Fenton processes mediated by W and Mo oxides for degradation/mineralization of azo dye methyl orange in photoassisted microbial fuel cells. **Applied Catalysis B: Environmental**, v. 245, p. 672–680, maio 2019a.

WANG, W. et al. Micro-electricity utilization performance and microbial mechanism in microbial fuel cell powered electro-Fenton system for azo dye treatment. **Biochemical Engineering Journal**, v. 186, p. 1–15, 2022b.

WANG, X.-Q. et al. Arsenite oxidation and removal driven by a bio-electro-Fenton process under neutral pH conditions. **Journal of Hazardous Materials**, v. 275, p. 200–209, jun. 2014.

WANG, X. et al. An eco-friendly Iron cathode electro-Fenton system coupled with a pH regulation electrolysis cell for p-nitrophenol degradation. **Frontiers in Chemistry**, v. 9, p. 1–10, 2022c.

WANG, Y.-T. et al. Enhancement of electrical properties by a composite FePc/CNT/C cathode in a bio-electro-Fenton microbial fuel cell system. **Journal of Nanoscience and Nanotechnology**, v. 20, n. 5, p. 3252–3257, 2019b.

WANG, Y. et al. Enhancement of emerging contaminants removal using Fenton reaction driven by H2O2-producing microbial fuel cells. **Chemical Engineering Journal**, v. 307, p. 679–686, 2017.

WANG, Y.; QIAN, P.-Y. Conservative fragments in bacterial 16S rRNA genes and primer design for 16S ribosomal DNA amplicons in metagenomic studies. **PLoS ONE**, v. 4, n. 10, 9 out. 2009.

WANG, Y. Z. et al. Enhanced azo dye removal through anode biofilm acclimation to toxicity in single-chamber biocatalyzed electrolysis system. **Bioresource Technology**, v. 142, p. 688–692, 2013b.

WATANABE, K.; KODAMA, Y.; HARAYAMA, S. Design and evaluation of PCR primers to amplify bacterial 16S ribosomal DNA fragments used for community fingerprinting. **Journal of Microbiological Methods**, v. 44, n. 3, p. 253–262, abr. 2001.

WEN, Q. et al. Electricity generation and brewery wastewater treatment from sequential anode-cathode microbial fuel cell. **Journal of Zhejiang University**, v. 11, n. 2, p. 87–93, 3 fev. 2010.

WHITBY, C. A microbial solution to oil sand pollution: understanding the microbiomes, metabolic pathways and mechanisms involved in naphthenic acid (NA) biodegradation. In: **Functional Microbiomes**. [s.l: s.n.]. p. 231–287.

WU, J. C. et al. Effect of FeSO4 on bio-electro-Fenton microbial fuel cells with different exchange membranes. **Materials Research Innovations**, v. 19, p. 51276–51279, 2015.

WU, L. C. et al. Highly efficient removal of victoria blue R and bioelectricity generation from textile wastewater using a novel combined dual microbial fuel cell system. **Chemosphere**, v. 258, p. 1–10, 2020a.

WU, Q. et al. Microbial fuel cell system: a promising technology for pollutant removal and environmental remediation. **Environmental Science and Pollution Research**, v. 27, n. 7, p. 6749–6764, 2020b.

XIA, T. et al. Power generation and microbial community analysis in microbial fuel cells: a promising system to treat organic acid fermentation wastewater. **Bioresource Technology**, v. 284, p. 72–79, jul. 2019.

XIA, Y. et al. Cellular adhesiveness and cellulolytic capacity in Anaerolineae revealed by omics-based genome interpretation. **Biotechnology for Biofuels**, v. 9, n. 1, p. 1–13, 2016.

XU, J. et al. Organic wastewater treatment by a single-atom catalyst and electrolytically produced H2O2. **Nature Sustainability**, v. 4, n. 3, p. 233–241, 9 nov. 2020a.

XU, L. et al. The integrated processes for wastewater treatment based on the principle of microbial fuel cells: a review. **Critical Reviews in Environmental Science and Technology**, v. 46, n. 1, p. 60–91, 2 jan. 2016.

XU, P. et al. The mechanism and oxidation efficiency of bioelectro-Fenton system with Fe@Fe2O3/ACF composite cathode. **Separation and Purification Technology**, v. 234, p. 116103, mar. 2020b.

XU, P.; XU, H.; SHI, Z. A novel bio-electro-Fenton process with FeVO4/CF cathode on advanced treatment of coal gasification wastewater. **Separation and Purification Technology**, v. 194, p. 457–461, 2018.

YADAV, A. et al. Microbial fuel cells for mineralization and decolorization of azo dyes: recent advances in design and materials. **Science of the Total Environment**, v. 826, p. 1–23, 2022.

YANG, H. Y. et al. Process and kinetics of azo dye decolourization in bioelectrochemical systems: effect of several key factors. **Scientific Reports**, v. 6, p. 1–9, 2016.

YANG, J.; CHEN, B. Energy efficiency evaluation of wastewater treatment plants (WWTPs) based on data envelopment analysis. **Applied Energy**, v. 289, p. 1–

15, maio 2021.

YANG, X. et al. Degradation of metoprolol from wastewater in a bio-electro-Fenton system. **Science of the Total Environment**, v. 771, p. 1–12, 2021.

YANG, Y. Recent advances in the electrochemical oxidation water treatment: spotlight on byproduct control. **Frontiers of Environmental Science and Engineering**, v. 14, n. 5, 2020.

YANG, Z. et al. Efficient degradation of organic compounds in landfill leachate via developing bio-electro-Fenton process. **Journal of Environmental Management**, v. 319, p. 1–12, out. 2022.

YAQOOB, A. A. et al. Outlook on the role of microbial fuel cells in remediation of environmental pollutants with electricity generation. **Catalysts**, v. 10, n. 8, p. 1–34, 2020.

YASEEN, D. A.; SCHOLZ, M. Textile dye wastewater characteristics and constituents of synthetic effluents: a critical review. **International Journal of Environmental Science and Technology**, v. 16, n. 2, p. 1193–1226, 2019.

YE, Y. et al. Effect of organic loading rate on the recovery of nutrients and energy in a dual-chamber microbial fuel cell. **Bioresource Technology**, v. 281, p. 367–373, 2019.

YE, Y. et al. Impacts of hydraulic retention time on a continuous flow mode dual-chamber microbial fuel cell for recovering nutrients from municipal wastewater. **Science of the Total Environment**, v. 734, p. 1–7, 2020.

YING, Z. et al. External potential regulated biocathode for enhanced removal of gaseous chlorobenzene in bioelectrchemical system. **Chemosphere**, v. 274, p. 1–8, 2021.

YOGALAKSHMI, K. N. et al. Nano-bioremediation: a new age technology for the treatment of dyes in textile effluents. In: SAXENA, G.; BHARAGAVA, R. N. (Eds.). . **Bioremediation of Industrial Waste for Environmental Safety**. [s.l.] Springer Nature Singapore, 2020. p. 313–347.

YONG, X.-Y. et al. Bio-Electron-Fenton (BEF) process driven by microbial fuel cells for triphenyltin chloride (TPTC) degradation. **Journal of Hazardous Materials**, v. 324, p. 178–183, fev. 2017.

YONG, Y.-C. et al. Increase of riboflavin biosynthesis underlies enhancement of extracellular electron transfer of Shewanella in alkaline microbial fuel cells. **Bioresource Technology**, v. 130, p. 763–768, fev. 2013.

YOU, J. et al. Efficient biodechlorination at the Fe3O4-based silicone powder modified chlorobenzene-affinity anode. **Journal of Hazardous Materials**, v. 457, p. 1–12, set. 2023.

YOU, S. J. et al. Power generation and electrochemical analysis of biocathode microbial fuel cell using graphite fibre brush as cathode material. **Fuel Cells**, v. 9, n. 5, p. 588–596, 2009.

YOUNG, B. J. et al. Toxicity of the effluent from an anaerobic bioreactor treating cereal residues on Lactuca sativa. **Ecotoxicology and Environmental Safety**, v. 76, p. 182–186, fev. 2012.

YU, X. et al. Automatic microbial electro-Fenton system driven by transpiration for degradation of acid orange 7. **Science of the Total Environment**, v. 725, p. 1–7, 2020.

YUAN, G.-E. et al. Integration of microbial fuel cell and catalytic oxidation reactor with iron phthalocyanine catalyst for Congo red degradation. **Biochemical Engineering Journal**, v. 120, p. 118–124, abr. 2017.

YULIASNI, R. et al. Introduction to microbial fuel cell (MFC): waste matter to electricity. In: **Biofuel Cells: Materials and Challenges**. [s.l: s.n.]. p. 123–144.

ZAFAR, S.; BUKHARI, D. A.; REHMAN, A. Azo dyes degradation by microorganisms – an efficient and sustainable approach. **Saudi Journal of Biological Sciences**, v. 29, p. 1–9, 2022.

ZAVALA, M. Á. L.; GUTIÉRREZ, I. C. C. Effects of external resistance, new electrode material, and catholyte type on the energy generation and performance of dual-chamber microbial fuel cells. **Fermentation**, v. 9, n. 4, p. 1–13, 2023.

ZHANG, L.-J.; TAO, H.-C. Bioelectro-Fenton system for environmental pollutant degradation. In: **Bioelectrochemistry Stimulated Environmental Remediation: From Bioelectrorespiration to Bioelectrodegradation**. [s.l: s.n.]. p. 245–267.

ZHANG, L. et al. Startup performance and anodic biofilm distribution in continuous-flow microbial fuel cells with serpentine flow fields: effects of external resistance. **Industrial and Engineering Chemistry Research**, v. 56, n. 14, p. 3767–3774, 2017.

ZHANG, L.; YIN, X.; LI, S. F. Y. Bio-electrochemical degradation of paracetamol in a microbial fuel cell-Fenton system. **Chemical Engineering Journal**, v. 276, p. 185–192, set. 2015.

ZHANG, P. et al. Accelerating the startup of microbial fuel cells by facile microbial acclimation. **Bioresource Technology Reports**, v. 8, n. 100347, p. 1–8, 2019a.

ZHANG, P. et al. Accelerating the startup of microbial fuel cells by facile microbial acclimation. **Bioresource Technology Reports**, v. 8, p. 1–8, 2019b.

ZHANG, Q. et al. Enhancement of fipronil degradation with eliminating its toxicity in a microbial fuel cell and the catabolic versatility of anodic biofilm. **Bioresource Technology**, v. 290, p. 1–7, 2019c.

ZHANG, X. et al. Insights into practical-scale electrochemical H2O2 synthesis. **Trends in Chemistry**, v. 2, n. 10, p. 942–953, 2020.

ZHANG, Y. et al. Microbial fuel cell hybrid systems for wastewater treatment and bioenergy production: Synergistic effects, mechanisms and challenges. **Renewable and Sustainable Energy Reviews**, v. 103, p. 13–29, 2019d.

ZHANG, Y. et al. Microbial fuel cell hybrid systems for wastewater treatment and bioenergy production: synergistic effects, mechanisms and challenges. **Renewable and Sustainable Energy Reviews**, v. 103, p. 13–29, abr. 2019e.

ZHANG, Y. et al. Treatment of textile wastewater by advanced oxidation processes – a review. **Water**, v. 13, p. 1–22, 2021.

ZHANG, Y.; WANG, Y.; ANGELIDAKI, I. Alternate switching between microbial fuel cell and microbial electrolysis cell operation as a new method to control H2O2 level in bioelectro-Fenton system. **Journal of Power Sources**, v. 291, p. 108–116, set. 2015a.

ZHANG, Y.; WANG, Y.; ANGELIDAKI, I. Alternate switching between microbial fuel cell and microbial electrolysis cell operation as a new method to control H2O2 level in Bioelectro-Fenton system. **Journal of Power Sources**, v. 291, p. 108–116, set. 2015b.

ZHANG, Z. et al. Contaminant removal and resource recovery in bioelectrochemical wastewater treatment. **Current Pollution Reports**, v. 8, n. 2, p. 159–176, 2022.

ZHAO, H.; ZHANG, Q. Performance of electro-Fenton process coupling with microbial fuel cell for simultaneous removal of herbicide mesotrione. **Bioresource Technology**, v. 319, n. 124244, p. 1–8, 2021.

ZHI, W. et al. Methods for understanding microbial community structures and functions in microbial fuel cells: a review. **Bioresource Technology**, v. 171, p. 461–

468, nov. 2014.

ZHONG, D. et al. Enhanced electricity generation performance and dye wastewater degradation of microbial fuel cell by using a petaline NiO@ polyaniline-carbon felt anode. **Bioresource Technology**, v. 258, p. 125–134, jun. 2018.

ZHOU, W. et al. Hydrogen peroxide generation from O2 electroreduction for environmental remediation: a state-of-the-art review. **Chemosphere**, v. 225, p. 588–607, 2019.

ZHUANG, L. et al. A novel bioelectro-Fenton system for coupling anodic COD removal with cathodic dye degradation. **Chemical Engineering Journal**, v. 163, n. 1–2, p. 160–163, 2010.

ZOU, R. et al. Feasibility and applicability of the scaling-up of bio-electro-Fenton system for textile wastewater treatment. **Environment International**, v. 134, n. 105352, p. 1–11, 2020.

ZOU, R. et al. Scaling-up of microbial electrosynthesis with multiple electrodes for in situ production of hydrogen peroxide. **iScience**, v. 24, n. 2, p. 1–9, fev. 2021.